Time-of-Flight Mass Spectrometry

ACS SYMPOSIUM SERIES 549

Time-of-Flight Mass Spectrometry

Robert J. Cotter, EDITOR
The Johns Hopkins University School of Medicine

Developed from symposia held at the 204th National Meeting of the American Chemical Society, Washington, DC, August 23–28, 1992, and the Pittsburgh Conference on Analytical Instrumentation, New Orleans, Louisiana, March 9–12, 1992



American Chemical Society, Washington, DC 1994



Library of Congress Cataloging-in-Publication Data

Time-of-flight mass spectrometry / Robert J. Cotter, editor.

p. cm.—(ACS symposium series, ISSN 0097-6156; 549)

"Developed from symposia held at the 24th National Meeting of the American Chemical Society, Washington, DC, August 23–28, 1992, and the Pittsburgh Conference on Analytical Instrumentation, New Orleans, Louisiana, March 9–12, 1992."

Includes bibliographical references and index.

ISBN 0-8412-2771-3

- Time-of-flight mass spectrometry—Congresses.
- I. Cotter, Robert J., 1943— . II. American Chemical Society. Meeting (204th: 1992: Washington, DC) III. Pittsburgh Conference on Analytical Instrumentation (1992: New Orleans, La.) IV. Series.

QC454.M8T56 1994 543'.0873—dc20

93-23638 CIP

The paper used in this publication meets the minimum requirements of American National Standard for Information Sciences—Permanence of Paper for Printed Library Materials, ANSI Z39.48—1984.

Copyright © 1994

American Chemical Society

All Rights Reserved. The appearance of the code at the bottom of the first page of each chapter in this volume indicates the copyright owner's consent that reprographic copies of the chapter may be made for personal or internal use or for the personal or internal use of specific clients. This consent is given on the condition, however, that the copier pay the stated per-copy fee through the Copyright Clearance Center, Inc., 27 Congress Street, Salem, MA 01970, for copying beyond that permitted by Sections 107 or 108 of the U.S. Copyright Law. This consent does not extend to copying or transmission by any means—graphic or electronic—for any other purpose, such as for general distribution, for advertising or promotional purposes, for creating a new collective work, for resale, or for information storage and retrieval systems. The copying fee for each chapter is indicated in the code at the bottom of the first page of the chapter.

The citation of trade names and/or names of manufacturers in this publication is not to be construed as an endorsement or as approval by ACS of the commercial products or services referenced herein; nor should the mere reference herein to any drawing, specification, chemical process, or other data be regarded as a license or as a conveyance of any right or permission to the holder, reader, or any other person or corporation, to manufacture, reproduce, use, or sell any patented invention or copyrighted work that may in any way be related thereto. Registered names, trademarks, etc., used in this publication, even without specific indication thereof, are not to be considered unprojected by law.

specific indication thereof, are not to be considered unprotected by law.

American Chemical
PRINTED IN THE UNITED STATES OF AMERICA
SOCIETY Library

1993 Advisory Board

ACS Symposium Series

M. Joan Comstock, Series Editor

V. Dean Adams
University of Nevada—
Reno

Robert J. Alaimo Procter & Gamble Pharmaceuticals, Inc.

Mark Arnold University of Iowa

David Baker University of Tennessee

Arindam Bose Pfizer Central Research

Robert F. Brady, Jr. Naval Research Laboratory

Margaret A. Cavanaugh National Science Foundation

Dennis W. Hess Lehigh University

Hiroshi Ito IBM Almaden Research Center

Madeleine M. Joullie University of Pennsylvania

Gretchen S. Kohl Dow-Corning Corporation Bonnie Lawlor
Institute for Scientific Information

Douglas R. Lloyd
The University of Texas at Austin

Robert McGorrin Kraft General Foods

Julius J. Menn
Plant Sciences Institute,
U.S. Department of Agriculture

Vincent Pecoraro University of Michigan

Marshall Phillips Delmont Laboratories

George W. Roberts North Carolina State University

A. Truman Schwartz Macalaster College

John R. Shapley University of Illinois at Urbana—Champaign

L. Somasundaram DuPont

Peter Willett University of Sheffield (England)

Foreword

THE ACS SYMPOSIUM SERIES was first published in 1974 to provide a mechanism for publishing symposia quickly in book form. The purpose of this series is to publish comprehensive books developed from symposia, which are usually "snapshots in time" of the current research being done on a topic, plus some review material on the topic. For this reason, it is necessary that the papers be published as quickly as possible.

Before a symposium-based book is put under contract, the proposed table of contents is reviewed for appropriateness to the topic and for comprehensiveness of the collection. Some papers are excluded at this point, and others are added to round out the scope of the volume. In addition, a draft of each paper is peer-reviewed prior to final acceptance or rejection. This anonymous review process is supervised by the organizer(s) of the symposium, who become the editor(s) of the book. The authors then revise their papers according to the recommendations of both the reviewers and the editors, prepare camera-ready copy, and submit the final papers to the editors, who check that all necessary revisions have been made.

As a rule, only original research papers and original review papers are included in the volumes. Verbatim reproductions of previously published papers are not accepted.

M. Joan Comstock Series Editor

Preface

MOST MASS SPECTROSCOPISTS WOULD AGREE that there is a resurgence of interest in time-of-flight (TOF) mass spectrometers. LeCroy Corporation, which manufactures digitizing oscilloscopes used in many such instruments, held a highly successful meeting on Instrumentation for Time-of-Flight Mass Spectrometry in November 1992, which was reported in the January 15, 1993, issue of Analytical Chemistry. And on October 3-7, 1993, the Asilomar Conference on Mass Spectrometry at Estes Park in Colorado was dedicated to that subject. This renewed interest in a mass analyzer first described more than 40 years ago is in large part an interest in matrix-assisted laser desorption-ionization (MALDI), a powerful new ionization technique that has made it possible to measure the molecular masses of proteins weighing several hundred kilodaltons and has resulted in the commercialization of MALDI-TOF instruments by at least seven manufacturers. At the same time, there is a genuine interest in the TOF analyzer itself, as evidenced by considerable activity in designing compatible electrospray ionization (ESI) sources, exploiting the high speed and duty cycle of the TOF for chromatography, and developing methods for obtaining structural information from "post-source" fragmentation. This latter activity motivated the organization of the symposium: Time-of-Flight Mass Spectrometers as Tandem Instruments that was held on August 24, 1992, during the annual meeting of the American Chemical Society in Washington, DC.

Tandem time-of-flight (TOF-TOF) instruments are indeed few in number, but reflectrons have been used for a number of years to observe and record product ion mass spectra. Thus, the contributions to the ACS symposium by Ronald Beavis, Michael Duncan, David Russell, Jack Holland, and me described the basic principles of reflectron focusing; the recording of metastable, collision-induced, and photo-induced dissociation spectra; hybrid and tandem time-of-flight instruments; and the combination of time-of-flight mass spectrometry with chromatography. These contributions formed the core of this volume. At the same time, it was our intention in assembling this volume to provide a more complete picture of the current state of time-of-flight mass spectrometry. Thus, we in-

cluded several contributions from the Time-of-Flight Mass Spectrometry symposium held in conjunction with the Pittsburgh Conference on Analytical Instrumentation on March 10, 1992, in New Orleans. Other chapters were added to provide a history of time-of-flight mass spectrometry, a description of basic principles, the possibilities for utilizing continuous ionization techniques (particularly electrospray), and applications to biological research. The result (we think) provides an excellent introduction to time-of-flight mass spectrometry for those beginning such work, as well as an up-to-date account for those already using the technique.

In Chapter 1, Dennis Price (University of Salford) describes the history of time-of-flight mass spectrometry from its first successful commercialization in 1955 to the present. This chapter was written specifically for this book.

The basic principles of time-of-flight mass spectrometry; the dependence of mass resolution on initial time, space, and kinetic energy distributions; and the use of a reflectron for energy focusing are then described in my overview for this book, Chapter 2. These concepts are brought up to date by discussions on the effects of metastable fragmentation of large ions (generally from biological molecules) on mass resolution, and the use of reflectrons to observe product ion mass spectra.

Chapters 3 to 6, from the ACS symposium, focus on the use of timeof-flight mass spectrometers as tandem instruments, that is for recording product ion mass spectra to obtain structural information. In Chapter 3, Ronald Beavis (Memorial University of Newfoundland) presents the principles of single- and dual-stage reflectrons in some detail and describes how product ion mass spectra may be obtained. In Chapter 4, Michael Duncan (University of Georgia) describes the photoinduced dissociation of ions in the turn-around region of the reflectron, where their low velocity results in improved dissociation cross section. This approach contrasts with other metastable and induced fragmentation schemes in the linear region, and results in different focusing conditions and mass scale. In Chapter 5, David Russell and co-workers (Texas A&M University) describe a hybrid tandem instrument using a double-focusing sector mass spectrometer as the first mass analyzer, a collision chamber, and a reflectron time-of-flight (RTOF) as the second mass analyzer. Finally, in Chapter 6, Timothy Cornish and I describe a tandem (TOF-TOF) instrument using pulsed collision induced dissociation.

Time-of-flight mass spectrometers are the most obvious choice for pulsed or random event techniques such as laser desorption (LD), MALDI, or plasma desorption mass spectrometry (PDMS), because the multiplex recording of all ions of all masses from each ionization event is far more reasonable than approaches that scan the mass range. At the same time, there is considerable interest in interfacing time-of-flight mass spectrometers with ionization techniques that are inherently continuous. In Chapter 7, Dodonov and co-workers (Russian Academy of Sciences) describe an atmospheric pressure ionization (API) instrument using ion storage, orthogonal extraction, and reflectron focusing that can be interfaced with virtually any continuous ionization technique. They demonstrate their results using electrospray ionization (ESI), citing high mass measurement accuracy and the ability to improve structural information by inducing collisions in the ESI source. This chapter is based on a poster presentation at the 12th International Mass Spectrometry Conference (August 26–30, 1991) in Amsterdam.

Just when you thought you knew all about time-of-flight mass spectrometry, Robert Conzemius (Iowa State University) describes in Chapter 8 the possibilities for correlating mass differences from species originating from single ionization events. In Chapter 9, Holland and co-workers (Michigan State University) continue their interest in mass spectrometry in the chromatographic time frame with an approach that uses (again) ion storage, pulsed extraction, and spectral deconvolution to achieve high duty cycle, high chromatographic integrity, and time-compressed chromatography. Recent advances in the sampling rates, bandwidths, and signalprocessing capabilities of waveform recorders, integrating transient recorders, and digital oscilloscopes have contributed to the proliferation of time-of-flight instruments now available commercially. In Chapter 10, Ihor Lys (Carnegie Mellon University) presents the basic principles of signal processing in time-of-flight instruments. Chapters 8 and 10 were selected from the symposium on Time-of-Flight Mass Spectrometry held at the Pittsburgh Conference on Analytical Instrumentation (March 10, 1992) in New Orleans, Louisiana, while Chapter 9 was culled from presentations at both the ACS symposium and the Pittsburgh Conference.

The volume concludes with the application of time-of-flight instruments to biological analysis. In Chapter 11, Amina Woods (Johns Hopkins University) describes how molecular-weight measurements can be used in conjunction with enzymes (trypsin, endoproteinases, and peptidases) to determine cleavage and phosphorylation sites in a herpesvirus protein. In Chapter 12, Martha Vestling (University of Maryland Baltimore County) provides an important link between the mass spectroscopist and the biologist by offering several examples of the ability to analyze samples transferred to the mass spectrometer directly from the gels used in gel electrophoresis. These last two chapters were invited, not presented at a symposium.

Together, these chapters provide a very comprehensive and up-to-date view of the theory, instrumentation, and applications of time-of-flight mass spectrometry.

Acknowledgments

I first acknowledge the considerable efforts expended by the authors of each chapter in preparing camera-ready manuscripts within a time frame that would produce an up-to-date account of a field that is progressing rapidly. It has been clear from the outset that there has been considerable interest on their part in producing the first comprehensive review of this subject. I also acknowledge the considerable assistance of the staff of ACS Books, without whom this would have been a far more difficult task. Finally, I acknowledge the editorial assistance of Darleen Stankiewicz and Jennifer Justice. Their efforts in transcribing and formatting manuscripts produced on a variety of word processors are greatly appreciated.

ROBERT J. COTTER
Middle Atlantic Mass Spectrometry Laboratory
Department of Pharmacology and Molecular Sciences
The Johns Hopkins University School of Medicine
Baltimore, MD 21205

October 29, 1993

Chapter 1

Time-of-Flight Mass Spectrometry

The Early Years as Chronicled by the European Time-of-Flight Symposia

Dennis Price

Department of Chemistry and Applied Chemistry, University of Salford, Salford M5 4WT, England

As shown in Table I, time-of-flight mass spectrometry has had a checkered history since it became commercially available following the innovations of the Wiley-McLaren design in 1955. The Bendix/CVC instruments were used for a wide range of applications facilitated by its very fast scan capability and/or ease of access to the ion source. However, because they were seen as having both low resolution and low sensitivity, these instruments never became widely utilised in the major areas of mass spectrometry.

The resurgence of interest in the time-of-flight technique since the mid '80's has been due to the advent at the forefront of mass spectrometry development of such techniques as laser and plasma desorption, laser ionisation and surface analysis, which require its ability to provide a complete spectrum for each ionisation event and also its unlimited mass range. In order for this renaissance to continue and expand, a wide base of commercially available instruments is required. As can be seen from Table II such a base now exists.

This chapter is intended to provide a brief history of the time-of-flight mass spectrometer (TOFMS) over the period 1955-90 based on the progress reported at various European time-of-flight symposia. In this it is intended to act as a prelude to the exciting developments which this author anticipates for the current decade. The following chapters will provide the reader with a foretaste of the future of time-of-flight mass spectrometry.

Time-of-flight mass spectrometers operate on the simple principle that a packet of ions, of differing mass/charge (m/z) ratios but equal energy or momentum, when projected into a constant electric field will separate according to their m/z ratios. Since z is usually unity, the separation is essentially one of mass. If the ions travel a fixed distance l to a detector, then the 'time-of-flight' (TOF) is given by

$$\left(\frac{1^2}{2V}\right)^{1/2} \left(\frac{m}{z}\right)^{1/2} \tag{1}$$

in the constant energy case (V is the accelerating voltage) and

0097-6156/94/0549-0001\$06.00/0 © 1994 American Chemical Society

Table I. History of time-of-flight mass spectrometry to 1990

- 1946 TOFMS first proposed by Stephens (1).
- 1948 First experimental account of TOF instrument "Ion Velocitron" by Cameron and Eggers (2).
- 1953 First TOFMS utilising pulsed electron beam (44).
- 1955 Katzenstein and Friedland instrument using pulsed electron beam and delayed ion ejection from source (3).
 Major improvement to TOFMS performance via two-grid ion source optimised for 'space' and 'energy' focussing, plus time-lag focussing, Wiley and McLaren (4).
- 1957 Bendix Corporation launch commercial TOFMS based on Wiley-McLaren design.
- 1959 GC/TOFMS reported by Gohlke (10).
- 1960 Harrington publishes first TOFMS review (45).
- 1963 Capillary GC/TOFMS reported by McFadden (46).
- 1966 Laser microprobe/TOFMS described by Vastola and Knox (47).
- 1967 First European TOFMS Symposium. Published proceedings (5) contain a review of Bendix instruments plus articles on their application to fast reactions, ion-molecule and ion-surface interactions, high temperature studies and industrial analysis.
- 1969 Second European Symposium (8), papers on kinetic studies, ionisation processes, analytical applications and general instrumentation.
- 1971 Mass Reflectron giving major improvement in TOFMS resolution (>2000) reported by Mamyrin (13).

 Third European TOFMS Symposium (12).
- 1973 Poschenrieder paper (24) concerned with time and space focussing in TOFMS using sector fields.
- 1974 Plasma desorption-TOFMS for high mass studies first reported by Macfarlane (16).
 Forth European Symposium now expended to induce all dynamic mass spectrometers. Proceeding (14) contain review of TOFMS literature and also time-focussing TOFMS.
- 1977 Fifth European Symposium; Boerboom et al. report used of CEMA for detection of ions produced by laser induced desorption (15).
- 1979 Laser desorption/TOFMS instrument (LAMMA) marketed by Leybold Hereaus.
- 1980 Sixth European Symposium.
- 1983 Seventh European Symposium (17). Increasing activity reported to be due to the advent of new ionisation techniques (plasma and laser desorption) which require TOFMS ability to provide a complete spectrum per event and also the unlimited mass range.
- 1986 Eighth European Symposium.
- 1987 Hillenkamp et al. announce detection of high mass ions (m/z > 100 kDa) using matrix assisted, laser desorption/ionisation TOFMS.
- 1989 Ninth European Symposium (28).

$$\frac{lm}{p}$$
 (2)

in the case of a constant momentum p.

The time-of-flight principle has been known since J.J. Thomson carried out his experiments on ionised particles. However, the first proposal for a mass spectrometer based on this principle is accredited to Stephens (1) whilst Cameron and Eggers (2) provided the first experimental account of such an instrument in 1948. Although the literature reports a number of attempts to improve on the Cameron and Eggers instrument it was not until 1955 that significant advances leading to a commercial instrument were published. The significant innovation was the pulsed operation of the ion source. Katzenstan and Friedland (3) used a pulsed electron beam and an ion push-out pulse, delayed with respect to the timing of the electron pulse, to remove the ion packet from the ionisation zone. However, it was the design of Wiley and McLaren (4), published the same year, which lead to the first successful commercial time-of-flight mass spectrometer marketed firstly by the Bendix Corporation and subsequently by CVC Products Limited (Rochester, New York).

Wiley and McLaren observed that ions of the same m/z ratio would reach the detector with a spread in arrival times (see Fig. 1) due to both spacial distribution at the instance of ionisation and also the initial kinetic energy distribution of the ions. Solution of the former effect is a problem in 'space resolution' and the latter effect 'energy resolution'. Wiley and McLaren devised a pulsed two-grid ion source with dimensions optimised for space and energy resolution.

The basic geometry of the Wiley-McLaren design is shown in Fig.2 together with typical dimensions and electric field strenghts for their instrument. The ion source has two accelerating regions. Whilst ions are being formed, the source backing plate voltage is the same as that of the first grid. At all times the second accelerating region, d, has an electric field E_d whilst the drift tube D is field free. Ions are accelerated out of the source to the detector when a positive pulse is applied to the source backing plate to produce an electric field, E_s . The duration of this pulse is sufficient to remove all the ions from the first field region. The double-field source introduced two new parameters, d and $E_d E_s$, not available to previous single source TOF designs, which not only increased flexibility, but also enabled easier operation, because only a fraction of the total voltage was pulsed, and higher resolution to be obtained. In this system any ion, with an initial energy U_o , will have a total flight time T which is the sum of its flight time through the three consecutive regions, i.e.

$$T = T_s + T_d + T_D \tag{3}$$

For convenience, Wiley and McLaren obtained the following expression for T when $U_o = O$ and the initial position in the ion source is s_o

$$T(O,s) = 1.02 \left(\frac{m}{2U_t}\right)^{1/2} \left(2k_o^{1/2}s_o + \frac{2k_o^{1/2}}{k_o^{1/2}+1}d + D\right)$$
 (4)

TABLE II. Commercially available TOFMS instruments

Manufacturer Type VC Scientific Products Ltd Wiley-McLaren Leybold - Heraeus GmbH LAMMA Cambridge Mass Spectrometry Ltd LIMA (now Kratos Analytical) ²⁵²Cf PDMS Bio-Ion Nordic VG Ionex **TOFMS-SIMS** Bruker - Franzen Analytik GmbH LD-MPI-TOFMS R.H. Jordan Co. LD-MPI-TOFMS Toftec Inc. Velocity compaction "LE-PD-ion beam" S.N. Nermag **TOFMS** LD/TOFMS Kratos Analytical Finnigan MAT LD/TOFMS LD/TOFMS Vestec Corporation Comstock Inc. Various ionisation modes e.g. laser, electron beam.

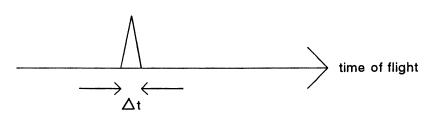


Figure 1. Spread (Δt) in flight times of ions of single m/z ratio.

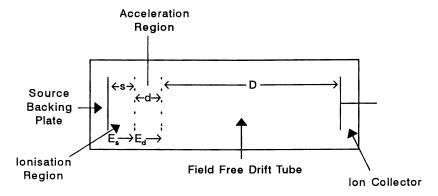


Figure 2. Schematic diagram showing the original Wiley-McLaren 2region ion source design (4). (Typical values: $s_0 = 0.2$ cm; d = 1.2 cm; D =40 cm; $E_s = 320 \text{ V cm}^{-1}$; $E_d = 1280 \text{ V cm}^{-1}$.)

where U_i is the ion velocity in the drift tube and k_o a constant determined by the instrument parameters as given by the following relationship.

$$k_o = \frac{\left(s_o E_s + d E_d\right)}{s_o E_s} \tag{5}$$

This relationship was used as the basis for estimating the space resolution (M_s) and energy resolution (M_{θ}) for typical parameter values of their new instrument. The overall resolution (M_s, θ) was predicted using the relationship

$$\frac{1}{M_{\bullet}\theta} = \frac{1}{M_{\bullet}} + \frac{1}{M_{\bullet}} \tag{6}$$

Typical values were given as $M_s = 400$, $M_\theta = 147$ and thus $M_{s,\phi} = 108$. The Wiley-McLaren paper includes discussion as to their choice of parameters such as ion source dimensions and field strengths and how these influence resolution.

The initial space distribution of the ions results from the physical width of the ionising electron beam, typically 1mm, and from ions formed outside the beam by secondary collisions as well as those that drift between the time that the ions are formed and the start of the draw-out pulse. Wiley and McLaren showed that a space focus condition exists when the height of the draw-out pulse is such that ions formed closest to the draw-out grid are overtaken by those formed the furthest away from that grid just as they reach the detector. The reason for the difference in velocities is that ions formed closest to the draw-out grid fall through a smaller potential gradient than those formed at a greater distance. In this way ions having the greatest distance to travel are accelerated to the largest velocity with those travelling the shortest distance having the lowest velocity.

Energy focusing is required because of variations in velocity are due to ions that have velocity components along the line of flight and against it. One of the ways this excess energy arises is thermal and is approximately 0.09eV in value. Compared to a typical final accelerating voltage of 3000V this energy is quite small and only has a significant effect on the time-of-flight of heavy ions.

Energy focusing was also improved by the introduction of a time-lag between the ionisation pulse and application of the draw-out pulse. Before draw-out those ions with velocities in the direction of flight will move to a position closer to the draw-out grid whilst those with velocities against the direction of flight will take up new positions a greater distance away from the draw-out grid. Hence during the delayed draw-out pulse ions with velocities opposite that of the flight direction will receive greater energy than those with velocities in the direction of flight and the focussing condition, achieved by adjustment of the time-lag and E_d/E_s ratio, occurs when the both types of ions reach the detector together. The time-lag system gives preferred treatment to energy resolution and therefore has the greatest usefulness when dealing with ions containing excess translational energies.

A commercial instrument based on the Wiley-McLaren design was launched by the Bendix Corporation in the late 1950's This was a low resolution instrument, the mass resolution being around 250-300 for organic species and 500 for inorganics. Its advantages were seen as the high scan rate (20 kHz), which gave potential for fast

reaction monitoring, and the very open geometry of the ion source which enabled easy coupling to a wide range of ancillary techniques. The instrument utilised a magnetic electron multiplier with multi-channel time-gated output (4). At the output end of the multiplier, the ion current pulses passed by a series of electronic gates. If a gate electrode was pulsed negative, any passing ion current pulse was diverted into that particular analogue output channel. The negative gating pulse duration was sufficient to collect only signal due to ions of a particular m/z ratio. Mass scanning was achieved by changing the time at which the gate electrode was pulsed during each cycle of the instrument. Alternatively, a number of gates could be set to provide simultaneous multi-ion monitoring. Also, complete individual spectra could be recorded by sending the multiplier output direct to a suitable oscilloscope and photographing the spectra displayed on the screen. The simultaneous multi-ion monitoring was viewed as potentially useful for gas chromatography work and Early reports of the use of this first commercial TOFMS were reaction studies. presented at various mass spectrometry symposia in the U.S.A. and, in particular, at various TOFMS users meetings arranged at the Bendix Corporation headquarters in Cincinnati.

The first European Time-of-Flight Mass Spectrometry Symposium was held at Salford in July 1967. At that time it was claimed that there were 300 TOFMS instruments in use throughout the world with some 50 or so in Europe. proceedings of this symposium were published to provide a TOFMS textbook (5) indicating the then state of development of the instrument and its major applications. A very full account of the Bendix time-of-flight instruments and ancillary techniques is provided by Damoth. The instruments, all based on the Wiley-McLaren design, ranged from the small MA-1 with a 20cm flight path to the large 3015, 1.5m flight path, equipped for both positive and negative ion signal output. The obvious utilisation of the very fast scanning capability of the TOFMS is to monitor very fast chemical reactions such as those initiated by flash photolysis, flash pyrolysis and A major problem in this type of application is the recording of the individual mass spectra generated at a rate of 20kHz. The proceedings contain the first authoritative assessment of this aspect of the TOFMS technique by R.T. Meyer Other areas covered include negative ions, then of relatively minor interest in the mass spectrometry field, ion reactions both in the gas phase and during sputtering from solid surfaces, high temperature (Knudsen Cell) studies and industrial analysis. The latter contribution described the application of a TOFMS as a gas chromatographic detector for the analysis of multicomponent mixtures of glycol ethers and ketones and also direct analysis of atmospheres in sealed containers, plastics and impurities in explosives. A bibliography of some 350 TOFMS publications to March 1968 was also included (7).

A second European Time-of-Flight Mass Spectrometry symposium took place at Salford in July 1969 and the proceedings were published as the first in a new series entitled Dynamic Mass Spectrometry (8). The volume as well as being concerned with general instrumentation, particularly resolution and sensitivity, indicates the main areas of TOFMS application at the end of the decade namely kinetic studies, ionisation processes and analytical work. Of particular interest is an early paper on the use of TOFMS as a selective detector for quantitative gas chromatography (9). This was an area for which its fast scan capability should have given the TOFMS an edge in the subsequent development of the GC/MS technique. In fact, Gohlke (10)

had first reported the use of the time-of-flight instrument for GC/MS in 1959. The opportunity was, however, missed and the quadrupole instrument became the major non-sector mass spectrometer utilised for commercial GC/MS instrument.

Volume 2 of the Dynamic Mass Spectrometry (11) series shows a change in policy to embrace the whole range of dynamic mass spectrometers including commissioned and submitted articles on quadrupole and ion cyclotron resonance as well as time-of-flight mass spectrometers. Some six contributions were concerned with the time-of-flight technique.

Carrico provided a theoretical account of an inhomogeneous oscillatory electric field time-of-flight mass spectrometer. The pre-eminence of time-of-flight mass spectrometry in the field of direct monitoring of fast gas reactions is extensively reviewed by Lippiatt and Price. This application is further emphasised by a report on a study of ammonium perchlorate decomposition. A study of the autodetachment of electrons in sulphur tetra- and hexa-fluoride was reported by Thynne and co-workers. Perhaps the article of most current interest is B.E. Knox's review of laser probe mass spectrometry. This provides an early indication of the potential of this technique and that time-of-flight mass spectrometry would have a major role in its development. The lead role played by the time-of-flight techniques in the various laser/mass spectrometry developments over the past decade proves how justified that prediction was.

The third European Time-of-Flight Mass Spectrometry took place in 1971, the proceedings being published in Volume 3 of the Dynamic Mass Spectrometry Series (12). This contains reviews of inhomogeneous oscillatory electric fields (Carrico) and negative ion studies (Thynne) together with some thirteen application papers. The latter fall into three groups. Five describe the monitoring of reactive intermediates generated by flash photolysis or a shock wave. Vaporisation or gas evolution from surfaces are the subject of a further three papers. The remaining articles deal with various instrumental developments.

In the early '70's Mamyrin and coworkers (13) published the first reports of the mass reflectron. This technique gave an order of magnitude improvement to the resolving power obtainable by the time-of-flight technique which has greatly facilitated the renaissance in time-of-flight mass spectrometry seen since the mid '80's. Figure 3 is a schematic representation as to how the reflectron provides for greatly enhanced energy resolution. The reflectron contains both decelerating and reflecting electric fields. For ions of the same m/z ratio entering these fields, those with higher energy (velocity) penetrate the decelerating field further before reflection than do slower lower energy ions. Consequently, the faster ions have a longer flight path and time through the reflectron than do the slower ions. This effect compensates for the reverse behaviour across the linear flight paths. The appropriate reflectron voltages can be adjusted so that the fast and slow ions reach the detector together, thus optimising energy resolution.

For the next Symposium in 1974 the format was expanded to include the whole field of dynamic mass spectrometry. It also began the long standing collaboration between the author and John Todd (University of Kent) to both organise these international meetings and edit the proceedings. Thus it was intended to provide a forum for the discussion of the current usage and future development of the dynamic mass spectrometric technique. The published proceedings (14) show a significant contribution made by the time-of-flight instrument. Price provided a

survey of its current state whilst Bakker gives a clear account of time-focussing time-of-flight mass spectrometry. In principle ions, of the same m/z ratio and initial velocity v_o , would have the same time-of-flight t_o . In practice this is never so because of differences in the initial velocities of the ions, $v\pm = v_o \pm \Delta v$. Taking into account this initial velocity spread, it can be shown that the time-of-flight of the ions can be expressed

$$t(\nu \pm) = t_o(1 \mp \beta + \beta^2 \mp \beta^3 +)$$
 (7)

where β represents the ratio $\Delta v/v_o$. First order time focussing is concerned with making $t(v\pm)$ independent of β , second order time focussing makes $t(v\pm)$ independent of β and β^2 and so on. Bakker's article is concerned with various approaches utilising static fields to obtain time focussing. Again the monitoring of rapid events was to the fore with reports on flash thermal analysis, electrical discharges through gases, combustion reactions and shock tube studies. Rice and Truby discuss the limiting effect of velocity distributions on such measured reaction rates. Donovan et al. reported continuation of the negative ion studies initiated by Thynne, whilst Piacente and Balducci presented dissociation energy data for indium phosphide and aluminium arsenide.

The 1977 Symposium (15) showed a marked decline of interest in time-of-flight mass spectrometry, only four papers on this topic being contributed. All were concerned with reaction studies. The fast reaction capability was utilised for work concerned with detonation reactions and also the kinetics of chlorine atom reactions initiated by the flash photolysis. The latter technique was also applied to aromatic molecules. Johnston described a novel Knudsen cell used to investigate high temperature systems. Also reported was the development of a Mass Thermal Analysis experiment which follows the course of a solid decomposition by monitoring the evolved gas as the temperature is ramped at a linear rate. This technique has the advantage over similar data obtained by thermogravimetric analysis in that the evolved products are directly identified by their mass spectra. This was illustrated by studies of the calcium oxalate and barium nitrate decompositions.

The mid-'70's brought the first announcement by Macfarlane and his co-workers (16) of the detection of ions of mass up to 5 kDa, then considered as the high mass region. Such ions resulted from bombardment of surface films with pulsed 100 MeV fission fragments from the radioactive decay of ²⁵²Cf, a technique now termed plasma desorption mass spectrometry (PDMS). The TOFMS was the ideal mass spectrometer for this application since it was the only instrument capable of providing the required mass analysis per ionisation event. The '80's were also to see various application of pulsed laser ionisation also benefit from this particular feature of the TOFMS. It was these innovations coupled to the improvement in resolution made available by Mamyrin's reflectron which lead to the current renaissance in time-of-flight mass spectrometry.

The last in the Dynamic Mass Spectrometry series (17) contains the proceedings of the 1980 meeting held at Canterbury, Kent. Compared to 1977, the time-of-flight technique made an increased contribution to the Symposium. A new time-focussing variation was described by Bakker et al. whilst Lincoln providing a detailed account of the use of a transient recorder to acquire data from laser

vaporisation studies. Application to study pulsed surface ionisation was reported by Olsson and co-workers. Further papers were concerned with various novel 'mass thermal analysis' inlets, process monitoring and control, together with kinetic studies of tungsten/halogen/oxygen systems, polymer degradations and flash photolysed aromatic systems. The versatility of the time-of-flight instrument was well illustrated in its use as an automated mass spectrometer for an underground coal gasification field test (Crawford et al.).

As indicated earlier by the reference to the review by Knox (18), analysis of solids and/or of surfaces by pulsed laser ionisation had for some time been an active area of academic research. In 1978, Leybold Heraeus made the first LAMMA instrument commercially available. This was a laser microprobe operating in the transmission mode for the analysis of thin films as sections. Subsequent developments incorporated a reflection as well as a transmission mode of laser-sample interaction together with a Mamyrin-type reflectron to provide the required resolving power for time-of-flight mass analysis. This was necessary because of the wide energy spread of the ions ejected from the sample by the high energy laser pulse. A rival instrument, the LIMA, was marketed by Mass Spectrometry Ltd., U.K. Clarke (19) provides a very readable account of this development of laser microprobe mass spectrometry.

The last years of the '70's and early '80's marked a turning point in the fortunes of the time-of-flight instrument with the emphasis moving away from the pulsed Wiley-McLaren design to new instruments based on new pulsed ionisation techniques such as plasma and laser desorption/ionisation which required high sensitivity and full spectrum analysis per ionisation event. The time-of-flight instrument is uniquely advantaged in this respect. Also, improvements in mass resolution offered by Mamyrin's reflectron were being used increasingly. updated review by Price and Milnes (20) published in the proceedings of the 1983 Symposium (21) reflect this trend. A high resolution (4000) instrument for multiphoton ionisation studies was described by Neusser et al. whilst Guest reported on developments of laser microprobe mass analysers (LAMMA instruments). Continued use for reaction studies was illustrated by work concerned with flash photolysis of isoxazole and the investigation of fire-retardant systems. discussed techniques for avoiding discrimination errors in the dynamic sampling of condensible vapours.

Another surface analysis technique, to which the time-of-flight technique was beginning to make a significant contribution, was that of secondary ion mass spectrometry (SIMS). For the analysis of secondary ions ejected from solid samples, the TOFMS has advantages over the quadrupole instrument which had previously been the major instrument used for this application. These are the greater than 100-fold increase in sensitivity, low mass-discrimination, simultaneous detection of the whole mass spectrum and the ability to function with pulsed ionisation. The latter is particularly desirable in the case of non-conducting materials such as polymers and ceramics in order to reduce or even eliminate surface charge build-up which can be a major hindrance to successful SIMS work. The SIMS/TOF technique has been pioneered by the Benninghoven groups at Munster (22) and that of Standing at Manitoba (23). It was when Benninghoven pointed out that because of its mode of operation the TOFMS was a very sensitive instrument for pulsed SIMS work, that the mass spectrometry community began to re-assess its previous view that the

TOFMS was a low sensitivity, low resolution instrument. The initial Benninghoven instrument incorporated energy compensation, based on calculations by Poschenrieder (24), to provide improved resolution for the time-of-flight analysis. The Manitoba instrument utilised a reflectron.

The 1986 Dynamic Mass Spectrometry Symposium was held at Canterbury. Roughly 50% of the programme was devoted to the time-of-flight instrument indicating the rapid developments which were to take place in the latter half of the Price and Milnes reviewed the current state of the art as a prelude to a number of papers describing particular applications. A commercial SIMS/TOF, of similar design to that of Benninghoven, was described by Waugh and Kingdom (25). Current improvements to the design of the LIMA laser microprobe instrument were reported by Mullock. The development by Bruker-Franzen Analytik GmbH of a commercial laser (IR) desorption/laser multiphoton ionisation/high resolution time-of-flight mass spectrometer was reported by Frey. The instrument had a resolution of 6000 at m/z 96. Only molecular ions were produced in the soft ionisation mode whilst increasing the ionisation laser power density resulted in hard ionisation yielding a fragmentation pattern for structure analysis. Cotter described the advantages of utilising a Wiley-McLaren source, with the draw-out field and time-lag focussing used to correct for spatial and energy distribution of the ions, for improving focussing in laser desorption and liquid SIMS experiments. In both cases metastable decomposition in the accelerating field can cause loss of resolution. further contribution was concerned with the Bio-Ion Nordic plasma desorption time-of-flight mass spectrometer whilst Blanchard discussed experimental and computer simulated data pertinent to the use of nonlinear fields for ion mobility Application of time-of-flight mass spectrometry to study chemical reactions was the subject of two contributions from the Salford group. extremely fast scan capability enabled studies of the time dependent behaviour of the major products evolved when various PVC composites were subjected to pulsed laser The ease of access offered by open ion source geometry enabled the development of a line of sight batch inlet system for the analysis of air sensitive, condensible compounds. Data obtained for a kinetic study of the decomposition of tungsten dioxide dichloride was reported. Proceedings of this symposium were not formally published although various articles on the papers presented have appeared in the literature (26,27).

The latest International Dynamic Mass Spectrometry Meeting, the 9th, took place in Salford in July 1989. In the opening session Price emphasised that the current resurgence in the time-of-flight technique was due to its ability to provide a complete mass spectrum per event and high mass capability. These are particularly advantageous in the areas of new ionisation techniques such as plasma and laser desorption which were at the forefront of mass spectrometry developments. A volume-optimised TOF-mass spectrometer utilising a multiple-reflection technique for resonance ionisation mass spectrometry (RIMS) studies on xenon was described by Schneider. An account of the use of RIMS for depth profiling in semiconductor devices was provided by McLean and Clarke. Thompson, Mullock and Dingle described a combined laser microprobe (LIMA) and low-dose static SIMS instrument which permits both bulk and near-surface materials analysis. The original interest in the TOF-instrument was as a monitor for very fast reactions. As stated previously, this was handicapped by the problems in recording the temporal behaviour of the

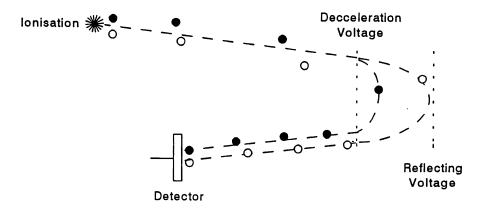


Figure 3. Schematic of the principle of Reflectron (o fast ion; • slow ion)

individual mass spectra obtained from very rapidly changing chemical systems. Lincoln showed that the advent of modern high-speed electronic systems has largely solved this problem.

A collection of some of the papers presented at this symposium have been published (28). These include a time-of-flight-mass spectrometry review (26) based on the talks given at both the 1986 and 1989 Meetings and also Lincoln's paper on fast data recording (29). An account of the Salford and NASA studies of fast reactions has also appeared (30).

At the start of the '90's, the time-of-flight instrument is at the cutting-edge of mass spectrometry development. This is because many of its advantages (Table III) make it the best choice of mass analysers for pulsed ionisation techniques such as plasma and laser desorption which promise so much because of their potential to provide valuable information concerning large molecules of biological and medical interest. Surface analysis is another area of increasing application whilst efforts are being made to utilise its very fast scanning capability to provide better monitoring of gas and liquid chromatographic column elutions.

It was when time-of-flight mass spectrometry was used to show that laser desorption could produce ions of mass 200 kDa (31) that the instrument came to the forefront of mass spectrometrists' attention. Currently, the main limitation on the accessible mass range is the efficiency of ion production and the sensitivity for their detection. In both areas the time-of-flight instrument has characteristic advantages which have lead to it playing the lead role in the development of the plasma desorption technique by Macfarlane and others and, more recently, laser desorption by Hillenkamp. The importance of both techniques has lead to the marketing of commercial instruments, Table II.

TABLE III. Advantages of the TOFMS

- Ideal where ionisation is pulsed or spatially confined.
- High initial energy spread of ions is admissible up to hundreds of eV.
- · Complete mass spectrum for each ionisation event.
- High transmission.
- Spectra can be obtained for extremely small samples, approaching 10-18 mole.
- High precision for ion concentration ratio measurements, same conditions for all ions in both analyser and detection system.
- Fastest scanning mass spectrometer with repetition rates of up to 100 kHz.
- · Unlimited mass range.
- Performance dependent on rise times and stability of electronic circuitry rather than mechanical alignment.
- · Relatively low cost.

Another important area in which the TOFMS is beginning to appear is that of Tandem Mass Spectrometry. The first successful attempt in this direction was by Stults et al. (32) who developed a TRIMS technique, time-resolved ion momentum Glish and Goeringer (33) have developed a quadrupole/TOFMS instrument in which the quadrupole is used to select the required precursor. TOFMS is then used to provide complete spectral analysis of the product ions generated in the collision cell. One important advantage is that this Q/T approach is sufficiently rapid to enable MS/MS analysis of limited quantities of sample or rapidly changing sample input as, for example, would be the case for chromatographic eluent monitoring. A tandem TOF/TOF mass spectrometer for studying polyatomic ion/surface collisions has been reported by Cooks et al. (34). A feature of this equipment is that the range of collision energies extends above 300eV. Internal energies as high as 30eV can be deposited in selected ions, thus facilitating controlled fragmentation and hence structural analysis. More recently a tandem instrument has been constructed with two linear TOF instruments and using fast atom bombardment for ionisation (35). Collision induced decomposition mass spectra have been obtained. With refinement, this approach has the potential to provide collision-induced decomposition spectra of all the components of a single complex mixture in a single experiment.

Despite its fast scanning capability, time-of-flight mass spectrometry has not played a lead role in the development of the GC/MS technique. Two problems inhibited such a role. Firstly, a resolving power better than 1000 for electron bombardment and, if possible, chemical ionisation, is required. Secondly, a data handling system for the vast amount of data generated in short time periods is

essential. Improvements in instrument design are beginning to solve the first requirement, and developments in high speed electronic circuitry and memory devices the second. The most promising approach to date, is that of Enke and his co-workers at Michigan State University (36) and will be discussed in detail later in this book. The coupling of a liquid chromatographic column via a continuous-flow interface to his liquid-SIMS/TOFMS system has been described by Cotter (37). An off-line sampling approach has been utilised by the Standing group in Manitoba (38). A review of enhancement of selectivity by coupling gas chromatography with wavelength selective multiphoton ionisation has been provided by Lubman (39).

The current increasing interest in the TOFMS is mainly due to its unique features which make it the ideal mass spectrometer for new ionisation techniques such as plasma and laser desorption. However, establishment in the more conventional sector of the market requires an instrument using simple and inexpensive electron bombardment with good sensitivity and resolving powers of several thousand. This author is optimistic that this will be achieved in the near future. Already Wollnik and co-workers (40) have reported resolving powers in the region of 20,000 for the tris (pentadecafluoroheptyl)-1,2,5,-triazine ions at 866 and 867. This work utilised a TOFMS designed for the analysis of ions with angle - and energy - spread as produced in a continuous electron bombardment source. Efforts are still being made to improve the resolving power of the conventional commercial Wiley-McLaren instrument. Sanzone et al. (41) have proposed an impulse field focussing technique whilst Enke's group (42) have considered various models for mass-independent space and energy focussing. Muga (43) has developed a commercial instrument based on a 'velocity compaction' technique in which a time-dependent acceleration voltage is used to compensate for the translational energy spread of ions ejected from a Wiley-McLaren ion source.

Literature Cited

- (1) Stephens, W.E., Phys. Rev., 1946, 69, 691.
- (2) Cameron, A.E. and Eggers, D.F., Rev. Sci. Instr., 1948, 19, 605.
- (3) Katzenstein, H.S. and Friedland, S.S., Rev. Sci. Instr., 1955, 26, 324.
- (4) Wiley, W.C. and McLaren, I.H., Rev. Sci. Instr., 1955, 26, 1150.
- (5) Time-of-Flight Mass Spectrometry, Price, D. and Williams, J.E., Eds., Pergamon Press, Oxford, England, 1969.
- (6) Meyer, R.T. in *Time-of-Flight Mass Spectrometry*; Editors D. Price and J.E. Williams, Pergamon Press: Oxford, England, 1969; pp. 61-87.
- (7) Joy, J.W.K.in *Time-of-Flight Mass Spectrometry*; Editors D. Price and J.E. Williams, Pergamon Press: Oxford, England, 1969; pp. 247-260.
- (8) Dynamic Mass Spectrometry, Price, D., Williams, J.E., Ed., Heyden & Son Ltd.: London, England, 1970, Vol. 1.
- (9) D. 'Oyly-Watkins, C, Hillman, D.E. Winsor, D.E., Ardrey, R.E., In Dynamic Mass Spectrometry, Price, D., Williams, J.E., Eds. Heyden & Son Ltd.: London, England, 1970, Vol. 1, pp. 163-174.
- (10) Gohlke, R.S., Anal. Chem., 1959, 31, 535.
- (11) Dynamic Mass Spectrometry, Price, D. Ed., Heyden & Son Ltd.: London, England, 1971, Vol. 2.

- (12) Dynamic Mass Spectrometry, Price, D. Ed., Heyden & Son Ltd.: London, England, 1972, Vol. 3.
- (13) Mamyrin, B.A., Karataev, V.I., Shmikk, D.V. and Zagulin, V.A., Soviet Phys., *JEPT*, 1973, 37, 45.
- (14) Dynamic Mass Spectrometry, Price, D., Todd, J.F.J., Eds., Heyden & Son Ltd.: London, England, 1976. Vol. 4.
- (15) Dynamic Mass Spectrometry, Price, D., Todd, J.F.J., Eds., Heyden & Son Ltd.: London, England, 1978, Vol. 5.
- (16) Mcfarlane, R.D. and Torgerson, D.F., Int. J. Mass Spectrom. Ion Phys., 1976, 21, 81.
- (17) Dynamic Mass Spectrometry, Price, D., Todd, J.F.J., Eds., Heyden & Son Ltd.: London, England, 1981, Vol. 6.
- (18) Knox, B.E., in *Dynamic Mass Spectrometry*, Price, D., Ed., Heyden & Son Ltd. London, England, 1971, Vol. 2, pp. 61-96.
- (19) Clarke, N.S., Chem. Brit., 1989, 484.
- (20) Price, D., Milnes, G.J., Int. J. Mass Spectrom, Ion Proc., 1984, 60, 61-81.
- (21) Price, D., Todd, J.F.J., Eds., Int. J. Mass Spectrom. Ion Proc., 1984, 60, 1-311.
- (22) Niehuis, E., Heller, T., Feld, H. and Benninghoven, A., J. Vac. Sci. Technol., 1987, A5, 1243.
- (23) Standing, K.G., Beavis, R., Ens, W., Tang, X. and Westmore, J.B., in *The Analysis of Peptides and Proteins by Mass Spectrometry*, NcNeal, C.J., Ed., Wiley, Chichester, England, 1988, pp. 267-278.
- (24) Poschenrieder, W.P., Int. J. Mass. Spectrom. Ion Phys., 1972, 9, 357.
- (25) Waugh, A.R., Kingham, D.R., Richardson, G.H. and Goff, N., *J. Phys. (Paris) Colloq.*, 1987, 48, C6-575.
- (26) Price, D., Milnes, G.J., Int. J. Mass Spectrom. Ion. Proc., 1990, 99, 88881-39.
- (27) Upton, J.R., Price, D., Pilkington, R.D., Sutcliffe, H., Int. J. Mass Spectrom. Ion. Proc., 1990, 96, 233-242.
- (28) Price, D., Ed. Int. J. Mass Spectrom. Ion Proc., 1990, 90, 1-167.
- (29) Lincoln, K.A., Int. J. Mass Spectrom. Ion Proc., 1990, 90, 41-51.
- (30) Price, D., Lincoln, K.A. and Milnes, G.J., Int. J. Mass Spectrom. Ion Proc., 1990, 100, 77-92.
- (31) Karas, M., Bahr, U., Ingendoh, A. and Hillenkamp, F., Agnew Chem. Int. Ed. Engl., 1989, 28, 760.
- (32) Stults, J.T., Holland, J.F., Watson, J.T. and C.G. Enke, *Int. J. Mass Spectrom*. *Ion Proc.*, **1986**, *169*; and also Eckenrode, B.A., Watson, J.T. and Holland, J.F.; loc. cit., **1988**, *83*, 177.
- (33) Gish, G.L. and Goeringer, D.E., Anal. Chem., 1984, 56, 2291.
- (34) Schey, K., Cooks, R.G., Grix, R. and Wollnik, H., Int. J. Mass Spectrom. Ion Proc., 1987, 77, 49.
- (35) Jardine, D.R., Morgan, J., Alderdice, D.S. and Derrick, P.J., *Org. Mass Spectrom.*, 1992, 27, 1077-83.
- (36) Erikson, E.D., Enke, C.G., Holland, J.F. and Watson, J.T., Anal. Chem., 1990, 62, 1079.
- (37) Chen, K.H. and Cotter, R.J., Rapid. Comm. Mass Spectrom., 1988, 2, 237.
- (38) Beavis, R.C. Ens, W., Main, D.E. and Standing, K.G., Anal. Chem., 1990, 62, 1259.
- (39) Lubman, D., Mass Spectrom. Rev., 1988, 7, 535 and 559.

- (40) Grix, R., Kutscher, R., Li, G., Gruner, U. and Wollnik, H., Rapid Comm. Mass Spectrom., 1988, 2, 83.
- (41) Browder, J.A., Miller, R.L., Thomas, N.A. and Sanzone, G., Int. J. Mass Spectrom. Ion Phys., 1981, 37, 99.
- (42) Yefchak, G.E., Enke, C.G. and Holland, J.F., Int. J. Mass Spectrom. Ion. Proc., 1989, 87, 313.
- (43) Muga, M.L., Anal. Instrum., 1987, 16, 31.
- (44) Wolff, M.M. and Stephens, W.E., Rev. Sci. Instru., 1953, 24, 616.
- (45) Harrington, D.B. in the Encyclopedia of Spectroscopy, Clark, G.L., Ed. Reinhold Publishing, New York, U.S.A., 1960.
- (46) McFadden, W.H., Teranishi, R., Black, D.R. and Day, J.C., J. Food Sci., 1963, 28, 316.
- (47) Knox, B.E. and Vastola, F.J., Chem. Eng. News, 1966, 44 (No.44), 48.

RECEIVED September 16, 1993

Chapter 2

Time-of-Flight Mass Spectrometry

Basic Principles and Current State

Robert J. Cotter

Department of Pharmacology and Molecular Sciences, Middle Atlantic Mass Spectrometry Laboratory, The Johns Hopkins University School of Medicine, Baltimore, MD 21205

Since time-of-flight mass spectrometers were first introduced, there has been the need to improve mass resolution, which depends largely upon the initial conditions of the ions at the time they are formed. For larger ions, metastable fragmentation presents an even more serious challenge, although such processes may be utilized to obtain product ion mass spectra in instruments equipped with a reflecting field. Initial conditions and internal energy are all determined during the ionization process, so that ion extraction, focusing, detection, recording and other aspects of time-of-flight analyzer design must be suited to the ionization method used. Thus, this chapter presents the basic principles governing time-of-flight mass measurement and resolution, describes the role of reflectrons and other energy focusing devices, and reviews several unique time-of-flight configurations that have been, or are currently being, used.

An attractive feature of the time-of-flight mass spectrometer is its simple design (Figure 1a). Ions are formed in a short *source* region (s), defined generally by a backing plate and an extraction grid. A positive voltage (V) placed on the backing plate imposes an electric field (E = V/s) across the source region, which accelerates all of the ions to the same kinetic energy:

$$\frac{mv^2}{2} - zeEs$$
 [1]

where m = the mass of the ion, v = its velocity, e = the charge on an electron, and z = number of charges. As the ions pass through the extraction grid they will have velocities which depend inversely upon the square root of their mass:

$$v = \left[\frac{2zeEs}{m}\right]^{1/2}$$
 [2]

0097-6156/94/0549-0016\$09.25/0 © 1994 American Chemical Society The ions then pass through a much longer drift region (D). Because they spend most of their time in this region, their time-of-flight measured at the detector is approximately:

$$t = \left[\frac{m}{2zeEs}\right]^{1/2}D\tag{3}$$

Typically, the source distance (s) is of the order of 0.5 cm, while drift lengths (D) ranging from 15 cm to 8 meters have been utilized. Accelerating voltages (V) generally range from 3kV to 30kV, and flight times are of the order of 5 to 100 microseconds.

Mass Calibration, Mass Measurement Accuracy and Mass Resolution

The time-of-flight spectrum can be converted directly to a mass spectrum using known values of the accelerating voltage and drift length:

$$\frac{m}{z} - 2eEs \left[\frac{t}{D}\right]^2$$
 [4]

In practice, however, one measures the flight times of ions of at least two known masses, and determines the constants a and b in the empirical equation:

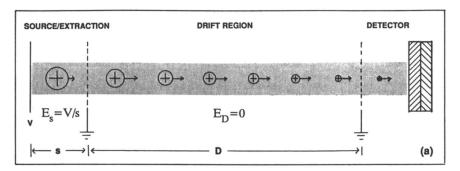
$$\frac{m}{z} = at^2 + b$$
 [5]

as a means for calibrating the mass spectrum and determining unknown masses. As shown in the plasma desorption mass spectrum of the peptide *RDASSDEE* (Figure 1b), the mass calibration peaks (in this case H⁺ and Na⁺) are generally obtained from the low mass region of the same spectrum.

In a simple *linear* time-of-flight mass spectrometer, mass resolution is generally of the order of one part in 300 to 400. Thus, the calibration peaks and low mass ions in the plasma desorption mass spectrum (Figure 1b) are resolved, while the protonated molecular ion for the peptide is not. The peak at m/z 1037.1 corresponds to the average mass of the unresolved isotopic cluster of species containing one or several ¹³C, ²H, ¹⁵N, ¹⁸O and ³⁴S atoms. Mass accuracy in this mass range is generally 0.1% or better, so that the isotopically averaged mass can be determined within 1 dalton.

Time, Space and Kinetic Energy Distributions

In 1955, W.C. Wiley and I.H. McLaren (1) reported the design for a pulsed *electron* impact (EI) ionization time-of-flight mass spectrometer that was successfully commercialized by the Bendix Corporation and continues to be available from CVC Products (Rochester, NY). In that report, they describe the effects of uncertainties in the time of ion formation, location in the extraction field and initial kinetic energy on



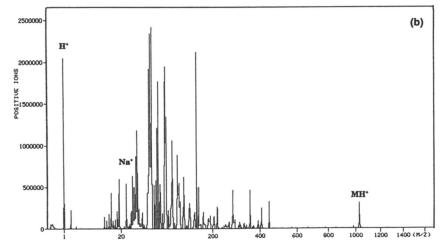


Figure 1. (a) Basic components of the linear TOF mass spectrometer. (b) PD mass spectrum of the endoproteinase Glu-C peptide RDASSDEEE from the assembly protein obtained from simian cytomegalovirus, showing the H⁺ and Na⁺ peaks used to calibrate the mass scale. (Reprinted with permission from Reference 4).

mass resolution. More recently, Riley et al. (2) have analyzed the effects of these initial temporal, spatial and kinetic energy distributions on mass resolution for *multiphoton ionization (MPI)* instruments where the temporal distribution (using a pulsed laser) is considerably narrower than the electron beam case.

Temporal Distribution. The effects of initial conditions of the ion on mass resolution can be described using Figure 2. In Figure 2a, two ions of the same mass that are formed at different times, but have the same kinetic energy, will traverse the drift region maintaining a constant difference in time and space. Because mass resolution on the time-of-flight mass spectrometer is given by:

$$\frac{\Delta m}{m} = \frac{2\Delta t}{t} \tag{6}$$

and the time interval (Δt) is constant, mass resolution can be improved by increasing the flight time (t), that is by using low accelerating voltages and/or long drift lengths. In the Wiley and McLaren instrument, the electron beam pulses used for ionization were of the order of 0.5 to 5 microseconds, necessitating the use of pulsed ion extraction to reduce Δt . In contrast, ionization by plasma desorption occurs in less than 10^{-9} seconds, while multiphoton ionization or laser desorption instruments generally employ lasers with pulse widths from 300 ps to 10 ns. In such cases, the width of Δt may be limited by the detector response and/or the time-to-digital or transient recorder (see below), rather than by uncertainties in the time of ion formation. In addition, if there were no contributions from spatial and/or initial kinetic energy distributions, equation [6] predicts that mass resolution will increase with increasing mass, since Δt will remain constant while t will increase with mass.

Spatial Distribution. When ions of the same mass are formed at the same time with the same initial kinetic energy, but are formed in different locations in the extraction field (Figure 2b), the ions formed near the back of the source will be accelerated to higher kinetic energy than ions formed closer to the extraction grid. The ions formed at the rear of the source enter the drift region later, but have larger velocities so that they eventually pass the ions formed closer to the extraction grid and arrive at the detector sooner. It is possible to adjust the extraction field so that ions of any given mass arrive at a space focus plane, located at a distance (2s) from the source, at the same time. The location of the space focus plane is independent of mass; however, ions of different masses arrive at this plane at different times.

Space focusing is generally achieved using low extraction voltages, while initial kinetic energy focusing (see below) demands the use of high extraction voltages. Thus, one approach to focusing is the use of two-stage extraction, where the larger extraction field is located at the space focus plane, which now acts as a virtual source of ions with a distribution of kinetic energies. For desorption techniques, in which ions are formed at a surface rather than in the gas phase, the spatial distribution is greatly minimized.

Initial Kinetic Energy Distribution. Ions formed with different initial kinetic energies (Figure 2c) will have different final velocities after acceleration and arrive at the detector at different times. This is the most difficult initial condition to correct

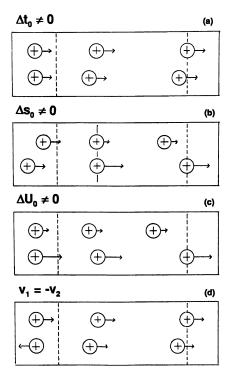


Figure 2. Effects of initial time, space and kinetic energy distributions on mass resolution. (a) Two ions formed at different times. (b) Two ions formed at different locations in the ion extraction field. (c) Two ions formed with different kinetic energies. (d) Two ions with the same initial kinetic energy that have initial velocities in opposite directions. (Reprinted with permission from reference 4).

in a linear instrument, since increases in drift length increase peak widths along with the separation of peaks of different mass. Thus (as described below) reflectrons and other energy-focusing devices are used in the mass analyzer to compensate for differences in kinetic energy in the source. When ions are formed in the gas phase, the initial kinetic energy distribution also includes ions with the same kinetic energy, but with their velocities in different directions (Figure 2d). These ions will be accelerated to the same final kinetic energy (and velocity), but will arrive at the detector at different times corresponding to their turn-around time in the source. This effect is minimized using longer flight distances.

Using an approach similar to that described by Wiley and McLaren (1), it is possible to derive an equation for the arrival time of an ion formed at time (t_0) :

$$t = t_s + t_D + t_0 \tag{7}$$

(where t_s = time in the source and t_D = time in the drift region), that reflects the initial temporal, spatial and kinetic energy conditions (3,4):

$$t = \frac{(2m)^{1/2}}{eE} [(U_0 + eEs_0)^{1/2} \mp U_0^{1/2}] + \frac{(2m)^{1/2}D}{2(U_0 + eEs_0)^{1/2}} + t_0$$
 [8]

The quantity: $(U_0 + eEs_0)$ is the final kinetic energy of an ion having an initial kinetic energy (U_0) and accelerated from an initial position (s_0) in the source. In the first term, this same kinetic energy is reached upon exiting the source regardless of the initial direction of the ion's velocity, while the time spent in the source reflects the turnaround time $(\mp U_0^{I/2})$. In the second term, the time spent in the drift region depends again upon the initial position (s_0) and kinetic energy (U_0) in the source, but not upon the initial direction of velocity. Thus, longer drift lengths (D) increase the magnitude of t_D , and decrease the effects of turn-around time as well as uncertainties in the time of ion formation (t_0) . In addition, large extraction voltages (V=Es) minimize the effects of initial kinetic energy.

Approaches to Improving Mass Resolution

In any mass spectrometer, mass resolution is determined by the peak widths for a given mass, relative to the separation of peaks of different mass. In the time-of-flight mass spectrometer, peak widths (Δt) are determined by uncertainties in the temporal, spatial and initial kinetic energy distributions, and can be determined by differentiating equation [8] with respect to Δt_0 , Δs_0 and ΔU_0 . In practice, mass resolution is achieved using a combination of three approaches: 1) elimination or minimization of the initial distribution, 2) correction of the initial distribution during ion extraction from the source, and 3) compensation of the effects of the initial distribution in the mass analyzer. Thus (for example) we have noted that ionization by pulsed lasers minimize the uncertainties in the time of ion formation. If the ions are formed from a smooth conducting surface parallel to the extraction grid, the spatial distribution is also minimized, so that the remaining initial kinetic energy distribution can be corrected by high extraction voltages and compensated by a reflectron located in the mass analyzer. Alternatively, initial kinetic energy

distributions can be minimized by collisional cooling (5), or by extracting ions orthogonal to the desorption direction (6).

Below we contrast two approaches. In the first the initial conditions for ions formed in the gas phase are compensated by a pulsed extraction technique known as time-lag focusing. In the second (which is more typical for current instruments utilizing plasma desorption or laser desorption ionization), temporal and spatial distributions are minimized by rapid desorption from surfaces, while initial kinetic energies are compensated by high voltage extraction and/or corrected by a reflectron.

Time Lag Focusing: Ions Formed in the Gas Phase. In their 1955 report, Wiley and McLaren (1) described a method for improving the mass resolution for ions formed in the gas phase by relatively broad (0.5 to 5 µs) pulses from an electron beam. Their method, known as time-lag focusing, was intended to compensate for the initial time, space and energy distributions using delayed, low voltage, pulsed ion extraction. The ions were actually formed in a field-free ion source, and extracted by a fast (10 ns rise time) drawout pulse to provide time correction. Thus, the time-offlight was measured as the time after application of the drawout pulse, rather than the ionization pulse. The drawout pulse was of the order of -150V to provide space focusing, while the ions were accelerated to final energies of 3keV using multiple stage extraction. Initial kinetic energy focusing was accomplished by delaying the drawout pulse for up to 10 µs after the ionization pulse. During that time, ions with initial velocities along the time-of-flight axis drift toward the front or back of the source. When the drawout pulse is applied, ions with velocities in the forward direction are accelerated less than those with velocities in the reverse direction, so that all ions (of a given mass) reach the detector at the same time.

While time-lag focusing provided correction for the initial kinetic energy spread, the optimal length of the time delay is (unfortunately) mass dependent. The Wiley-McLaren instrument used a *boxcar* method for recording mass spectra from repetitive (10 kHz) ionization cycles, so that the length of the time delay was simply increased in successive cycles. While suitable for the boxcar approach, time-lag focusing is not practical for current instruments, which utilize time-to-digital converters or transient digitizers to record all ions (of all masses) in each time-of-flight cycle.

At the same time, many aspects of the Wiley-McLaren scheme to focus ions formed in the gas phase are now being revisited. In our laboratory, time-delayed pulsed ion extraction has been utilized to focus ions formed off-axis by infrared laser desorption (7), to observe metastable fragmentation (8), and to permit the use of broad pulse primary ion beams with a liquid matrix (9), approximating the conditions of fast atom bombardment or dynamic SIMS. The latter can be used with a continuous flow probe interface connected to a high performance liquid chromatograph (10). In this case, the fast extraction pulse provides temporal focusing, while the low voltage, multiple stage extraction provides space focusing for ions formed from a liquid matrix. More importantly, initial formation of the ions in a field-free ion source provides a crude trapping device, since ions of relatively high mass will drift very slowly from the extraction volume. For ions of m/z 1000, formed at thermal energies, the source half-life is of the order of 6 microseconds (11). Thus, ionization pulses of 10 µs are practical and, if the cycle time is 10 kHz, provide a considerable increase in duty cycle. More elaborate trapping methods have been described by Wollnik et

al (12) using an electrostatic potential well, and by Lubman and co-workers (13) using a quadrupole ion trap. Both schemes are again intended to raise the duty cycle and, thereby, the sensitivity.

Ions Desorbed from Surfaces. Most modern time-of-flight instruments minimize the temporal and spatial distributions by desorbing ions from an equipotential surface using a pulsed laser, MeV particles or a pulsed KeV primary ion beam. Such instruments are much simpler, since they utilize static (rather than pulsed) extraction fields. There is no uncertainty in s_0 , and all ions gain the same energy (eV) from acceleration. Thus, equation [8] can be rewritten as:

$$t = \frac{(2m)^{1/2}[(U_0 + eV)^{1/2} \mp U_0^{1/2}]}{eV} + \frac{(2m)^{1/2}D}{2(U_0 + eV)^{1/2}}$$
 [9]

If the drift length (D) is much larger than the source, then the flight time is approximately:

$$t - \frac{(2m)^{1/2}D}{2(U_0 + eV)^{1/2}}$$
 [10]

for an ion with an initial kinetic energy of U_0 . If one compares this flight time with that of an ion having zero initial kinetic energy:

$$t' = \frac{(2m)^{1/2}D}{2(eV)^{1/2}}$$
 [11]

the difference in arrival times (Δt) due to initial kinetic energy spread is then:

$$\Delta t = \left(\frac{m}{2}\right)^{1/2} \left[\frac{1}{(eV)^{1/2}} - \frac{1}{(eV + U_o)^{1/2}}\right] D$$
 [12]

and the mass resolution is given by:

$$\frac{\Delta m}{m} - 2 \left[\frac{(eV + U_0)^{1/2} - (eV)^{1/2}}{(eV)^{1/2}} \right]$$
 [13]

which can be simplified to:

$$\frac{\Delta m}{m} \cong 2 \left[\left(1 + \frac{U_0}{eV} \right)^{1/2} - 1 \right]$$
 [14]

leading to the approximate relationship:

$$\frac{\Delta m}{m} \cong \frac{U_0}{eV}$$
 [15]

Thus, if the drift length is long with respect to the source region, equation [15] suggests that mass resolution is independent of both mass and drift length. In addition, it also suggests that desorption of ions with an energy spread of 1 eV that are extracted from a 10kV source should yield a mass resolution of one part in 10,000! Such results are not observed in linear instruments.

Practical Mass Resolution Limitations for Linear Instruments

The inability to observe mass resolutions of the order predicted by equation [15] can be attributed in part to practical limitations in the design of time-of-flight instruments. Many of these limitations continue to be minimized by improvements in detector and ion recording technology. Other limitations, primarily those due to initial kinetic energy spread and metastable fragmentation, arise from the ionization process itself.

Uncertainties in Initial Time and Position of Ion Formation. Stability of the high voltage power supplies used for ion acceleration, detector response, jitter (in triggering transient recorders) and digitizer rate will set lower limits to the peak widths that can be recorded. In addition, irregularities of the sample surface and irregular fields in the region of extraction grid wires, while not increasing the energy spread, will result in different path lengths and times for ions to exit the ion source. In our laboratory, we have utilized very smooth surfaces, a 600 ps pulsed nitrogen laser, a detector with 1.2 ns response time and 1 Gsample/s (1 ns time resolution) transient recording to obtain peak widths as low as 4.0 ns and mass resolution as high as one part in 1528 on a short (21 cm) linear instrument (Cornish, T.J.; Cotter, R.J., unpublished).

Because samples have a finite thickness, ions are desorbed at slightly different locations in the extraction field and are thereby accelerated to different final energies. When high extraction fields are used, this may correspond to several volts. This spatial uncertainty may be particularly acute for ions desorbed from the non-conducting nitrocellulose layer commonly used in plasma desorption mass spectrometry (14,15). Because uncertainties in s_0 are all effectively converted to distributions in the final kinetic energy, they can be corrected by a reflectron or other energy focusing device in the analyser. However, they limit the mass resolution in linear instruments, which are the most commonly used.

In addition, ions may be formed above the surface at times later than the ionizing pulse, contributing to uncertainties in both s_0 and t_0 . This may be particularly true of even electron species (MH⁺ and MNa⁺ ions) that are likely to be formed in the gas phase by secondary (ion molecule) reactions, and may account for the common observation that mass resolution is better for inorganic (atomic) ions than for organics. Recently, time delay experiments by Hillenkamp et al. (16) suggest that ionization can occur several nanoseconds after the laser pulse in MALDI, while even longer times were observed earlier in our laboratory for IR laser desorption (7).

The Kinetic Energy Problem. The initial kinetic energy distribution arises directly from the ionization process. In the electron impact method utilized by Wiley and

McLaren (1), kinetic energy distributions were basically thermal (around 0.1 eV). Thus, the time-lag itself was not as significant a factor in improving their resolution as was the pulsed, low voltage ion extraction for temporal and spatial focusing. In general, the initial kinetic energy distributions for desorption techniques (used to ionize non-volatile molecules directly from the condensed phase) are considerably higher. These techniques include plasma desorption (17), laser desorption (18) and secondary ion mass spectrometry (19).

In the matrix-assisted laser desorptionlionization (MALDI) technique developed by Hillenkamp and Karas (20), peptides and proteins (or other biomolecules) are deposited on a sample probe in solutions containing a high excess of a UV-absorbing compound such as nicotinic acid. Laser desorption of the resultant crystals results in matrix ions with initial kinetic energies of about 1 ev in the forward direction, and kinetic energy spreads of comparable magnitude. Experiments in several laboratories (21-23) have shown that the analyte ions are desorbed with mean velocities and velocity distributions comparable to that of the matrix ions. Thus, both average energies (in the forward direction) and kinetic energy distributions increase approximately linearly with mass. For a protein, this may be of the order of tens or hundreds of electron volts. This has detrimental effects upon both mass resolution and accuracy, since the peak centroids will appear at times that are shorter than should be expected for their mass.

Metastable Fragmentation and Its Effects on Mass Resolution

With the advent of short pulse lasers, improved detector response and faster transient digitizers, the problems of time measurement accuracy can be greatly minimized. The initial spatial and kinetic energy distributions, after ion acceleration, are both converted into distributions in the final kinetic energy. They pose serious problems for linear instruments, but can be corrected by energy focusing devices such as the reflectron which is described below. Thus, it would appear that the question of mass resolution could be addressed as a simple ion optical problem. However, a number of investigators have noted (24,25) that the prompt fragmentation observed for small organic molecules may occur over a longer time frame (microseconds) for larger biomolecules having a greater number of internal degrees of freedom. The effects on mass resolution are particuarly problematic when they occur in regions where electric fields are used to focus or accelerate ions, rather than the field free drift regions. Metastable fragmentation of large biological molecules poses a considerably greater challenge to the development of high performance time-of-flight mass spectrometers than the initial temporal, spatial and kinetic energy distributions described by Wiley and McLaren (1).

Fragmentation in the Source/Accelerating Region. Fragmentation occurring during ion extraction and acceleration has the most detrimental effects upon the time-of-flight mass spectrum. If an ion of mass m_1 decays at a point α s in the source/acceleration region to an ion of mass m_2 , its final kinetic energy as it enters the drift region will be given by:

$$\frac{1}{2}m_2v^2 - \left(\frac{m_2}{m_1}\right)eE\alpha s + eE(1-\alpha)s$$
 [16]

Its final velocity will determine its time-of-flight in the drift tube:

$$v^2 = \frac{2eE\alpha s}{m_1} + \frac{2eE(1-\alpha)s}{m_2}$$
 [17]

and can be compared with the velocity of its apparent mass m^* :

$$v = \left[2eEs\left(\frac{\alpha}{m_1} + \frac{1-\alpha}{m_2}\right)\right]^{1/2} - \left[2eEs\left(\frac{1}{m^*}\right)\right]^{1/2}$$
 [18]

to show that the ion will appear at an apparent mass:

$$m^* = \frac{m_1 m_2}{\alpha m_2 + (1 - \alpha) m_1}$$
 [19]

intermediate between the precursor and product ion masses. Because fragmentation may involve any number of precursor/product ion pairs and can occur randomly in the acceleration region, most of the ions detected will contribute to the general baseline noise in the spectrum, with a resultant loss in sensitivity. However, the rate of fragmentation is highest in the early stages of acceleration and decays with time. For large molecules, Bunker and Wang (26) have noted that fragmentation rates are highest for processes involving the losses of small neutral groups, resulting in the formation of product ions whose masses are slightly lower than that of the precursor ion. These ions appear at lower mass than the precursor ions, but are unresolved from the precursor ions since they have slightly reduced kinetic energies. Thus, they appear as tailing on the low mass side of the precursor ion peak. The resultant peak broadening produces considerable loss in mass resolution, and shifts peak centroids to lower mass.

Fragmentation in the Flight Tube. Ions spend most of their time in the drift region. Studies by Chait (24) and Demirev et al. (25) have shown that the metastable fragmentation time frame for large peptides (5,000 to 20,000 daltons) is of the order of tens of microseconds, so that fragmentation of these ions occurs predominantly in the flight tube. Because there are no electric fields in the drift region, precursor ions and their product ions and neutrals will all have the same velocity, and therefore the same time-of-flight as the precursor ion. Thus, fragmentation in this region is largely inconsequential, provided that the ions and neutrals do not encounter additional electric fields. In fact, such fields *are* encountered as the ions approach detectors, or are energy focused by a reflectron. Detectors may result in considerable peak broadening, while reflectrons can result in loss of ion signal to the baseline noise. Thus, linear time-of-flight instruments generally provide higher sensitivity for the analysis of large biological molecules.

The Effects of Postacceleration. The electronics console on the Bendix Model 2000 mass spectrometer included a control for observing the products of metastable fragmentation in the flight tube. This control provided a retarding potential to a grid placed at the end of the flight tube, at a short distance from the entrance to the detector. When activated, the molecular ion peak could be seen to split into three distinct peaks, corresponding to the neutral product (m_N) , molecular ion (m_1) and fragment ion (m_2) , respectively, from the reaction: $m_1 \rightarrow m_2 + m_N$. The neutral product is, of course, unaffected by the retarding field and arrives in the shortest time. The molecular and fragment ions are both retarded, with the fragment ion retarded to the greatest extent. Some years later, this technique was revisited by Chait and Field for describing the metastable fragmentation of chlorophyll-a (27).

As one might expect, an analagous situation occurs for instruments which utilize post-acceleration of ions prior to detection. Post-acceleration is generally employed to improve detection efficiency for high mass ions by increasing their velocity of impact at the detector. However, when metastable fragmentation occurs in the flight tube, post-acceleration will have different effects upon the velocities of the precursor ions and their ionic and neutral products. In particular, the precursor ions will have energies after post-acceleration equal to:

$$\frac{m_1 v^2}{2} = e \ (V + V_p) \tag{20}$$

where V_p = post-acceleration voltage. Their final velocities as they strike the detector will be given by:

$$v = \left[\frac{2e}{m_1}(V + V_p)\right]^{1/2}$$
 [21]

This velocity is, of course, higher than that of the neutral fragments, which retain the same velocity as the precursor ion prior to post-acceleration:

$$v = \left[\frac{2e}{m_1}V\right]^{1/2}$$
 [22]

Product ions, on the other hand, will have energies after post-acceleration equal to:

$$\frac{m_2 v^2}{2} - e \left(\frac{m_2}{m_1} V + V_p \right) \tag{23}$$

which corresponds to a final velocity:

$$v = \left[\frac{2e}{m_2} \left(\frac{m_2}{m_1} V + V_p \right) \right]^{1/2}$$
 [24]

This can be more conveniently arranged to:

$$v = \left[\frac{2e}{m_1} \left(V + \frac{m_1}{m_2} V_p\right)\right]^{1/2}$$
 [25]

to show that the product ions will have velocities greater than either the precursor ion or the product neutrals. Since all species originating from a particular precursor arrive at the end of the flight tube at the same time, their differences in arrival times at the detector will depend upon their final velocities. The product ions arrive first, followed by the precursor ion and the neutral products. The actual separation in time will depend upon the magnitude of the post-acceleration voltage, the length of the post-acceleration region, and the distance between that region and the detector.

For high mass ions, metastable fragmentation in the flight tube is generally extensive. A number of different fragments are formed, some of which involve the losses of small neutral molecules such that m_2 is only slightly less than m_1 . Since these are not resolved, this results in considerable peak broadening. Thus, post-acceleration can be detrimental to mass resolution and, in many cases, to mass measurement accuracy if extensive metastable fragmentation results in shifting the time-centroid of the unresolved peak.

In the matrix-assisted laser desorption technique, molecular ion mass measurements in excess of 300,000 daltons have been carried out. Since it is generally understood that detection efficiency depends upon the impact velocity of the ions at the detector, ion kinetic energies of 20 to 30 keV are commonly utilized for such large ions. Given the problems described above, this is best accomplished using 20 to 30 kV extraction in the acceleration region, rather than lower voltage extraction followed by post-acceleration. At the same time, many instruments using high voltage extraction have at least some post-acceleration between the flight tube and the detector, that results from the voltage bias on the front end of the detector. The most common configurations place the source backing plate at 20 to 30 kV and the flight tube at ground potential. Ions exiting the flight tube are then accelerated as they approach detectors with the first dynode (or channelplate) biased between 1800 to 3000 volts, resulting in some loss of mass resolution. For techniques, such as plasma desorption mass spectrometry, which detect single ion pulses, dual channelplate detectors can be biased so that the front channelplate is at ground and the collector anode at high (negative) voltage, since the pulses can be capacitively coupled to the preamplifier and recording device. This solution can be used as well for techniques, such as laser desorption, in which analog signals are recorded. Alternatively, the flight tube itself can be floated to match the voltage at the first dynode of a particle detector. In any case, it is essential in the linear time-of-flight mass spectrometer to eliminate all electrical fields along the ion transmission axis following initial ion acceleration.

Time-Delay Techniques. There have been numerous instances in which the fast atom bombardment (FAB) mass spectrum of a peptide has revealed extensive fragmentation for determining the amino acid sequence, while the plasma desorption mass spectrum has resulted in recording only the molecular ion. While it is tempting to attribute such differences to the method of ionization, the differences in the mass spectra are due primarily to the different analyzers used. Fast atom bombardment is generally carried out on double-focusing and quadrupole mass spectrometers, since it provides the stable, continuous ion beams that are essential for such scanning instruments. Ions are formed in a field-free ion source, where they reside for several microseconds before entering the extraction/acceleration region. Plasma desorption occurs as a series of random ionization events that produce (on average) about 3 ions/event, so that they are best recorded on an instrument that can record the entire mass range for each event. Thus, this technique is used almost exclusively with timeof-flight analyzers. Since timing is based upon the precise moment of ionization, it is essential that the ions be extracted promptly. Thus, the ions are generally formed in a region of high electric field, and extracted into the drift region within a few nanoseconds. The extensive fragmentation that occurs in the microsecond time frame within the drift region in time-of-flight mass spectrometers (as described above) suggests that the fragmentation observed in FAB mass spectra results primarily from the opportunity for ions to undergo fragmentation prior to extraction/acceleration and mass analysis.

The use of lower extraction fields in the time-of-flight mass spectrometer does not solve the problem, since fragmentation during extraction produces ion signals with indeterminant mass. In our laboratory, we have developed a series of time-of-flight instruments which form ions in a field free region, and extract those ions from 10 to 50 microseconds later. The method is similar to that of Wiley and McLaren in that it uses pulsed two-stage extraction, with high spatial focusing of ions that are adrift in a field-free source region.

We have been interested for a number of years in the possibilities for rapid identification of bacteria and other micro-organisms from the polar lipids observed by direct desorption of intact or lysed cells (28,29). Figure 3a shows the FAB mass spectrum of lysed E. coli cells which is dominated by the desorption of protonated phosphatidylethanolamine species at m/z 704 and 732 carrying different fatty acyl groups. The fragment ion peaks at m/z 563 and 691 result from the loss of the polar phosphoethanolamine head group. While these fragments occur promptly within the time frame of the double-focusing instrument, subsequent investigation of the product ion and constant neutral loss (CNL) spectra of these compounds suggests considerable metastable fragmentation over several microseconds (30). The plasma desorption mass spectrum of the same lysed cells is shown in Figure 3b. The molecular ions observed at m/z 749 and 777 are M+2Na-H⁺ ions. No fragmentation is observed and the peaks are broad, both consequences of metastable fragmentation. Figure 3c is the liquid SIMS time-of-flight mass spectrum of the same sample obtained after a 20 µs delay. The mass spectrum is essentially the same as that obtained on the sector instrument. Figure 3d is the infrared laser desorption mass spectrum obtained after a delay time of 50 µs. The peaks at m/z 743 and 771 correspond to MK+ ions, and fragmentation is again observed. In addition, the mass resolution is significantly improved in comparison to the plasma desorption mass spectrum obtained by prompt extraction.

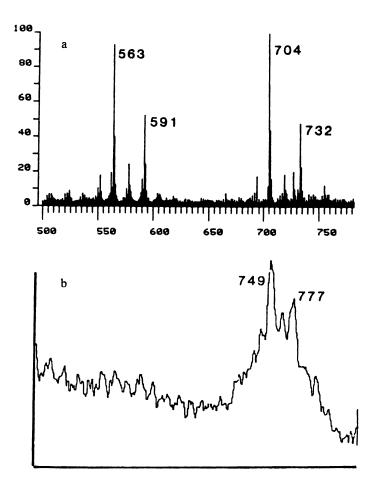


Figure 3. Mass spectra of phospholipids desorbed from bacterial cells. (a) FAB mass spectrum. (b) PD mass spectrum. (Reprinted with permission from Reference 4.)

Thus, an effective approach to dealing with the metastable fragmentation and, its effects on mass resolution and fragment ion information in time-of-flight mass spectra, is to incorporate time delays of sufficient length to enable complete metastable relaxation.

Reflectrons and Other Energy Focusing Devices

From the above discussion it should be obvious that it is generally possible to minimize (practically) the temporal and spatial distributions problems, using short pulsed ionization sources, desorption from equipotential surfaces and fast detectors. However, the initial kinetic energy distribution, which is a property of the ionization

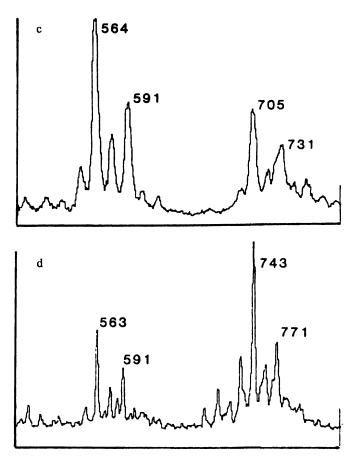


Figure 3. Continued. Mass spectra of phospholipids desorbed from bacterial cells. (c) Time-delayed liquid secondary ion TOF mass spectrum. (d) Time-delayed IRLD TOF mass spectrum. (Reprinted with permission from Reference 4.)

technique employed, remains as the primary initial condition that is not easily corrected in a simple linear instrument. Time-lag focusing was proposed early on by Wiley and McLaren, but this approach is not, however, practical on modern instruments in which time-to-digital converters and transient recorders are utilized to capture ion signals across the entire mass range in each time-of-flight cycle.

Electrostatic Energy Analyzers. An obvious approach would be to utilize an electrostatic analyzer (ESA, similar to that used in double-focusing instruments) either in front of a field-free drift length, or as the flight region itself. While the ESA is an effective means for reducing the kinetic energy spread, it should be remembered that it is less important that the energy spread be reduced at the detector than that ions with different kinetic energies arrive at the detector at the same time. Thus the

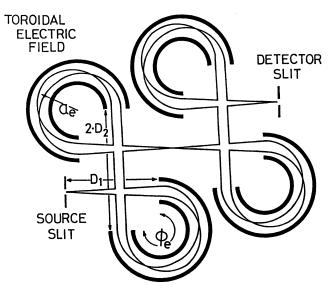


Figure 4. Time-of-flight mass spectrometer of Sakurai et al. (Reprinted with permission from Reference 32).

electric sectors from double-focusing instruments are generally unsuitable, since ions with different energies exit the sector at different times.

An electric sector which provides time focusing was designed by Poschenroeder (31). The more energetic ions travel a longer path through this 180° energy analyzer, arriving at the exit at the same time as slower, less energetic ions. A more recent design, incorporating four compact ESA elements, was reported by Sakuri et al. (32), and is shown in Figure 4.

The Dual-Stage Reflectron of Mamyrin. In 1973, Mamyrin et al. (33) introduced an energy-focusing device known as a reflectron, which consists of a series of retarding lenses as shown in Figure 5a. Similar to the Poschenroeder, the reflectron utilizes an electrical field to turn the ion trajectories around 180°, that is: back along their initial flight axis. In practice, the ions return at a slight angle to permit location of the detector adjacent to the ion source. The more energetic ions penetrate the retarding field of the reflectron to greater depth, so that they travel along a longer path, arriving at the detector at the same time as the less energetic ions.

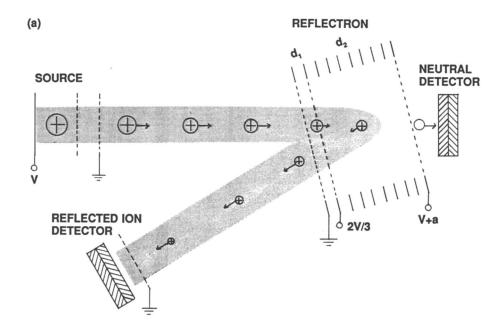
The Mamyrin reflectron was a dual stage device. Ions pass through an entrance grid, usually set at the potential of the flight tube, and are retarded to about one third of their initial kinetic energy by the time that they pass through the second grid, located at about 10% of the total reflectron depth. The ions are turned around in the second longer stage which is terminated by a plate (or grid, when a detector is located behind the reflectron), whose potential is slightly above that of the ion source. In their 1973 paper, Mamyrin and coworkers demonstrated mass resolutions better than one part in 3500 for the peak at m/z 1278 in the isotopic cluster of the trimer of rhenium bromide, an impressive resolution that cannot be realized routinely in current instruments.

Reflectrons using the basic Mamyrin design have been incorporated in many of the time-of-flight instruments reported since 1973. They are utilized in the commercial laser microprobe instruments offered by Leybold-Hereaus (Koln, Germany) and Cambridge Mass Spectrometers, Ltd. (now Kratos/CMS, Manchester, UK), as well as instruments manufactured for resonance enhance multiphoton ionization (REMPI) by R.M. Jordan, Inc. At the same time, reflectrons have not been particularly advantageous for techniques, such as plasma desorption and laser desorption, which are utilized for the analysis of large biological molecules. Because many of these large ions undergo metastable fragmentation in the flight tube (or in the reflectron itself), their products are not reflected back at times corresponding to the precursor ion mass, so that (unlike the linear instrument) these species do not contribute to the focused mass spectrum. Thus, for high mass molecules improved mass resolution may be realized at considerable expense in sensitivity.

Fragmentation may be induced by collisions with the grids utilized in time-of-flight mass spectrometers, so that gridless reflectrons have also been designed (34). In the dual stage reflectron, fringe fields around the grid wires are particularly severe in the first stage where the largest voltage drop occurs over a small distance. This results in considerable ion scattering, which reduces the transmission and overall sensitivity. This effect is more pronounced in instruments using high voltages, that is: instruments designed for high mass analysis. Thus, linear instruments continue to be favored for high mass analysis. Additionally, coaxial reflectrons have also been designed (35). These commonly use a set of matched channelplates as detectors, equipped with a hole in the center for passage of the ion beam emerging from the source (Figure 5b). Because channelplates are utilized, the coaxial configuration is best suited for methods which detect single ion pulses, rather than analog signals. An instrument described by Tanaka et al. (36) used a coaxial reflectron as the entire flight distance.

The Single-Stage Reflectron and Metastable Fragmentation. Standing and coworkers introduced a single-stage reflectron, or ion mirror (37). Because the retarding field strength is shallow, similar to that of the second stage of the dual-stage reflectron, the ion mirror must be considerably longer to achieve comparable mass resolution. However, its major advantage is realized for techniques (described below) that are used to record product ion mass spectra from metastable or induced fragmentation. In this case, the ion mirror provides a linear mass scale for the product ion spectra.

Mass Calibration in Reflectron Instruments. In reflectron instruments, ions spend a portion of their time in two field-free regions $(L_1 \text{ and } L_2)$ and the remainder of the time passing into and out of the reflectron, where they turn around at a distance (d = penetration depth). If $L = L_1 + L_2$ is the combined length of the drift regions, then the time that an ion spends in the field-free regions is given by:



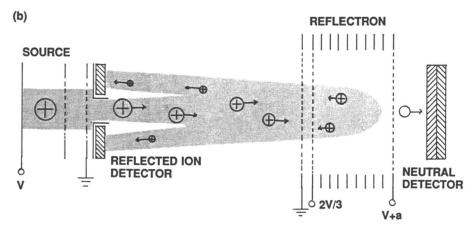


Figure 5. Reflectron designs. (a) Dual-stage Mamyrin reflectron. (b) Coaxial reflectron. (Reprinted with permission from Reference 4).

$$t' - \left[\frac{m}{2eV}\right]^{1/2} L - k'm^{1/2}$$
 [26]

which is equivalent to equation [3]. When the ions enter a single-stage reflectron, they decelerate in a time equal to:

$$t'' - \left[\frac{2m}{eV}\right]^{1/2} d - k'' m^{1/2}$$
 [27]

After turning around, they are reaccelerated in the same time. Thus, the total time to traverse both drift regions and pass through the reflectron distance twice is:

$$t = \left[\frac{m}{2eV}\right]^{1/2} (L_1 + L_2 + 4d) = km^{1/2}$$
 [28]

where the factor of 4 results from two passes through the reflectron, with an average velocity half that of the linear regions. Because equation [28] follows a square root law, empirical equations for calibrating the mass scale:

$$t = am^{1/2} + b$$
 [29]

where the constants a and b are determined from the flight times of known masses, are equally valid for reflectron as well as linear instruments.

For the single-stage reflectron, Standing (38) has noted that optimal focusing is achieved when $L_1 + L_2 = 4d$, which means that ions spend equal amounts of time in the field-free and reflectron regions (i.e. t' = t''). Using equation [28] it is possible to illustrate in simple fashion how the reflectron achieves energy focusing. For an ion with an initial kinetic energy (U_0) in the forward direction, the total flight time will now be given by:

$$t = \left[\frac{m}{2(eV + U_0)}\right]^{1/2} (L_1 + L_2 + 4d)$$
 [30]

The increase in ion kinetic energy means that the ion will spend less time in the field-free regions $(L_1 \text{ and } L_2)$ which have fixed distances. However, the penetration depth (d) will increase, so that the total time in equation [30] will be exactly the same as the time in equation [28]; and the ions will be in focus.

A more thorough treatment of the energy focusing properties of reflectrons is given by Beavis (Chapter 3). While it is far simpler to derive these equations for single-stage reflectrons, the dual-stage reflectron behaves in a similar manner.

Metastable Fragmentation. An ion which fragments in the first field-free region (L_l) produces a neutral product that is not reflected (and therefore does not contribute to the ion signal as in linear instruments) and a fragment ion whose arrival time at the detector corresponds to neither the precursor or product ion mass. When a mass spectrum is being recorded, metastable product ions complicate the spectrum by producing weak signals at seemingly random positions along the time (mass) scale. The situation is rather similar (in fact) to the broad metastable peaks that are observed in mass spectra obtained from double-focusing instruments.

The flight times of product ions from such metastable transistions are predictable, however; and can be interpreted if one can identify the precursor. Thus, there are two approaches to utilizing the reflectron time-of-flight mass analyzer for producing product ion spectra. The first (and perhaps the most obvious) approach is to select ions of a single mass for passage through the first drift region. One example of this approach has been developed by Owens (39), in which a timed gate is located at the space focus plane located in the first drift region. The ions passed by the gate are then fragmented by photodissociation using a pulsed UV laser, and the product ions are detected after reflection. The intact precursor ions (m_1) are recorded at the same flight times as observed in the normal mass spectrum. Product ions (m_2) have the same velocity as the precursor ions and (therefore) spend the same time (t') in the field-free regions. However, they enter the reflectron with energies equal to:

$$KE - \left[\frac{m_2}{m_1}\right] eV ag{31}$$

and penetrate the retarding field of the reflectron to a much shallower depth:

$$d = \frac{m_2 V}{m_1 E}$$
 [32]

where E = the field strength (V/d) in the reflectron. From equation [27] and substitution of the reflectron depth, their flight times (t'') in the reflectron region will then be given by:

$$t_2'' - 2\left[\frac{2m_2b}{eE}\right]^{1/2} - 2\left[\frac{2m_1^2V}{eE^2m_1}\right]^{1/2} - k''m_2$$
 [33]

while the precursor ions spend a time $(t'' = k''m_i)$ in the reflectron. Thus a mass scale can be established:

$$t_2 = \left[\frac{m_2}{m_1}\right] t_1'' + t_2'$$
 [34]

which shows a linear dependence upon mass, and results in a product ion mass spectrum for a given precursor.

Correlated Techniques. The second approach was introduced by LeBeyec and coworkers (35) using a coaxial dual-stage reflectron, and has been developed by Standing et al. (37) using an ion mirror. In this approach, all ions are permitted to enter the reflectron. A detector is also located at the rear of the reflectron and records neutral species resulting from metastable decay in the first field-free drift length. Because these neutrals appear at times corresponding to the mass of the precursor ion, it is then possible to only register ions in the reflectron detector when a neutral corresponding to the precursor mass is received. The resultant spectrum, known as a correlated reflex spectrum (35), can only be obtained from methods which employ single ion pulse counting. The method is illustrated in Figure 6, from data obtained by the Manitoba group (37). Figure 6a shows the spectrum obtained when the ion mirror voltages are turned off, essentially a linear time-of-flight mass spectrum. In Figure 6b, the reflectron voltages are turned on, and the first detector records the neutral species only, while in Figure 6c the second detector records the reflected mass spectrum at much higher mass resolution. Figures 6d and 6e are coincidence mass spectra, in which ions are recorded only when neutrals corresponding to the decay of MH⁺ and MNa⁺ ions, respectively, are registered on the detector behind the reflectron.

We should, of course, note a third approach by Duncan and coworkers (40). In this case fragmentation is induced by photodissociation in the *turn-around* region of the reflectron where the ions are briefly at rest. The product ions pass through the reflectron field only once, and from the same penetration depth. Thus, the reflectron behaves as an ion source, with product ions following a square root law. This approach is described in detail in Chapter 4.

Tandem Mass Spectrometry. In the double-focusing (EB) mass spectrometer, the electrostatic energy analyzer (E) can be used to improve the mass resolution of spectra acquired normally by scanning the magnetic field (B), or to obtain product ion mass spectra by linked scanning at constant B/E. Analogously, the reflectron can be utilized to improve mass resolution of time-of-flight spectra, or to obtain product ion mass spectra using one of the techniques described above. In both sector and time-of-flight instruments one observes metastable transitions occurring in the field-free region ahead of the energy-focusing device, and mass analysis is based upon the fact that product ions have different kinetic energies, i.e. $(m_2/m_1)eV$. When normal mass spectra are recorded, mass is proportional to B^2 in the sector instrument and to t^2 in the time-of-flight. Conversely, product ion mass spectra in both instruments follow a linear law. Finally, when used to provide mass dispersion, neither the ESA or reflectron provide the same optimal focusing for product ion spectra as they do for normal spectra.

Thus, if one has followed the evolution of sector instruments from the double-focusing mass spectrometer to triple analyzers (EBE), hybrid instruments (EBqQ) using quadrupole collision cells (q) and mass analyzers (Q), and four sector (EBEB) tandems, then one might expect a similar course for time-of-flight instruments as well. In fact, a number of tandem instruments have been constructed. Cooks and coworkers (41) have described an instrument using two linear time-of-flight analyzers, with fragmentation induced by surface induced dissociation (SID), as well as a more recent

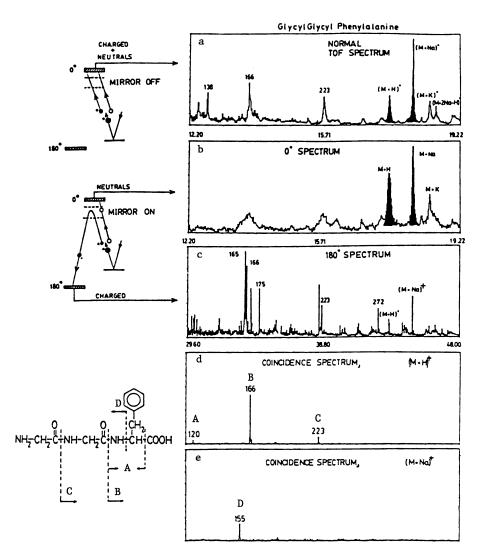


Figure 6. Mass spectra obtained from the Manitoba time-of-flight. (a) Normal mass spectrum of Gly-Gly-Phe obtained at the first detector with the reflectron turned off. Mass spectra of the neutral fragments obtained at the first detector (b) and reflected ions at the second detector (c) with the reflectron on. Coincidence mass spectra for the MH⁺ (d) and MNa⁺ (e) ions. (Reprinted with permission from Reference 37).

version in which the second mass analyzer is a reflectron design (42). Jardine et al. (43) have also used two linear analyzers with a gas collision cell. Russell and coworkers (44,45) have developed a sector/time-of-flight hybrid instrument which is described in Chapter 5, while Cornish and Cotter (46) have constructed a tandem time-of-flight (TOF/TOF) mass spectrometer using two reflecting analyzers, that is described in Chapter 6.

Recording the Ions

The resurgance of interest in the time-of-flight mass analyzers owes as much to the development of faster, more precise timing electronics as it does to the introduction of ionization methods that can now realize the almost unlimited mass range of this analyzer. It was not mass resolution, in fact, which diminished the initial enthusiasm for the Bendix instruments. Quadrupole mass spectrometers, developed in the 1960s, were capable of scanning the mass range within seconds, and outpaced the time-of-flight as on-line detectors for packed column gas chromatography. With the development of high speed transient recording, Holland et al. (47) have predicted the eventual evolution from the time-slice detection approach used by Wiley and McLaren to full time-array detection using integrated transient recording that will provide duty cycles of 100% and superb chromatographic integrity. These goals are described in detail in Chapter 9. Here, we describe the methods that have been used to date.

Oscillographic and Boxcar Methods. Wiley and McLaren (1) initially recorded their time-of-flight mass spectra as an oscillographic trace triggered by the drawout pulse. The trace was then photographed. That method was used as well by Mamyrin and coworkers in their initial report (33).

The Bendix Model 2000 mass spectrometer used a continuous dynode magnetic electron multiplier whose anode was connected to the oscilloscope output. The detector was also equipped with a deflection gate for diverting the ion signal to a separate anode for single ion monitoring, or for scanning the mass spectrum. In each 100 microsecond time-of-flight cycle a 10 to 40 ns portion of the ion signal was diverted to this anode and amplified. The time delay between the drawout pulse and the deflection pulse was incremented each cycle, and the resultant amplified signal connected to a recorder which produced a mass spectrum over a period of several minutes. This boxcar approached was successful since the same ion signal could be generated repetitively (10 kHz). It was not possible to use this approach for recording the results from a single pulsed laser event, so that later instruments developed for laser pyrolysis studies (48) generally continued to use oscillographic recording. More importantly, the duty cycle was much too low. Electron impact is used in most mass spectrometers for continuous ionization, but in this case the electron beam was pulsed for 1 microsecond in each 100 microsecond cycle: an ionization duty cycle of 1%. The recording of 10 ns time slices represents a recording duty cycle of 10⁻⁴ for a combined duty cycle of 10⁶! It was this aspect of the commercial time-of-flight instruments of the 1960s that could not compete with fast scanning quadrupoles for GC/MS analyses.

In the 1970s, electronic techniques were developed that enabled one to record ions of any mass in each time-of-flight cycle. In general there have been two distinct development paths for recording time-of-flight mass spectra. The first began with

multichannel analyzers designed for recording nuclear events and developed into the current multistop time-to-digital converters (TDCs) that are now used in plasma desorption mass spectrometry. These methods are used primarily (but not exclusively) to record the results of events that occur randomly. In addition, they are used when only one or a few ions are produced in each time-of-flight cycle. The second began with the development of waveform recorders using rapid, sequential analog-to-digital conversion to store a waveform or transient. These recorders were intended to replace boxcar methods for recording transients that could not be generated repetitively. These have developed into the current fast digital oscillscopes that are now used to provide a full mass spectrum from a single laser shot. These two approaches are described briefly here, while a more detailed evaluation of their performance is provided by Lys (Chapter 10).

Time-to-Digital Conversion. In the early 1970s, Vestal (49) developed a coincidence time-of-flight mass spectrometer for Johnston Laboratories (Baltimore, MD) that was used to obtain photionization mass spectra. The ionization source was a mercury lamp from which photons in the vacuum ultraviolet (VUV) range were selected by a grating monochrometer. Gas phase photoionization of a neutral molecule produced a positive ion which was extracted into the flight tube, and an electron that was extracted in the opposite direction and recorded by a start detector. The amplified pulse from the start detector was passed through a discriminator and then to a time-topulse height converter (TPHC) which generated a linear voltage ramp. At some later time, the positive ion was recorded by the stop detector at the end of the flight tube. This pulse was also passed through a discriminator and used to terminate the voltage ramp. The TPHC then output a pulse whose amplitude corresponded to the voltage of the ramp at the time of its termination. This was then fed to a Technical Measurements Corporation (Oak Ridge, TN) multichannel pulse height analyzer (PHA), which recorded the event in one of 1024 channels. The cycle was repeated until sufficient events were accumulated to provide a mass spectrum with good signal/noise.

In 1974, Macfarlane and Torgerson (17,50) developed the method known as plasma desorption mass spectrometry (PDMS). This is also a coincidence method, since the source of ionization (a 10 microcurie sample of ²⁵²Cf) emits two high energy (40 to 100 MeV) fission fragments in opposing directions. One of these is recorded at a start detector, while the other is used to desorb (ionize) non-volatile molecules deposited on a thin aluminum foil. A block diagram of this instrument is shown in Figure 7a. The arrival time of the resultant ion is registered by a stop detector, and the amplified pulses from both detectors are fed to constant fraction discriminators (CFD), which provide more accurate timing for peaks of varying height than discriminators based upon an amplitude threshold. The time-to-pulse height converter and multichannel analyzer described above are replaced with a multistop time-to-digital converter. This improves the probability of observing a molecular ion following fission events which also desorb low mass ions.

In addition to the Texas A&M group (17), plasma desorption mass spectrometers have been developed at Rockefeller (24), Orsay (35), Uppsala (14), Darmstadt (51) and Argonne Laboratories (52). They were commercialized by BIO-ION Nordic (Uppsala, Sweden) and have more recently been marketed by Applied Biosystems, Inc. (Foster City, CA). The commercial instruments are now installed

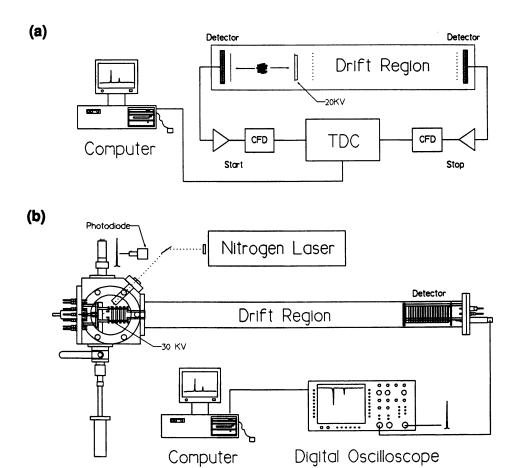


Figure 7. Block diagrams of TOF mass spectrometers. (a) BIO-ION plasma desorption mass spectrometer. (b) MALDI mass spectrometer developed in our laboratory. (Reprinted with permission from Reference 4).

in more than fifty laboratories worldwide, and are used primarily for the structural analysis of peptides and small proteins. An example of spectra produced by this technique was shown in Figure 1b.

Integrated Transient Recording. In 1975, Hillenkamp and coworkers (53) introduced the laser microprobe for elemental analysis of biological samples with high spatial resolution. The LAMMA 500 was commercialized by Leybold-Hereaus (Koln, Germany) and utilized an 8-bit, 100 Msample/sec Biomation 8100 waveform recorder manufactured by Gould (Cupertino, CA) to digitize the spectrum produced from a single laser shot. The ability to digitize the analog signal from a single laser shot (rather than record and accumulate single ion events) was essential since a specific location on the biological tissue was generally vaporized by the laser shot. In 1978, Kistemaker introduced laser desorption as a method for the mass analysis of nonvolatile and thermally labile molecules, using a double-focusing mass spectrometer with a spatial array detector (18). In 1983 our laboratory introduced an infrared laser desorption time-of-flight instrument (7) using the Biomation 8100 downloaded to an Apple II+ computer to provide signal add/averaging of successive analog mass spectral transients. Simultaneously, this approach was also used on the LAMMA 1000 which was developed for laser desorption.

Integrated transient recording (ITD) became available commercially with the introduction of the model 3500SA signal averaging transient recorder by LeCroy Corporation (Spring Valley, NY). This instrument was capable of recording and averaging 8-bit, 100 Msample/sec spectra at the rate of 100 spectra/sec. More convenient (and less costly) were their later offerings of a 100 Msample/sec model 9400 digital oscilloscope, and the faster 400 Msample/sec model 9450 oscilloscope. Linear Instruments (Reno, NV) offers a 300 Msample/sec digitizer that can be placed in a slot in a 386 or 486-based PC. Currently the Tektronix (Beaverton, OR) model TDS540 and LeCroy (Spring Valley, NY) 7200 series digital oscilloscopes provide 1 Gsample/sec digitization rates.

These recording devices have been fundamental to the success of matrix-assisted laser desorption/ionization (MALDI) mass spectrometry, introduced by Karas and Hillenkamp (54), and Tanaka et al. (36). This technique has been used to measure the molecular weights of proteins in excess of 300 kdaltons (55,56), generally obtained from only a few laser shots. Figure 7b shows a block diagram of a MALDI instrument developed in our laboratory using a pulsed nitrogen laser (57). Figure 8 shows the mass spectrum of the endoproteinase Arg-C digest of an insertion mutant of Staph. nuclease obtained from eight laser shots (58). Matrix-assisted laser desorption has, in fact, generated much of the recent and intense interest in time-of-flight mass spectrometers as instruments for biological research. Commercial MALDI instruments are now offered by Vestec Corporation (Houston, TX), Finnigan (Hemmel-Hempstead, UK), Bruker-Franzen (Bremen, Germany), VG Analytical (Manchester, UK).

At the same time, Holland et al. (47) have espoused the benefits of 100% duty cycle instruments for high chromatographic resolution in capillary GC/MS configurations, coupled with the ability to provide spectral deconvolution of coeluting species. Their approach combines ion storage techniques to improve the ionization duty cycle with higher transient recording repetition rates to improve recording duty cycle, and is detailed in Chapter 9.

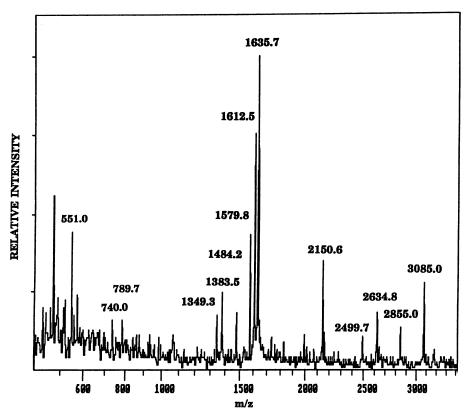


Figure 8. MALDI mass spectrum of *Staphylococcus* nuclease containing a glycine insertion. (Reprinted with permission from Reference 4).

Pulsed, orthogonal extraction and continuous ionization

There are now an emerging group of new instruments that address the initial kinetic energy spread problem by extraction of ions at right angles to the direction of their major velocity components. The infrared laser desorption and liquid SIMS instruments used to acquire the time-delay spectra in Figures 3c and 3d are early examples of this approach (7,9). As shown in Figure 9a, ions are desorbed off-axis to the time-of-flight direction and drift into the field-free source region, with the higher velocity ions arriving first. After a suitable delay, ions can be extracted which have low velocities in the off-axis direction which are corrected by a set of deflectors. In addition, these ions have even lower velocities in the time-of-flight direction prior to extraction.

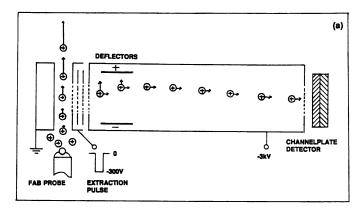
Bergmann et al. (59) have described a time-of-flight mass spectrometer for analysis of high mass clusters emitted from a cluster beam source off-axis to the time-of-flight direction. In their case, ions are formed by a pulsed laser in the center of the source and off-axis velocities are corrected by a quadrupole lens system with asymmetric voltages. More recently, Dodenov and coworkers (6) have coupled an electrospray ionization (ESI) source to a Mamyrin-type time-of-flight instrument as shown in Figure 9b. Pulsed, orthogonal extraction in this case enables them to utilize the time-of-flight with a continuous source, as well as to accomodate the very broad kinetic energy spreads of ions produced by this ionization method. Figure 9c shows the ESI mass spectrum of bovine insulin obtained on this instrument. The details of this approach are described by Dodenov in Chapter 7.

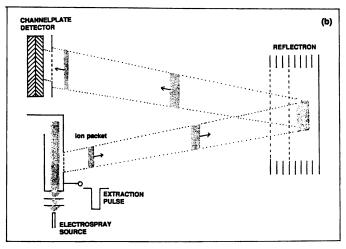
Finally, Guilhaus et al. (60) have constructed an instrument in which a continuous ion beam is focused tightly to produce ions with velocity components in one direction, which are then extracted orthogonally into a linear time-of-flight mass analyzer. The resultant packet of ions expands in the off-axis direction only slightly before striking the detector, since the kinetic energy due to extraction is considerably larger than the mean kinetic energy in the off-axis direction. In addition, the cycle repetition rate can be made high enough to extract adjacent ion packets and, thereby, record all of the ions that are produced. In addition, because the ions spend considerable time in the beam prior to extraction, there are likely to be fewer problems with metastable decay.

Conclusions and Predictions

The overwhelming success of the matrix-assisted laser desorption/ionization technique for determining the molecular weights of intact proteins has resulted in considerable attention to the time-of-flight mass spectrometer as an instrument with unlimited mass range. Indeed, preliminary work with the desorption of oligonucleotides (61-63) has led to predictions by many researchers that the time-of-flight mass spectrometer is destined to play a significant role in the Human Genome Project.

At the same time, such instruments are more likely to be used for the types of problems decribed in this volume by Woods (Chapter 11) and Vestling (Chapter 12). The current slate of inexpensive instruments now being offered by several manufacturers suggests that these instruments will be found in the laboratories of protein chemists, biochemists and molecular biologists, operated by researchers who would not consider themselves to be mass spectroscopists. For this group, the





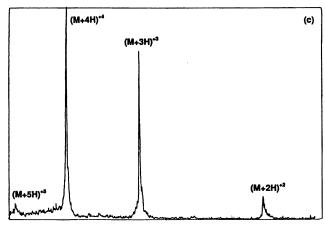


Figure 9. Pulsed ion extraction. (a) Diagram of the liquid secondary ion mass spectrometer described by Olthoff et al. (Adapted with permission from Reference 9). (b) Diagram of the ESI instrument and (c) the mass spectrum of bovine insulin reported by Dodenov et al. (Adapted with permission from Reference 6).

development of tandem instruments that can provide structural information: amino acid sequences, glycosylation sites, etc., will be important.

Finally, the ability to acquire repetitive spectra rapidly using fast integrated transient recording combined with fast spectral deconvolution should spur the development of compact, relatively low mass instruments that would outperform the current quadrupole and ion trap mass spectrometers as benchtop detectors for capillary gas chromatography.

Acknowledgments

Development of time-of-flight mass spectrometry in our laboratory has been supported by a grant (GM-33967) from the National Institutes of Health.

Literature Cited

- (1) Wiley, W.C.; McLaren, I.H. Rev. Sci. Instrumen. 1955, 26, 1150.
- (2) Opsal, R.B.; Owens, K.G.; Riley, J.P. Anal. Chem. 1985, 57, 1884.
- (3) Cotter, R.J. Biomed. Environ. Mass Spectrom. 1989, 18, 513-532.
- (4) Cotter, R.J. Anal. Chem. 1992, 64, 1027A-1039A.
- (5) Li, L.; Lubman, D.M. Anal. Chem. 1988, 60, 2591-2598.
- (6) Dodenov, A.F.; Chernushevich, I.V.; Laiko, V.V. presented at the 12th International Mass Spectrometry Conference, Amsterdam, August 26-30, 1991.
- (7) Van Breemen, R.B.; Snow, M.; Cotter, R.J. Int. J. Mass Spectrom. Ion Phys. 1983, 49, 35.
- (8) Tabet, J.-C.; Jablonski, M.; Cotter, R.J.; Hunt, J.E. Int. J. Mass Spectrom. Ion Processes 1985, 65, 105.
- (9) Olthoff, J.K.; Honovich, J.P.; Cotter, R.J. Anal. Chem. 1987, 59, 999-1002.
- (10) W.B. Emary, I. Lys, R.J. Cotter, R. Simpson and A. Hoffman, Anal. Chem. 62 (1990) 1319-1324.
- (11) Tabet, C.-C.; Cotter, R.J. Int. J. Mass Spectrom. Ion Processes 1983, 54, 151.
- (12) Grix, R.; Gruner, U.; Li, G.; Stroh, H.; Wollnik, H. Int. J. Mass Spectrom. Ion Processes 1989, 93, 323-330.
- (13) Lubman, D.M.; Michael, S.M.; Chien, M. Proceedings of the 40th ASMS Conference on Mass Spectrometry and Allied Topics, Washington DC, 1992.
- (14) Jonsson, G.; Hedin, A.; Hakansson, P.; Sundqvist, B.U.R.; Save, G.; Nielsen, P.F.; Roepstorff, P.; Johansson, K.E.; Kamensky, L.; Lindberg, M. Anal. Chem. 1986, 58, 1084.
- (15) Cotter, R.J. Anal. Chem. 1988, 60, 781A.
- (16) Hillenkamp, F. paper presented at the International Conference on Biological Mass Spectrometry, Kyoto, September 23, 1992.
- (17) Macfarlane, R.D.; Skowronski, R.P.; Torgerson, D.F. Biochem. Biophys. Res. Commun. 1974 60, 616.
- (18) Posthumus, M.A.; Kistemaker, P.G.; Meuselaar, H.L.C.; Ten Noever de Brauw, M.C. Anal. Chem. 1978, 50, 985.
- (19) Benninghoven, A.; Jaspers, D.; Sichtermann, W. Appl. Phys. 1976, 11, 35.
- (20) Karas, M.; Hillenkamp, F. Anal. Chem. 1988, 60, 2299.
- (21) Beavis, R.C.; Chait, B.T. Chem. Phys. Lett. 1991, 5, 479.

- (22) Huth-Fehre, T.; Becker, C.H. Rapid. Commun. Mass Spectrom. 1991, 8, 378-382.
- (23) Pan, Y.; Cotter, R.J. Org. Mass Spectrom. 1992, 27, 3-8.
- (24) Chait, B.T. Int. J. Mass Spectrom. Ion Phys. 1983, 53, 227.
- (25) Demirev, P.; Olthoff, J.K.; Fenselau, C.; Cotter, R.J. Anal. Chem. 1987, 59, 1951-1954.
- (26) Bunker, D.H.; Wang, F.M. J. Am. Chem. Soc. 1977, 99, 7457.
- (27) Chait, B.T.; Field, F.H. J. Am. Chem. Soc. 1984, 106, 1931.
- (28) Heller, D.N.; Cotter, R.J.; Fenselau, C.; Uy, O.M. Anal. Chem. 1987, 59, 2806-2809.
- (29) Platt, J.A.; Uy, O.M.; Heller, D.N.; Cotter, R.J.; Fenselau, C. Anal. Chem. 1988, 60, 1415-1419.
- (30) Heller, D.N.; Murphy, C.; Cotter, R.J.; Fenselau, C.; Uy, O.M. Anal. Chem. 1988, 60, 2787-2791.
- (31) Poschenroeder, W. Int. J. Mass Spectrom. Ion Phys. 1971, 6, 413.
- (32) Sakurai, T.; Fujita, Y.; Matsuo, T.; Matsuda, H.; Katakuse, I., *Int. J. Mass Spectrom. Ion Proc.* 1985, 66, 283.
- (33) Mamyrin, B.A.; Karataev, V.I.; Shmikk, D.V.; Zagulin, V.A. Zh. Eksp. Teor. Fiz. 1973, 64, 82-89.
- (34) Grix, R.; Kutscher, R.; Li, G.; Gruner. U.; Wollnik, H. Rapid Commun. Mass Spectrom. 1988, 2, 83.
- (35) Della-Negra, S.; LeBeyec, Y. Anal. Chem. 1985, 57, 2035.
- (36) Tanaka, K.; Waki, H.; Ido, Y.; Akita, S.; Yoshida, Y.; Yoshida, T. Rapid Commun. Mass Spectrom. 1988, 2, 151.
- (37) Standing, K.G.; Beavis, R.; Bollbach, G.; Ens, W.; LaFortune, F.; Main, D.; Schueler, B.; Tang, X.; Westmore, J.B. Anal. Instrumen. 1987, 16, 173.
- (38) Tang, X.; Beavis, R.; Ens, W.; LaFortune, F.; Schueler, B.; Standing, K.G. Int. J. Mass Spectrom. Ion Processes 1988, 85, 43-67.
- (39) King, R.C.; Owens, K.G. Proceedings of the 40th ASMS Conference on Mass Spectrometry and Allied Topics, Washington DC, 1992.
- (40) Cornett, D.S.; Peschke, M.; LaiHing, K.; Cheng, P.Y.; Willey, K.F.; Duncan, M.A. Rev. Sci. Instrum. 1992, 63, 2177-2186.
- (41) Schey, K.L.; Cooks, R.G.; Grix, R.; Wollnik, H. Int. J. Mass Spectrom. Ion Processes 1987, 77, 49-61.
- (42) Schey, K.L.; Cooks, R.G.; Kraft, A.; Grix, R.; Wollnik, H. Int. J. Mass Spectrom. Ion Processes 1989, 94, 1-14.
- (43) Jardine, D.R.; Morgan, J.; Alderdice, D.S.; Derrick, P. Org. Mass Spectrom. 1992, 27, 1077-1083.
- (44) Strobel, F.H.; Solouki, T.; White, M.A.; Russell, D.H. J. Am. Soc. Mass Spectrom. 1990, 2, 91-94.
- (45) Strobel, F.H.; Preston, L.M.; Washburn, K.S.; Russell, D.H. *Anal. Chem.* **1992**, 64, 754-762.
- (46) Cornish, T.J.; Cotter, R.J. Anal. Chem. 1993, 65, 1043-1047.
- (47) Holland, J.F.; Enke, C.G.; Allison, J.; Stults, J.T.; Pinkston, J.D.; Newcomb, B.; Watson, J.T. Anal. Chem. 1983, 55, 497A.
- (48) Vastola, F.J.; Pirone, A.J.; Giver, P.H.; Dutcher, R.R. In *Spectrometry of Fuels*; Friedel, R.A., Ed.; Plenum Press: New York, NY, 1970; pp. 29-36.
- (49) Vestal, M.A., private communication.

American Chemical

- (50) Macfarlane, R.D.; Torgerson, D.F. Science, 1976, 191, 920.
- (51) Becker, O.; Furstenau, N.; Krueger, F.R.; Weiss, G.; Wien, K. Nucl. Instrum. Methods 1976, 139, 195.
- (52) Fischel, D.; Hunt, J.E. Org. Mass Spectrom. 1987, 22, 799-801.
- (53) Hillenkamp, F.; Kaufmann, R.; Nitsche, R.; Unsold, E. Appl. Phys. 1975, 8, 341.
- (54) Karas, M.; Bachmann, D.; Bahr, U.; Hillenkamp, F. Int. J. Mass Spectrom. Ion Processes 1987, 78, 53.
- (55) Karas, M.; Bahr, U.; Ingendoh, A.; Hillenkamp, F. Angew. Chem., Int. Ed. Engl. 1989, 28, 760.
- (56) Spengler, B.; Cotter, R.J. Anal. Chem. 1990, 62, 793-796.
- (57) Chevrier, M.R.; Cotter, R.J. Rapid Commun. Mass Spectrom. 1991, 5, 611-617.
- (58) Keefe, L.J.; Lattman, E.E.; Wolkow, C.; Woods, A.; Chevrier, M.; Cotter, R.J. J. Appl. Crystalog. 1992, 25, 205-210.
- (59) Bergmann, T.; Martin, T.P.; Schaber, H. Rev. Sci. Instrum. 1989, 60, 792.
- (60) Dawson, J.H.J.; Guilhaus, M. Rapid Commun. Mass Spectrom. 1989, 3, 155-159.
- (61) Spengler, B.; Pan, Y.; Cotter, R.J.; Kan, L.-S. Rapid Commun. Mass Spectrom. 1990, 4, 99-102.
- (62) Tang, K.; Allman, S.L.; Chen, C.H. Rapid Commun. Mass Spectrom. 1992, 6, 365-368.
- (63) Huth-Fehre, T.; Gosine, J.N.; Wu, K.J.; Becker, C.H. Rapid Commun. Mass Spectrom. 1992, 6, 200-213.

RECEIVED October 12, 1993

Chapter 3

The Interpretation of Reflectron Time-of-Flight Mass Spectra

Ronald C. Beavis

Department of Physics, Memorial University of Newfoundland, St. John's, Newfoundland A1B 3X7, Canada

The time-of-flight mass spectrometer is currently undergoing a renaissance as an analytical instrument in biochemistry. This paper will discuss the ion optics of these instruments in detail, with particular emphasis on "reflectron" type instruments and the effects produced by the unimolecular decomposition of an ion while it is passing through a reflectron mass analyzer.

The simplest time-of-flight mass analyzer is a "linear" device, which measures the flight time of a pulse of ions from an ion source to a detector, through a region of field-free vacuum (Figure 1). In a linear machine, the detector faces towards the ion source. The ions from the source are all assumed to have the same kinetic energy. The mass measurement is obtained by applying the following simple equation:

$$m = q (\alpha \tau + \beta)^2, \tag{1}$$

where τ is the time-of-flight, m & q are the mass and charge of an ion, respectively, and $\alpha \& \beta$ are calibration constants that depend on the dimensions of the instrument and the details of the signal recording electronics. In practice, α and β are determined experimentally, calculated from the flight times and masses of known peaks in a particular mass spectrum. The mass resolution that can be achieved by this type of mass spectrometer is limited by the temporal width of the initial ion pulse from the ion source, and the velocity distribution of the ions. The ion velocity distribution results in a distribution of arrival times at the detector, broadening the signal from the detector corresponding to a single ion species.

The second type of time-of-flight analyzer is referred to as a reflectron, and it is illustrated in Figure 2 ("reflectron" is a contraction of the name originally proposed, "mass-reflectron" (1)). Ions are produced by a pulsed ion source, preferably with a short (nanosecond) temporal pulse width. The ions then traverse a field-free region, followed by a two stage ion mirror that reflects the ions through an angle $\phi \leq \pi$. The reflected ions then pass through a second field-free region and

0097-6156/94/0549-0049\$06.00/0 © 1994 American Chemical Society

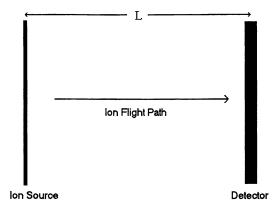


Figure 1 A linear time-of-flight mass analyzer.

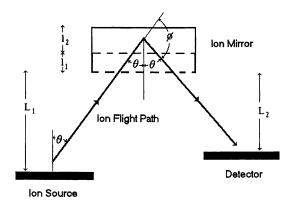


Figure 2 A reflectron time-of-flight mass analyzer with a two-stage mirror.

strike a detector. If the ion mirror voltages and dimensions are chosen to match the lengths of the field-free regions, it is possible to use this combination of ion optical elements to remove the time effects produced by the velocity distribution of ions generated by the ion source. The ability to correct for the additional temporal distribution caused by a the velocity distributions commonly found in real ion sources has made the reflectron a popular instrument for applications where a maximum mass resolution is desired. The calibration function for a reflectron is the same as for a linear instrument (equation 1), although the constants will have different values, depending on the geometry and voltages of the reflectron.

The temporal correction produced by a reflectron depends on the component of the ion's initial velocity (v, bold face indicates a vector) normal to the plane of the ion mirror (this is the direction of the instrument's ion optical axis):

$$v = |\mathbf{v}| \cos(\theta) . \tag{2}$$

Therefore, the equations of motion for an ion in a reflectron will be developed in terms of the ion's velocity and velocity distribution. The energy distribution of ions leaving the source can be substituted for the velocity distribution in the special case when $\phi = \pi$ (and $\theta = 0$, v = |v|). Instruments with $\phi = \pi$ have been constructed by several groups, although $\phi < \pi$ instruments are far more common. The use of velocity, rather than energy, for calculations also simplifies the mathematical notation necessary to describe the situation.

An important point to note in Figure 2 is the orientation of the planes characteristic of the ion source, the ion mirror, and the detector. All of these planes must be parallel for the reflectron to produce maximum temporal compensation for the ion source's intrinsic velocity distribution. The time-of-flight of an ion in such an arrangement is determined by the component of an ion's velocity in the direction normal to the ion mirror plane (the axial component) and the dimensions of the instrument along that direction. The velocity component parallel to the plane (the radial component) determines the angle θ , but it does not affect the time-of-flight of the ion. The relationship between the detector, ion mirror and ion source planes has occasionally been incorrectly drawn in the literature, leading to some confusion as to their correct orientations.

Another type of instrument capable of correcting for ion source velocity distributions was proposed by Bakker (2) and later by Poschenrieder (3). In this type of instrument, the ion mirror is replaced by an electrostatic sector, which bends the ions though an angle near π . This analyzer (called a *spiratron* by Bakker) has not been exploited extensively, because of the difficulty involved in constructing a sufficiently large, high angle electric sector, compared to the much easier to construct ion mirror in a reflectron.

The purpose of this chapter is the mathematical description of the behavior of ions in a reflectron analyzer. The treatment given below borrows heavily on the work of others. Rather than give specific references to individual papers at each step, the reader is invited to examine (4-9) (and particularly the extensive references in (8)) to see the motivations for my derivations and practical examples of working reflectrons.

The Effect of Ion Source Velocity Distributions

The principal that a reflectron uses to compensate for the initial velocity distribution of ions exiting the detector is conceptually quite simple, but requires an understanding of the effects caused by an ion velocity distribution. Let us assume that an ion source produces an extremely short pulse of a single ionic species with mass m from a flat, equipotential surface. Also, assume that these ions are produced with a distribution of axial velocities that has a mean value v_0 . Then the axial velocity of a particular ion in the ion pulse can be written $v = v_0 + \delta v$.

Linear Analyzers. In the linear instrument in Figure 1, ions will have a mean flight time $\tau_0 = L/v_0$. The flight time of ions with any particular velocity v will therefore be given by $\tau = L/v$. The distribution of flight times about τ_0 can be characterized in terms of the distribution of initial ion axial velocities,

$$\Delta \tau = \tau - \tau_0 = L \left[(v_0 + \delta v)^{-1} - (v_0)^{-1} \right]. \tag{3}$$

This equation shows that ions with $v > v_0$ will arrive with $\tau < \tau_0$ and ions with $v < v_0$ will arrive with $\tau > \tau_0$. This behavior leads to a broadening of the flight time distribution recorded by the detector and therefore a reduction in the mass resolution of the analyzer. The effect can be compensated for by increasing the value of v_0 . This type of compensation is not usually very effective, because increasing v_0 will lead to an increase in δv in most ion sources, resulting in little net improvement to the analyzer's resolution.

Another way to formulate the problem is to expand the flight time in the vicinity of τ_0 in terms of the axial velocity, using a Taylor series,

$$\tau(v) = \tau_0(v_0) + [\partial \tau(v)/\partial v] \delta v + [\partial^2 \tau(v)/\partial v^2] (\delta v)^2 + \dots, \tag{4}$$

where the derivatives are evaluated at v_0 . Examining the appropriate derivatives for a linear instrument, all of the terms in this series are non-zero for all choices of L and v_0 .

Reflectron Analyzers. The situation is different for a reflectron. The flight time of an ion through the analyzer can be broken down into three distinct components, corresponding to the flight times in the three different electric fields in a reflectron. In this analysis, it is assumed that the ion has sufficient initial velocity to penetrate through the first stage of the ion mirror, but it is slow enough to be reflected by the second stage.

The flight time in the field-free portion of the analyzer is given by

$$\tau_{\rm ff} = (L_1/v) + (L_2/v) \tag{5a}$$

where L_1 and L_2 are the lengths of the first and second field-free legs of the analyzer (measured normal to the mirror plane) and v is the axial component of the ion's velocity as it exits the ion source plane. The flight time therefore depends upon the sum of the two lengths ($L = L_1 + L_2$) and not the relative length of either leg.

The time-of-flight for an ion during its reflection by the two-stage electrostatic mirror can be divided into the time spent in the first and second stages of the mirror. The flight time in the first mirror stage (τ_{1m}) is given by

$$\tau_{1m} = 2\left(\frac{l_1 m}{q \Re f_1}\right) \left[v - (v^2 - 2q \Re f_1/m)^{1/2} \right], \tag{5b}$$

where \aleph is the potential difference used to accelerate the ions in the ion source, l_1 is the length of the first stage (measured normal to the mirror plane) and f_1 is the fraction of \aleph held across the first stage. The factor of 2 arises because the ion must pass through the first stage twice, once entering and once leaving the mirror. The flight time of an ion through the second mirror stage (τ_{2m}) is given by

$$\tau_{2m} = 2 \left(\frac{m l_2}{q \aleph f_2} \right) [v - (q \aleph f_2 \tau_{1m}) / (l_1 m)], \qquad (5c)$$

where l_2 is the length of the second stage (measured normal to the mirror plane) and f_2 is the fraction of \aleph held across the second stage of the mirror (N.B.), the definition of \aleph as the ion source potential means that in a practical mirror $f_1 + f_2 > 1$). The first term in parenthesis represents the acceleration in the second mirror region and the second term is the initial velocity of the ion, less the velocity lost in the first mirror region.

Equations 5a, 5b and 5c can be combined to give the total flight time of an ion in a reflectron (τ) , as a function of the ion's initial axial velocity, its mass, the dimensions of the reflectron and the mirror voltages:

$$\tau(v,L,l_1,l_2,f_1,f_2,\aleph) = \tau_{ff}(L,v) + \tau_{1m}(v,m,l_1,f_1,\aleph) + \tau_{2m}(v,m,l_1,f_1,l_2,f_2,\aleph).$$
 (6)

For historical and pedagogical reasons, τ is usually expanded in terms of τ_0 and ν_0 using (4), and if $f_1 + f_2 \ge 1$, then there will be a set of lengths and voltages such that

$$[\partial \tau / \partial v] = 0 \text{ and } (7a)$$

$$[\partial^2 \tau / \partial v^2] = 0 \,, \tag{7b}$$

where the derivatives are evaluated at v_0 . Equations 7a & 7b are the basis of two-stage reflectron design, because when these conditions are met, the effect of a velocity spread on an ion's arrival time at the detector is minimized. The resulting correction for initial velocity spread is referred to as a "second-order correction". Practically, it is better to solve equation 6 numerically, to achieve a solution for any real ion optics arrangement. In § 4.1 (below), a practical example will demonstrate that the simultaneous solution of equations 7a and 7b leads to a saddle point for a given set of reflectron dimensions, *i.e.*, there is only one possible combination of ion mirror voltages. If the ion velocity distribution is narrow enough that the third term in equation 4 is very small, then equation 7b is no longer significant. A reflectron designed using only equation 7a as a design constraint is referred to as having a "first-order correction". A special case of a first-order instrument is when $f_1 = 0$. The first stage of the mirror no longer affects the flight of the ion and therefore l_1 simply becomes an extension of L_1 and L_2 . The resulting ion mirror is called a single-stage (or one-stage) mirror.

Ion Unimolecular Decomposition

Ions formed in an ion source (i.e., parent ions) may have internal vibrational and electronic excitations caused by the ion formation process. If the ions have sufficient internal energy, unimolecular reactions can occur, resulting in the fission of the ion into two fragments. For singly charged parent ions, one of these fragments will be an ion and the other fragment will be neutral. The time scale for these unimolecular decompositions is often of the same order of magnitude as the transit time of an ion through the mass analyzer. It may be of interest to determine the mass of the fragment ions, if the unimolecular decompositions occur in such a way as to produce fragment ions that are characteristic of the covalent structure of the parent ion. Therefore, it is necessary to determine the effect of unimolecular decomposition during flight.

Linear Analyzers. In a linear analyzer, a unimolecular decomposition has very little effect on the observed mass spectrum. After the ion has left the ion source, it does not experience any external forces until it reaches the detector. Therefore, after the decomposition the center-of-mass of the fragments continues to travel with the same velocity as the parent ion. In the centre-of-mass reference frame, the fragments will have non-zero velocities, depending on the energy released by the unimolecular reaction ζ . If the fragments have masses m_i (ion) and m_n (neutral), then the centre-of-mass velocities of the fragments must satisfy these conditions:

$$m_i \mathbf{v}_{icm} = -m_n \mathbf{v}_{ncm}$$
, and (8a)

$$\zeta = \frac{1}{2}m_{\rm i}|\mathbf{v}_{\rm icm}|^2 + \frac{1}{2}m_{\rm n}|\mathbf{v}_{\rm ncm}|^2$$
 (8b)

The worst possible case would be if the time constant for unimolecular decay $t_d << \tau$, implying that all of the ion decay occurs near the ion source. This results in the axial velocity of an fragment ion being changed by a factor corresponding to the centre-of-mass velocity of the fragment:

$$v_i' = v_i + \mathbf{n} \cdot \mathbf{v}_{icm} , \qquad (9)$$

where n is a unit vector in the direction of the ion optical axis. So long as $v >> |\mathbf{v}_{icm}|$, the effect of the decomposition will be similar to a small velocity distribution added to the ion source velocity distribution. This behavior means that a linear time-of-flight analyzer cannot be used to determine the mass of fragment ions.

Reflectron Analyzers. Unimolecular ion decomposition produces three different effects in a reflectron, depending on where in the analyzer the composition occurs. If the ion fissions in the second field-free region, the effect is analogous to a decay in a linear machine, i.e., a slight broadening of the ion signals. Therefore, decays in the second field-free region cannot be used to determine a fragment ion's mass.

If the ion fissions in either stage of the mirror, then the resulting fragment ions will travel along new trajectories that depend on both the mass of the fragment ion and where the fission occurred. The dependence on the fragment's initial position in the mirror produces a range of flight times for a given m_i, resulting in a very broad signal corresponding to fragment ions with the same mass but different decay positions. These broad peaks could be used to determine the mass of the fragment

ion, but in practice the peaks are of such poor quality (low signal-to-noise ratios and mass resolutions) that they cannot be used analytically.

Ions that decay in the first field-free region have flight times (τ') that can be used to determine the mass of the fragment ions. Assuming that $|\mathbf{v}_{icm}| << v_0$, the flight time of an ion through the first field-free region does not change, regardless of where the fission occurs. Similarly, the flight time through the second field-free region is also unperturbed, because the fragment emerges from the mirror with the same velocity it entered the mirror. Therefore, can be written in the same form as equation 5a and it does not depend on the mass of the fragment:

$$\tau'_{\text{ff}} = (L_1/v) + (L_2/v)$$
. (10a)

The flight time of the fragment ion through the mirror is more complicated, but it only depends on the mass of the fragment ion and not on the position of the fission. If the parent ion's mass is m and the fragment ion's mass is m_i , then let $\mu = [m/m]$. This fraction represents the partitioning of the parent ion's kinetic energy between the fragments: the kinetic energy of a fragment ion is just $m_i \aleph$. This energy partitioning means that some fragment ions will not have sufficient kinetic energy to penetrate through the first mirror region: the ions will be reflected without ever entering the second region. Therefore, the flight-time in the first mirror stage will depend on μ according to the following conditions:

$$\mu < f_1 \implies \tau'_{lm} = \left(\frac{v l_1 \mu m}{f_1 q \aleph}\right) \quad ; \text{ (reflected in 1st region) or}$$

$$\mu > f_1 \implies \tau'_{lm} = 2\left(\frac{l_1 m}{q \aleph f_1}\right) \quad [v - (v^2 - 2q \aleph f_1/(\mu m))^{1/2}]. \quad (10b)$$

A similar set of conditions and equations hold for the second stage of the mirror,

$$\mu < f_1 \implies \tau'_{2m} = 0$$
 ; (reflected in 1st region) or

$$\mu > f_1 \quad \Rightarrow \qquad \tau'_{2m} = 2 \left(\frac{\mu m l_2}{q \aleph f_2} \right) \left[\nu - (q \aleph f_2 \tau_{1m}) / (l_1 \mu m) \right]. \tag{10c}$$

The total flight time can then be written as

$$\tau'(m,\mu) = \tau'_{ff}(m) + \tau'_{1m}(m,\mu) + \tau'_{2m}(m,\mu). \tag{11}$$

Note that the complicated functional dependencies of equation 6 have been eliminated, by requiring the dimensions and voltages to satisfy equations 7a and 7b.

Practical Examples

Figures 3 - 6 illustrate graphically the points made mathematically in the previous section. They represent the expected behavior of a reflectron time-of-flight mass analyzer, for a given solution to the focussing conditions (equations 7a & 7b). The equations were solved numerically, using a commercial algebra and calculus package (Mathcad 3.1, MathSoft Inc., Cambridge, Ma.).

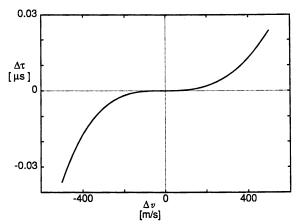


Figure 3 The second-order flight time correction function for a two-stage reflectron. The parameters chosen for this solution are given by the following: $\aleph = 5000 \text{ V}$, m = 10000 u, $f_1 = 0.679$, $f_2 = 0.451$, $L_1 + L_2 = 1.0 \text{ m}$, $l_1 = 0.0100 \text{ m}$ & $l_2 = 0.0668 \text{ m}$.

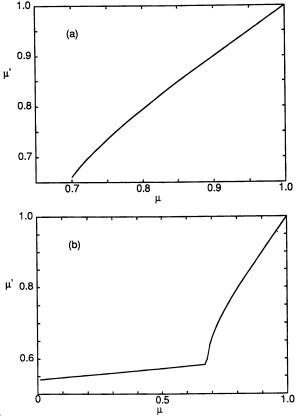


Figure 4 The function relating μ' to μ for the reflectron analyzer defined in the caption of figure 3. Figure 4a is an expansion of the "linear" region of figure 4b.

In Time-of-Flight Mass Spectrometry; Cotter, R.; ACS Symposium Series; American Chemical Society: Washington, DC, 1993.

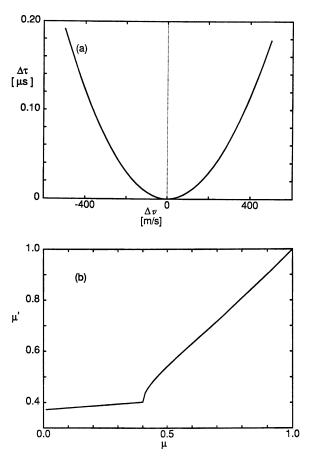


Figure 5 Functions describing the behavior of a first-order, two-stage reflectron, defined by the following parameters: $\aleph = 5000 \text{ V}$, m = 10000 u, $f_1 = 0.400$, $f_2 = 0.730$, $L_1 + L_2 = 1.0 \text{ m}$, $l_1 = 0.0100 \text{ m}$ & $l_2 = 0.145 \text{ m}$. Figure 5a is the flight time correction function and figure 5b relates μ' to μ .

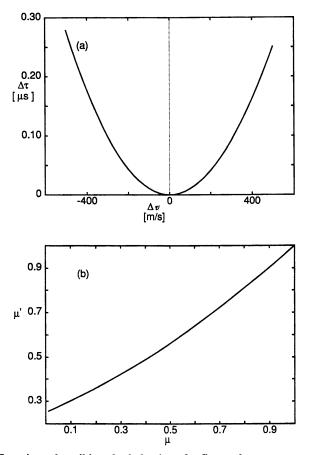


Figure 6 Functions describing the behavior of a first-order, two-stage reflectron, defined by the following parameters: $\aleph = 5000 \text{ V}$, m = 10000 u, $f_1 = 0.000$, $f_2 = 1.130$, $L_1 + L_2 = 1.0 \text{ m}$, $l_1 = 0.000 \text{ m}$ & $l_2 = 0.283 \text{ m}$. Figure 6a is the flight time correction function and figure 6b relates μ' to μ .

A Second-Order, Two-Stage Reflectron. The expected behavior of a second order reflectron is shown in Figures 3 & 4. The dimensions, voltages, ion velocity and mass used to solve the differential equations 7a and 7b are given in the Figure captions. Figure 3 demonstrates the second-order correction produced by the analyzer. The ordinate $\Delta \tau$ represents the deviation in τ produced by a velocity different from v_0 , i.e.,

$$\Delta \tau(v) = \tau(v) - \tau(v_0) . \tag{12}$$

In the vicinity of v_0 , $\Delta \tau \approx 0$, and therefore in this velocity regime, the time-of-flight of an ion depends on its mass, not on its velocity. It is worthwhile to note that there is only one set of dimensions and voltages that will produce this type of curve, once one of the dimensions or voltages has been set (see the dependences in equation 6). Therefore, in practice it is difficult to tune a second-order reflectron to produce a true second-order correction. Additional temporal distributions caused by mechanical tolerances in analyzer dimensions and the finite duration of the ion source pulse usually limit the resolution of the analyzer to a value that is less than predicted by equation 12. To achieve a mass resolution $(m/\Delta m) = 10000$, the distance ions travel (projected onto the ion optical axis) must be the same to within 1:20000 (a machining tolerance of 5 μ m/meter). Achieving mechanical precision to this degree requires detailed consideration of the fine dimensions of all components, particularly the detector's.

The behavior of an ion produced by a unimolecular decomposition in the first field-free region is illustrated in Figures 4a & 4b, for the reflectron defined in Figure 3. In these graphs, the abscissa is μ , defined above as the ratio of the fragment ion's mass to the intact molecule's mass. The ordinate is the ratio of the apparent mass of the fragment ion (as measured by the reflectron) to the intact molecule's measured mass, μ' . The value of μ' was calculated using flight times obtained from equation 11 in the calibration equation (equation 1). Figure 4a shows the behavior for ions that satisfy the second set of conditions in equations 10b and 10c. As expected, the measured mass of the fragment is very close to the true mass of the fragment, because the flight time through the instrument only depends on the mass of the ion (to second order). Figure 4b shows the full range of behavior for ions of any μ . The sharp break in slope that occurs at μ < 0.67 is caused by changing from the second set of conditions in equation 10b & 10c to the first set. Physically, this is caused by the fragment ion having too little kinetic energy to penetrate through the first mirror region. The cusp and different dependencies for μ' produced by the conditional statements in equations 10b and 10c make a second-order reflectron a difficult analyzer to use for the measurement of μ over a wide range of values.

A First-Order, Two-Stage Reflectron. As mentioned in § 2.2, it is not always necessary (or desirable) to solve equations 7a & 7b simultaneously. A reflectron designed using only equation 7a corrects for the velocity distributions produced by many types of ion sources. Relaxing the second constraint also means that there are many possible solutions, rather than the one possible second-order solution.

One of these first-order solutions is illustrated in Figure 5. The shape of Figure 5a can be compared with the second-order case in Figure 3. The range of Δv where $\Delta \tau$ is approximately independent of v is smaller than in Figure 3, but this range is sufficient for many purposes. The behavior of fragment ions is similar to that

shown in Figure 4b, but the cusp has been moved to a lower value of μ , and the approximately linear portion of the curve has been extended. Therefore, this solution to the reflectron equations will be more useful in measuring μ , but only for $\mu > 0.4$. The shallow slope of the curve below 0.4 would make the functional relationship between μ and μ' difficult to use in practice.

A First-Order, One-Stage Reflectron. A special case of the first-order, two-stage reflectron can be found by requiring that $f_1 = 0$ (and therefore $l_1 = 0$). This solution is represented by Figure 6. The velocity distribution correction in Figure 6a is valid for a narrower range of values than the first-order, two-stage solution, but it is still analytically useful. More importantly, the cusp that is present in all two-stage solutions has been eliminated in Figure 6b. The relationship between μ and μ ' can be given analytically:

$$\mu' = \frac{1}{4} + \frac{1}{2} \mu + \frac{1}{4} \mu^2. \tag{13}$$

Equation 12 can be easily rearranged to give an expression for μ in terms of μ ':

$$\mu = 2 \sqrt{\mu' - 1}$$
 (14)

This very simple calibration function, valid for all values of μ (0 - 1) and μ' (0.25 - 1.0), makes the first-order, one-stage reflectron the best choice for determining the mass of fragment ions.

Acknowledgments

I would like to thank Werner Ens, Ken Standing and Ulrich Boesl for many discussions on the design and operation of reflectron mass analyzers.

Literature Cited

- Karataev, V.I.; Mamyrin, B.A.; Shmikk, D.V. Sov. Phys.-Tech. Phys. 1972, 16, 1177.
- 2. Bakker, J.M.B. Int. J. Mass Spectrom. Ion Phys. 1971, 6, 291.
- 3. Poschenrieder, W.P. Int. J. Mass Spectrom. Ion Phys. 1972, 9, 357.
- 4. Mamyrin, B.A.; Shmikk, D.V. Sov. Phys. JETP 1979, 49, 762.
- Gohl, W.; Kutscher, R.; Laue, H.J.; Wollnick, H. Int. J. Mass Spectrom. Ion Phys. 1983, 48, 411.
- 6. Boesl, U.; Grotemeyer, J.; Walter, K.; Schlag, E.W. Anal. Instrum. 1987, 16, 151.
- 7. Grix, R.; Kutscher, R.; Li, G.; Grüner, U.; Wollnick, H. Rapid Comm. Mass Spectrom. 1988, 2, 83.
- 8. Bergmann, T.; Martin, T.P.; Schanber, J. Rev. Sci. Instrum. 1989, 60, 792.

RECEIVED September 16, 1993

Chapter 4

Cluster—Ion Photodissociation and Spectroscopy in a Reflectron Time-of-Flight Mass Spectrometer

K. F. Willey, D. L. Robbins, C. S. Yeh, and M. A. Duncan¹

Department of Chemistry, University of Georgia, Athens, GA 30602

We describe a configuration for a reflectron time-of-flight mass spectrometer incorporating laser photodissociation of mass-selected ions, and the application of this instrument to studies of metal-containing cluster ions. Metal cluster cations and metal-containing ion-molecule complexes are produced in a molecular beam with a pulsed-nozzle cluster source. We describe here details of the instrument operation for studies of these systems. They exhibit novel cluster photochemistry and vibrationally resolved cluster ion spectroscopy. Advantages and disadvantages of this instrument are discussed.

As reflected in this volume, time-of-flight (TOF) spectrometers have many important advantages for modern mass spectrometry. They are ideally suited for experiments employing pulsed laser ionization, ablation, or desorption. multichannel aspect of mass analysis and ion detection allows rapid data acquisition and processing. It is therefore possible to couple TOF devices to instrument systems requiring fast and repetitive on-line analysis. systems have historically had poorer resolution than many other spectrometers, the introduction of the reflectron time-of-flight (RTOF) design has improved resolution so that it is now acceptable for many applications (1-7). Perhaps the greatest advantage of TOF systems is their high mass range. While most magnetic or electrostatic field instruments are restricted to charge-to-mass ratios of less than 10-20 kDa, TOF instruments now routinely detect species in the range of several hundred kDa. This capability is essential for analysis problems involving high molecular weight polymers, biological molecules, or other novel materials.

A serious disadvantage of TOF and RTOF instruments until recently has been the difficulty in utilizing these instruments for tandem mass spectrometry ¹Corresponding author

0097-6156/94/0549-0061\$06.00/0 © 1994 American Chemical Society (MS/MS) (8-14). By dissociation of a selected "parent" ion, and the measurement of its fragmentation spectrum, tandem experiments reveal the molecular sub-units present. Tandem experiments are required in many complex environments in which there are a mixture of possible components and the identity of a particular ion mass cannot be uniquely established. They are also useful in establishing the structure of the parent ion. This latter feature is especially important in biological mass spectrometry, where structural characterization, or "sequencing" of constituents, is a general goal. In the present report, we describe a new configuration for the reflectron time-of-flight instrument which makes tandem TOF measurements more convenient (15). This design uses laser excitation for ion activation. We describe representative studies of the dissociation of metal cluster cations, metal-benzene ion-molecule complexes, and magnesium-CO₂ ion-molecule complexes produced in molecular beam environments. These studies illustrate the capability of the instrument and demonstrate how it may be adapted for other mass spectrometry applications.

Instrument Operation

The molecular beam machine for the experiments here is shown in Figure 1. Ions are produced by laser vaporization in a pulsed nozzle cluster source external to the mass spectrometer. After vaporization and condensation, cluster ions undergo a supersonic expansion in a helium or argon expansion gas. Therefore, these ions are internally cold. After their formation and cooling, the expanded ions are collimated into a beam by a skimmer. The molecular beam passes through the source region of the time-of-flight mass spectrometer about 50 cm downstream from the vaporization/ionization source.

The TOF source region is normally held at ground potential to avoid deflection of the molecular ion beam. When a pulse of cluster ions arrives in the source region, pulsed acceleration plates extract the positive ions from the molecular beam into the time-of-flight tube assembly. For measurements of the distribution of ions and cluster ions produced by the source, the total time-of-flight is measured through the entire reflectron assembly. This mode of operation is entirely similar to that used in previous experiments in other laboratories, where the reflectron is employed to achieve improved resolution in the time-of-flight measurement.

Figure 2 shows a representative cluster ion distribution measured in this way for magnesium - CO_2 ion-molecule cluster complexes. To obtain this spectrum, we vaporize a magnesium rod sample using a pulsed expansion of pure CO_2 or CO_2 in argon. As shown, mass peaks of the form $[Mg(CO_2)_N]^+$ are the main features observed in the mass spectrum. The ionization potential of magnesium is about 7.6 eV, while that of CO_2 is 13.5 eV. We therefore expect that the charge in these clusters is localized on the metal ion, i.e. $Mg^+(CO_2)_N$. The photodissociation experiments and ion spectroscopy experiments described below confirm this expectation. By varying the choice of the metal which is vaporized, the expansion gas used, and the nozzle geometry employed, we can produce cluster distributions similar to this for a variety of pure metal systems (M_N^+) or metal-molecular systems (M^+-R_N) .

The primary application for the reflectron system in our laboratory is laser

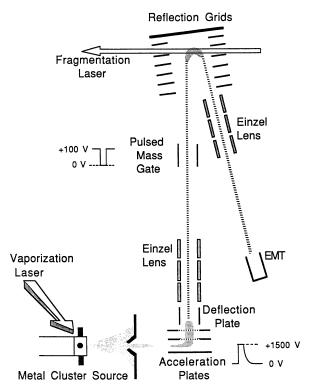


Figure 1 - The reflectron time-of-flight mass spectrometer configuration used for mass-selected photodissociation experiments.

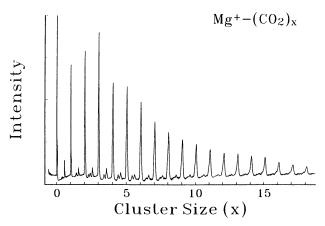


Figure 2 - The distribution of ${\rm Mg}^+-({\rm CO}_2)_{\rm X}$ clusters produced by laser vaporization of magnesium in a pure ${\rm CO}_2$ expansion.

photodissociation of these metal containing cluster ions to explore their structures and bonding properties. For these experiments, we have developed a configuration to introduce the laser into the reflectron system to photoexcite mass-selected ions (15). In this design, ions are extracted from the molecular beam as described above. The time-of-flight in the first section of the drift tube is used to achieve mass selection of the desired ion. This is accomplished with pulsed deflection plates, which transmit one mass at a time, and are located just prior to the reflection field. Ions other than the selected mass arriving at a particular time are deflected from the trajectory to the detector by these plates. Laser excitation of the selected ion takes place at the turning point in the ion trajectory in the reflecting field. Following excitation, the undissociated parent ion and any resulting photofragment ions are reaccelerated out of the reflection field into the second flight tube section. The time-of-flight through this section provides the analysis of the fragment ion masses.

This design is different from previous ones for photodissociation in linear TOF instruments (8-10) and from previous configurations used for reflectron TOF instruments (11-14). It has two advantages. First of all, ions are excited with the laser at the turning point in their trajectory, where their motion is slowest. The typical time window in the excitation region is 2-3 usec. Therefore, intersecting the ion beam with a pulsed laser (5 nanosecond pulsewidth) is less critical than it is in designs where fast (kilovolt) ions are excited with a similar pulsed laser. Secondly, fragment ions are formed at the deepest point in the reflectron field so that they all can follow similar trajectories down the second flight tube to the detector. In other designs, where fragmentation occurs before the reflecting field, each different fragment follows a unique trajectory through the reflecting field. The field applied to the reflectron needs to be adjusted to transmit each fragment ion to the detector, and only a narrow mass region is focused at any one setting. In our design, all fragments can be detected on every laser shot, and the long second drift section (1.2 meter) provides good fragment mass resolution.

The disadvantage of this design is that the exact shape of the ion beam in the excitation region is not generally known and is highly dependent on the particular instrument design. It is necessary to know the overlap of the laser with the ion beam to measure absolute dissociation cross sections. As we have described previously, there may be some mass discrimination in this configuration, depending on the experimental conditions and instrument design (15). Careful attention to these details is required to obtain good results.

Pure Metal Clusters

Photodissociation of a variety of pure metal cluster ions and alloy cluster ions have been described by our research group (15-19). Figure 3 provides two selected examples which illustrate the general kinds of mechanisms we observe. In the upper spectrum, we show the dissociation spectrum at 308 nm of the Pb_{17}^+ parent ion, which produces a series of fragments in the N=6-10 range. More extensive fragmentation is observed at higher laser power, when multiphoton absorption becomes efficient. Excitation at other energies, or at other cluster sizes near N=17 produce similar fragmentation spectra, with the fragment series

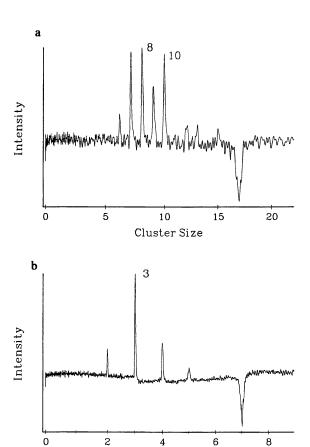


Figure 3 - a) The photodissociation mass spectrum of the Pb_{17}^{+} cluster obtained at 308 nm. The parent ion depletion is plotted negative, while fragment ions are plotted in the positive direction. b) The photodissociation mass spectrum for Bi_7^{+} at 308 nm.

Cluster Size

shifting according to the conditions. In other words, there are no "magic number" fragments for this system. This lead cluster system has been studied in detail in our lab, allowing the general mechanism of photodissociation to be inferred. This mechanism appears to be sequential loss of atoms, i.e., "evaporation," whose extent is determined by the average binding energy of atoms in the cluster and the energy deposited by the excitation. Interestingly, the Pb₁₇⁺ cluster described here is one of the highest molecular weight species ever studied with mass-selected laser photodissociation (3522 amu), and it illustrates the capability of our instrument for studies of large molecules.

Another photodissociation mechanism is illustrated by the ${\rm Bi_7}^+$ spectrum also shown in Figure 3. The ${\rm Bi_3}^+$ fragment ion is formed preferentially at all laser energies studied. Other bismuth cluster parent ions in the N=4-9 size range all produce the N=3 cation as their most prominent fragment. Unlike the lead system above, fragmentation here appears to be dominated by the preferential formation of an especially stable product ion. A similar fragmentation mechanism, driven by formation of a stable cation, has been observed for antimony (16), silicon (8), and several other main group cluster systems. In a way closely related to this, several cluster systems fragment by loss of a stable neutral from many cluster sizes. For example, small carbon cations (8) lose C_3 and small tellurium cations (17) lose Te_4 . Clearer patterns are recognizable in alloy cluster systems of the group IV-group V metals (e.g., Pb/Sb), where preferential cluster sizes and stoichiometries are eliminated in dissociation (19).

Unfortunately, neither of these general photodissociation mechanisms lends itself to easy interpretation of the detailed structure and bonding in these clusters. Especially stable cluster sizes can be identified, but their structures can only be guessed. Analysis of the energy dependence of cluster atom evaporation may be used to estimate the average dissociation energies, but these attempts are frustrated by various experimental problems. One prevalent one is multiphoton absorption, which is difficult to eliminate in these strongly absorbing systems.

Metal-Molecular Complexes

Metal-molecular cluster complexes containing a variety of metal ions surrounded by small molecules have been produced in a number of laboratories using the same molecular beam technology used to produce pure metal clusters. These systems are interesting as models for the fundamental interactions in metal-ligand bonding, metal ion solvation, and adsorption on metal Photodissociation experiments, as described below, have been able to probe the energetics of bonding in these systems and their spectroscopy. Photodissociation mechanism are potentially more varied in metal-molecular complexes than they are in pure metal systems. The chromophore on which excitation occurs may be the metal center or the molecular species. The bond-breaking may also occur at the metal center (if there are more than one metal atom present), on the ligand(s), or between the metal and ligand(s). Intracomplex rearrangements/reactions are also possible. As indicated below, our initial studies have already revealed some of the variety of behavior anticipated for these systems.

Photodissociation of metal-benzene cluster complexes reveals a previously unrecognized process for gas phase metal systems - "dissociative charge transfer" (20). This process is illustrated in Figure 4 for the Fe⁺-benzene system. As indicated, excitation at low energy (wavelengths to the red of 280 nm) produce simple cleavage of the metal ion-benzene bond, yielding the Fe⁺ product ion. At higher energies, a second channel corresponding to the benzene cation is observed. Since the parent ion has been mass selected, this channel must arise from the following dissociation process:

$$Fe^+-C_6H_6 + h\nu \rightarrow Fe + C_6H_6^+$$

As indicated, the complex has broken the metal-ligand bond and transferred the charge from the iron atom to benzene. Formation of the benzene ion cannot occur on the ground state potential surface because the ionization potential of benzene (9.24 eV) is greater than that of iron (7.87 eV). This process must instead occur on an excited electronic surface corresponding to a charge-transfer electronic state. While charge-transfer electronic transitions are well-known in condensed phase inorganic chemistry, this process had not been observed in a gas phase ion complex prior to our studies.

We have now observed that dissociative charge transfer plays an important role in essentially all metal-benzene complexes, and, indeed, in nearly all metal-organic complexes we have studied. In order for this process to be observed, the excitation laser energy must exceed the ground state dissociation energy (D_0'') of the complex and the ionization potential difference (Δ IP) between the metal atom and the ligand molecule. Therefore, charge transfer dissociation processes are expected for different metal complexes in different regions of the UV-visible spectrum. Large Δ IP values or large dissociation energies shift the threshold for this process to higher energy. Conversely, if the threshold for the dissociative charge transfer process can be measured, an upper limit on the dissociation energy of the complex can be determined:

$$D_0'' \leq h v_{CT} - \Delta IP$$

We have used this method to obtain upper limits on the dissociation energies of Ag⁺-benzene (30.1 kcal/mol), Fe⁺-benzene (62.1 kcal/mol), and Mg⁺-benzene (26.9 kcal/mol) (20). Strictly speaking, these are only upper limits to the true values. However, comparisons to other experiments and to theoretical calculations indicate that the values determined by this method are in fact quite close to the actual dissociation energies. This is significant, because the photodissociation method is far more generally applicable than other "exact" methods for determining metal-ligand binding energies. Consequently, the values we have already determined represent a sizable fraction of all such energetic data which is available.

Magnesium- CO_2 complexes illustrate two other significant aspects of the photodissociation dynamics of metal-molecular complexes which we have observed. As shown in Figure 2, clusters of the form Mg^+ - $(CO_2)_N$ may be formed containing multiple CO_2 molecules. Because of the large IP difference between magnesium and CO_2 , these species have the charge localized on the

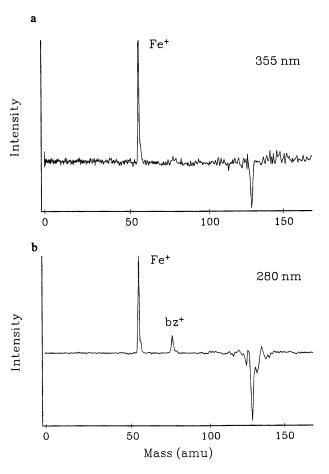


Figure 4 - ${\rm Fe}^+$ -benzene photodissociation at 355 nm (a) and 280 nm (b). Charge transfer dissociation only occurs at the shorter wavelength.

metal atom. The binding in these system has been predicted (21) to be purely electrostatic, and therefore these complexes may resemble "solvated" metal ions in a "microsolvent" environment. Photodissociation of these complexes takes place by successive evaporation of solvent species. This behavior is shown in Figure 5, where the photodissociation mass spectrum of Mg⁺-(CO₂)₇ is shown. At the excitation wavelength studied (280 nm), evaporation of about five CO₂ molecules takes place on the timescale of the experiment. However, this data also indicates another more interesting photodissociation product corresponding to formation of MgO⁺-(CO₂)₂. Careful studies show that this fragment channel results from an "intracluster" reaction in the excited state of the ion-molecule complex,

$$Mg^{+}(CO_{2})_{7} + h\nu \rightarrow Mg^{+*}(CO_{2})_{7} \rightarrow MgO^{+}(CO_{2})_{6}CO$$

 $\rightarrow MgO^{+}(CO_{2})_{2} + 4CO_{2} + CO$

Carbon dioxide molecules do not absorb at the energy of excitation here (280 nm), but the solvated magnesium ion does. The chromophore for the chemistry is the ${}^2S \rightarrow {}^2P$ atomic resonance line, which occurs in isolated Mg⁺ at 279 nm. The reaction of CO₂ with magnesium is endothermic in the ground state, but the excitation which places the lone valence electron into an excited p orbital provides enough electronic energy to initiate the reaction. This reaction is efficient in all magnesium/CO₂ complexes which we have studied (up to N=10).

A final aspect of photodissociation experiments made possible by the reflectron system in our laboratory involves the study of ion spectroscopy. Ions only photodissociate at wavelengths at which they absorb light. Therefore, it is possible to measure the fragment ion yield as a function of the excitation wavelength to map out the ion absorption spectrum. We have done this for several pure metal cluster ions and for metal ion-molecule complexes. The ${\rm Mg}^+$ - ${\rm CO}_2$ ion illustrates the kind of information which can be obtained.

 ${
m Mg}^+{
m -CO}_2$ has been the subject of *ab initio* calculations by Bauschlicher and coworkers which have predicted the structure of the complex in both its ground and excited electronic states (21). The bonding is predicted to result from charge-quadrupole interactions, which produces a linear structure in both the ground and excited states. In the ground state, the interaction between the ${
m Mg}^+({}^2{
m S})$ state and the ${
m CO}_2$ molecule in a colinear arrangement results in a ${}^2{
m E}^+$ complex state. In the first excited state, however, the ${
m Mg}^+({}^2{
m P})$ state can interact with the ${
m CO}_2$ in two ways. One arrangement has the excited p orbital perpendicular to the molecular axis, while the other has the p orbital along the axis. These arrangements result in two electronic states, the ${}^2{
m II}$ and ${}^2{
m E}$ states, respectively. Since it has the positive core of the ${
m Mg}^+$ exposed to the ${
m CO}_2$ quadrupole, the ${}^2{
m II}$ state is more strongly bound than either of the ${}^2{
m E}$ states (ground or excited). The ${}^2{
m E} \rightarrow {}^2{
m II}$ transition is therefore predicted to be red shifted with respect to the atomic resonance line, lying in the 340 nm region.

When we tune our photodissociation laser into the wavelength region where absorption is predicted for this $^2\Sigma \rightarrow ^2\Pi$ transition, we find a strong dissociation signal (22). Tuning the laser while monitoring the Mg⁺ fragment ion produces a structured spectrum, as shown in Figure 6. This spectrum consists of

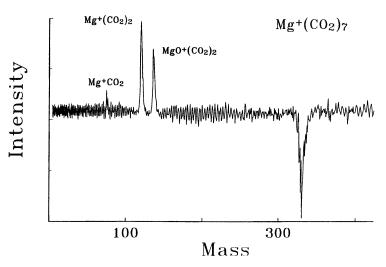


Figure 5 - The photodissociation mass spectrum of ${\rm Mg}^+({\rm CO}_2)_7$ at 280 nm, showing the ${\rm Mg}^+({\rm CO}_2)_2$ and ${\rm MgO}^+({\rm CO}_2)_2$ fragmentation channels.

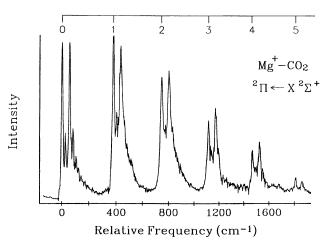


Figure 6 - Photodissociation spectroscopy of the $^2\Sigma^+ \rightarrow ^2\Pi$ electronic transition in Mg $^+$ -CO $_2$. The origin is at 26,625 cm $^{-1}$ (337.6 nm).

about a dozen peaks, with a pattern of doublets spaced by about 50 cm⁻¹ in a progression with spacings of about 380 cm⁻¹. This spectrum has been discussed in detail elsewhere (22). It is assigned to a progression in the metal-CO₂ stretching mode with an excited state frequency of 382 cm⁻¹. The 50 cm⁻¹ doublets arise from the spin-orbit splitting in the excited ²II state. This structure and vibrational frequency are completely consistent with the predictions of theory, confirming that this complex is indeed linear.

The observation of an extended progression in the metal-molecular stretching coordinate makes it possible to investigate the bonding energy in this complex. We fit the progression to a Morse potential in the excited state with an excited state well depth of 11,194 cm⁻¹ (32.0 kcal/mol). Using this number with the measured origin of the electronic transition and the known energy of the atomic resonance line in the isolated Mg⁺, we are able to derive the ground state bond energy of 14.7 kcal/mol. This is in good agreement with the *ab initio* prediction of 16.4 kcal/mol (21). This is the first time that the binding energy in a metal ion-molecular complex has been determined spectroscopically.

Conclusion

We have described a new configuration of a reflectron time-of-flight mass spectrometer system which makes it possible to achieve mass selected laser photodissociation on a variety of metal cluster ions. Dissociation dynamics, energetics, and ion spectroscopy can be studied with this device. While the focus here is on metal cluster ions produced in molecular beam experiments, the design concepts described here are general. For example, we have already incorporated these ideas into a reflectron system for matrix-assisted laser desorption of biological molecules. This system is in operation, and initial photodissociation experiments are being attempted. This system and others like it have exciting potential for the study of mass spectrometry and tandem mass spectrometry on large molecules.

Acknowledgements

The research described in this paper is supported by the National Science Foundation (metal complexes), the Air Force Office of Scientific Research (metal complexes), and the U.S. Department of Energy (pure metal clusters). We gratefully acknowledge the support from these agencies.

Literature Cited

- Mamyrin, B.A.; Karataev, V.I.; Shmikk, D.V.; Zagulin, V.A. Zh. Eksp. Teor. Fiz. 1973, 64, 82.
- Boesl, U.; Neusser, H.J.; Weinkauf, R.; Schlag, E.W. J. Phys. Chem. 1982, 86, 4857.
- 3. Lubman, D.M.; Bell, W.E.; Kronick, M.N. Anal. Chem. 1983, 55, 1437.
- 4. Kuehlwind, H.; Neusser, H.J.; Schlag, E.W. Int. J. Mass Spectrom. Ion Phys. 1983, 51, 25.
- 5. a) Kuehlwind, H.; Neusser, H.J.; Schlag, E.W. J. Phys. Chem. 1984, 88,

- 6104. b) Kuehlwind, H.; Neusser, H.J.; Schlag, E.W. J. Phys. Chem. 1985, 89, 5600.
- 6. Martin, T.P.; Bergmann, T.; Gröhlich, H.; Lange, T. J. Phys. Chem. 1991, 95, 6421.
- 7. Bergman, T.; Martin, T.P.; Schaber, H. Rev. Sci. Instr. 1989, 60, 347; <u>ibid</u>, 792.
- 8. a) Bloomfield, L.A.; Freeman, R.R.; Brown, W.A. Phys. Rev. Lett. 1985, 50, 2246. b) Bloomfield, L.A.; Geusic, M.E.; Freeman, R.R.; Brown, W.A. Chem. Phys. Lett. 1985, 121, 33. c) Geusic, M.E.; McIlrath, T.J.; Jarrold, M.F.; Bloomfield, L.A.; Freeman, R.R.; Brown, W.A. J. Chem. Phys. 1986, 84, 2421. d) Geusic, M.E.; Jarrold, M.F.; McIlrath, T.J.; Freeman, R.R.; Brown, W.A. J. Chem. Phys. 1987, 86, 3862.
- 9. Brucat, P.J.; Zheng, L.S.; Tittel, F.K.; Curl, R.F.; Smalley, R.E. J. Chem. *Phys.* **1986**, *84*, 3078.
- 10. Liu, Y.; Zhang, Q.L.; Tittel, F.K.; Curl, R.F.; Smalley, R.E. J. Chem. Phys. 1986, 85, 7434.
- a) Alexander, M.L.; Levinger, N.E.; Johnson, M.A.; Ray, D.; Lineberger, W.C. J. Chem. Phys. 1988, 88, 6200. b) Levinger, N.E.; Ray, D.; Alexander, M.L.; Lineberger, W.C. J. Chem. Phys. 1988, 89, 5654.
 c) Papanikolas, J.; Gord, J.R.; Levinger, N.E.; Ray, D.; Vorsa, V.; Lineberger, W.C. J. Phys. Chem. 1991, 95, 8028.
- 12. Posey, L.A.; Johnson, M.A. J. Chem. Phys. 1988, 89, 4807.
- Grotemeyer, J.; Boesl, U.; Walter, K.; Schlag, E.W. J. Am. Chem. Soc. 1986, 108, 4233.
- 14. Tembreull, R.; Lubman, D.M. Anal. Chem. 1986, 58 1299.
- 15. a) LaiHing, K.; Cheng, P.Y.; Taylor, T.G.; Willey, K.F.; Peschke, M.; Duncan, M.A., *Anal. Chem.* 1989, 61, 1458. b) Cornett, D.S.; Peschke, M.; LaiHing, K.; Cheng, P.Y.; Willey, K.F.; Duncan, M.A., *Rev. Sci. Instrum.* 1992, 63, 2177.
- 16. Geusic, M.E.; Freeman, R.R.; Duncan, M.A. J. Chem. Phys. 1988, 88, 163.
- 17. Willey, K.F.; Cheng, P.Y.; Taylor, T.G.; Bishop, M.B.; Duncan, M.A. J. Phys. Chem. 1990, 94, 1544.
- 18. Taylor, T.G.; Willey, K.F.; Bishop, M.B.; Duncan, M.A. J. Phys. Chem. 1990, 94, 8016.
- 19. LaiHing, K.; Willey, K.F.; Taylor, T.G.; Duncan, M.A. J. Phys. Chem., submitted.
- a) Willey, K.F.; Cheng, P.Y.; Pearce, K.D.; Duncan, M.A., J. Phys. Chem. 1990, 94, 4769. b) Willey, K.F.; Cheng, P.Y.; Bishop, M.B.; Duncan, M.A., J. Am. Chem. Soc. 1991, 113, 4721. c) Willey, K.F.; Yeh, C.S.; Robbins, D.L.; Duncan, M.A. J. Phys. Chem. 1992, 96, 9106.
- a) Bauschlicher, C.W.; Partridge, H., J. Phys. Chem. 1990, 95, 3946. b)
 Bauschlicher, C.W.; Partridge, H., Chem. Phys. Lett. 1991, 181, 129. c)
 Sodupe, M.; Bauschlicher, C.W.; Partridge, H., Chem. Phys. Lett. 1992, 192, 185. d)
 Bauschlicher, C.W., private communication.
- a) Willey, K.F.; Yeh, C.S.; Robbins, D.L.; Duncan, M.A., Chem. Phys. Lett. 1992, 192, 179. b) Yeh, C.S.; Willey, K.F.; Robbins, D.L.; Duncan, M.A. J. Phys. Chem. 1992, 96, 7833.

Chapter 5

Tandem Time-of-Flight Mass Spectrometry

A Magnetic Sector—Reflectron Time-of-Flight Mass Spectrometer

F. H. Strobel and D. H. Russell

Department of Chemistry, Texas A&M University, College Station, TX 77843

A magnetic sector (EB)/reflectron time-of-flight (R-TOF) is described with emphasis on the method of data acquisition. This chapter covers the basic instrumentation used for the EB/R-TOF development, the general requirements of the tandem TOF experiment, and the use of the instrument for fundamental studies. Clusters of the type [B---H⁺---B'] formed by Cs⁺ ion desorption ionization of a mixture of glycerol (B) and nitroaniline, (B') are used to demonstrate pulsed laser photodissociation experiments. Such experiments are designed to probe H⁺-transfer reactions of electronically excited molecules. Metastable ion spectra of ions formed by laser desorption are used to demonstrate tandem mass spectrometry of ions formed by pulsed ionization methods.

Structural biological mass spectrometry is synonymous with tandem mass spectrometry. The major advances in the field of biological mass spectrometry can be traced to the development and evolutionary improvements in ionization methods such as field desorption (FD) (1), 252 Cf-PDMS (2), fast-atom bombardment (FAB) (3), particle beam methods (4), thermo-spray (5), electrospray (6), and matrix-assisted laser desorption (7). Similarly, the progress realized in structural biological mass spectrometry have paralleled developments in tandem mass spectrometry. complexity of biological samples, in terms of purity, complicates the assignment of ions in the mass spectrum in terms of fragment ions of the analyte. Also, desorption ionization methods cause considerable sample degradation and the products of the degradation process contribute to the mass spectrum, but such fragments may not yield useful structural information about the analyte. In fact, it can be very difficult to distinguish between real signal (signals due to the analyte or fragment ions of the analyte) and noise (signals that are due to impurities and degradation processes). Tandem mass spectrometry can provide unambiguous identification of the fragment ions because representative ions of the intact molecule, [M+H]⁺, [M+Na]⁺, [M-H]⁻, etc., are activated to energies above the dissociation threshold, and the product ions are then mass-analyzed by MS-II.

> 0097-6156/94/0549-0073\$06.50/0 © 1994 American Chemical Society

At precisely the point in the development of tandem mass spectrometry where real biology, molecular biology, and biochemistry problems can be tackled currently available state-of-the-art instrumentation limits further developments. That is, the ionization methods are now sufficiently developed that virtually any class of biomolecule can be formed as a gas phase ionic species (8). The very best tandem mass spectrometers can be used for studies of molecules up to approximately m/z 10,000; however, the activation methods most widely used, e.g., collision-induced dissociation (CID), has a very low yield of structurally significant fragment ions, especially for analytes with molecular weights of approximately 2500 daltons or greater (9). Consequently, the usual protocol for structural mass spectrometry of large molecules (say MW > 2500-3000 daltons) involves degradation (enzymatic) of the analyte, separation of the molecular fragments with mass spectrometric analysis of the molecular fragments (10). Alternatively, ESI which produces multiple-charged ionic forms of the intact molecule can be combined with tandem mass spectrometry (11). As with any emerging technology it is too early to predict the final developments and how much difficulty will actually be encountered in the overall development of ESI/TMS.

Lasers play an increasingly important role in biological mass spectrometry (12), but it is clear that optimum utilization of lasers for structural biological mass spectrometry requires considerable instrument development. Tandem mass spectrometers designed specifically to take advantage of laser experiments to probe the structure of large molecules possess enormous potential, but virtually all the tandem mass spectrometry instruments commercially available are designed for CID, and adapting these instruments to pulsed laser experiments is far from trivial (13). The ideal structural biological mass spectrometry instrument would be capable of analysis of molecules with molecular weights of 5,000-500,000 daltons, but the development of structural probes of large molecules is just now emerging; we know nothing about the energy requirements for dissociation of such large molecules. There are even questions as to whether such large molecular systems can be adequately described by RRKM theory (14).

Until very recently the idea of performing structural mass spectrometry on large molecules appeared highly unlikely. Recent developments in ESI and MALDI demonstrate that relatively large populations of ionic, intact high molecular weight biomolecules can be produced with relative ease. Given that sufficiently large numbers of ions can be produced, the question becomes how do we tackle the problem of activating the ionic molecules to energies above the "dissociation threshold?" Another equally important question, however, is what information is sought from such studies? The objective of most tandem mass spectrometry studies of biomolecules is primary structure, but clearly the fragmentation of large biomolecule is influenced by secondary or higher order structure (15). Although recent studies on surface-induced dissociation (SID) suggest that large amounts of internal energy can be deposited into ionic systems by such methods (most probably by multiple collisions with the surface atoms), the instrumentation required to produce analytically useful data on large ionic molecules is equally as cumbersome as that required for CID studies. Another factor to consider is what type(s) of instruments are compatible with structural mass spectrometry of large molecules. In the authors view the leading candidates are rf-ion traps (16), Fourier-transform ion cyclotron resonance (FTICR) (17), and tandem time-of-flight (TOF) instruments (18).

The activation method of choice for studies involving large molecules is photodissociation, and the preferred laser wavelengths for photodissociation are 266 nm, 193 nm, and 118 nm. These wavelengths are useful because aromatic amino acid residues absorb strongly at 266 nm, the amide bond absorbs strongly at 193 nm, and the C-C framework strongly absorbs at 118 nm. In addition, the energy provided by each photon corresponds to 4.7 eV, 6.3 eV, and 10.5, respectively, an amount of energy that should dissociate the ionic molecule by either single- or multiphoton processes.

The objective of performing photodissociation on a large ionic molecule places serious demands on instrument technology. For example, a single laser shot (MALDI) can yield 10⁴-10⁶ ions. If the photodissocation efficiency is 10⁻⁵ that means that from an ensemble of 10⁶ ions only 10 photofragment ions are produced. Clearly, the experiment requires sensitivity that can only be achieve by single ion correlation methods. Thus, the experimental methods we have chosen for developing large molecule structural mass spectrometry is tandem TOF. The work described in this chapter is intended to survey the current level of development of this field. Our work in this area began by developing a hybrid magnetic sector/TOF tandem instrument. The objectives of this work were to evaluate various designs of the TOF that would be useful for the research and a convenient method for preparing the ions for development of MS-II. This chapter reviews the design of the instrument and demonstrates the experiment and operation modes of the apparatus.

Tandem Time-of-Flight Instruments

Time-of-Flight (TOF) mass spectrometry has several advantages that can be exploited for expanding the scope of tandem mass spectrometry. These advantages include single ion counting which can increase the sensitivity, compatibility with pulsed ionization/excitation techniques, and unlimited mass range. In recent years there has been growing interest in developing tandem TOF mass spectrometry. For example, Enke and coworkers have described a mass spectrometer that simultaneously measures momentum (magnetic analyzer) and velocity (TOF) of ions, and they demonstrated this method can be used to acquire normal mass spectra as well as collision-induced dissociation (CID) spectra (19). Glish and co-workers developed a tandem quadruple/TOF instrument and demonstrated the utility of the instrument for tandem mass spectrometry experiments (20). The reported data on the quadruple/TOF instrument was comparable (in terms of mass resolution) to data obtained with a mass-analyzed ion kinetic energy (MIKES) spectrometer.

Several research groups are now working on developing tandem TOF instruments for performing studies that ranges from cluster chemistry to biological applications (21). The work performed to date on such instruments clearly illustrate the high performance capabilities and an analytically useful range of sensitivities. On the basis of this early work it is quite clear that TOF methods will play an increasingly important role in tandem mass spectrometry. However, it is equally clear that new instrument concepts and new experimental methods will evolve and improve both performance and sensitivity of the instruments.

The early tandem TOF instruments utilized linear TOF, and there are distinct advantages for using reflectron TOF mass analyzer. The most frequently cited

advantage of R-TOF is the improved mass resolution, e.g., mass resolution of 35,000 has been demonstrated with an R-TOF. R-TOF instruments also provide an excellent means for performing tandem mass spectrometry experiments. Because the R-TOF functions in the same manner as an sector type electrostatic energy analyzer, e.g., ions having different kinetic energies follow different trajectories through the electric field, ions formed by dissociation in the field-free region leading to the reflectron will have different resident times in the reflectron. Thus, energy dispersion measurement is obtained by measuring the flight time of the ion through the reflectron. LeBeyec and coworkers developed a neutral-ion correlation method to acquire metastable ion mass spectra using a R-TOF instrument (22). The neutral-ion correlation method has been extensively used by Standing (23) for studying metastable ion dissociation reactions of ions formed by Cs+-SIMS and we recently reported on the development of a magnetic sector (EB)/ R-TOF tandem mass spectrometer that also used this method for data acquisition (18). The magnetic sector instrument provides a highly collimated beam of mass selected ions. The mass resolution of the MS-I exceeds 100,000. In addition, the use of a highly collimated ion beam simplifies the alignment procedure for laser-ion beam photodissociation. This instrument can also be used for performing keV energy collision-induced dissociation. The ability of the instrument to be used with continuous ionization sources has been demonstrated (24). This chapter focuses on the use of the instrument for performing tandem mass spectrometry with pulsed ionization (matrix-assisted laser desorption ionization (MALDI) and Cs⁺ ion gun) and photodissociation by using pulsed lasers. The first application will involve photodissociation using a pulsed N₂ laser and a pulsed Nd:YAG laser. The second experiment will involve the use of a N₂ laser for performing tandem mass spectrometry on ions formed by matrix-assisted laser desorption.

Description of the EB/R-TOF Instrumentation

The tandem magnetic sector (EB)/reflectron time-of-flight (TOF) instrument is shown in Figure 1 and a schematic representation of the apparatus is shown in Figure 2. The instrument consists of a Kratos MS-50 and a home-built R-TOF (MS-II). The instrument is equipped with a 30 keV Cs⁺ ion gun (Phasor Scientific) that has been modified to operate in continuous or pulse modes, an excimer laser (Questek model 2440) for performing pulsed laser desorption ionization and/or laser-ion beam photodissociation, and a Laser Science, Inc. cartridge type N₂ laser (model VSL 337 and VSL 337ND) that can be used for either ionization or photodissociation. TOF spectra can be obtained by using a time-to-digital converter (TDC) (LeCroy model 4208 TDC), a 350 Mhz digital oscilloscope (LeCroy model 9450), or a CAMAC transient recorder (LeCroy model TR8828D 200 MHz digitizer). All of the TOF data acquisition modules are interfaced to PC/AT computers by using a National Instruments GPIB mainframe card. Event sequences for the various experiments are controlled by an EG&G Princeton Applied Research digital delay generator (model 9650).

The R-TOF has a total flight path of 2 meters and the reflection angle is approximately zero degrees (25). The advantages of a collinear reflectron are high ion transmission and high mass resolution in comparison to that obtained with larger (5°-20°) reflecting angles. The collinear arrangement is also convenient for positioning detectors to detect both neutrals and ions. For example, neutrals formed

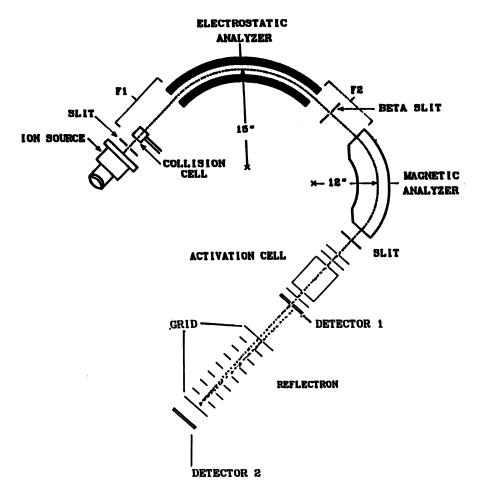


Figure 1. Diagram of the tandem magnetic sector/reflectron time-of-flight mass spectrometer.

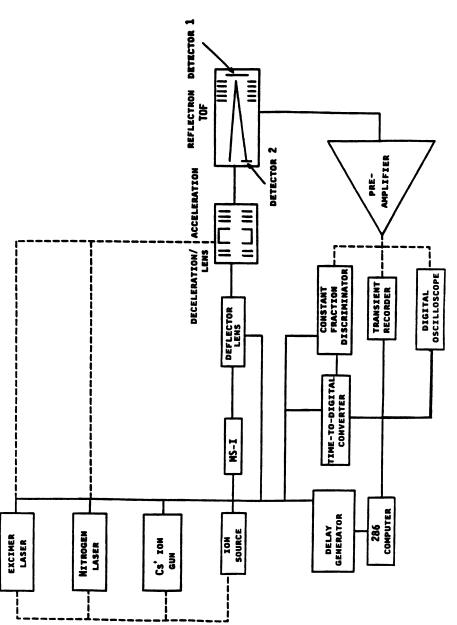


Figure 2. Schematic representation of the EB/R-TOF instrument.

by metastable ion dissociation reactions, collision-induced dissociation (CID), or photodissociation in the region between MS-I and MS-II are detected by a microchannel plate detector (detector #1) positioned behind the reflectron. Ions are detected by the microchannel plate detector (detector #2) positioned at the entrance to the R-TOF. The reflector assembly is 40 cm in length and composed of 33 electrodes that have a 7 cm inner diameter. The front plate of the reflectron is a grid with 98% transmission. A linear electric field gradient in the reflectron is produced by a resistor bridge placed in the vacuum system. The R-TOF vacuum is maintained by a 60 l per second turbo molecular pump.

Most reflectrons are classified as either single-stage or two-stage reflectrons depending on the number of linear electric field gradients used in the reflector. The choice of single-stage or two-stage reflectron is usually based on the desired operation of the device. For example, two-stage reflectrons are preferred for high resolution measurements. Typically such measurements are performed on ions having a relatively narrow range of kinetic energies. The criteria we used in the designing of the tandem R-TOF are (i) the collection efficiency of the neutrals formed by chargeexchange and/or dissociation of the mass selected ion, (ii) the collection efficiency of all products ions which are formed by decay in the field-free region, and (iii) the ability to separate (in time) all the product ions formed by unimolecular dissociation in the field free region (26). The design of reflectrons used for high resolution mass measurements of ions formed by direct ionization in the ion source are not satisfactory for product ions formed by dissociation in the field-free region because the fragmentation ions have a broad range of kinetic energies. In particular, two-stage and gridless single-stage reflectrons have limited kinetic energy ranges. A non-grided reflectron can improve the collection efficiency for ions having a relatively small distribution of kinetic energies, but the non-grided reflectron has a low transmission efficiency for ions having a large range of kinetic energies. The two-stage reflectron provides high resolution for a small range of kinetic energies; however, ions with significantly lower kinetic energies are not separated because they do not penetrate into the region of the reflectron, which have small electric gradient (27). Therefore, for broad band tandem MS experiments, a grided single-stage reflectron is preferred.

Data Acquisition

Several data acquisitions methods can be used for obtaining tandem mass spectra using the EB/R-TOF, e.g., pulsed Cs⁺-liquid SIMS with TDC, laser desorption using a transient recorder; however, each of these methods has some limitations. In order to achieve the desired sensitivity and resolution with a R-TOF, the ions must be formed with an infinitely short pulse (1-10 ns) and yield sufficient numbers of ions to accumulate a statistically significant number of product ions. Although pulse widths of 1-10 nanosecond can be obtained by rastering a conventional Cs⁺ ion gun across a small slit (28), this mode of operation requires summing a large number of events (10⁴ or greater) to obtain a complete mass spectrum. Because the efficiency of CID of large molecules is quite low, ranging from a few percent to 0.1-0.5%, an even larger number of ionization events would be required to acquire tandem mass spectral data. If the CID efficiency is 0.1%, 10⁷ primary ions or greater would be required to yield a significant number (10³-10⁴) of product ions. This is further complicated by the partitioning of the ions to the available reaction channels. In

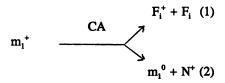
addition, as the ion yield or CID efficiency decreases, as is observed with increasing molecular weight, the number of events required to collect a statistically significant data set also increases. Standing estimates that MALDI yields approximately 10⁴ ions on each laser pulse (29), however, the numbers of ions per laser pulse varies with the laser power density, type of matrix used, and with the matrix-to-analyte ratio. A complicating factor associated with laser desorption ionization, and especially MALDI, is the temporal evolution of ions following laser excitation (30). We have previously shown that the arrival time distribution of MALDI formed ions extends to 50-70 us, the exact arrival time distribution of the ions depends on several factors (31). A different approach to pulsing the ion beam is to use a low current density ion beam (say 100-10,000 ions/s) which can be considered as a series of infinitely short pulses that contain one ion of interest. Because the timing of the pulse is not known, two particles (say an ion and a neutral) that strike different detectors can be used to synchronize the time-of-flight clock (32). The method of using the neutral and the ion for obtaining tandem mass spectra is refered to as neutral-ion correlation.

A particular advantage of the neutral-ion correlation experiment is that either continuous or pulsed ionization/excitation can be used for the TOF measurements. For example, dissociation reactions (unimolecular dissociation, CID, or photodissociation) of the mass-selected m_1^+ ion that occur in the field-free region between MS-I and the reflectron produce a fragment ion (m_2^+) and a neutral (m_3°) , and the velocity of m_2^+ and m_3° are the same as that of m_1^+ . The neutral fragment will not experience any force due to the reflectron and will strike detector #1 and produce a signal. m_2^+ will be decelerated upon entering the reflectron, eventually reaching zero velocity, at which point its direction is reversed. m_2^+ is then re-accelerated back to its initial velocity. Because the initial velocities of the fragment ions is independent of the m/z value, the time that an ion spends in the reflectron depends upon the rate of deceleration and reacceleration. The rate of deceleration/reacceleration is proportional to the m/z of m_2^+ . Therefore, the difference in the arrival time of the neutral and the arrival time of m_2^+ is dependent upon the m/z of the ion.

In order to improve the signal-to-noise ratio of neutral-ion correlation experiment, we developed an on-line pile-up rejection method (33). In the neutral-ion correlation experiment, the occurrence of a dissociation reaction of the mass-selected ion is indicated by the neutral product striking the detector positioned behind the reflectron (7,8), and the ion is detected by the detector positioned to receive the reflected ions. Thus a dissociation reaction yields two products, an ion and a neutral, that must be correlated. As with all event correlation experiments it is important to keep the flux of the events low in order to minimize the number of "false" correlation events, e.g., background signals from uncorrelated events.

As the mass-selected ion (mass selected by MS-I) traverses the field-free region between MS-I and MS-II fast neutrals are produced by two processes, reaction 1 and 2. The collision between m_1^+ and the target gas results in conversion of translational energy of m_1^+ into internal energy (collisional activation (CA), but collisional ionization of the target gas can also occur and yields a neutralized form of m_1 . The neutral form of m_1 may be the intact molecule or neutral fragments. Results from neutralization - reionization experiments suggest that both intact molecules and fragment neutrals are formed (34). These results are also consistent with collision-induced emission studies reported by Holmes. Reaction 2 produces an ion (the original target atom) and a neutral (m_1°) but the ion has near-thermal kinetic

energy and is not extracted from the collision cell, thus the only detectable product (detectable in the tandem mass spectrometry experiment) of reaction 2 is the fast-neutral. The arrival time of F_i^+ at the ion detector is delayed in time relative to the neutral because the flight path of the ion is greater, thus the difference in arrival time of the neutral and ion can be used for TOF analysis of the ionic products of reaction 1. The occurrence of reaction 1 is confirmed by correlation of an ion with a neutral, whereas fast-neutrals formed by reaction 2 do not correlate with an ion.



m₁° denotes a neutral species and whether the neutral is an intact molecule or a fragment of the molecule is not known.

The principle source of background signal associated with coincidence measurements arises when the count rates for "true" coincidence signals are low and the count rate of "false" coincidence signals is relatively high. For example, false coincidence gives rise to signal distortion if a neutral formed by reaction 2 strikes the detector (a "start" signal for the ion TOF clock) and within the ion acquisition time window a second neutral formed by reaction 1 strikes the detector. measurement for the ion is in error by Δt , the difference in arrival time between neutral 1 and neutral 2 (Figure 3). Because Δt is random, the end result is noise in the spectrum. In addition, the probability for background signal in a coincidence experiment is directly proportional to the time window allowed for detection of F_i⁺, which is determined by the flight time of the ion. Typically, time windows of 10-100 us are required for acquisition of the full range MS-II mass spectrum assuming ion energies of 1-8 keV and m/z values of 100-5000 for m₁⁺. Such a large time window for the MS-II mass spectrum limits the maximum allowable pulse rate for m₁⁺ to approximately 10,000 to 50,000 neutrals per second. Data acquisition rates of 10-50 KHz exceeds the capabilities of the instrument hardware, thus it is necessary to acquire a statistical sampling of the actual number of neutrals formed. Because the number of products formed by reaction 2 exceed the number of products from reaction 1 by more than a factor of 10, signal-averaging is not an efficient means for improving the S/N ratio. Although the S/N ratio can be improved by summing together narrow segments of the TOF spectrum, e.g., sampling a narrow time window, this method increases the total data acquisition time for the experiment. In addition, this procedure is practical only if the signal for m₁⁺ is constant in time, e.g., often times the liquid-SIMS spectrum changes (in terms of analyte versus matrix background signal) (35) as the sample is depleted, thus the time-averaged spectra are composite MS-II spectra for analyte and matrix background ions.

The "pile-up" rejection S/N enhancement can be accomplished in two ways: (i) acquire and store all the neutral-ion arrival events and process the data off-line (36), or (ii) develop a hardwired system for performing the experiment on-line. We chose to use an on-line system because this permits evaluation of the data as it is

acquired. On-line evaluation of the data is important because some samples yield acceptable S/N ratios with minimum acquisition times, either because the dissociation efficiency is high or a large amount of sample is available, but other samples require much longer acquisition times to achieve acceptable S/N levels. The circuitry used for the neutral-ion correlation/"pile-up" rejection and the resulting spectra has been described elsewhere (37).

Photodissociation

Although there is considerable interest in the fundamentals of photodissociation and the use of photodissociation as a method for ion activation in tandem mass spectrometry, the numbers of studies on complex molecules or even model compounds of biological molecules are very limited. The advantage of photodissociation is the amount of energy deposited into the ion as defined by the energy of the photon; issues of average energy uptake and what fraction of the energy loss is partitioned as internal energy of the ion do not complicate the issue. The most serious disadvantage of photodissociation is that the yield of product ions is low if single-photon absorption is maintained, and studies of multiphoton dissociation (MPD) processes require a high degree of variability of the laser power density. Several laboratories have published photofragment ion spectra of complex molecules, but these spectra are composite metastable ion, CID, and photofragment ion spectra. It is difficult to obtain a true photofragment ion spectrum because the efficiency of photodissociation of large ionic systems is quite low (10⁻²-10⁻⁴) and the background ion counts that arise by metastable ion and CID processes may be as much as a few percent relative abundance of the "main ion" beam. In order to obtain a true photofragment ion spectrum it is necessary to subtract the background metastable/CID spectrum. Subtraction of the background spectrum can be done by modulation of the laser source and synchronously detecting the ion signal (e.g., lock-in amplifier) (34) or by ion counting methods (35). Another problem that frequently complicates the acquisition of the photofragment ion spectrum is the increased neutral background that arises from the laser beam striking metal components within the vacuum system. This yields a photofragment ion spectrum that is very similar to the CID spectrum because the fragment ions are formed by collision with laser evaporated/ablated neutral species.

The experimental sequence for obtaining photodissociation spectra is contained in Figure 4. The first step in the photodissociation experiment is to pulse the Cs⁺ ion gun to obtain a 20-50 us pulse of ions, and the ion of interest is mass selected using MS-I. Firing of the photodissociation laser is synchronized to the ionization pulse and the flight time of the mass-selected ion from the source to the photodissociation region. The synchronization is established by measuring the arrival time distribution of the ions on the line-of-sight detector (positioned behind the reflectron (see Figure 1)), and calculating the flight time from the photodissociation region. Using this method to synchronize the laser with the ion arrival time eliminates problems associated with the electronic delays of the pulsed Cs⁺ ion gun. In addition, photofragment neutrals that arrive within a 10 us wide gate (pre-set and synchronized with the laser) are used to obtain a spectrum. The time differences between the neutrals that arrive within the gate period and the ions that arrive within a variable time period are calculated and histogramed on the computer. To obtain a true

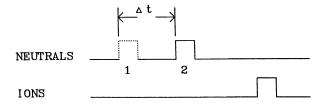


Figure 3. Pulse sequence of ions and neutrals with two neutrals (1 and 2) that yield false coincidence.

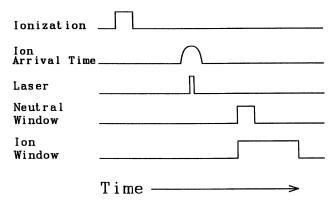


Figure 4. Experimental sequence for obtaining photodissociation spectra.

photofragment ion spectrum, the data must be corrected for background ions that result from unimolecular dissociations and/or CID. The CID is caused by residual gases and by gases evolved when the laser strikes the walls of the vacuum chamber. To reduce the amount of gases produced by the laser, a window is placed on the both sides of the vacuum chamber to allow most of the laser light to escape. The photofragment ion spectrum is obtained by subtracting the metastable ion/CID spectra from photodissociation /metastable ion/CID spectra. Figure 5 contains a background spectrum, a background/photodissociation spectrum and a photofragment ion spectrum for [4-nitroaniline-H⁺-(glycerol)] obtained by using 266 nm for photoexcitation.

Photodissociation Studies of H*-Transfer Reactions within Clusters

H⁺-transfer reactions are one of the most fundamental reactions in chemistry; therefore, an understanding of the factors that influence H+-transfer is immensely important to our understanding of chemistry (36). H⁺-transfer reactions play an important role in the unimolecular reactions of gas phase ionic species and ionization methods such as FAB, MALDI, and electrospray ionization, (ESI) etc. Considering the importance of H^+ -transfer reactions in desorption ionization processes, e.g. $[M+H]^+$ species must be formed by a H⁺-transfer reaction, there have been very few studies of H⁺-transfer reactions of large molecules. We view desorption ionization in terms of a "cluster emission model," and, in particular, we view the ionization of the analyte occurring via H⁺-transfer between an excited (rovibronic) matrix molecule and a ground state analyte molecule (37). We are interested in using laser-ion beam photodissociation to probe H⁺-transfer reactions within cluster species as well as understanding the effect of cluster size on such reactions. To develop the experiment we are examining H⁺-transfer within a H⁺-bound dimer of the type [B---H⁺---B]. The [B---H⁺---B] ion is formed by desorption ionization, mass selected by MS-I, photoexcited by the laser (tuned to an absorption wavelength of either B or B'), and the photofragment ions are detected by MS-II (the R-TOF).

The protonated clusters are formed by 15keV Cs⁺- liquid SIMS on a mixture of nitroaniline, glycerol, and HCl. Ionization of this mixture forms complexes of the type [NA-H⁺- G_n], where n = 1-5. Two isomers of nitroaniline were used (3-nitroaniline (3-NA) and 4-nitroaniline (4-NA)) in these preliminary studies. The ionic complexes are mass-selected by MS-I and photoexcited with either 337 nm (N₂ laser) or 266 nm (Nd:YAG laser). The only photofragment ion of the clusters studied to date arise by loss of a neutral molecule, e.g., either B or B. The photodissociation (337nm or 266 nm) of the ionic cluster occurs by electronic excitation of the nitroaniline. 4-nitroaniline has a strong absorption band between 300 - 420 nm (max - 365 nm) and the typical benzoid absorption band centered around 250 nm. The 300 - 420 nm absorption band is absent in the spectrum of the 4-nitroanilinium ion, protonation of the NH₂ group eliminates electron delocalization between the NO₂ and NH₂ groups, thus a [4-NA---H⁺--- G_n] species that has a 4-nitroanilinium solvated by glycerol do not photodissociate.

3- and 4-nitroaniline (NA)/glycerol (G) clusters were selected for the preliminary studies. These compounds were selected because the basicities are similar (NA-199 kcal mol⁻¹ and G-196 kcal mol⁻¹). The acidities of the electronically excited anilines is much greater than that of ground state species. For example, the pk_a of 4-nitroanilinium ion (solution state) in the ground state is -4.33 and the pk_a of the

excited state is -13. Thus, the change in $pk_a [pk_a(S_1)-pk_a(S_0)]$ is - 9; indicating the excited state is 10^9 times more acidic than the ground state. The much greater acidity of the excited state results in a rapid shift in the equilibrium and H⁺-transfer to the solvent (glycerol). Photodissociation studies provide a convenient way to study H⁺-transfer reactions of electronically excited state species. There are two additional factors that must be considered in these studies: (i) the rate of internal conversion of 4-nitroaniline S_1 verses the rate of H⁺-transfer, and (ii) the structure of the H⁺-bound species. For H⁺-transfer to be an important decay route for S_1 requires very rapid H⁺-transfer, e.g., $k = 10^9$ s⁻¹, the radiative relaxation rate of the S_1 excited state (38). For H⁺ bound dimer species, e.g., [B---H⁺---B⁻] such rapid H⁺-transfer is probably reasonable, whereas for large cluster species H⁺-transfer may be rapid but ion-pair formation (dissociation of the cluster) may be the rate-limiting step. That is, the S_1 excited state may relax via H⁺-transfer to form a solvated ion pair, but the ground state species undergo H⁺-transfer to reform neutral species.

Table 1 contains the photodissociation data for the $[NA-H^+-G_n]$ clusters. The photoexcitation of $[3-NA-H^+-G]$ results in loss of nitroaniline to form protonated glycerol $[GH^+]$, whereas photoexcitation of $[4-NA-H^+-G]$ results in loss of glycerol to yield $[4-NA-H^+]$. In the case of $[4-NA-H^+-G_2]$ loss of glycerol (to form $[4-NA-H^+-G]$) and nitroaniline (to form $[G_2H^+]$) are competitive processes.

The basicity of the 4-nitroaniline (199.8 kcal/mol) is greater than that of glycerol, and loss of glycerol is the dominate product ion in the metastable ion spectrum of [4-NA-H⁺-G] (39). The loss of glycerol indicates that photoexcited 4-nitroaniline is a stronger base than glycerol. The photodissociation data for [4-NA-H⁺-G] is inconsistent with the molecular orbital calculations. The basicity of excited state 4-nitroaniline is expected to be lower than glycerol.

The reason for the lack of H⁺-transfer to the glycerol could be caused by the geometry of the cluster prohibiting the H⁺-transfer. Further evidence that the geometry could be hindering the H⁺-transfer is found in the photodissociation of the [nitroaniline-H⁺-glycerol₂] cluster which shows the loss of neutral nitroaniline for both 3- and 4-nitroaniline, because the cluster containing two glycerols is more likely to be solvating the 4-nitroaniline.

The observed loss of 3-NA from photoexcited [3-NA-H⁺-G] cluster suggests the 3-nitroaniline has a lower proton affinity than glycerol. The gas phase basicity of 3-nitroaniline has not been previously determined to our knowledge, but it probably does not differ much from that of 4-nitroaniline (199.8 kcal/mole)(40). The 199.8 kcal/mole may be used as a rough estimate of the gas phase basicity of the 3-nitroaniline. The gas phase basicity of glycerol has been determined to be 196 kcal/mole, however, a large entropy change is associated with the basicity (41).

The ratio of relative abundances of BH⁺ and B'H⁺in the CID spectrum is determine by the rate of dissociation to product ions, thus the relative abundances can be used to determine the relative H⁺ affinities of the species in the H⁺-bound clusters (42). In the CID experiment the excitation energy is distributed randomly throughout the molecule, independent of the rate of intramolecular energy distribution. Conversely, in the photodissociation experiment the energy is initially deposited into the cluster by a specific molecular chromophore, the rate of randomization of this energy depends upon the local environment of the neighboring "solvent" molecules and coupling between the chromophore and the solvent. In the absence of strong coupling between the molecule pairs the rate of H⁺-transfer should be rapid with respect to the decay channels.

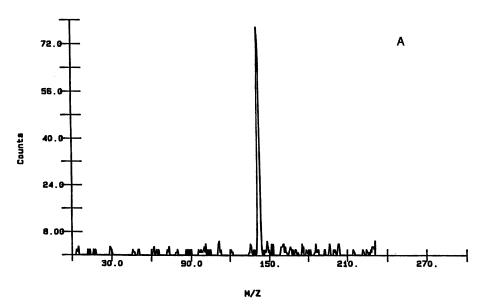


Figure 5.A) Photodissociation spectra of 4-nitroaniline-H⁺-glycerol.

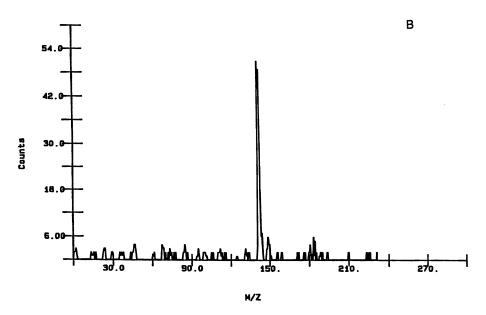


Figure 5.B) Photodissociation and background spectra of 4-nitroaniline-H⁺-glycerol.

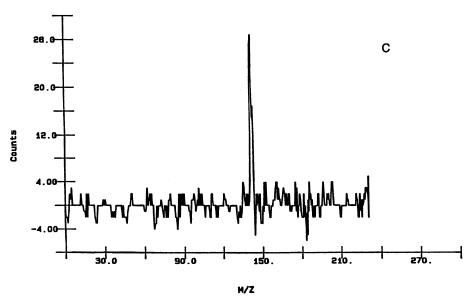


Figure 5.C) Background spectra of 4-nitroaniline-H⁺-glycerol.

Table 1.	Photodissociation	of [(Glycerol),	-H+-Nitroaniline]	Complexes
----------	-------------------	-----------------	-------------------	-----------

Number of		Neutral loss				
Glycerols	Nitroaniline	Glycerol		Nitroaniline		
		337 nm	266 nm	337 nm	266 nm	
n=1	4-Nitroaniline	+	+	*	*	
	3-Nitroaniline	-	*	+	+	
n=2	4-nitroaniline		+ (66%)		+ (33%)	
	3-nitroaniline		-		+	

- + indicates an observed photodissociation signal
- indicates a decrease in the metastable ions formed
- * indicates no signal was observed

Tandem Mass Spectrometry with MALDI

Matrix-assisted laser desorption ionization (MALDI) has greatly impacted molecular weight mass spectrometry of peptides and proteins, but the potential of MALDI, in combination with tandem mass spectrometry, for structural characterization is far less developed. The slow adaptation of MALDI as an ionization method for tandem mass spectrometry can be attributed to incompatibilities of scanning instruments with pulsed ionization/excitation sources, but the EB/R-TOF instrument is well suited for tandem mass spectrometry of laser desorbed ions. We have initiated studies of the tandem mass spectrometry of laser desorption. These initial studies have concentrated on comparing data obtained by MALDI/EB/R-TOF with data obtained from Cs⁺ ion L-SIMS and on developing the experimental methods required for MALDI/tandem mass spectrometry.

MALDI is performed on the EB/R-TOF instrument by using a low-power N_2 laser (Laser Science VSL-337; 337nm, 120 u joules per pulse, 3 nsec pulse width). A slurry of sinapic acid, (5mg/ml to 500 mg/ml) and 1 ml of glycerol is prepared. 1 ug of analyte and slurry matrix are mixed on the probe tip. The laser is then focused to approximately 0.1 mm² on the probe tip, and the resulting ions extracted. The ion of interest is mass-selected, and after a period of time corresponding to the flight time of the mass-selected ion through the sector instrument, neutrals and ions signals are collected and correlated as described above.

The overall rate of data acquisition for this experiment is limited by the low duty-cycle pulsed N₂ laser. For example, at a repetition rate of 20 Hz (maximum rep. rate of the laser) the laser is on for only 60 ms/s. In addition, there are significant trade-offs required in data acquisition. For example, if the fragmentation efficiency of the m, ion is 1%, a single fragment ion is obtained for each 100 m, ions formed. Thus, to obtain a fragment ion for each laser pulse 100 m₁⁺ ions must be formed/pulse. 100 ions per laser pulse can be achieved, even 104-105 ions per pulse can be achieved, but these ions must be extracted and collimated prior to analyze by MS-I. We have found that metastable ion counts of 0.1-1/laser pulse can be obtained under practical experimental conditions, and that good signal-to-noise for the minor fragment ions required 10³ to 10⁵ laser shots. This corresponds to a total data acquisition time of 8 - 80 minutes. Stable ion currents can be obtained for 8 - 10 minutes using nearly all the standard MALDI matrices, e.g., 4-nitroaniline, sinapic acid, etc., but to obtain stable ion currents for up to 80 -100 minutes requires the use of liquid matrices, e.g., 4-nitrobenzyl alcohol, or slurries of solid-matrices, e.g., sinapic acid/glycerol or sinapic acid/4-nitro benzyl alcohol. These preliminary studies illustrate the utility of the EB/R-TOF experiment combined with pulsed laser photodissociation to probe H⁺-transfer reactions within cluster species.

Figures 6-8 contains metastable ion spectra obtained using Cs⁺ liquid-SIMS and MALDI. The L-SIMS data was recorded using neutral-ion correlation/pile-up rejection and the MALDI/metastable ion spectra were obtained by any neutral-ion correlation. Consequently, the S/N for MALDI/ metastable ion spectra is not as good as that for L-SIMS.

The spectra for the MALDI and L-SIMS are very similar indicating that the internal energies of the dissociating ions formed by L-SIMS and MALDI are similar.

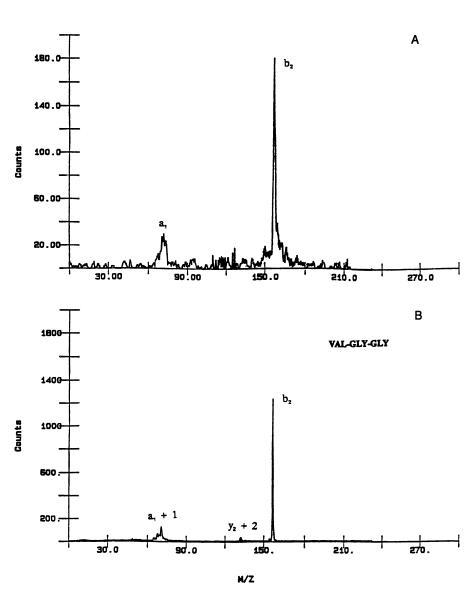


Figure 6. Metastable ion spectrum of val-gly-gly (M+H⁺)from ions formed by A)MALDI B)L-SIMS.

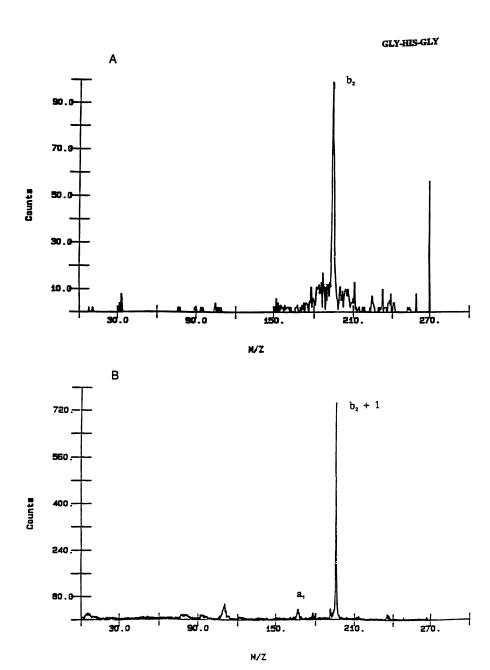


Figure 7. Metastable ion spectrum of gly-his-gly $(M+H^+)$ from ions formed by A)MALDI B)L-SIMS.

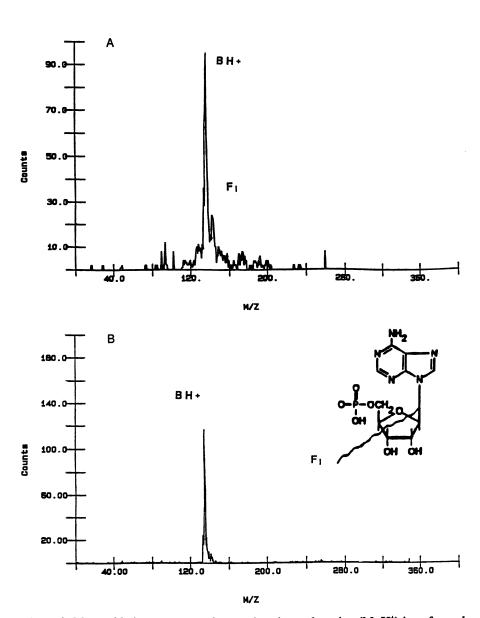


Figure 8. Metastable ion spectrum of monophosphate adenosine $(M+H^+)$ ions formed by A)MALDI B)L-SIMS.

Because the ion population sampled is the same for both experiments (30-100 used after the ionization pulse), metastable ion spectra for MALDI and L-SIMS formed ions should be very similar. It should be noted that the energies of the ions that decay are similar, the absolute number of ions that decay cannot be determined in the manner which these experiments were performed. Other compounds may reveal some differences in the spectra, but a comparison of the dissociation using the same experiment is needed.

Future of Tandem Time-of-Flight Mass Spectrometry

The EB/R-TOF instrument has developed very rapidly. In just over two years the tandem sector/TOF experiments evolved from a paper concept to a working experiment. The early work on pulsed FAB clearly demonstrated improved sensitivity for pulsed ionization relative to CW ionization (43) and the earliest experiments with MALDI on tandem TOF further illustrates this point (44). Both pulsed FAB or pulsed liquid-SIMS and MALDI can be combined with EB/R-TOF instrumentation for performing ultra-high sensitivity tandem mass spectrometry experiments.

Tandem TOF instrumentation will continue to evolve as methods such as MALDI find applications in biology and biochemistry. Although EB/R-TOF instruments are limited in terms of upper mass range (between m/z 5000 and 10000) for MALDI applications, the increased resolution afforded by the magnetic sector MS-I can be an advantage for many important problems. Clearly, the performance of the EB/R-TOF is comparable to multi-sector instruments and offers the same advantages of array detectors (single ion counting) for high sensitivity. Ion counting and neutralion correlation experiments are clearly limited to low ion current applications. Thus, the advantages of instruments such as the EB/R-TOF are realized in applications at the edge of instrument sensitivity. This is not a critical limitation because it is always possible to reduce the numbers of ions formed or admitted to the analyzer if the count rate is too high.

A major limitation with photodissociation of large ions (m/z>500) is that the efficiencies for producing photofragment ions is low, typically 10⁴. This is an intrinsic limitation for the dissociation dynamics of large molecules and can be reduced only by increasing the number of incident ions that are excited, increasing the energy of the absorbed photon, or increasing the reaction time for dissociation. Combining the pulsed ion beam techniques, high-power pulsed lasers for performing photodissociation, and TOF analysis of the photofragment ions is expected to result in substantial enhancements in photofragment ion yields. The EB/R-TOF instrument accomplishes all the state objectives and the preliminary photodissociation experiments are very encouraging.

Literature Cited

- (1) Lattimer, R.P., Hansen, G.E., Macromolecules, 1981, 14, 1776.
- (2) Macfarlane, R.D., in *Methods in Enzymology*, Vol. 193 Mass Spectrometry, J.A. McCloskey, Academic Press, San Diego, CA, **1990**, 263-279.
- (3) Barber, M., Bordoli, R.S., Elliott, G., Sedgwick, R.D., Tyler, A.N., *Anal. Chem.* 1982, 54, 645A.
- (4) Willough, R.C., Browner, R.F., Anal. Chem., 1984, 56, 2626.

- (5) Blakely, C.R., Vestal, M.L., Anal. Chem., 1983, 55, 750; b). Vestal, M.L., Fergusson, G.J., Anal. Chem., 1985, 57, 2372; c). Vestal, M.L., Science, 184, 221, 275.
- (6) Yamashita, M., Fenn, J.B., J. Phys. Chem., 1984, 88, 4451; b). Edmonds, C.G., Smith, R.D., in Methods in Enzymology, Vol. 193 Mass Spectrometry Academic Press San Diego, CA 1990, 412-431.
- (7) Hillenkamp, F., Karas, M.,; in *Methods in Enzymology*, Vol. 193 Mass Spectrometry, Academic Press, San Diego, CA 280-295; b). Hillenkamp, F., Karas, M., Beavis, R.C., Chait, B.T., *Anal. Chem.*, 1991, 63, 1193A.
- (8) Burlingame, A.L., Baillie, T.A., Russell, D.H., Anal. Chem., 1992, 64, 467R-502R.
- (9) Hayes, R.N., Gross, M.L., in *Methods in Enzymology*, Vol. 193 Mass Spectrometry, Academic Press, San Diego, CA 1990, 237-263.
- (10) Lee, T.D., Shively, J.E., in *Methods in Enzymology*, Vol. 193 Mass Spectrometry, Academic Press, San Diego, CA, 1990, 361-374.
- (11) Loo, J.A., Udseth, H.R., Smith, R.D., Rapid Comm. Mass Spectrom., 1988, 2, 207; b). Smith, R.D., Loo, J.A., Barinaga, C.J., Edmonds, C.T., Udseth, H.R., J. Am. Soc. Mass Spectrom., 1990, 1, 53.
- (12) Cooks, R.G., Grant, E.R., Science, 1990, 250, 61.
- (13) Tecklenburg Jr., R.E., Russell, D.H., Mass Spectrom. Rev., 1990, 9, 405.
- (14) Griffin, L.L., McAdoo, D.J., J. Am. Soc. Mass Spectrom., 1993, 4, 11-15; b). Schlag, E.W., Levine, R.D., Chem. Phys Lett., 1989, 163, 523-530.
- (15) MacFarlane, R.D., in *Methods in Enzymology*, Vol. 193 Mass Spectrometry, McCloskey, J.A., Academic Press, San Diego, CA, 1990, 263-279.
- (16) Louris, J.N., Cooks, R.G., Syka, J.E.P., Kelly, P.E., Stafford, G., Todd, J.F.J., Anal. Chem., 1987, 59, 1677.
- (17) Solouki, T., Russell, D.H., Appl. Spectros., 1993, 47, 211.
- (18) Strobel, F.H., Preston, L.M., Washburn, K., Russell, D.H., *Anal. Chem.* 1992, 64, 754.
- (19) Stults, J.T., Enke, C.G., Holland, J.F., Anal. Chem., 1983, 55, 1323.
- (20) Glish, G.L., Goeringer, D.E., Anal. Chem., 1984, 56, 2291.
- (21) Cornett, D.S., Peschke, M., Lailting, K., Cheng, P.Y., Willey, K.F., Duncan, M.A., Rev. Sci. Ist., 1992, 63, 2177-2186; b). Jardine, D.R., Morgan, J., Alderdice, D.S., Derrick, P.J., Org. Mass Spectrom., 1992, 27, 1077-1083.
- (22) Della-Negra, S., LeBeyec, Y., Anal. Chem., 1985, 57, 2035.
- (23) Tang, X., Ens, W., Standing, K.G., Westmore, J.B., Anal. Chem., 1988, 60, 1791.
- (24) Strobel, F.H., Preston, L.M., Washburn, K.S., Russell, D.H., *Anal. Chem.*, 1992, 64, 754.
- (25) Della-Negra, S., Le Beyec, Y., Int. J. Mass Spectrom. Ion Proc., 1984, 61, 21.
- (26) Strobel, F.H., Russell, D.H., (manuscript in preparation).
- (27) Strobel, F.H., Russell, D.H., (work in progress).
- (28) Standing, K.G., Chait, B.T., Ens, W., McIntosh, G., Beavis, R., Nucl. Inst. Meths., 1982, 198, 33; b). Hues, S.M., Colton, R.J., Wyatt, J.R., Rev. Sci. Instrum., 1989, 60, 1239.
- (29) Ens, W., Mao, Y., Mayer, F., Standing, K.G., Presented at the 38th ASMS Conference on Mass Spectrometry and Allied Topics, Tucson, AZ, June 3-8, 1990, p. 24-25.

- (30) White, M.A., Strobel, F.H., Russell, D.H., 39th ASMS Conference on Mass Spectrometry and Allied Topics, Nashville, TN, May 19-24, 1991, p. 334-335
- (31) Strobel, F.H., Preston, L.M., Washburn, K.S., Russell, D.H., *Anal. Chem.*, 1992, 64, 754.
- (32) Torgerson, D.F., Skowronski, R.P., MacFarlane, R.D., Biochem. Biophys. Res. Commun., 1974, 60, 616.
- (33) Williams, O.M., Sandle, W.J., J. Phys. E., 1970, 3, 741.
- (34) Mukhtar, E.S., Griffith, I.W., March, R.E., Harris, F.M., Int. J. Spectrom. Ion Phys., 1981, 38, 333.
- (35) Jarrold, M.F., Illies, A.J., Bowers, M.T., J. Chem. Phys. 1983, 79, 6086.
- (36) See for example Steadman, J., Syage, J.A., J. Phys. Chem. 1991, 95, 10326;
 b). Kin, S.K., Li, S., Bernstein, E.R., J. Chem. Phys., 1991, 95, 3119;
 c). Jouvet, C., Lardeux-Dedonder, C., Richard-Viard, M., Solgadi, D., Tramer, A., J. Phys. Chem., 1990, 94, 5041.
- (37) Gimon, M.E., Preston, L.M., Solouki, T., White, M.A., Russell, D.H., Org. Mass Spectrom., 1992, 27, 827-830.
- (38) Seliskar, C.J., Khalil, O.S., McGlynn, S.P., in Excited States, Kim, E.C., Ed., Academic Press, New York/London, 1974, 288-291.
- (39) Strobel, F.H., Russell, D.H., (manuscript in preparation).
- (40) Rolli, E., Houriet, R., Spectros. Int. J., 1984, 3, 177.
- (41) Sunner, J.A., Kulatunga, R., Kebarle, P., Anal. Chem., 1986, 58, 1312.
- (42) McLucky, S.A., Cameron, D., Cooks, R.G., J. Am. Chem. Soc., 1981, 103, 1313.
- (43) Teckllenburg, Jr., R.E., Castro, M.E., Russell, D.H., Anal. Chem., 1989, 61, 153.
- (44) Strobel, F.H., Solouki, T., White, M.A., Russell, D.H., J. Am. Soc. Mass Spectrom., 1990, 2, 91-94.

RECEIVED October 12, 1993

Chapter 6

A Dual-Reflectron Tandem Time-of-Flight Mass Spectrometer

Timothy J. Cornish and Robert J. Cotter

Middle Atlantic Mass Spectrometry Facility, The Johns Hopkins University School of Medicine, Baltimore, MD 21205

A compact, laser desorption tandem time-of-flight mass spectrometer has been developed utilizing two electrically isolated flight tubes separated from each other by a collision cell. A pulsed valve produces a beam of argon gas to promote collision induced dissociation (CID) fragmentation of mass selected ions. Each flight tube has a 2-stage reflectron which can be used in the dual role of energy focusing and mass dispersing the product ions in the tandem mode. A second acceleration region has been inserted directly beyond the collision region to study the effects of mass dispersion by post-acceleration in conjunction with dispersion by the second ion mirror. Mass selective gating into the collision region is accomplished without slits by applying a low energy deflection pulse and subsequent loss of ions through the second reflection region and final leg Results are presented demonstrating the double of the drift region. reflectron mode for high resolution studies, and the tandem mode to induce fragmentation of several laser desorbed compounds.

Tandem mass spectrometry has been demonstrated to be a very effective method in elucidating molecular structure, particularly in the analysis of biomolecular compounds. Generally, the first mass spectrometer in a tandem instrument is used to select a single ion (the precursor ion) from the normal mass spectrum. Following some type of dissociation, the final mass spectrometer is subsequently used to analyze the secondary ions (product ions) generated from the fragmentation process. The three techniques most often used to promote fragmentation of the mass selected ions are photo-dissociation, surface induced dissociation (SID), and collisionally induced dissociation (CID). For sequencing proteins, CID is often relied upon because of its general applicability to numerous classes of compounds. The 4-sector mass spectrometer has been quite successfully developed for this type of MS/MS analysis, but the instrument is expensive, rather slow, and requires significant expertise to operate. For these reasons, there have been a number of attempts to introduce much simpler and less expensive time-of-flight mass analyzers into either hybrid or stand-alone versions of the

0097-6156/94/0549-0095\$06.00/0 © 1994 American Chemical Society tandem mass spectrometer configuration. CID is difficult to perform, however, in a TOF mass spectrometer because of increased background pressure resulting from addition of the collision gas, and reduced resolution of the product ion spectrum due to energy spread caused by the collision event. Therefore, surface induced dissociation or photo dissociation have traditionally been regarded as the most obvious choice for time-of-flight applications.

Russell et al. (1) have developed a magnetic/TOF hybrid instrument in which the magnetic portion of the instrument isolates the mass of interest under high resolution conditions, followed by collision-induced dissociation and mass analysis of the product ions in a reflectron time-of-flight MS. Other types of tandem time-of-flight instruments utilize a single reflectron TOF only. In one case, demonstrated by Duncan et al., (2) gate selected ions are photo dissociated by a laser focused into the rear of the ion mirror thereby producing product ion dispersion in the second leg of the instrument. In another method developed by Schlag et al., (3) the first sector consists of a short, linear TOF in which the mass selected primary ions are tightly spaced-focused to a point which is then intersected by the beam of a photodissociation laser. Product ion spectra are generated by scanning the mirror voltages. The technique of neutral and product ion coincidence in a reflectron TOF, first proposed by LeBeyec et al.(4) and later studied by Standing et al.(5) represents yet another type of tandem instrument for the study of metastable decomposition. Recently, Jardin et al.(6) have discussed a TOF/-TOF designed in a linear configuration incorporating an electrically floating collision cell for the study of charge exchange and CID product ions.

Reliable, non-specific fragmentation of proteins into their component amino acids is the principle reason for pursuing collision induced dissociation (CID) in many tandem MS instruments. The goal of this research project is to design a tandem mass spectrometer replacing the two magnetic sectors with two independent reflectron time-of-flight sectors and employing CID for MS/MS protein analysis. Unit resolution up to 3000 daltons would be sufficient to study peptides and enzymatic digestion products of larger proteins. In this chapter, the dual reflectron tandem TOF instrument and its design rationale are discussed along with an overview of the results obtained thus far. These include preliminary data from the instrument operating in the single and double reflectron modes, data collection factors affecting resolution and performance, and operation of the collision cell to perform CID in the tandem TOF mode.

Instrumentation

The basic design of the dual reflectron tandem time-of-flight mass spectrometer (7) is shown in Figure 1. The 32" aluminum vacuum chamber houses two stainless steel, electrically isolated flight tubes A 2-stage ion mirror, assembled from components purchased from Kimball Physics (Wilton, N.H.), is mounted onto each flight tube and offset from the flight axis by 3°. The ionization region consists of a single stage extraction region in which ions are accelerated to 4000 V. This region is followed by an einsel lens and a set of steering elements. The laser beam strikes the immersion-type probe surface at grazing incidence. The detectors consist of matched sets of microchannel plates (Galileo Electro Optics) mounted in shielded cases and fitted with conical stainless steel anodes. Figure 2 traces the triggering scheme of the data collection system.

A 1.2 mJ/pulse nitrogen laser (Photon Technology International) is used for sample

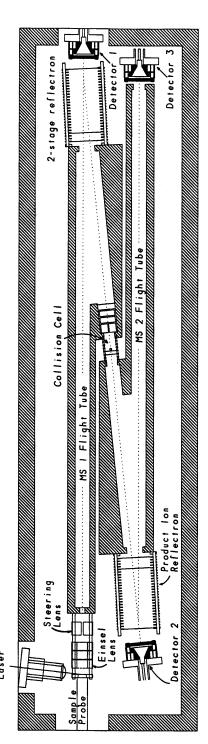


Figure 1. Dual Reflectron Tandem Time-of-Flight Mass Spectrometer.

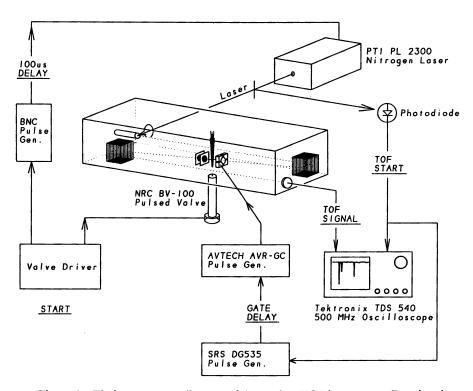


Figure 2. Timing sequence diagram of the tandem TOF instrument. (Reprinted with permission from Reference 8).

desorption and ionization. The analog signal is collected without external amplification using a Tektronix TDS 540 (1 Gsam/sec, 500 MHz bandwidth) digitizing oscilloscope and processed on a PC using a custom designed time-of-flight software program (ILys Software, Pittsburgh, PA) Normally, each mass spectrum represents between 20 to 30 single shot spectra averaged within the oscilloscope prior to transfer to the data processing computer.

Design Considerations

In order to achieve good mass resolution, it was necessary to pay particular attention to the temporal characteristics of the ion signals detected. Resolution is normally expressed by $m/\Delta m = t/2\Delta t$, where t is the total flight time and Δt is the peak width at half height (see Chapter 2). Since t is fixed by the drawout voltage and the flight tube length, we have concentrated on minimizing the analog peak width. In theory, very high mass resolution can be achieved if infinitely narrow peaks are produced in the ion source and detected with high precision. It is therefore necessary to consider the instrumental factors that increase the time spread of the signal recorded at the digitizer. The pulse duration of the laser determines the absolute minimum peak width that can be produced. In this case, the desorbing laser has a peak width of 600 ps, sufficiently short to insure that it is not the limiting factor in producing narrow time-of-flight peaks.

In addition to the ion energy distribution discussed earlier (see Chapter 2), the detectors and digitizers used in recording the signal also contribute to the observed peak width. The microchannel plate detectors were found to produce single ion pulse profiles of approximately 1 ns risetime and 1.5 ns FWHM. If all energy spreads were corrected for by the ion reflectrons, the detector response time would fix the upper limit of mass resolution obtainable. In practice, peak widths of less than 4 ns are rarely observed. The isotope series of PBD dye shown in Figure 3c represents our record for a high resolution time-of-flight spectrum ($t \approx 48 \, \mu s$; $\Delta t = 5.5 \, ns$; resolution > 4000).

Single and Double Reflectron Operation

The dual reflectron flight tube configuration was designed so that the first leg energy focuses ions to be mass selected, while the second serves to energy focus the product ions generated during the collision. In the preliminary stage of development, the double reflectron TOF geometry had to be tuned and characterized. A detector behind the first reflectron, used for collecting data in the linear TOF mode, is used primarily for tuning purposes to determine the amount of ions present in the first reflectron before the opposing potentials were applied.

Figure 3 is a comparison of the three operating modes using PBD laser dye as the test compound. Several observations can be made based this comparison. There is a significant energy spread observed using the linear TOF mode (Figure 3a) because the energy distribution acquired during the laser desorption process is uncorrected. The 299 Da peak has a width of 26 ns and the isotopic pattern is unresolved. In the single reflectron mode (Figure 3b), the width of the parent peak is reduced to 15 ns while the flight time has more than doubled, resulting in a spectrum with a resolution of roughly 1500. By utilizing both reflectrons, the peak widths are further reduced down to approximately 6ns producing a spectrum clearly resolving the isotopic pattern to better than 1 part in 4000. Since the ultimate goal of this project is to produce tandem mass

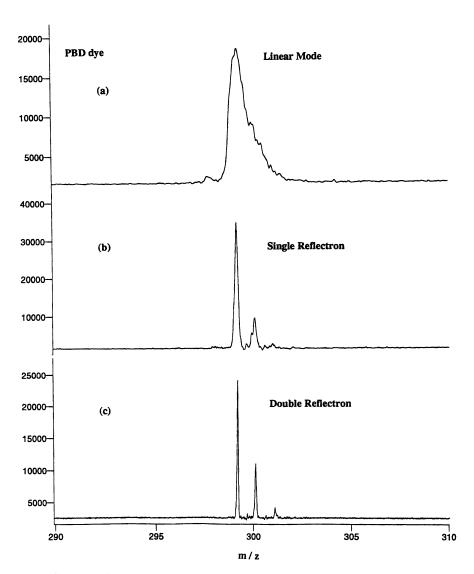


Figure 3. a) Linear mode mass spectra of PBD laser dye. b) Same as a) except spectrum was collected in the single reflectron mode.

c) PBD mass spectrum collected in the double reflectron mode.

spectra of peptides and small proteins, we have included the double reflectron spectrum of Gramicidin S showing a resolution of over 3000 for the (M+Na⁺) isotope cluster (Figure 4).

Tandem Time-of-Flight Studies

Two additions to the tandem time-of-flight instrument were required in order to perform CID experiments (8). First, there must be a capability to mass select ions without reducing the resolution or sensitivity of the ion signal. Gating (selection of single mass ions) was accomplished by applying a -100 V, 100 ns pulse at the appropriate delay time to one of the steering elements adjacent to the collision cell (see Figure 2 detail of the collision region). This element is held at +100 V during the mass selection mode of operation. While this is not a sufficiently high voltage to deflect the 4 kV ions completely out of the flight path, it is high enough to disrupt the trajectory of the ions through the second reflectron so that they collide with the flight tube wall before reaching the final detector. Even though all masses are present in the collision cell during CID operation, only those collision products of the gate selected ions will reach the detector.

The second modification involves the incorporation of a collision cell which would provide sufficient gas density for fragmentation of the ion beam yet would not raise the background pressure of the instrument significantly. This has been accomplished using a pulsed valve which delivers a high density of argon gas directly into the ion flight path. With appropriate timing between the valve pulse and the laser firing (see Figure 2), the primary ion signal is readily adjustable to any level of attenuation. The pulsed jet itself has a FWHM of approximately 200 μ s, sufficiently short to eliminate the need for a second pump in the vicinity of the collision cell. Background pressures are found to increase from about $1x10^{-6}$ to $6x10^{-6}$ during the valve pulse. Two additional grids separated by 0.05" were installed directly beyond the collision cell to define a second acceleration region.

Mass Dispersion

After the collision event, it is necessary to provide a means of temporally separating the product ions from their precursors since the velocities of all ions at this point are identical. This applies as well to the decay of metastable ions along the field free drift regions. Because ions of every mass would arrive at the detector simultaneously, no mass dependent information would be gained. To accomplish mass dispersion of the CID product ions, either an acceleration potential can be applied directly beyond the collision cell, or the second ion reflector can be employed.

Although this instrument was designed to incorporate either form of product ion mass dispersion, the data presented here demonstrate the separation of fragment ion peaks from their respective precursor ions by the second reflectron. This behavior is described precisely (5) for a 1-stage ion mirror by the relationship:

$$qE_f = ma = m(v_0/t) \tag{1}$$

where q is the charge of the ion, E_f is the field strength, v_0 is the ion velocity of mass m. The time spent in the reflectron is given by:

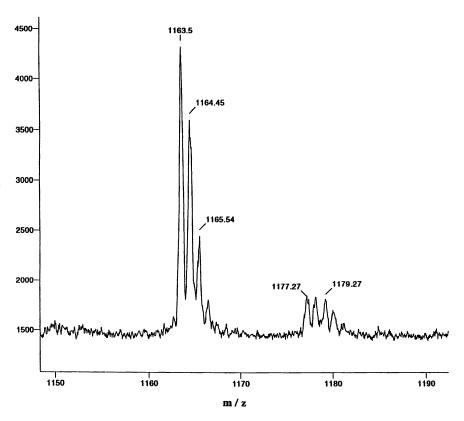


Figure 4. Double reflectron spectrum of Gramicidin S. (Reprinted with permission from Reference 8).

$$t = (2mv_0/qE_f) (2)$$

Two cases of ions passing through the reflectron are now considered. The first is its usual operation as an energy focusing device in which ions are accelerated out of the source with the same nominal energy E_k (4000 V in this case). Here, E_k is constant and the velocity of each ion is determined by the relationship:

$$v_0 = (2E_1/m)^{1/2} (3)$$

Substituting (3) into (2) yields:

$$t = k(m/m^{1/2}) = k(m)^{1/2}$$
 (4)

where k is a proportional constant. Since the time in the reflectron is proportional to the square root of the mass, the mass calibration is contiguous with the time spent in the drift regions. The alternate case occurs during metastable decomposition or induced fragmentation of the primary ion beam. In these situations, the precursor and product ions have the same velocity rather than the same energy. Referring to equation (2), v_0 is now constant so that

$$t = k(m) \tag{5}$$

and the time spent in the reflectron is <u>linearly</u> proportional to its mass. All ions enter the reflectron with the same velocity and penetrate to a depth directly proportional to their mass. It is important to note that the time spent in the drift regions (t_{drift}) does nothing to disperse the ions. Mass calibration can be determined from the relationship:

$$t_{prod} = (m_{prod}/m_{pre})t_{pre} + t_{drift}$$
 (6)

in which t_{pre} is the precursor ion's flight time referenced to the time of collision.

Mass dispersion in a 2-stage reflectron is not linear across the entire mass range due to the sharp change in the field gradient between the first and second stages of the mirror. Here, there are two separate conditions that result in linear mass dispersion. The first occurs when ions have sufficient kinetic energy to penetrate deeply into the second stage of the reflectron. The other is found in the first stage of the mirror for small mass ions lacking the energy required to pass beyond the middle grid. This abrupt change in field gradient produces a mixture of calibration slopes. Those ions found in the middle mass range which clear the first stage but cannot pass deeply into the second region are calibrated on a curve connecting the two linear regions.

The two reflectrons in the tandem TOF configuration therefore serve somewhat different purposes: the first is used solely for energy focusing of the precursor ions while the second simultaneously energy focuses and mass disperses the product ions. Post accelerating the product ions following the collision event will increase mass dispersion to a degree dependent upon the re-acceleration voltage applied. The higher the magnitude of the post acceleration potential, the greater the (m)^{1/2} contribution to the dispersion.

Operation of the Tandem Time-of-Flight

Figure 5 shows a series of CID spectra using the matrix α -cyano-4-hydroxy cinnamic acid as the test compound. In Figure 5a, the 190.1 amu peak represents the MH⁺ peak, and the 172.1 and 146.1 are due to the loss of water and CN groups respectively. Gate selected ions of mass 172 Da (E_{coll} = 4 kV) were collided with the pulsed jet of argon. The small peak observed at 20 μ s in Figure 5b is a metastable decay product of 172.1 Da ion. Figure 5c shows the affect of turning on the pulsed valve, producing fragmentation peaks at 146.1, 122.2, and 100.3 Da. Ion signal attenuation of the 190.1 Da peak is about 35% under these pulsed beam conditions. It is clear that the higher mass fragments are better resolved than are the smaller masses, mainly because the reflectron is tuned to energy focus the precursor ions. Moreover, smaller mass fragments experience more disruption in trajectory and velocity during the collision event than the heavier fragments and are thus more difficult to energy focus.

The tandem TOF spectrum of the dye rhodamine 6-G is shown in Figure 6. The 429.2 peak (M-15)⁺ was selected and collided with argon to produce a series of peaks separated by roughly 15 Da (Figure 6b). Post acceleration of 500 V was applied after the collision in order to improve the extraction efficiency yet not significantly alter the linearity of the observed fragment ion spectrum. In addition, the potential on the rear grid of second reflectron was reduced from 4020 V to 3950 V in order to filter out the remainder of the fragment ions formed during the original 4kV acceleration in the source region. Under these conditions, the 429.2 peak is substantially reduced in intensity while the entire product ion spectrum is shifted to slightly longer flight times.

This TOF-TOF CID spectrum was compared to a linked B/E scan of a magnetic sector instrument (Kratos Concept 1H double focusing mass spectrometer), again using argon as the collision gas but applying an 8kV lab frame collision energy. The resulting spectrum, plotted in Figure 6c, provides a good indication of performance of the tandem TOF instrument. Since the mass scale is known to be linear in the B/E scan, the linearity or lack thereof in the TOF spectrum can be determined. It is evident that, in spite of the 500 V post acceleration potential and the 2-stage reflectron configuration, the time-of-flight peaks match well with those from the sector instrument (Figures 6b and 6c). The fragments shown in this spectrum are the higher mass ions that penetrate far into the second reflectron region and therefore fall in the linear portion of the calibration curve.

Conclusions

We have shown that a dual reflectron tandem time-of-flight mass spectrometer is feasible for the CID study of small organic compounds and should be quite useful for the analysis of larger biological molecules as well. Very good mass resolution, selective gating without the use of restrictive slits, and the implementation of a pulsed molecular beam as the neutral gas collision source have been successfully demonstrated in this compact TOF/TOF design. In addition, mass dispersion in a tandem TOF has been discussed and evaluated for this instrument. The application of CID analysis to peptides and proteins will be the focus for the future development of this technique.

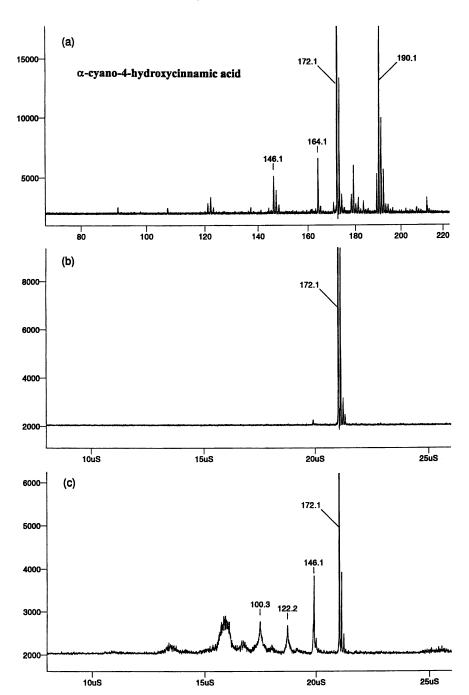


Figure 5. a) Complete TOF mass spectrum of α-cyano-4-hydroxycinnamic acid. b) Spectrum of 172.1 Da peak isolated for the CID experiment.

c) CID product ion spectrum of the 172.1 Da peak using argon as the collision gas. (Reprinted with permission from Reference 8).

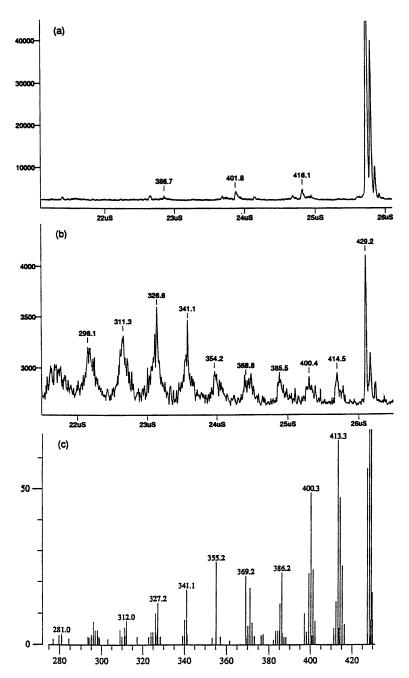


Figure 6. a) TOF mass spectrum of rhodamine 6-G. b) Tandem TOF CID product ion spectrum of rhodamine gating on the 429.2 Da peak. c) Product ion mass spectrum of 429.2 Da peak obtained by linked (B/E) scan on a double focusing mass spectrometer. (Reprinted with permission from Reference 8).

Acknowledgments

This work was supported by grant (GM 33967) from the National Institutes of Health, and carried out at the Middle Atlantic Mass Spectrometry Laboratory, a National Science Foundation Shared Instrumentation Facility.

Literature Cited

- Strobel, F.H.; Preston, L.M.; Washburn, K.S.; Russell, D.H. Anal. Chem. 1992, 64, 754.
- Cornett, D.S.; Peschke, M.; LaiHing, K.; Cheng, P.Y.; Willey, K.F.; Duncan, M.A. Rev. Sci. Instrumen. 1992, 63, 2177.
- Weinkauf, R.; Walter, K.; Weickhardt, C.; Boesl, U.; Schlag, E.W. Z. Naturforsch. 1989, 44a, 1219.
- 4. Della-Negra, S.; LeBeyec, Y. Anal. Chem. 1985, 57, 2035.
- 5. Standing, K.G.; Beavis, R.; Bollbach, G.; Ens, W.; Lafortune, F.; Main, D.; Schueler, B.; Tang, X.; Westmore, J.B. Anal. Instrumen. 1987, 16, 173.
- 6. Jardine, D.R.; Morgan, J.; Alderdice, D.S. Organic Mass Spectrom. 1992, 27, 1077.
- 7. Cornish, T.J.; Cotter, R.J. Rapid Commun. Mass Spectrom. 1992, 6, 242.
- 8. Cornish, T.J.; Cotter, R.J. Anal. Chem. 1993, 65, 1043.

RECEIVED September 16, 1993

Chapter 7

Electrospray Ionization on a Reflecting Time-of-Flight Mass Spectrometer

A. F. Dodonov, I. V. Chernushevich, and V. V. Laiko

Institute of Energy Problems of Chemical Physics, Russian Academy of Sciences, Chernogolovka, Moscow Region, 142432, Russia

A novel time-of-flight mass spectrometer with an ion mirror for continuous ionization sources has been developed. High sensitivity is achieved with moderate mass resolution (R > 1000) in this instrument, and the factors limiting the resolution are discussed. Several electrospray mass spectra demonstrate the main characteristics of this mass spectrometer.

There are several reasons for the renaissance in the development of the time-of-flight (TOF) mass spectrometry technique during the last decade. In the first place are the well-known advantages of TOF MS: a mass range limited only by the ion detector, high ion transmission, relatively low cost, the ability for simultaneous registration of ions of all masses (1,2, also see this book), and full spectrum sensitivities equal to that in the single ion monitoring regime. The second reason is the development of several approaches for improving the mass resolution of TOF MS. The most common method is the application of the electrostatic mirror originated by Mamyrin et al. (3). Finally, TOF MS is the best choice for the new pulsed ionization techniques such as plasma and laser desorption since it provides a complete spectrum per each event.

During the same period several new atmospheric pressure ionization (API) techniques have been developed which make possible an extremely sensitive and rapid analysis of molecular or elemental composition of gases, liquids, solutions and solid probes. These API techniques include corona discharge and radioactive foil ionization (4), electrospray ionization (5,6), ion-spray (7), thermospray (8) and inductively coupled plasma (ICP). Thus, it seemed attractive to us to design a TOF mass spectrometer with the above-mentioned ion sources and enjoy the advantages of both TOF MS and API methods. Unfortunately, all these ionization methods are inherently continuous and cannot be directly coupled with TOF mass analyzers without a tremendous loss of sensitivity. An example of interfacing a continuous chemical ionization source to the TOF mass analyzer was described by Pinkston et. al. (9). The need to extract short ion packets with a small energy spread resulted in a decrease of sensitivity: only 0.0025% of total ion current contributed to the recorded spectra.

0097-6156/94/0549-0108\$06.00/0 © 1994 American Chemical Society From 1985 to 1987 we designed and fabricated a new reflecting TOF mass spectrometer capable of mass analyzing continuous ion beams without loss of sensitivity (10,11). The present paper describes this instrument and its further development with an emphasis on results obtained with an electrospray ion source.

Instrument Layout and Principles

The atmospheric pressure ionization time-of-flight mass spectrometer is shown schematically in Figure 1. It consists of the following main parts: 1 - replaceable API source, 2 - vacuum interface with differential pumping system, 3 - time-of-flight ion storage modulator, 4 - deflection plates, 5 - ion drift region, 6 - two-stage ion mirror, 7 - ion detector, 8 - guard grid at high potential, and 9 - vacuum chamber. In brief the device works in the following manner. Any API source 1 is arranged outside the vacuum chamber 9, which is differentially pumped by a 5 L/s rotary pump and two 500 L/s turbo-molecular pumps. Low-energy ions (5 - 25 eV) entering the vacuum in the direction normal to the axis of the drift region are focused into a parallel beam and introduced into the time-of-flight ion storage modulator 3 where they continue moving under field-free conditions. With the frequency equal to several kilohertz (dependent on the largest mass to be analyzed) ions are pushed out from the ion storage modulator 3 to the drift region 5. A pair of deflection plates 4 is placed in the drift region to correct the ion trajectory. In order to keep the ion source and ion storage modulator potentials close to the ground, the drift region is floated at ± 2 kV. The cylindrical guard grid 8 serves to prevent penetration of the ground potential of the vacuum chamber 9 into the drift region. Having passed once through the drift region the ions enter a two-stage electrostatic mirror 6 which equalizes the time-of-flight of ions of the same mass with different initial coordinates and energies. Reflected ions pass through the drift region once again and finally reach the detector 7. The latter is a secondary electron multiplier made of two rectangular microchannel plates 63 x 43 mm². The multiplier is isolated from ground potential; therefore post-acceleration of heavy ions and negative ion registration are possible. A decoupling capacitor (4700 pF) is used to transmit the ion current pulses and enable these to be recorded near ground potential. The pulses are amplified and recorded by a stroboscopic registration system with 10-nanosecond resolution designed in-house. In the negative ion mode all potentials except that of multiplier are reversed.

A more detailed scheme of the time-of-flight ion storage modulator is shown in Figure 2. Operation of this part of the device does not depend strongly upon the type of ion source used; that is: it is assumed here that ions start their motion from a point source with zero initial energy, a skimmer orifice 1 being the point source. Ions are then accelerated and focused into a parallel beam by a grid 2 and a quadrupole lens 3. The latter narrows the beam in the x-direction, while widening it in the y-direction, thus coupling the axial symmetry of the source with the planar symmetry of the modulator. Part of the beam (usually about half of the ions) enters the ion storage modulator through a slit 4 (2 x 10 mm²). Initially, a repeller plate 5 and the first grid 6 are at ground potential, and ions move towards the ion collector 7 which helps to adjust and control the ion current entering the modulator. When the space between plate 5 and grid 6 is filled with ions, both push-out and draw-out voltage pulses are applied simultaneously to plate 5 and the second grid 8, respectively; and the ion packet is drawn into the acceleration region between grids 8 and 9. Ions entering the

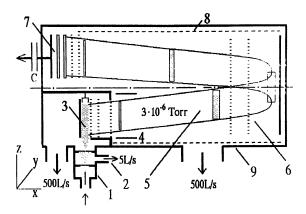


Figure 1. Construction of the API TOF mass spectrometer with an ion mirror.

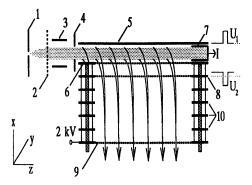


Figure 2. Schematic diagram of the time-of-flight ion storage modulator.

modulator at the time the pulse is applied are deflected by the push-out pulse and removed to the frame of grid 6. The value of the draw-out voltage pulse is selected to ensure a homogeneous electric field across the whole gap from plate 5 to grid 8. This prevents ion scattering near the wires of grid 6 where the defocusing effect could be strong for ions with low kinetic energy. The output grid 9 is held at 2 kV and is connected to the guard grid 8 in Figure 1. All of the grids were made on stainless steel rectangular frames from tantalum wire of 50 µm diameter. The wires are stretched in z-direction and spaced by 1 mm except for grids 6 and 8, which are twice as dense. To prevent field distortions in the acceleration region, guard frames 10 are placed between grids 8 and 9. The frames are connected by a built-in voltage divider.

A strong electric field in the acceleration region results in field penetration into the ion storage gap between plate 5 and grid 6, and part of the ion beam is therefore drawn-out into the drift region continuously. To avoid field penetration, a small potential of the opposite polarity should be applied to grid 8 between the draw-out pulses. The value of this potential can be calculated by relationship [1] derived from the equations given in (12):

$$U - E\left(\frac{a}{2\pi}\right) \ln \frac{a}{2\pi r}$$
 [1]

where E is the field strength in the acceleration region, a is the distance between the parallel wires of the grid, and r is the radius of the wires. In our case this value is equal to 5.6 V.

The ion mirror design is similar to that of the ion storage modulator. It consists of two grids, 18 guard frames and a plate, forming two regions with uniform fields of different strength. The first grid is connected to the cylindrical guard grid, while the second grid and the plate potentials were adjusted to ensure time focusing of ions with different initial coordinates and energies (see the next section). The main parameters of the instrument are summarized in Table I.

It is obvious from the previous description that there are two processes taking place simultaneously at any moment of operation except during the pulse time. The first process is the accumulation of input ions in the ion storage modulator; the second is the time-of-flight separation of ions in the drift region. To coordinate the ion motion in the x and z directions and maximize sensitivity, several requirements must be fulfilled. The filling time of the modulator must not exceed the flight time of the same ions in the drift region. Consequently, relationship [2] must hold:

$$U/u \le (L^*/b)^2 \tag{2}$$

where U and u are the ion energies in the drift region and in the modulator, L^{\bullet} is an effective drift length (exceeding L in Table I) and b is the length of the ion storage region. The mass spectrum repetition rate (corresponding to the frequency of application of the push-out and draw-out pulses) must be low enough to enable the heaviest ions of mass M to fill the storage modulator:

$$f < \sqrt{2eU/M/b} \tag{3}$$

When relationships [2] and [3] are fulfilled, any mass peak area is proportional to the corresponding ion concentration in the storage modulator. Thus, for ions of masses M_1 and M_2 equation [4] may be written:

$$S(M_1)/S(M_2) - I(M_1)/I(M_2) * \sqrt{M_1/M_2}$$
 [4]

where I(M) and S(M) are the corresponding input ion currents and peak areas. Thus, at the given upper mass limit (i.e., constant frequency) sensitivity is better for heavy ions due to their lower velocity in the z direction. To enable the ion trajectories to reach the detector, one more requirement must be fulfilled:

Table I: API TOF Mass Spectrometer Dimensions and Potentials in the Positive Ion Mode

Potentials, V:	
skimmer 1 (u)	5 + 25
focusing grid 2	-21
repeller plate 5 (base/pulse, U_1)	0/180
grid 6	0
grid 8 (base/pulse, U_2)	5.6/-120
grid 9 $(U_2 + U_3)$	-2000
ion drift region	-2000
ion mirror grid 1	-2000
ion mirror grid 2	
with respect to grid 1 (U_T)	1510.8
ion mirror plate	
with respect to grid 2 (U_K)	853.4
detector grid 1	-2000
detector grid 2	-5000
Distances, mm:	
repeller plate 5 to grid 6 (d_1)	3
grid 6 to grid 8 (d_2)	2
grid 8 to grid 9 (d_3)	32
total field-free region length (L)	1516
ion mirror:	
grid 1 to grid 2 (d_T)	49
grid 2 to plate (d_{κ})	91
initial ion packet dimensions:	
in x-direction	2 ÷ 3
in y-direction	< 20
in z-direction	50

Transmission through all grids: > 50%

$$U/u - (L^*/B)^2$$
 [5]

where B is the distance between the centers of the ion storage modulator and the detector. In this case no additional deflection is needed. The application of deflection plates 4 (Figure 1) to bend ion trajectories is undesirable since it decreases the resolution (see the next section).

To conclude this section, it is necessary to mention three other groups where TOF mass spectrometers with "orthogonal acceleration" of ions have been developed independently (13-17). The design of Guilhaus and Dawson (13-15) resembles our API TOF, but differs in at least two important features: there is no ion mirror, and accumulation of ions is not utilized to maximize sensitivity. The first one results from a wide-spread mistake that the application of the reflectron is restricted to the sources where ions are accelerated simultaneously from a well defined plane (e.g., laser or plasma desorption). Cotter and coauthors used a similar method in their continuous SIMS instrument (16). The apparatus described in (17) is also not a reflecting instrument, and was designed to probe ion clusters. During 1991 and 1992 two additional groups have constructed TOF mass spectrometers with orthogonal acceleration of ions, using atmospheric pressure ionization of gases (18) and electrospray ionization (ESI) of solutions (19).

Mass Resolution

The most significant limitation on the resolution of the API TOF mass spectrometer may be imposed by the following factors: coordinate spread of ions in the ion storage modulator and consequent energy spread; initial kinetic energy spread of ions; deflection of ions in the ion drift region; rise time of the push-out and draw-out pulses; and ion scattering in a nonuniform field near the grids. All of these are important enough to be discussed here.

Time spread compensation in a two-stage electrostatic mirror. The accumulated ions start their motion in the x-direction from points with coordinates differing within 3 mm (equal to the gap width d_1 from plate 5 to grid 6) and acquire energies in this gap differing from 0 to 180 eV (corresponding to the push-out pulse voltage U_1). Both coordinate and energy spreads can lead to a spread in the time-of-flight of ions if not compensated by the ion mirror. To obtain the ion mirror parameters necessary for this compensation (following procedures developed in (3,20)), we first calculate the total flight time neglecting the initial energy spread in x-direction:

$$t - \sqrt{\frac{m}{2q}} \left[2 \left(\frac{d_1}{U_1} - \frac{d_2}{U_2} \right) \sqrt{kU_1} + 2 \left(\frac{d_1}{U_2} - \frac{d_3}{U_3} \right) \sqrt{kU_1 + U_2} \right]$$

$$+2\left(\frac{d_3}{U_3}+\frac{2d_T}{U_T}\right)\sqrt{kU_1+U_2+U_3}$$
 [6]

$$+ 4 \left(\frac{1}{E_K} - - \frac{d_T}{U_T} \right) \sqrt{kU_1 + U_2 + U_3 - U_T} + \frac{L}{\sqrt{kU_1 + U_2 + U_3}}$$

where m/q is the mass to charge ratio of the ion, k is a dimensionless coordinate of ion starting plane (k = 1 near plate 5 and k = 0 near grid 6), and E_K is the field strength in the second stage of the mirror; all the other notations are given in Table I. For the second order time focusing of ions, second and third terms of the Taylor series expansion of t(k) should be set to zero at k=1/2. So equations [7] should be solved

$$\left(\frac{\partial t}{\partial k}\right)_{k=1/2} - 0 \quad \left(\frac{\partial^2 t}{\partial k^2}\right)_{k=1/2} - 0$$
 [7]

giving the unknown parameters of the mirror U_T and E_K :

$$U_{T} - U_{1} \frac{c_{2}p_{0} - c_{1} - Lp_{0}^{-3/2} - 2d_{T}p_{0}^{-3/2}}{c_{2} + \frac{d_{3}}{p_{0}}p_{0}^{-3/2} - \frac{3}{2}Lp_{0}^{-5/2}} - p_{T}U_{1}$$
[8]

$$E_{K} - U_{1} \left(\frac{d_{T}}{p_{T}} + \sqrt{p_{0} - p_{T}} \left[p_{0}^{-1/2} \left(\frac{L}{4p_{0}} - \frac{d_{3}}{2p_{3}} - \frac{d_{T}}{p_{T}} \right) - \frac{c_{1}}{2} \right] \right)^{-1}$$
 [9]

where p_i (i = 1,2,3,K or T) are the dimensionless voltages $p_i = U_i/U_1$, p_0 is the mean ion energy in the drift space ($p_0 = 1/2 + p_2 + p_3$) and $c_{1,2}$ are defined by equations [10] and [11]:

$$c_1 - \left(d_1 - \frac{d_3}{p_3}\right) \left(\frac{1}{2} + p_2\right)^{1/2}$$
 [10]

$$c_2 - \left(d_1 - \frac{d_3}{p_3}\right) \left(\frac{1}{2} + p_2\right)^{1/2}$$
 [11]

Equations [8] to [11] are already simplified taking into account that the field strength is equal in the gaps d_1 and d_2 . Substituting the values of potentials and distances from Table I into equations [8], [9] and [6], one can find a theoretical limit for the "bottom" mass resolution (i.e. the lower resolution limit) of our API TOF instrument: $R_1 = 28200$. Although this value for R_1 is large enough for the total resolution to be limited by some other factors, it seemed interesting to us to find the conditions for the third-order time focusing of ions, so that the total flight time would be independent of k to third order. The problem arose when the second generation API TOF device was

designed and it was easy to alter its dimensions. So, the acceleration gap width d_3 was chosen to be the third unknown parameter in addition to U_T and E_K , and equations [7] were supplemented by the requirement that the third derivative of t(k) is equal to zero at k = 0.5. Analytical calculations are hardly possible for the resulting bulky equations. Nevertheless, it can be shown that only if E_3 is less than E_1 third order focusing is possible. Finally, the value of d_3 corresponding to the best resolution was found by means of numerical simulations. A new set of parameters differing from that in Table I was used in the calculations: $U_1 = 140 \text{ V}$; $U_2 = 93.3 \text{ V}$; $U_3 = 1906.7 \text{ V}$; d_1 = 3 mm; d_2 = 2 mm; d_T = 28.7 mm; d_K = 40 mm; L = 706 mm. Equations [8] and [9] were used in the calculations to ensure second order time focusing for each value of d_3 . The results of these simulations are shown in Figures 3 and 4. Each curve in Figure 3 represents a relative time-of-flight difference [t(k) - t(0.5)]/t(0.5) for ions starting from different initial coordinates k, gap width d_3 being a parameter. Curves 1 and 3 have a shape close to a cubic parabola, while a highly symmetric curve 2 confirms that the cubic term in Taylor's expansion has vanished and the third order time focusing is achieved. The "bottom" resolution as a function of d_3 is shown in The greatest resolution $R_1 = 303000$ is achieved when $d_3 = 48$ mm. Unfortunately, this frightening resolution value has nothing to do with the total resolution of the real device. Many other factors limiting the resolution cannot be compensated to the same extent.

The influence of the initial energy spread of ions on the resolution can be partly compensated by the mirror. In this case the total flight time is

$$t = \sqrt{\frac{m}{2q}} \left[-2\frac{d_1\sqrt{\varepsilon}}{u_1} + 2\left(\frac{d_1}{U_1} - \frac{d_3}{u_3}\right)\sqrt{\varepsilon + kU_1 + U_2} \right]$$

$$+ 2\left(\frac{d_3}{U_3} + \frac{2d_T}{U_T}\right)\sqrt{\varepsilon + kU_1 + U_2 + U_3}$$

$$+ 4\left(\frac{1}{E_k} - \frac{d_T}{U_T}\right)\sqrt{\varepsilon + kU_1 + U_2 + U_3 - U_T}$$

$$+ \frac{l}{\sqrt{\varepsilon + kU_1 + U_2 + U_3}}$$
[12]

where $e\varepsilon$ is the initial kinetic energy of ion in the x-direction. Comparing equation [6] and [12], it is easy to notice that they differ in two aspects: kU_1 is replaced by $(\varepsilon + kU_1)$, and an additional term is present in equation [12]: $-(2d_1/U_1)(\varepsilon m/2q)^{1/2}$. This term is equal to a half of the "turn-around time" which is known to be not compensated in any static fields. Thus, it is impossible to fulfill the requirements of the second order time focusing (equations [7]) for the whole equation [12], but it seems reasonable to

do it ignoring the term corresponding to the turn-around time. It is obvious that the result will be the same as in equations [8] - [11]. Taking into consideration the value obtained for R_1 , one can see that the final time spread is equal to the turn-around time.

In the API TOF spectrometer the initial energy spread is determined mainly by imperfect focusing of ions into a parallel beam. To appreciate the resolution R_2 due to the turn-around time, three types of ion focusing were examined: 1 - ideal focusing into a parallel beam, 2 - no focusing at all (i.e. ions move radially from a point source), 3 - focusing to the center of the accumulation region (in z-direction), maximizing the ion current on the collector 7. In the last two cases the maximum angle between the ion velocity vector and z-axis is roughly the same: $\theta_{max} \approx 0.05$. The maximum initial energy in x-direction is therefore equal to $\varepsilon = u \sin^2 \theta_{max} \approx 0.0125$ and the resolution

$$R_2 - \frac{t}{2\Delta t} - \frac{L^* U_1}{8d_1 \sqrt{\varepsilon U_0}} \approx 6000$$
 [13]

where t is the total flight time, Δt is the turn-around time, L^* is the effective drift length, and U_0 is the mean ion energy in the drift region. In the first case the angle θ_{max} is determined basically by the effective diameter of the skimmer orifice d_{eff} which is assumed to be $d_{eff} \approx (2 + 3) \cdot d \approx 0.2 + 0.3$ due to some ion scattering after skimmer. This gives us $\theta_{max} = d_{eff}/f \approx 0.005$, where f is the focal length of the lens, and $R_2 \approx 600000$.

Influence of ion deflection. Most of the reflecting TOF mass spectrometers contain deflection plates to correct ion trajectories. The main drawback of such an adjustment is that the ion packet gets bent after deflection. In the first approximation the slope of the ion packet after deflection turns out to be equal to the deflection angle of the ion trajectory (20). This limits resolution by the value:

$$R_3 - \frac{L^* dU_0}{\Delta U \ hl}$$
 [14]

where ΔU and d are the voltage and distance between the deflection plates, l is their length, and h is the ion packet length in z-direction. In our initial experiments we had to use deflection plates, since the ion energy u was larger (25 eV) than that required by equation [5] (\approx 5 eV). As a result, $\Delta U = 200$ V was applied to the plates to deflect ions from the tube axis, with resolution being as low as 440. Since the focusing grid was placed after skimmer, it became possible to lower u to 5 eV. Therefore, ion deflection is not used now in the device.

Other limitations. It is usually supposed that the rise-time of draw-out and push-out pulses must be shorter than the desirable ion current pulse duration. This is not the case when a two-stage ion mirror is used. To prove this statement, computer simulations were made. The rise-time of both pulses was approximated by a linear function consisting of 50 voltage steps. The main result of these simulations for the rise-time $\tau = 100$ ns is shown in Figure 5 where "bottom" resolution R_4 is plotted versus ion mass, other parameters being the same as in Figures 3,4. It is noteworthy

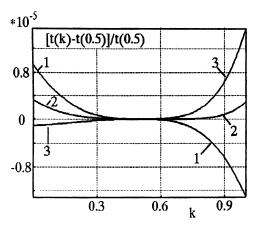


Figure 3. Calculated relative time-of-flight difference plotted as a function of the starting coordinate k for $d_3 = 40$ mm (1), $d_3 = 48$ mm (2) and $d_3 = 56$ mm (3).

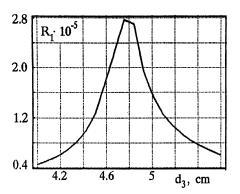


Figure 4. Calculated bottom resolution R_1 plotted as a function of d_3 .

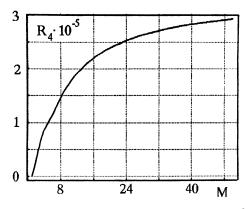


Figure 5. Calculated mass dependence of bottom resolution R_4 for rise-time of the pulses $\tau = 100$ ns.

that the rise time of the pulses does not affect seriously the resolution for ions heavier than 20 Da.

The axial velocity of the ion may be changed by scattering from the grids, thus producing a spread of flight times. In a reflecting instrument, however, the mirror compensates part of the velocity spread which appears in the accumulation region. On the other hand, the mirror cannot compensate the scattering from its own grids. Expressions for scattering from grids have been derived in (21). The maximum scattering angle for paraxial rays

$$\alpha_{\text{max}} = \frac{a(E_2 - E_1)}{4V}$$
 [15]

where $E_{1,2}$ are the electric fields on both sides of the grid, V is the ion energy near the grid, and a is the spacing between grid wires, all the wires being parallel to z-axis. Substituting the values from Table I, $\alpha_{(1)max} \approx 0.01$ was obtained for grid 9 of the modulator, $\alpha_{(2)max} \approx 0.004$ for the entrance grid of the mirror and $\alpha_{(3)max} = 0.006$ for the middle grid. As the scattering occurs twice on both mirror grids, the total maximum angle after the reflection will be $\alpha_{max} = \sum \alpha_{(i)max}$. Assuming that only the second half of the flight time is "spoiled" by scattering, the relative change in flight time is given by

$$\Delta t/t - 1/4 \left(\sum \alpha_{(i)\text{max}}\right)^2 - 2.5 \ 10^{-4}$$
 [16]

The corresponding "bottom" resolution is $R_5 \approx 2000$.

Provided that all grids and plates are plane and parallel to each other, ions are focused into a parallel beam and the deflection of ions is not used, the overall resolution of the API TOF instrument is limited by the ion scattering from the grids. The great potential of the third order time focusing cannot be used in this device and is interesting mainly from a theoretical point of view.

Application of Electrospray on API TOF Mass Spectrometer

Several API-sources have been coupled to our TOF instrument: ion sources with corona discharge, with tritium foil, with UV-lamp and electrospray ionization (ESI) (22,23). The latter seems to be the most popular ionization technique today. Together with laser and plasma desorbtion (LD, PD), secondary ion mass spectrometry (SIMS) and fast atom bombardment (FAB), ESI has had a revolutionary effect in the integration of mass spectrometry in biological research (24,25). Some results of the API TOF device operation with ES are discussed in this section.

Ion Source Design. The ESI ion source is schematically shown in Figure 6. It is partly similar to those conventionally used (5,7,24) and consists of a stainless steel capillary 1 (0.1 mm i.d., 0.5 mm o.d.) which protrudes ~2 mm from a glass capillary 2 (~1 mm i.d. at the tip), a gas curtain electrode 3, a nozzle 4 (orifice diameter 0.4 mm), an additional focusing electrode 5 and skimmer 6 (orifice diameter 0.1 mm). A voltage of between +2.5 and +5 kV (for positive ions) is applied to capillary 1. A flow of dry air or oxygen (~100 cm³s⁻¹) assists the nebulization and suppresses corona discharge. A syringe pump controls the flow of analyte liquid at typically 2 μ L/min.

A countercurrent flow of dry nitrogen (~100 cm³s⁻¹) is used as a gas curtain for large droplets. A voltage of 1 kV is applied between electrode 3 and nozzle 4 to pull ions through the gas curtain towards the nozzle. Both nozzle and skimmer electrodes are flat, the orifices made in stainless steel foil 0.1 mm thick. A strong nonuniform field near the skimmer orifice, which helps to focus and decluster ions in the case of conical skimmer, is obtained by an additional focusing electrode 5, placed near skimmer. The ion source construction allows one to move nozzle 3 along the axis with respect to skimmer 5. Thus, the optimal conditions for ion transmission were obtained (20). It turned out that for any nozzle diameter in the range from 0.2 to 0.5 mm and any pumping speed from 1 to 5 L/s, the nozzle - skimmer separation Δz should $\Delta z \approx 2.5x_{\rm M}$, where $x_{\mathbf{M}}$ is the distance from the nozzle orifice to Mach disc. This empirical relationship provides the maximum ratio of the ion current per neutral gas flow through the skimmer orifice. In our standard conditions $\Delta z \approx 8$ mm. An additional requirement must be fulfilled for the electrode potentials: nozzle potential U_n must be equal to $U_{\bullet} \approx 0.75 \Delta U$, where ΔU is the focusing electrode potential, both potentials measured relative to skimmer. It is noteworthy that in these conditions ions move against the electric field part of their way from the nozzle to skimmer. Typical voltages are $\Delta U = 200 \text{ V}$ and $U_n = 150 \text{ V}$, corresponding to a total declustering and low degree of fragmentation of ions. Typical values of ion current measured on different electrodes are listed in Table II.

Table II. Typical Values of Ion Current Measured on Different Electrodes

Ion current from capillary	$(10^{-6} + 10^{-7})A$
Ion current through nozzle orifice	$(10^{-8} \div 10^{-10})A$
Ion current on collector 7 (Figure 2)	$(10^{-11} + 10^{-13})A$
Ion current on detector 7 (Figure 1)	$(10^{-12} + 10^{-15})$ A

Results and Discussion

Two mass spectra shown in Figures 7a and b demonstrate sensitivity (a) and resolution (b) of the API TOF instrument coupled with ES-source. The first spectrum was recorded for gramicidine S dissolved in pure methanol, the concentration being 2·10⁻⁶M. Two thousand spectra were accumulated with 8 kHz mass spectra repetition frequency. Thus, ~1.5 minutes are necessary to obtain this spectrum with our stroboscopic registration system (250 points) or 0.25 seconds if a transient recording system is used. If the analyte liquid consumption could be restricted by this time interval, only 16 femtomoles of gramicidine would be necessary to record this spectrum.

To evaluate the resolving power, a monoisotopic peak of malachite green was used (Figure 7b). The total flight time of molecular ion (m/z = 329) is $t = 58.8 \,\mu$ s, and the time spread at half height is 30 ns; the resolution is therefore ~1000. Taking into account the time resolution of the stroboscopic registration system (10 ns), it is clear that the resolution of the mass spectrometer itself is much better. Mass resolution could be determined more precisely for the peaks of ions with greater m/z ratio, if they were not broadened by an isotopic distribution. Furthermore, the time spread of heavy ions (starting with $m \approx 1000$) is not proportional to flight time, as it

is generally assumed, and resolution decreases for higher masses (24). The reasons for this fact are not quite clear now. Insufficiently high vacuum can account only for a part of this additional time spread.

To obtain information on ion structure, collision-induced dissociation (CID) is commonly used with electrospray ionization (5,6,24). CID can occur both in a special collision chamber or in an intermediate region of a differential pumping system (6). In the API TOF instrument CID takes place between the focusing electrode 5 and skimmer 6 (Figure 6), where a sufficient field strength is ensured by the value of ΔU . Two mass spectra of multiply charged ions of melittin (MW = 2846 Da) are given in Figures 8a and b, differing in the value of ΔU : $\Delta U = 200 \text{ V}$ for Figure 8a and $\Delta U = 350 \text{ V}$ for Figure 8b. The first spectrum contains only molecular ion peaks, while increasing voltage to $\Delta U = 350 \text{ V}$ makes it possible to break chemical bonds and obtain a fragment ion spectrum. In the case of melittin, doubly and triply charged "y" type sequence ions are produced in CID (see (25) for a description of peptide fragment labelling nomenclature). Although the efficiency of CID decreases for heavier ions, it enables one to obtain limited sequence information or confirm the primary structure of a peptide.

Accurate mass determination has been one of the strengths of ESI mass spectrometry and is easily obtained on the API TOF instrument. One or two ion peaks in the mass spectrum are necessary to calibrate the mass scale. Usually singly- and doubly-protonated ions of gramicidin S with m/z = 1142.5 and m/z = 571.75 are used for calibration. Both reference m/z values and those obtained from the calibrated spectrum are isotopically averaged. A typical accuracy of mass determination for ion masses $m \le 10000$ is 0.05%, being a little worse for fragment ions. The molecular weight of hen egg lysozyme was determined from the mass spectrum given in Figure 9. The sample was dissolved at 10^{-3} M in 50% acetonitrile, 50% water, 1% acetic acid (v/v/v), and 2000 spectra were accumulated. A standard procedure described by Fenn (5) was used for the molecular weight determination. Thus, the experimental value $MW_{exp} = 14304.4$ Da was obtained from the five largest peaks in Figure 9. This value is quite close to that calculated from the amino acid sequence: $MW_{calc} = 14306$ Da.

Conclusions

We have shown here that the application of the TOF mass spectrometry is not confined to pulsed ionization methods. Most of the continuous ionization techniques may be coupled to TOF mass analyzers in the way described in this paper. The main advantage of the original construction lies in the fact that high sensitivity is compatible with moderate mass resolution. The initial energy spread of ions affects, only slightly, both resolution and sensitivity. Up to now not all the resources of the API TOF instrument have been utilized. We have demonstrated that the resolving power of our device is limited by the ion scattering from the grids. Therefore, it seems attractive to make use of the gridless reflector (26) to enhance both resolution and sensitivity. Some work has been done in this direction.

Finally, it would be useful to turn back to the beginning of this paper: the advantages of TOF mass spectrometry. It is well-known that ESI does not require an unlimited mass range, since multiple charging of ions reduces the m/z values to m/z < 4000 Thomsons. However, this is not the case when thermospray or some other continuous ionization techniques are used, where multiple charging is less abundant.

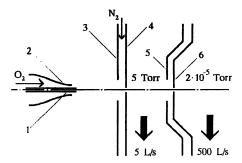


Figure 6. Schematic diagram of the electrospray ion source.

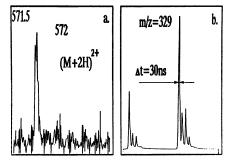


Figure 7. ESI mass spectra demonstrating sensitivity (a) and resolution (b) of the API TOF instrument.

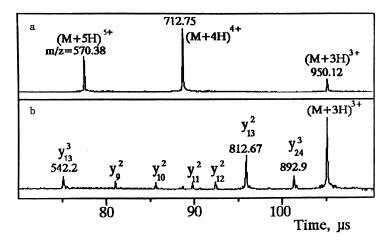


Figure 8. ESI mass spectra of melittin recorded at $\Delta U = 200V$ (a) and $\Delta U = 350V$ (b).

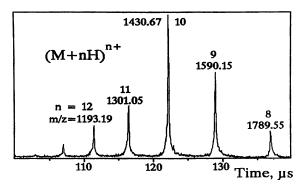


Figure 9. ESI mass spectrum of hen egg lysozyme.

The stroboscopic registration system will be replaced in the near future by an integrating transient recording system allowing simultaneous registration of ions of all masses. This means that approximately 1 second will be required to record the mass spectrum given in Figure 9. The possibility of fast spectrum acquisition together with pneumatically-assisted nebulization of large flows of analyte liquid (7) will enable us to interface high-performance liquid chromatography to the API TOF mass spectrometer.

In the longer term, we expect to interface an inductively-coupled plasma (ICP) source to our instrument for laser evaporation of solid probes.

Acknowledgements

We thank Dr. A.N. Verentchikov and Dr. V.A. Shkurov for help and discussions during our initial steps in electrospray of peptides. We are also grateful to Dr. A.V. Tolmachov for computer simulations of the ion trajectories.

Literature Cited

- Emary, W.B.; Lys, I.; Cotter, R.J.; Simpson, R.; Hoffman, A., Anal. Chem., 1990, 62, 1319-1324.
- (2) Holland, J.F.; Newcomb, B.; Tecklenburg, Jr., R.E.; Davenport, M.; Allison, J.; Watson, J.T.; Enke, C.G., Rev. Sci. Instrum., 1991, 62, 69-76.
- (3) Mamyrin, B.A.; Karataev, D.V.; Schmikk, D.V.; Zagulin, V.A, Sov. Phys. JETP, 1973, 37, 45.
- (4) French, J.B.; Thomson, B.A.; Davidson, W.A.; Reid, N.M.; Buckley, J.A., in Mass Spectrometry in Environmental Sciences; Karasek, F.W.; Hutzinger, O.; Safe, S., Eds.; Plenum Press: New York, 1985, Chapter 6.
- (5) Fenn, J.B.; Mann, M.; Meng, C.K.; Wong, S.F.; Whitehouse, C.M., Mass Spectrometry Reviews, 1990, 9, 37-70.
- (6) Alexandrov, M.L.; Gall, L.N.; Krasnov, N.V.; Nikolayev, V.I.; Pavlenko, B.I.; Shkurov, V.A., Reports of Academy of Sciences (Russian), 1984, 277, 379-383.

- (7) Bruins, A.P.; Covey, T.R.; Henion, J.D, Anal. Chem., 1987, 59, 2642-2646.
- (8) Blakley, C.R.; Vestal, M.L., Anal. Chem., 1983, 55, 750-754.
- (9) Pinkston, J.D.; Rabb, M.; Watson, I.Th.; Allison I., Rev. Sci. Instrum., 1986, 57, 583-592.
- (10) Dodonov, A.F.; Chernushevich, I.V.; Dodonova, T.F.; Raznikov, V.V.; Tal'rose, V.L., (inventors), *Inventor's Certificate No. 1681340A1*, USSR (February 25, 1987).
- (11) Dodonov, A.F.; Chernushevich, I.V.; Dodonova, T.F.; Raznikov, V.V.; Tal'rose, V.L., (inventors), *International Patent Appl.*, *PCT/SU89/00228* (April 1989).
- (12) Lukoshkov, V.C., Proceedings of the Academy of Sciences of the USSR (Physical Series), 1944, 8, 243-247.
- (13) Dawson, J.H.J; Guilhaus, M., Rapid Comm. Mass Spectrom., 1989, 3, 155-159.
- (14) Dawson, J.H.J.; Guilhaus, M., (inventors), Australian Provisional Patent P16079 (December 1987), Unisearch Limited.
- (15) Coles, J.; Stutsel, M.; Guilhaus, M., 40th ASMS Conference on Mass Spectrometry and Allied Topics, Abstracts of Papers, 1992, 10-11.
- (16) Olthoff, J.K.; Lys, I.A.; Cotter, R.J., Rapid Comm. Mass Spectrom., 1988, 2, 171-175.
- (17) Kennedy, R.A.; Kung, C.-Y.; Miller, J.P. in *Ion and Cluster Ion Spectroscopy* and Structure; Maier, J.P., Ed.; Elsevier, 1989; pp 213-239.
- (18) Sin, C.H.; Lee, E.D.; Lee, M.L., Anal. Chem., 1991, 63, 2897-2900.
- (19) Boyle, J.G.; Whitehouse, C.M., Anal. Chem., 1992, 64, 2084-2089.
- (20) Chernushevich, I.V., Doctoral Thesis: Institute of Energy Problems of Chemical Physics, Russian Academy of Sciences, Chernogolovka, 1991.
- (21) Konstantinov, O.V.; Mamyrin, B.A.; Schebelina, L.E.; Schebelin, V.G., J. Techn. Phys. (Russian), 1986, 56 (6), 1075-1081.
- (22) Tal'rose, V.L.; Dodonov, A.F.; Chernushevich, I.V., Pittsburg Conference on Analytical Chemistry and Applied Spectroscopy, Abstracts of Papers, March 3-8, 1991, Chicago, Illinois, 1991, 299P.
- (23) Dodonov, A.F.; Chernushevich, I.V.; Laiko, V.V., 12th Int. Mass Spectrometry Conference, Book of Abstracts, August 26-31, 1991}, p. 153.
- (24) Smith, R.D.; Loo, J.A.; Edmonds, C.G.; Barinaga, C.J.; Udseth, H.R., Anal. Chem., 1990, 62, 882-899.
- (25) Carr, S.A.; Hemling, M.F.; Roberts, G.D., Anal. Chem., 1991, 63, 2802-2824.
- (26) Grix, R.; Kutsher, R.; Li, G.; Gruner, U.; Wollnik, H., Rapid Comm. Mass Spectrom., 1988, 2 (5), 83-85.

RECEIVED October 12, 1993

Chapter 8

Radically New Time-of-Flight Mass Spectrometric Instrumentation

Making Single-Ion Concepts Provide Higher Performance

Robert J. Conzemius

Ames Laboratory, Iowa State University, Ames, IA 50011

Two techniques are described which utilize more radical concepts than current mass spectrometric approaches to characterization of solid specimens. Enhancement in interpretation and instrument performance as well as simplification of components are gained. The first technique uses quite conventional 300-picosecond uv laser desorption of very low numbers of ions which are subsequently tested for tendencies to be co-desorbed and/or dependent upon the total number of ions created. The second technique is more radical in its approach and uses single ion projectiles to cause desorption directly from a solid specimen of single or very few secondary ions. This new concept of mass measurement is in essence mass difference spectrometry. It promises very high mass resolution along with observation of speciation in the solid specimen.

Advances in instrumental techniques have made revolutionary improvements in analytical characterization and in these advances, mass spectrometry (MS) has played a prominent role. However, there are three areas where MS has had difficulty making significant inroads. These areas are:

- Radical reductions in instrument complexity and cost have not been realized;
- MS has not contributed significantly to the direct observation of speciation;
- Improvements in means for producing ions directly from specimens of interest have generally placed burdens on ion optical systems rather than enhancing their performance. An example of a strong driving force for advance of technology but usually associated with placing a significant burden on the ion optics and upon the entire instrument design has been the recent emphasis upon introducing liquids directly into the ion source (1-3).

The purpose of this development has been to investigate what can be done to eliminate or at least minimize the complexities and the cost associated with MS while permitting the observation of speciation and by allowing the ion production phenomenon to complement the ion optical system. In doing this it would be desirable to eliminate the need for rf voltages (Quadrupoles), magnetic fields (Sector

0097-6156/94/0549-0124\$09.25/0 © 1994 American Chemical Society CONZEMIUS

Instruments), pulsed voltages (Time-of-Flight), intricate scanning requirements (MS/MS), large numbers of instrument parameters (Plasma discharges, Variable flow rates, high pump speeds, etc.), and the comparatively high costs for instrument maintenance (Rapid deterioration of components due to high currents and pressures). My approach to this endeavor was to consider concepts contrary to current trends. Rather than increasing ion signals, why not let them approach zero levels. The approach also allowed freedom to eliminate the mass spectrum as a necessary or even best means to obtain the information carried by ions emitted from an ion source.

Lets look at MS differently. Mass spectra are composites of "n" ionization events where n is commonly very large. The scientist works backwards from these composites and postulates which individual ionization events caused the spectra to occur. Various ion optical schemes have been designed and refined to improve mass resolution, sensitivity, and instrument versatility such as scanning modes to aid the scientist in the interpretation. We could be placing too much emphasis and burden on the ion optical systems to aid in the interpretation of these composite mass spectra? Why not look directly at individual atomic and molecular events?

The first of the two techniques described here is within the domain of MS but approaches it from a different perspective. The second technique is a radical approach toward accomplishing the above goals. In this second technique single ions will be viewed as individual chisels upon the surface of the specimen (4, 5). Other work with TOF-MS considering phenomena such as "spontaneous desorption" (6), "coincidence counting" with ²⁵²Cf fission fragment bombardment of the specimen (7, 8), and "ion correlation" with MeV particle bombardment of the specimen (9) do not take the radical approach described here requiring the excitation to be caused by single atomic particles and then requiring the individual atomic and molecular desorption events to be the essential, sole source of information.

The First Technique: Single-Event Laser-Desorption Time-of-Flight Mass Spectrometry

The combination of laser desorption (LD) with mass spectrometry has grown rapidly in recent years particularly in the characterization of thermally labile, highly polar organic and biologically significant compounds (10). LD and other "soft" ionization techniques such as fast atom bombardment (2), secondary ion mass spectrometry (11), field desorption (12), and ²⁵²Cf plasma desorption (13) have greatly enhanced the ability of MS to characterize complex organic and biological substances.

Time-of-flight mass spectrometry (14) (TOF-MS) is ideally suited to LD because the analyzer and source are pulsed techniques and TOF-MS has a theoretically unlimited mass range and efficient ion transmission. The renaissance of TOF-MS has also been stimulated by the rapid development of fast electronics and computer techniques and by improvements in mass resolution (15) and mass range (14) of the TOF analyzer. Efforts have also been made to further improve mass resolution by shortening the duration of the ion production, e.g., the use of short-pulse UV lasers in TOF-MS atom-probe research (16). In general, however, the lasers currently used for LD-TOF-MS have had pulse widths in the range of 3 - 20 ns and have utilized matrix assisted laser desorption (14) for specimens of high molecular weight. Although these TOF-MS developments have been touted as simple instruments, in fact their complexity for reasonably high performance systems still represents a quite

highly developed technology in pulsing, sample preparation, and ion optical components.

This Approach to LD-TOF-MS. We have found that subnanosecond laser pulses are very useful for LD. Figure 1a gives a depiction of the general scheme for the Single Event(SE)-LD-TOF-MS which was constructed locally (23-24). The ion source uses 300-picosecond nitrogen laser excitation which delivers pulses adjusted down to about 10 microjoules to desorb very low numbers of ions containing parent ions, pseudoparent ions, and/or ions containing structurally significant fragments of the specimen. A depiction of the ion source is given in Figure 1b. A sample of ten microliters containing approximately one microgram analyte per ml. is deposited with a syringe onto the 200 Angstrom thick gold film. The energy content of the laser pulse is increased until approximately 1/2 of the pulses produced one or more ions and data is then collected from approximately 1000 laser pulses.

Application. Our early efforts emphasized instrumental development and the use of inorganic compounds (17-18) to test performance. More recent work has been directed toward the detection and characterization of polycyclic aromatic hydrocarbons (PAHs) and nitrogen-containing heterocycles (N-HC). Of particular interest are the more polar organic compounds, which are difficult to detect by GC or GC/MS, and in detecting these compounds from samples without requiring extensive extraction and fractionation. We have found these compounds to respond nicely to this technique in producing mass spectra and approximately 75 different compounds have been tested thus far. Quite simple mass spectra can be obtained as shown in Figures 2 and 3 for samples of 6-aminochrysene and benzo(ghi)perylene respectively.

Single Event Information. Because of their simplicity these spectra are very useful. However, our interest is not in obtaining mass spectra per se, but rather in extracting and studying additional information present in the raw data. This information is gained by studying dependencies upon "multiplicity" and "ion association" for ions produced within individual excitations in the ion source. Multiplicity is simply the number of ions detected per laser pulse and our interest is whether production of specific ions is dependent upon the total number of ions produced. Ion association is the tendency for ions to be co-produced within the same laser pulse desorption (i.e. as opposed to being randomly co-produced). Preliminary results are very interesting and show excellent promise for containing information regarding specimen contaminants, structure, and ion formation mechanisms that cannot be obtained from interpretation of conventional (i.e., averaged or summed composite) LD mass spectra. To accomplish these results, the instrumentation stores separately the arrival time of all individual ions from each ionization pulse so that all information present in the data can be tested by examining the data in retrospect.

Multiplicity. Table I gives the specific ion multiplicity at each m/z and the composite ion multiplicity for all the ions from the data which yielded the spectrum in Figure 3. The data show the parent ion at m/z 276 and the (parent + 1) at m/z 277 had preferred production at lower multiplicities. I like to identify such ions as being "independent" as opposed to ions produced at higher multiplicities which I refer to as "gregarious" ions. For example the lower m/z ions at 23, 27, 39, and 41, and the

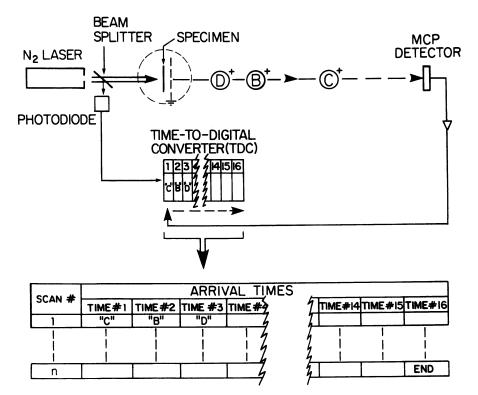


Figure 1a. Schematic diagram of SE-LD-TOF-MS system.

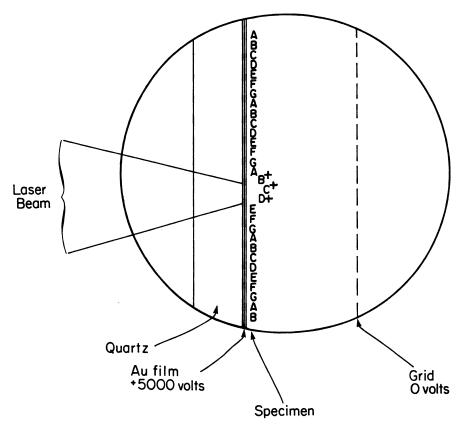


Figure 1b. Ion source for SE-LD-TOF-MS.

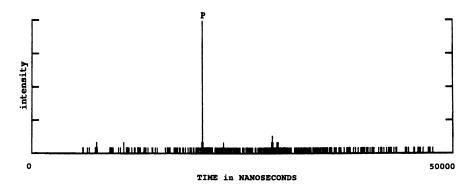


Figure 2. SE-LD-TOF-MS spectrum of 6-Aminochrysene.

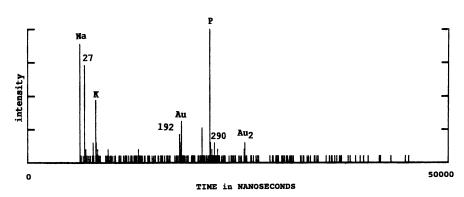


Figure 3. SE-LD-TOF-MS spectrum of Benzo(ghi)perylene.

ions due to gold at m/z 197 and 394 are gregarious ions. They tend to be observed only when several other ions are also present. A plot illustrating the tendency for all the structurally significant ions to be independent is given in Figure 4a. This tendency is quite common for the compounds studied and can be even more pronounced for some specimens as shown in Figure 4b for a sample of 9, 10-diphenylanthracene where <u>only</u> parent ions were produced at a multiplicity of one. The condition of the specimen, the environment of the laser excitation, and possible ionization processes which cause these observations should all be pertinent to the application of the technique to analytical situations.

Table I. Specific Ion and Composite Ion Multiplicity of SE-LD-TOF-MS data from Benzo(ghi)perylene

Specific														
Ion	MULTIPLICITY													_Total
m/z Ident.	1	2	3	4	5	6	7	8	9	10	11	12	15*	# Obs.
23. Na	5	4	8	5	4	17	10	39	21	9	6	4	1	133
27. C ₂ H ₃	6	13	11	7	17	11	6	33	22	5	5	2	1	139
39. K	4	3	6	0	3	4	7	20	17	4	5	2	1	76
41. K	1	0	0	0	0	1	1	2	2	1	3	0	0	11
192. P-84	1	2	4	2	1	2	1	3	2	0	0	1	0	19
197. Au	1	3	5	7	9	7	4	17	16	3	1	2	0	75
252. P-24	1	3	5	2	2	3	3	8	2	0	0	1	0	30
276. P	29	31	33	20	15	16	18	19	16	2	2	2	1	204
277. P+1	11	16	13	15	8	6	3	9	6	0	1	1	1	90
290. P+14	0	1	2	2	1	2	0	3	2	0	0	0	0	13
301. P+25	2	0	1	1	2	1	1	0	0	0	0	0	0	8
394. Au ₂	0	1	2	1	<u>3</u>	_2	2	8	_5	0	1	0	0	<u>25</u>
Composite	61	77	90	62	65	72	56	161	111	24	24	15	5	823
Composite	UI	,,	70	02	UJ	12	20	101	111	24	24	IJ	J	023

^{*}No ions observed at multiplicaties of 13, 14, and 16.

Ion Association. The techniques for computing ion association have been described (19) and the means for illustrating ion association can utilize the form of an "ion association map" (20) where the m/z identifications of the ions are written out and those ions found to be associated above an arbitrary confidence level are joined by solid lines. Such a map for a sample of anthracene is shown in Figure 5 which depicts the composite LD-TOF-MS spectrum at the top and the ion association map at the bottom of the figure for the higher intensity m/z ions. Solid lines joining the m/z assignments indicate that the computations of ion association yielded confidence levels greater than 98 percent for the ion pair to be detected within the same laser pulse. It is evident from the map that the low mass ions at m/z 23, 27, 39, and 41 tend to be created together and likewise the parent ion, the (parent + 1) ion, and the ion at m/z 167 tend to be created together. I refer to ions which are found to be

8. CONZEMIUS

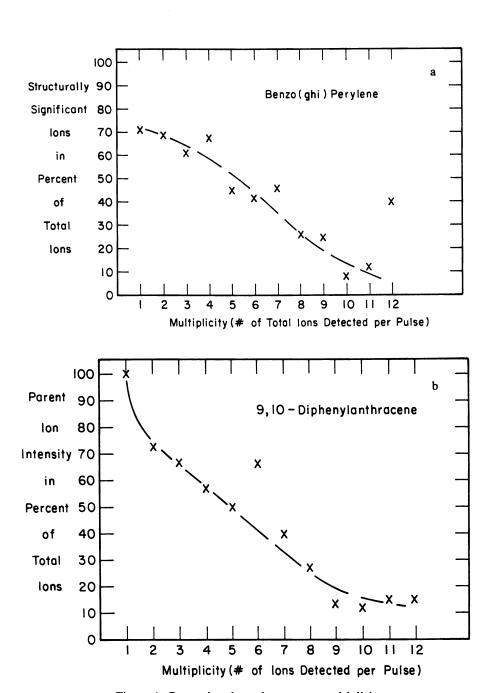


Figure 4. Parent ion dependence upon multiplicity.

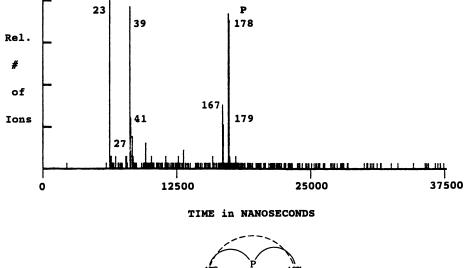
associated as "friendly" ions and conversely, "unfriendly" if they are not associated. An ion association map is shown in Figure 6 for data obtained from a sample of 2, 3-benzofluorene. The parent ion at m/z 216 and the gold ion at m/z 197 are seen to be friendly. The parent ions for these types of compounds have commonly been found to be friendly with the gold monomer ions.

Conclusion and Summary of The First Technique. The information obtained from investigations of multiplicity and ion association regarding the nature of the ion as gregarious, independent, friendly or unfriendly with other ions is considered pertinent and complementary to the composite mass spectrum. I expect these phenomena to be useful in extracting information regarding the condition of the specimen, the environment of the laser excitation, and the ionization processes. When scientists start using these computed "ion tendencies" they may not wish to return to only having the composite mass spectrum where this information has been scrambled.

The Second Technique: A Radical Approach - Mass Difference Spectrometry

Presume we have a solid specimen whose surface contains a The concept. nonrandom configuration of elements, compounds, or bonded species (i.e. the moieties are speciated) as depicted in a simplified manner in Figure 7a. We would like to characterize this nonrandom nature with atom or molecule level spatial resolution and we would like to obtain the information without high cost instrumentation or extensive scientific manpower. Mass Difference Spectrometry may accomplish this task. Presume that a very low and temporally random current of single projectiles such as single ions or fast atoms can be accelerated to the surface and that at least some of these primary projectiles individually sputter secondary particles from the surface as indicated in Figure 7b. Presume furthermore that the specimen is maintained in a field gradient such that the secondary ions can be accelerated away from the specimen toward an ion detector. If no secondary ions are produced we simply continue to let the clock keep running and wait for them to be produced. If a single secondary ion is created, then it can be detected, but its time of arrival at the detector will have no fixed time relationship to other secondary ions arriving at the detector since the primary projectiles causing these ions are random in their arrival rate at the specimen. However, if two or more secondary ions are produced by a single primary projectile then the time of traverse to the remote detector is related directly to the square roots of the co-desorbed ions. If these ions are subsequently co-desorbed at a later time during the experiment, the time relationship defining traverse to the detector will be the same and the differences in their time of arrival at the detector should be reproduced since the ions were produced simultaneously(i.e. the square roots of their masses and the same electric field again defines the time of traverse). Lets now adjust the average rate of arrival of the primary projectiles (i.e. the flux) at the specimen to a sufficiently low rate such that the average time between individual projectiles causing secondary ions to be desorbed is much greater than the differences in the time of arrival at the detector of the co-desorbed ions. We should then be able to observe these occurrences of subsequent co-desorption and perhaps some special advantages will accrue because of the nature of the phenomenon: The difference in the times of desorption for co-desorbed ions should be very small due to the subnanosecond time scale for the impact event (21). The co-desorbed species

CONZEMIUS



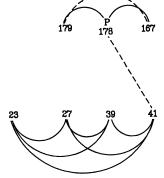


Figure 5. SE-LD-TOF-MS spectrum and ion association map for Anthracene.

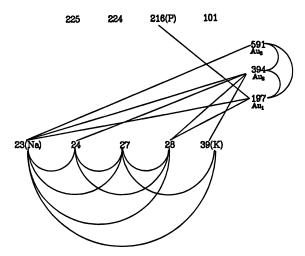


Figure 6. Ion association map for 2,3-Benzofluorene.

In Time-of-Flight Mass Spectrometry; Cotter, R.; ACS Symposium Series; American Chemical Society: Washington, DC, 1993.

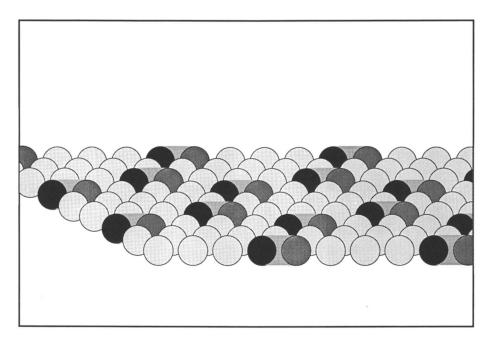


Figure 7a. Surface of solid with speciated moieties.

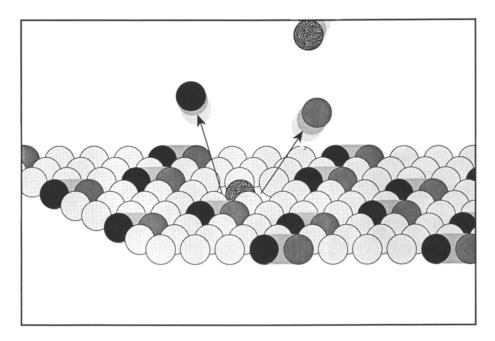


Figure 7b. Desorption of speciated moieties by a single ion.

should be expected to originate from a relatively small region of the specimen. They should be near each other but not necessarily bonded on the surface (21). To presume dimensions on the order of a molecule would not appear to be extreme.

Instrumentation for the Basic Measurement. The practical hardware necessary for conducting the experiment is quite simple. A computer based description of the basic parameters has been described (22). Figure 8 illustrates the general algorithm. An ion gun creates the primary projectiles which are accelerated without mass separation toward the specimen at the left of the figure. It is convenient to use ion projectiles whose charge is opposite to the sign of the voltage on the specimen from which the secondary ions (i.e. A and B in Figure 8) are accelerated to the detector. recording algorithm at the detector is again very simple. Only the differences in the arrival times of the secondary ions is recorded as illustrated in Figure 9 where time is indicated as a continuously running clock at the top, the occurrences of the arrival of secondary ions is indicated by a star (i.e. four arrivals indicated), and the quantities stored in the computer are the differences in the arrival times (DT) indicated at the bottom of the figure. We store a continuous stream of DT's, accurate to one ns, in the computer. Normally the average rate of arrival of secondary ions is adjusted to approximately ~600 Hz (i.e. ~10⁻¹⁶ Amp) and the experiment is allowed to run until 106 total DT's have been accumulated. If the ions are all produced randomly, the average difference in the time of arrival would be ~1.7 ms.

Random Observations and Predictions. Lets first purposefully create a random source of ions and see how the data handling system deals with it. This was done by replacing the specimen with the ion gun and pointing it directly at the detector. The voltage on the gun was set to +6000 Volts and the current of the cesium coated filament of the ion gun was then slowly increased to allow a stable rate of ion arrivals at the detector. Ten different ion arrival rates were used to study tendencies for co-desorption. When these ions are accelerated with a random but steady average rate, then the arrival of these ions can be predicted with respect to the number expected within specified observation periods. Lets select an observation period of 60,000 ns. After each experiment a software program searches the data for ion arrivals which were followed by subsequent ion arrivals within 60,000 ns (ie. a search for ion pairs which arrive within 60,000 ns of each other). If no subsequent arrival occurred within 60,000 ns, the ion was simply counted as a "1-hit burst" and the search continued. If two secondary ions arrive within 60,000 ns these DT's are stored in a file labelled as 2-hit bursts. Similarly, if more than two ions arrive within 60,000 ns their DT's are stored in respective files as n-hit bursts. Thus, the actual time differences are stored in separate files for each type of n-hit burst. The results of all ten experiments are given in Table II. The average rate of ion arrival to the detector is given in column one for each experiment and the total number of observed bursts and the number of bursts computed (i.e. predicted) due to random occurrences are given in columns 2 and 3 for 1-hit bursts, columns 4 and 5 for 2-hit bursts, columns 6 and 7 for 3-hit bursts, and columns 8 and 9 for 4-hit bursts. The values for the predicted number of n-hit bursts due to random occurrences were computed using equation 1 where the probability for random arrivals following a 1st ion arrival, within the time interval, is based upon an assumed exponential distribution of arriving ions (23) since the measuring time interval is not fixed (i.e. the longer you wait for

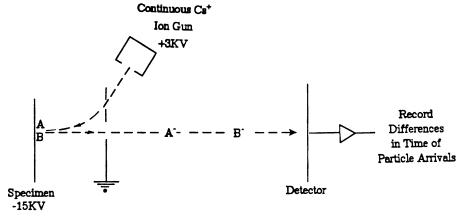


Figure 8. Schematic diagram of system for mass difference spectrometry.

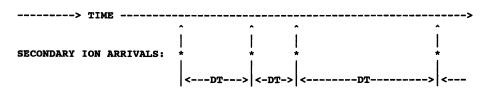


Figure 9. Measuring scheme for recording time differences.

Average

a second ion to arrive after observing a first one, the higher the probability of observing it).

$$P(t>T) = e(exp(-T*u))$$
 (1)

where: P(t>T) = the probability that a 2nd arriving ion will arrive time T after previously detected ion with "u" expected rate

Table II. Ions observed within the 60,000 ns intervals from a Cs+ ion source yielding random ion rates of production

	_								
Rate of									
Ion		<u># c</u>	of n hit bu	rsts using	a 60,000	ns delimit	<u>er</u>		
Arrival	<u>n</u> :	= 1	<u>n =</u>	<u>= 2</u>	<u>n =</u>	<u>: 3</u>	$\underline{\mathbf{n}=4}$		
Hz	<u>Actual</u>	Predict	<u>Actual</u>	Predict	<u>Actual</u>	Predict	<u>Actual</u>	Predict	
4	10695	10694	2	3	0	0	0	0	
-			_	_	U	•	Ū	•	
53	17816	17814	54	56	1	0	0	0	
70	11758	11754	45	54	0	0	0	0	
94	7880	7870	35	45	0	0	0	0	
220	15539	15549	213	204	4	3	0	0	
222	36662	36605	431	485	3	6	0	0	
247	80402	80372	1155	1182	15	17	0	0	
413	32434	32435	797	794	18	19	0	0	
459	72342	72213	1836	1960	50	53	0	1	
461	145039	144695	3642	3948	71	108	2	3	

These data are plotted in Figures 10a and 10b for 2-hit bursts and 3-hit bursts respectively in percent of bursts observed and in the percent computed bursts for predicted, random occurrences of ions arriving within 60,000 ns at the ten different average ion arrival rates. These figures show reasonable agreement between the observed number of bursts and the number computed for bursts due to random occurrences of arriving ions. The purpose of these experiments was to demonstrate that the data treatment can predict with reasonable confidence the arrival of random ion signals to the detector. This was considered pertinent since discussions with practitioners of secondary ion mass spectrometry indicated that co-desorptions from a single projectile may be so low that they would not be evident above temporally random events. These experiments with random n-hit bursts provide a basis for demonstration of the detection of non-random events.

Nonrandom Negative Ions. The ion gun was returned to the configuration in Figure 8 and a sample of NaF was inserted. The cesium ion gun was set to a positive 6,000 volts and the specimen (main ion source) was set to a negative 12,500 volts. The ion optical configuration of the ion gun and its orientation were set empirically in accordance with basic ion optical calculations. The ion gauge was turned off and the

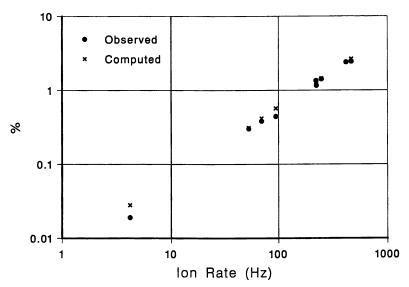


Figure 10a. Two-hit burst dependence upon random ion arrival rate.

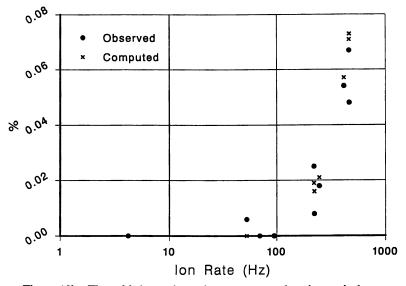


Figure 10b. Three-hit burst dependence upon random ion arrival rate.

ion arrival rate at the detector was observed to be less than one arrival per second. The filament current of the ion gun was then adjusted and allowed to stabilize to yield secondary ion arrivals from the specimen for twelve different experiments.

The twelve average secondary ion arrival rates are given in column 1 of Table III and the total number of bursts recorded for each experiment are given in column 2. The total number of recorded and computed n-hit bursts are given in the same format as in Table II.

Table III. Negative ions observed in the 60,000 ns intervals from an ion source yielding nonrandom ion rates of production

Ion											
Arriva	ıl	Number of 60,000 ns Intervals observed with n Ions									
Rate	Total	<u>n</u> =	<u>= 1</u>	<u>n =</u>	= 2	<u>n =</u>	3	<u>n = 4</u>			
<u>Hz</u>	Bursts	<u>Actual</u>	Predict	Actual Predict		Actual	Predict	Actual Predict			
11	1844	1768	1843	72	1	2	0	2	0		
30	5021	4794	5012	205	9	20	0	1	0		
33	11576	11107	11553	443	23	25	0	1	0		
56	21596	20713	21524	823	72	53	0	5	0		
71	11431	10929	11382	480	49	20	0	2	0		
130	21361	20379	21195	921	165	57	1	3	0		
177	905251	863451	895665	39221	9485	2355	100	204	1		
190	106278	101280	105076	4679	1189	295	13	20	0		
198	38569	36772	38113	1714	451	121	5	10	0		
308	48684	46113	47793	2381	875	174	16	13	0		
464	72189	67763	70208	4102	1928	303	53	21	1		
645	98757	91913	95007	6266	3608	527	137	48	5		

Figures 11a and 11b contain plots of the percent 2-hit and 3-hit bursts respectively for the observed and predicted random occurrences at the twelve different arrival rates. The data show the observed 2-hit and 3-hit bursts to be independent of ion rate at low data rates and then increase at higher rates. The increase at higher rates is at least partially due to greater contributions from random ion arrivals. Figure 12 contains a plot of the percent observed 2-hit, 3-hit, and 4-hit bursts corrected for the contributions predicted from random ion arrivals. With these corrections, the 2-hit bursts show only a slight decrease at higher rates, whereas only slight increases are indicated for the 3-hit and 4-hit bursts at higher average ion arrival rates. These slight tendencies at higher ion arrival rates are probably not significant but rather due to errors in computations of the predicted, random occurrences. The plots in figure 12 indicate that nonrandom phenomena are occurring. Are these phenomena due to co-desorptions?

Mass Difference Spectra for Negative Ions. We have been collaborating with a research group studying the identification of neuropeptides released from rat spinal cord tissue when electrically stimulated. Figure 13a is a histogram for an

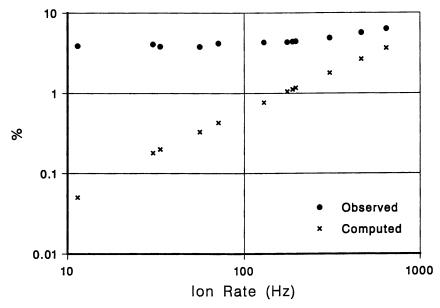


Figure 11a. Negative ion 2-hit burst dependence upon secondary ion arrival rate.

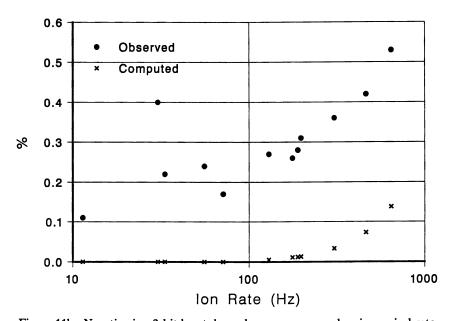


Figure 11b. Negative ion 3-hit burst dependence upon secondary ion arrival rate.

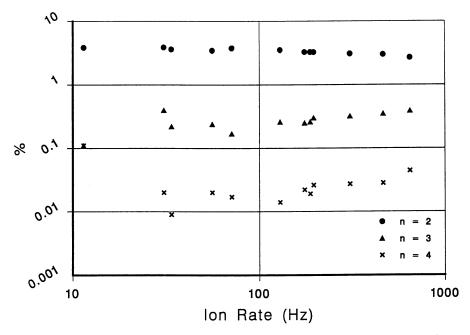


Figure 12. Corrected dependence of 2-hit, 3-hit, and 4-hit bursts upon negative, secondary ion arrival rate.

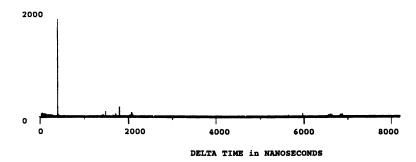


Figure 13a. Negative ion histogram for extract from neural fluid.

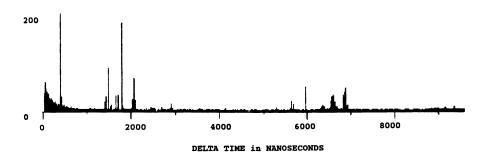
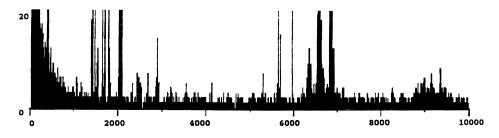


Figure 13b. Ordinate at $10\times$.

accumulation of 10⁶ DT's obtained with this specimen in the configuration of Figure 8. The number of occurrences of DT's are given on the ordinate and the abscissa contains the time range from 0 to 8000 ns with one ns resolution. The histogram shows the presence of peaks confirming that nonrandom phenomena are being repeated at certain time differences. By increasing the sensitivity to a full scale of 200 (i.e. X10 increase) as shown in Figure 13b we find many more ion pairs indicating a rich source of information. Figure 13c is the same spectrum shown with X100 sensitivity. The richness of information shown in Figure 13c may appear to be overly crowded as indicated by the histogram in the time range 6200 to 7000 ns. Figure 13d, an expansion of this time range, indicates however that it contains nicely resolved peaks. A magnification of the large peak at ~400 ns is given in Figure 14 for DT's obtained in this time span from 2-hit bursts and 3-hit bursts. When the instrument parameters are included in the computation of the mass differences that may be causing this peak the results agree with the mass of H⁻ and an electron which would be a prime consideration for co-desorbed negative species. The peak is quite



DELTA TIME in NANOSECONDS

Figure 13c. Ordinate at $100 \times$.

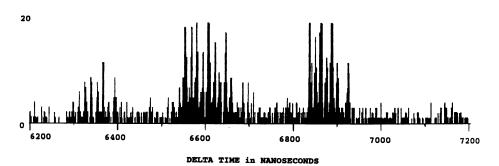


Figure 13d. Time range 6200 to 7000 ns.

sharp indicating the potential for high resolution especially when considering that neither pulsing nor any compensation for ion energy spreads which occur upon desorption have been utilized. Secondly, this e - H peak may be the largest but it is evident from Figures 13a-d that the addition of high resolution to these observations should possess great potential for analytical usefulness when full interpretation of the peaks has been achieved. The high resolution must yet be proven by the addition of ion energy compensation into the ion optics. Even with the linear system of Figure 8 a histogram obtained with a sample of the pentapeptide Tyr-Gly-Gly-Phe-Leu yielded a five ns. wide peak at a DT of 8344 which agreed with the mass difference between the deprotonated parent ion and an electron (24).

The reader may be tempted to conclude that the most useful information is only contained in 2-hit bursts in which one of the arriving particles is an electron. Our experience is that the most immediately useful and interesting information is contained in 3-hit bursts. Table IV contains a list of triply desorbed particles found in 3-hit bursts from a sample of the tripeptide Leu-Gly-Phe.

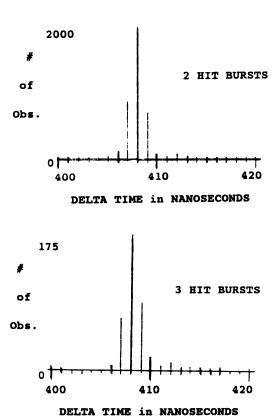


Figure 14. Time range of 400 to 420 ns for 2-hit and 3-hit bursts.

Codesorbed Species				Number Observed	<u>C</u>	odes	<u>orbed</u>	Sp	<u>ecies</u>	Number Observed	
e	+	Н	+	CH	21	е	+	Н	+	С	6
e	+	H	+	OH	20	е	+	H	+	C2	6
е	+	Η	+	Glycerol-1	16	e	+	H	+	C2H2	6
е	+	H	+	0	14	е	+	H	+	Cl	6
е	+	H	+	C2H	14	е	+	H	+	Glycerol-	1 6
е	+	176	+	194	14	е	+	H	+	42	6
е	+	Η	+	P-1	14	е	+	H	+	43	4
e	+	H	+	71	13	е	+	CH	+	0	4
C2H	+	P-1	+	P + OH	11	е	+	88	+	Glycerol-	1 4
e	+	H	+	Glycerol	11	е	+	CH	+	59	3
е	+	H	+	59	9	е	+	59	+	Glycerol-	1 3
е	+	H	+	89	7	е	+	71	+	Glycerol-	1 3
						е	+	Ο	+	P-1	3

Table IV. Negative ions found in 3-hit bursts in Leu-Gly-Phe

A considerable amount of leverage is gained in the interpretation of 3-hit particles which may be histogramed in three different sets: one containing the DT's between the first two arriving particles (DT₁₂), one containing the DT's between the first and third arriving particles (DT₁₃), and one containing the DT's between the second and third arriving particles (DT₂₃). Figure 15a gives the histogram for the DT₁₂'s for the time range 4800 to 5100 ns. The small DT_{12} peak at 4852 ns can be established by software techniques (25) as being due to C2H and the deprotonated parent ion co-desorbed pair. Figure 15b gives the histogram in the time region of 4400 to 5800 for only the DT₁₃'s found in the 3-hit bursts which also contained a DT₁₂ between 4850 and 4855 (i.e. determined earlier to be due to co-desorption of C₂H and the (P-1) negative ion pair. Figure 15c gives the histogram in the time region of 0 to 1400 ns for the DT₂₃'s with the same additional criterion for DT₁₂. Based upon the preceding evidence, presume that we have produced, detected, and at least partially identified 2-hit and 3-hit co-desorbed negative ions. In MS, positive ions are frequently considered more useful. Without the advantage of having the H and e species as co-desorbed partners, what can we expect?

Nonrandom Positive Ions. An ion gun was inserted to allow production of SF_6 as ion projectiles. The gun potential was set to -6000 Volts and the ion accelerating potential for the specimen was set to +7500 Volts. Again the species from the ion gun are not mass resolved so that identification of the bombarding ion(s) is not known. The ion gun is operated with very low electron energy and thus SF_n should predominate. A sample of Leu-Gly-Phe tripeptide was inserted and the ion gauge turned off. Sulfur hexafluoride was inlet to the ion gun source, allowing the main system to rise to ~1 X 10^{-6} Torr. The filament current was then adjusted to yield secondary ion arrivals at the detector for 24 different ion arrival rates and total ion accumulations as shown in columns one and two of Table V. Columns three through ten contain the actual number of "n" type bursts observed and the number predicted using equation 1 for n = 1, 2, 3, and 4.

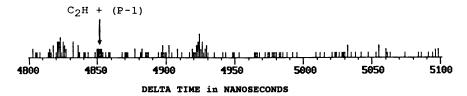


Figure 15a. Histogram of first two arriving ions(DT₁₂) from 3-hit bursts.

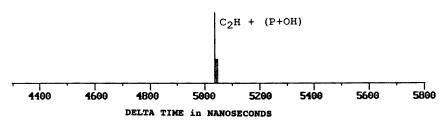


Figure 15b. Histogram of DT_{13} 's with C_2H and (P-1) as the DT_{12} .

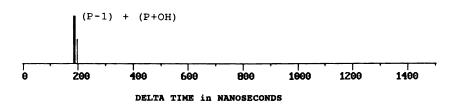


Figure 15c. Histogram of DT₂'s with C₂₃H and (P-1) as the DT₁₂.

Figures 16a and 16b contain plots of the percent observed and predicted random n-hit bursts relative to total bursts. The data indicate that ~0.2 percent of the arriving secondary positive ions are contained within three hit bursts and that ~ six percent are contained within 2-hit bursts. The 2-hit bursts show a slight increase and the 3-hit and 4-hit bursts give greater increases at higher average ion arrival rates than for negative secondary ions. Possible causes for these increases other than possible errors in the computations of predicted random ion arrivals will not be discussed here. As with the negative ion data these plots again indicate that nonrandom phenomena are occurring.

Table V. Positive ions observed in the 60,000 ns intervals from an ion source yielding nonrandom ion rates of production

T	7 - 0 -	ag		o .	r product					
Ion	,							.l Y		
Arriva				er of 60,000 ns Intervals observed with n Ions						
Rate	Total	<u>n</u> =	_	<u>n</u> =			= 3	$\underline{n=4}$		
\underline{Hz}	<u>Bursts</u>	<u>Actual</u>	<u>Predict</u>	<u>Actual</u>	<u>Predict</u>	<u>Actual</u>	Predict	Actual I	redict	
13	4265	4036	4262	219	3	10	0	0	0	
17	1301	1227	1300	70	1	3	0	1	0	
21	3314	3124	3310	173	4	15	0	0	1	
24	3906	3722	3900	176	6	8	0	0	0	
25	1972	1873	1969	96	3	3	0	0	0	
26	8361	8016	8348	329	13	15	0	1	0	
52	4105	3863	4092	233	13	9	0	0	0	
60	19158	18150	19090	959	68	46	0	4	0	
62	9925	9416	9888	467	37	39	0	3	0	
99	16848	16029	16741	754	106	56	1	9	0	
111	8929	8522	8870	379	59	26	0	2	0	
120	38031	35924	37758	1938	271	152	2	15	0	
171	26738	24895	26465	1663	270	168	3	9	0	
178	13865	12947	13717	843	146	69	2	5	0	
181	56119	52076	55514	3615	599	388	6	36	0	
229	17534	16142	17295	1241	236	137	3	12	0	
230	68615	61080	67673	6685	929	766	13	78	0	
232	35027	31801	34543	2884	478	299	7	37	0	
457	65945	57179	64160	7605	1737	1021	47	130	1	
458	32748	28346	31860	3840	864	508	23	45	1	
466	138042	124279	134233	12311	3704	1298	102	136	3	
658	191896	171579	184468	18269	7141	1845	276	180	11	
686	99869	89294	95839	9516	3868	940	156	106	6	
693	50382	45097	48331	4752	1968	485	80	39	3	
373	30302	13071	TUJJI	7152	1700	.05	00	٠,	_	

Mass difference spectra for positive ions. A sample of NaF was deposited onto the specimen mount and positive secondary ions were collected. Figure 17 shows histograms of DT's for 2-hit bursts and for 3-hit bursts for the NaF sample. As with American Chemical

Society Library

In Time-of-Flight 55 as 6 the title by Water, R.; ACS Symposium Series Water Light The Property of Series Water But 1993.

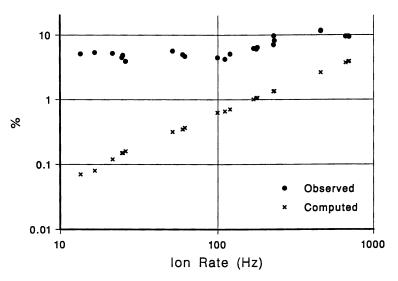


Figure 16a. Positive ion 2-hit burst dependence upon secondary ion arrival rate.

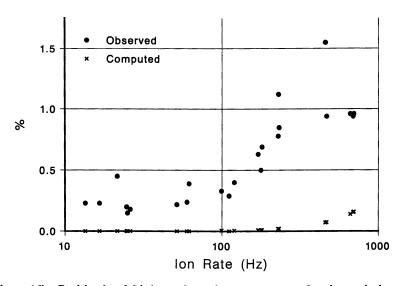


Figure 16b. Positive ion 3-hit burst dependence upon secondary ion arrival rate.

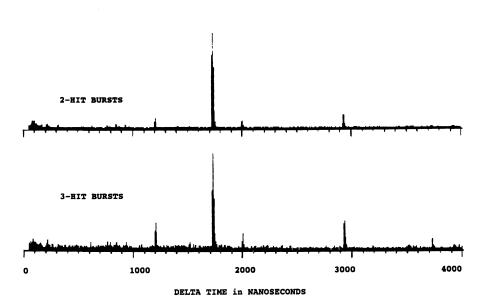


Figure 17. Histogram of positive ion 2-hit and 3-hit bursts for NaF.

negative secondary ions, the histograms again yield distinct peaks indicating nonrandom, positive ion pairs are being repeated. Lets look very briefly at a technique for interpreting the 3-hit bursts from this data. Figures 18a, 18b, and 18c contain histograms of all the DT₁₂'s, DT₂₃'s, and DT₁₃'s respectively from the 3-hit bursts. The peak at 1720 ns agrees with the mass difference between the Na⁺ and Na₂F⁺ ions. Figure 19a gives a histogram where the DT₁₂ agrees with the Na⁺ and Na₂F⁺ pair (i.e. the DT's in this histogram are due to ions trailing this pair to the detector). Figure 19b gives the histogram where the DT₁₃ agrees with the Na⁺ and Na₂F⁺ pair (i.e. the DT's in this histogram are due to ions detected between this pair). Figure 19c gives the histogram where the DT₂₃ agrees with the Na⁺ and Na₂F⁺ pair (i.e. the DT's in this histogram are due to ions preceding this pair to the detector). Computation of the masses co-desorbed with the Na⁺ - Na₂F⁺ pair are given in Table VI for each of the three cases in the histograms.

The tentatively identified molecular ion species are ordered according to intensity with the most highly observed M_x species at the top of the listings. Several computer based techniques have been developed for aiding interpretation but their descriptions are not within the scope of this text.

Table VI. Ions Co-desorbed with Na and Na₂F in Three Hit Bursts

Computed f Data in Figur			nputed fron		Computed from Data in Figure 19c.			
<-DT ₁₂ -><-D	I<-DT	₁₂ ->l<-D7	Γ ₂₃ ->l	<> $ <-DT_{12}-> <-DT_{23}-> $ M_x^+ Na^+ Na_2F^+				
M, Arrives: F	In-l	between		Preceding	Na ⁺ and	Na₂F⁺		
<u>Mx</u>			Species		Mx		2	
107	Na ₂ F ₂	27	C_2H_2		1	Н		
149			NaFH (or C ₃ H ₇	15	CH ₃		
68		29		,	14	CH_2		
275	Na_7F_6	41	C_3H_5		12	C		
174		55	NaO ₂		13	CH		
67		42	NaF		19	H ₃ O or	F	
133		39	NaO or	·K	2	H_2		
363		28	C_2H_4					
323		26	C_2H_2					
108								
105								
77								

Figures 20a and 20b give histograms at X1 and X10 ordinate sensitivity respectively and at one nanosecond abscissa resolution for positive secondary ions from the same

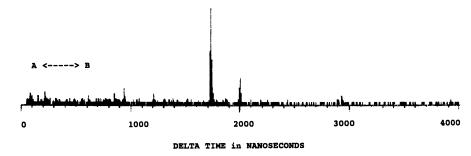


Figure 18a. Histogram of DT₁₂'s of positive ion 3-hit bursts for NaF.

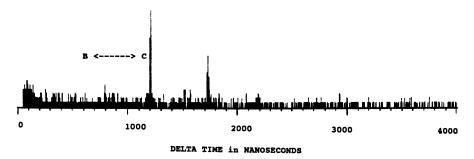


Figure 18b. Histogram of DT₂₃'s of positive ion 3-hit bursts for NaF.

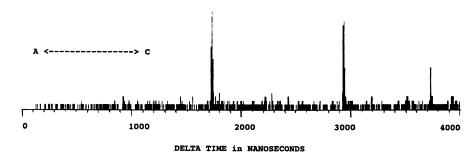


Figure 18c. Histogram of DT₁₃'s of positive ion 3-hit bursts for NaF.

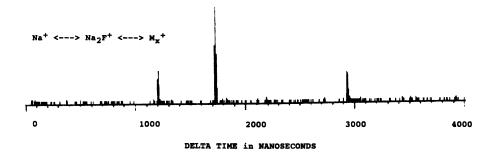


Figure 19a. Histogram of DT's when DT₁₂ agrees with Na+ and Na₂F+.

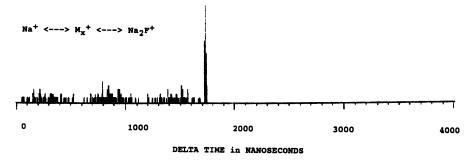


Figure 19b. Histogram of DT's when DT₁₃ agrees with Na+ and Na₂F+.

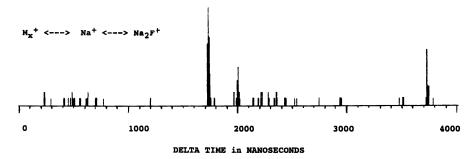


Figure 19c. Histogram of DT's when DT₂₃ agrees with Na+ and NaF+.

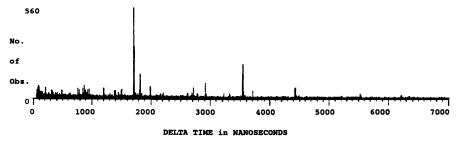


Figure 20a. Positive ion histogram for extract from neural fluid.

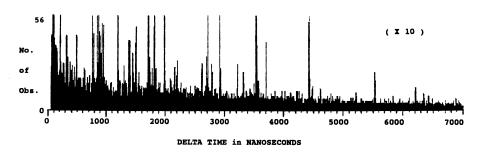


Figure 20b. Positive ion histogram for extract at 10× sensitivity.

extract as the sample for Figure 13. Here most of the peaks are observed between 0 and 7,000 ns. The further interpretation and presentation of these data is in preparation.

Conclusion and Summary of the Second Technique

This work gives credence to the hypothesis that a single projectile causes a significant number of two, three, and more simultaneous desorptions of secondary ions. The **ATOMICALLY** phenomenon given CO-EXCITED is the name: DESORPTION(ACED) to indicate the nature of the event: the desorption of more than one species is caused by excitation due to one atom or projectile. implications of the presence of this phenomenon appear to indicate significant analytical usefulness. ACED species are sputtered simultaneously, therefore the subsequent acceleration and time-of-flight measurements which include compensation for ion energy spreads should be made with very high accuracy since the time-zero error is negligible. ACED species are sputtered from a very small region of the specimen, on the order of the dimension of relatively small molecules. This implies that the ACED species carry with them information regarding speciation of particles on the surface of the specimen. ACED species should provide information pertaining to desorption mechanisms which are very important issues when considering means for improving presentation of specimens to the desorption ion sources.

The data shown here indicate that considerable fragmentation occurs with ACED species. The fragmentation should be considered an enrichment of the information present, considering the effort made to cause fragmentation in MS/MS studies. The information carried by ACED species would appear to speak to ion structure from an entirely new point of view. ACED species contain not only low mass fragments but also high mass species including parent and pseudoparent ions.

The beauty of mass difference spectrometry in gaining the ACED data is that the instrumentation is greatly simplified. The phenomenon does the work. Rf voltages, magnetic fields, pulsed voltages, or any scanning are not required. The number of instrumental parameters is very small and the operating ion currents are at the noise levels of most mass spectrometers. With these ultra low ion current rates, ion guns and ion source components should be expected to last for years. The detector experiences no high input signals and is required only to work with a dynamic range of unity. The ACED phenomenon in the ion source complements the ion optical system rather than burdening it.

A mass spectrum is not obtained. However, the spectrum is really a composite of individual events which the scientists would prefer to measure individually. This work is designed to allow the scientist to utilize this preference. The interpretation of the mass difference histograms presents a paradise for individuals interested in the development of software and takes on an analogy to the completion of a crossword puzzle. The dependence of the interpretation upon computer techniques is considered an advantage given the great improvement in computer hardware and software as well as the very significant reduction in cost for powerful systems.

The extremely low rates used here for sputtering of the specimen may be considered a mixed blessing. Very small amounts of the specimen need to be sacrificed to obtain the data and charge buildup on nonconducting specimens should be quite minimal. However, interferences in the data may be expected if the

specimen is not clean and if the vacuum system allows contamination while the data is being accumulated.

Some evident means for enhancement of these ACED phenomena should be mentioned. Neutral secondary particles generally exceed the numbers of secondary ions desorbed from the surface. The combination of single projectile excitation with multiphoton ionization of the neutral components may provide a very significant increase in the amount of information available from a single projectile. Singly desorbed secondary ions are isolated temporally. They can be made useful by fragmentation into daughter products followed by exclusive identification of the ion and neutral daughters (26). This MS/MS type of information can be accomplished by simple linear electrostatic field separation of the daughters with subsequent detection and identification of both the parent ion and the ion daughter(s). It would be surprising if specimen presentation (21) and close control of projectile (27) would not greatly enhance the information obtained with ACED ions.

Will mass difference spectrometry become a significant tool for the future? I think so. And maybe the future is not so far off.

Acknowledgments

CONZEMIUS

The work on the SE-LD-TOF-MS was funded by the Morgantown Energy Technology Center of the U. S. Department of Energy, Morgantown, WV. The work was performed at Ames Laboratory which is operated for the U.S. Department of Energy by Iowa State University under contract No. W-7405-ENG-82. The work on mass difference spectrometry was conducted under a technology transfer effort with joint support of the U.S. Department of Commerce through the Center for Applied Technology Development, Iowa State University and of the National Institute of Health through RESIFT, Inc., Ames IA. The work was conducted at the Iowa State University Research Park, Ames Iowa. Several individuals contributed to the efforts: John J. Richard, Lorinda Hemmingson, Isabel Hendrickson, Gregor A. Junk, and Dr. Albert E. Baetz. Three individuals contributing significantly to the development of the mass difference spectrometer were John F. Homer in data acquisition, Donald Carr in general data interpretation and display, and Thomas Hendrixson in the interpretation of 3-hit bursts. Dr. Mirjana J. Randic of the Iowa State University College of Veterinary Medicine provided the samples for the evaluation of application to identification of neuropeptides.

Literature Cited

- 1. Boyle, J. G.; Whitehouse, C. M. Anal. Chem. 1992, 64, 2084-2089.
- 2. Caprioli, R. M. Anal. Chem. 1990, 62, 477A-485A.
- Denoyer, E. R.; Fredeen, K. J.; Hager, J. W. Anal. Chem. 1991, 63, 445A-457A.
- U.S. Patent No. 4,818,862, "Characterization of Compounds by Time-of-Flight Measurement Utilizing Random Fast Atoms," issued April 4, 1989.
- 5. U.S. Patent No. 4,894,536, "Singly Event Mass Spectrometry," issued January 16, 1990.

- Della-Negra, A. S.; Deprun, C.; Le Beyec, Y.; Rollgen, F.; Standing, K.; Monart, B.; Rolbach, G. Int. J. Mass Spectrom. Ion Processes 1987, 75, 319-327.
- Park, M. A.; Gibson, K. A.; Quinones, L.; Schweikert, E. A. Science 1990, 248, 988-990.
- 8. Chait, B. T. Int. J. Mass Spectrom. Ion Processes 1983, 53, 227-242.
- Della-Negra, S.; Jacquet, D.; Lorthiois, I.; Le Beyec, Y. Int. J. Mass Spectrom. Ion Processes 1983, 53, 215-226.
- 10. Cotter, R. J. Anal. Chem. 1992, 64, 1027A-1039A.
- 11. Benninghoven, A.; Sichtermann, W. Anal. Chem. 1978, 50, 1180.
- 12. Lattimer, R. P.; Schulten, H. R. Anal. Chem. 1989, 61, 1201A-1215A.
- 13. Cotter, R. J. Anal. Chem. 1988, 60, 781A-793A.
- Hillenkamp, F.; Karas, M.; Beavis, R. C.; Chait, B.T. Anal. Chem. 1991, 63, 1193A-1203A.
- Mamyrin, B.A.; Karataev, V. I.; Shmikk, D. V.; Zagulin, V. A. Sov. Phys.-JETP(Engl. Transl.) 1973, 37, 45.
- Tsong, T. T.; Kinkus, T. J. Phys. Rev. B:Condensed Matter 1984,29,
 probe with n2 laser
- 17. Huang, L. Q.; Conzemius, R. J.; Junk, G.A.; and Houk, R. S. Anal. Chem. **1989**, 60, 1490-1494.
- Conzemius, R. J.; Adduci, D.; Huang, L. Q.; Junk, G. A.; and Houk, R. S. Int. J. Mass Spectrom. Ion Processes 1989, 90, 281-293.
- Huang, L. Q.; Conzemius, R. J.; Junk, G.A.; and Houk, R. S. Int. J. Mass Spectrom. Ion Processes 1989, 90, 85-96.
- Schoer, J. K.; Houk, R. S.; Conzemius, R. J.; Schrader, G. J. J. Am. Soc. Mass Spectrom. 1990, 1, 129-137.
- 21. Garrison, B. J. J. Am. Chem. Soc. 1982, 104, 6211.
- Carr, D. "A computer-based alternative to ordinary mass spectrometry", Thesis, 1990, Iowa State University, Ames, IA 50010
- Kennedy, J.B.; Neville, A. M. Basic Statistical Methods for Engineers and Scientists; 2nd Ed.; Thomas Y. Crowell Co.: New York, N. Y., 1976.
- Conzemius, R. J.; Carr, D. W.; Homer, J.; Baetz, A. E. Proceedings of the 38th ASMS Conference on Mass Spectrometry and Allied Topics, Tuscon, Arizona, June 3-8, 1990.
- Private communication. R. Conzemius. Ames Laboratory, Iowa State University, Ames, Ia. 50011.
- Conzemius, R. J.; Svec, H. J. Int. J. Mass Spectrom. Ion Processes 1990, 103, 57-66.
- Hand, O. W.; Tapan, K. M.; Cooks, R. G. Int. J. Mass Spectrom. Ion Processes, 1990, 97, 35-45.

RECEIVED June 18, 1993

Chapter 9

Achieving the Maximum Characterizing Power for Chromatographic Detection by Mass Spectrometry

J. F. Holland¹, J. Allison², J. T. Watson^{1,2}, and C. G. Enke²

Departments of ¹Biochemistry and ²Chemistry, Michigan State University, East Lansing, MI 48824

Since the initial application of mass spectrometry (MS) as a detector for chromatography (gas chromatography, circa 1960) (1,2), the relative rates of information along the two axes has been a major concern. Such a hyphenated technique as GC/MS involves two distinct axes of information with significantly different time frames. For each "sampled" point along the chromatographic axis, an entire mass spectrum must be acquired. Therefore, the required rate of data collection along the mass spectrometric axis far exceeds the sampling rate along the chromatographic axis. As shown in Figure 1, utility of a full range mass spectrometry analysis requires that the rate of spectral generation be sufficient so as not to lose information along the chromatographic axis. The initial GC-MS application utilized the time-of-flight mass spectrometer (TOFMS) (1), however, due to shortcomings that will be described below, the magnetic sector (3), and later the quadrupole mass spectrometer (4), became the dominant types to be used. The ultimate shift to the quadrupole was based on several factors which include: reasonable cost, relatively small size, high tolerance for pressure, and ease of computerization. The readily attainable full mass range scan speeds of the quadrupole, approximating one per second, were adequate for the detection of eluents from packed column chromatography and little or no information was lost from this time domain. However, the advent of capillary column chromatography created a need for a much faster rate of mass spectral generation in order not to lose chromatographic information. Our experience has determined that state-of-the-art high-performance capillary column chromatography using stationary bonded phases can achieve reproducibility of 1/20 of a second, subsequent to retention index calibration. Based on this reproducibility, for maximum utility of the information present, a Nyquist

> 0097-6156/94/0549-0157\$06.00/0 © 1994 American Chemical Society

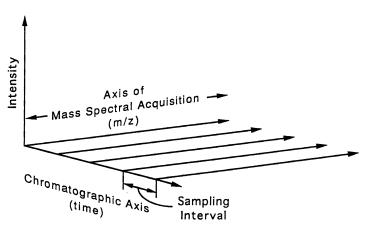


Figure 1 The three dimensional nature of GC-MS data illustrating the dependence of the chromatographic sampling interval on the mass spectral generation rate.

requirement of 40 mass spectra per second would be required to preserve the chromatographic information. Proper analysis of the information in a single Gaussian peak at this state-of-the-art would require a minimum of 12 points to reconstruct the profile of an isolated chromatographic peak for quantitation, 20-40 points per peak for maximum accuracy in the elution time measurement, and 40 or more total points to best represent eluting peak profiles in any deconvolution routines that may be required for distinguishing unresolved components. None of these data rate requirements can be achieved by existing commercial instrumentation. As spectral generation rates are increased, sensitivity falls off rapidly, and, for scanning mass spectrometers mass spectral skew is introduced from the changing analyte concentration during the scan. The maximum practical full mass range scan rates for current instrumentation are 2-5 scans/sec for the quadrupole, 1-5 scans/sec for the magnetic sector, and 10 scans/sec for the ion trap. These rates are also very near the fundamental limits for each of these mass analyzing techniques. Embodiments of Fourier transform mass spectrometry are array detectors (in the frequency domain) and not scanning detectors; however, to date, they have not been docmented to be sufficient for chromatographic applications. At the present state-of-the-art, to meet the speed requirements detailed above would impose restrictions on the transform efficiency that would severely reduce the sensitivity and resolution, and attenuate the dynamic range to an unacceptable level.

Because of the inherent limitations of commercial GC/MS systems, to achieve desirable data collection rates, compromises abound in the practice of the art. Rapid limited-range scanning and selected-ion monitoring produce a data density sufficient to preserve chromatographic information, however, these techniques ignore most of the mass spectral information that is present. Loss of mass spectral data is exceedingly detrimental, particularly in the case of mixtures of unknown components. Only by replicate sample analyses, can all of the mass spectral information be obtained, while not sacrificing chromatographic information. Full mass range scanning at the top of an eluting peak captures complete, although often badly skewed, mass spectral data, but at the expense of losses in chromatographic information. In summary, all of the compromising techniques sacrifice either mass spectral information or chromatographic information or require multiple analyses of the sample, encumbering excessive time and resource expenditures. In fact, the need for speed in capillary chromatographic detection is only one of the applications developing that will mandate faster collection of mass spectral data. High-speed chromatography, capillary zone electrophoresis and supercritical fluid chromatography require still greater detector speed and sensitivity.

Presently, there are no commercial GC/MS instruments that can accommodate applications of high resolution chromatography without sacrifice of either information or time. This problem was addressed by the MSU Mass Spectrometry Facility several years ago concerning applications of mass spectrometry to capillary gas chromatography (5). It was determined that only Time-of-Flight Mass Spectrometry (TOFMS) had the innate speed to accommodate the bandpass of information exhibited by the chromatographic resolution. It is now clear that only TOFMS has the potential to accommodate any situation where the composition of the sample is changing in time frames requiring more than 10 mass spectra per second. In addition to the chromatographic techniques mentioned above, there are several non-chromatographic techniques that require ever-increasing rates at which mass spectral information must

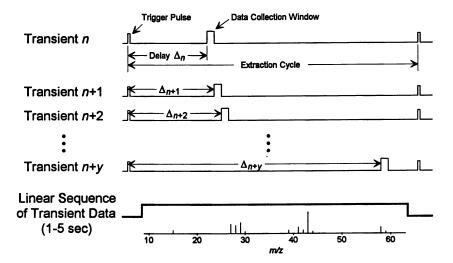
be obtained. A major technique of this type is MS/MS, which requires twodimensional mass axis scanning. Usually, the precursor mass axis is stepped to the m/z values of interest while the product mass axis is scanned. The spectral generation rate of the product analyzer limits the number of precursor values that can be obtained for a given sample amount or residence time. Therefore, the product mass analysis should be very rapid in order that maximum MS/MS data be obtained with traditional sample introduction techniques. Indeed, the combination of a magnetic sector for precursor isolation with the rapid TOF analyzer for product resolution functions with speed sufficient to accommodate packed column chromatographic separation (6). If both axes can be fast, i.e., a TOF/TOF MS/MS instrument, the temporal range of applications may drop into the capillary chromatographic time frame allowing complete MS/MS data fields to be obtained within the elution peak width of single, highly resolved components. Incidently, this is a major objective of research investigations in this area (7.8).

In spite of its inherent speed, TOFMS failed to maintain its initial headstart in applications to gas chromatography because of several factors. A major factor was the manner in which the mass spectral information has been collected. A single extraction pulse in the ion source produces a "transient" at the detector which can contain the information for a complete mass spectrum. The predominant method of data collection has been that of time-slice detection (TSD) which ignores over 99.9 percent of the information available at the detector by collecting only a small portion of the information available in each transient waveform. As shown in Figure 2, contiguous increasing of the delay prior to data collection from successive transients provides data for a sequentially generated (scanned) mass spectrum. In order to take advantage of the speed of the time-of-flight analyzer and, at the same time, not sacrifice mass spectral information, techniques utilizing time array detection (TAD) have been developed. As shown in Figure 2, these techniques capture and utilize all of the information within each transient providing the basis for faster spectral generation rates and greater sensitivity.

There are two requirements for the utility of time array detection. These are a sufficient bandpass of the data collection and processing electronics such that all of the information contained in each and every transient can be detected and utilized. The second major requirement is that all of the ions throughout the mass spectrum, from low to high m/z, strike the detector in temporal focus. The first requirement, high measurement bandpass, was fulfilled by the development of the integrating transient recorder (ITR) (9). The second requirement, that all ions striking the detector be in focus, has been resolved by several different methods. These include the combination of a magnetic sector with the time-of-flight, the combination of an electric sector with the time-of-flight, the pulsing of a continuous ion beam along the optical axis, and the use of a single extraction field with an ion mirror for regenerating the spatial focus plane on the detector.

The combination of a magnetic sector with a time-of-flight analyzer produces ions in focus having been generated, accelerated and selectively isolated on the basis of momentum by the action of the magnetic field and the ion optics of the mass spectrometer (10). Timed pulsing (beam deflection) of the beam emerging from the object slits of the mass spectrometer makes the attachment of the time-of-flight analyzer feasible. This novel instrumentation enabled a technique called TRIMS (Time Resolved Ion Momentum Spectroscopy) in which two arguments, one of

Time Slice Detection



Time Array Detection

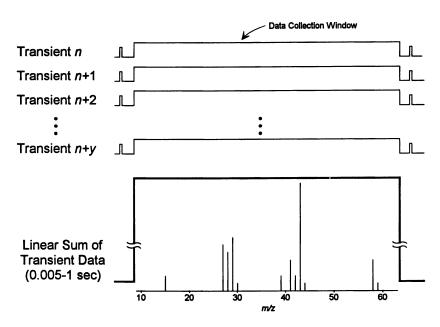


Figure 2 A comparison between time slice detection with subsequent linear sequencing and time array detection with successive transient summation.

momentum and one of velocity, enables the mass-to-charge of any ion to be unambiguously determined irrespective of its energy. Using TAD, this approach also enables MS/MS data to be collected on the time frame of packed column chromatography. Another approach to gain mass-independent focusing involved the combination of an electric sector and the TOF analyzer attached to a point focusing ion source, again utilizing beam deflection of the emerging continuous beam for TOF operations (11). This instrumentation allowed the development of a technique called TRIKES (Time Resolved Ion Kinetic Energy Spectroscopy) and was useful in experimentation presaging the utility of TAD in mass spectrometry. Non-static acceleration waveforms were investigated in a technique called dynamic field focusing (DFF) which would enable mass-independent focusing for a linear time-of-flight analyzer (12). The feasibility of this technique was confirmed by modeling, however, cost and resources available precluded actual construction.

The most successful approach in obtaining mass-independent focusing at the detector was achieved utilizing an ion mirror with a single field source extraction and accelerating potential (13,14). The single field extraction mechanism produces a space focus plane in the vicinity of the ion source. The subsequent ability of the ion mirror to reproduce this plane at the surface of the detector enables a path length and time duration sufficient for separation of ions with succeeding m/z values, while at the same time minimizing the packet width of isomass ions striking the detector. The combination of the ion mirror (reflectron) TOFMS geometry shown in Figure 3 and the ITR have resolved the two mandatory conditions for the application of TAD in time-of-flight mass spectrometry. That is, all of the ion information in each and every transient can be collected and utilized by the integrating transient recorder and the reflectron enables all of the ions across the mass spectrum to be in focus and, hence, provide the maximum mass spectral information.

Data Rate Analysis for Maximum Sample Utilization

Special requirements are imposed upon a mass spectrometric system that is to be used for chromatographic detection. These requirements come from the bandwidth and dynamic range of the chromatographic elution profiles and the small amount of analyte material contained therein. Elution profiles with temperal widths, now approaching one second for microbore capillary GC, require a spectral generation rate of 40 spectra per second for adequate sampling of the peak shapes. For spectra capable of providing quantitative information, to obtain a dynamic range of only 100 at a relative precision of 5% (assuming no noise), about 10⁴ ions should be collected for the base peak in the 25 ms available for the collection of each spectrum. A mass filter scanning over a 500 amu range with a mass resolution of 1000 could spend a maximum of 25 ms measuring the ion current for the base peak. An analog detector would have to measure a current of 64 pA in 25 ms with a precision of 5% or an ion counting circuit would have to count at an average rate of 400 MHz. requirements are substantially beyond the state of the art for detection even if the mass filters could scan that rapidly.

Among time-of-flight mass spectrometry detector techniques are the scanning boxcar (TSD), arrival time detection, transient recording, and integrating transient recording. In the case of a time slice detector with division of the time scale into 1000 time windows, collecting the transient value for each window of each of the 40

ion source extractions per second would require, without summation, an extraction rate of 40 kHz, and thus a maximum flight time of only 25 ms. This is a situation similar to that of the scanning filter. The peak in the transient that provides a base peak reading to achieve the dynamic range and precision described above should again contain 10⁴ ions. If the base peak were 10% of the total ion current, this would require an ion collection rate of better than one hundred thousand ions per extraction. This amounts to an intensity of 4 million ions per microsecond. Multiple boxcars will reduce these demands correspondingly, but the number of boxcar circuits must be very large before this approach becomes tractable.

Ion arrival time detectors have a counter associated with each element of time resolution. When an ion arrives, the counter for that arrival time is incremented. Arrival time detectors ignore all but the first ion to arrive in a given time increment. To avoid pile-up error of greater than 5%, it is necessary to have an average count rate per channel that is less than one-third the transient generation rate. To obtain 10⁴ counts in the base peak arrival time, 3 x 10⁴ extractions will be required. To do this every 25 ms will require a source extraction rate of 1.2 MHz (flight time analysis of 833 ns). Multistop arrival-time detectors allow ions of more than one arrival time to be counted during the same extraction, but they do not alter the basis of the above calculation. This calculation demonstrates that, for chromatographic detection, it is necessary to detect multiple ions of the same arrival time during each extraction. Therefore, for TAD of dynamic samples, analog detection circuitry is required.

Commercial analog transient digitizers are based on a 200 MHz or 400 MHz analog-to-digital converter. In order to adequately sample the typical transient waveform, an intensity value is stored every 2.5 or 5 ns during the time over which the ion arrivals are being recorded. For an ion extraction rate of 10 kHz the resulting data file will be 20,000 or 40,000 conversions in length. This number can be reduced somewhat by delaying the start of the conversion by a time equal to the flight time of the lowest mass ion of interest. The memory capacity of commercial transient recorders will only allow a few of these records to be stored so the data need to be condensed within the transient recorder or transferred out of it to the host computer and data system. Transfer of the transient record from memory to a resident disc or to a host computer requires tens of milliseconds and this transfer time determines the rate at which transients can be collected. Since the mass spectrometer can generate 10,000 transients per second, every millisecond of transfer time results in 10 transients that were not recorded. Lowering the recorded transient rate decreases the sample use efficiency, the dynamic range, or both. Even if faster electronics could provide faster data transfer rates, the mass of data represented by 20,000 byte records generated at the rate of 10,000 per second over the entire time of a 30 minute chromatogram (360,000 megabytes) is impractical to either store or review. Of course, it is not necessary to sample the ionization source composition at 10 kHz; the sample composition is not changing that rapidly. Optimally, one would like to average some number of successive transients to produce an averaged spectrum at the desired chromatographic sampling rate, thus achieving optimal spectral generation rate and maximum sample utilization efficiency.

Two summing or averaging modes are offered in most commercial transient recorders. In the true summing mode, the summing circuits do not operate as fast as the acquisition circuits; hence, summation does not involve sequential transients. With the LeCroy 9450, for instance, the maximum transient recording rate with true

summing of non-successive transients and transfer of the summed set to the host computer is approximately 10 summed averages per second with records 20,000 data points in length (15). The moving average mode, also provided in this instrument, is faster, but it is not a true average; it is a weighted sum with the most recent transient weighted more heavily than the earlier ones. In order to provide a true sum of transients generated continuously, it is necessary for the transient digitizer to contain dedicated fast summing circuitry, as we have done with the integrating transient recorder developed in our laboratory (9) and illustrated in Figure 4. Successive summation of contiguous transients is accomplished by using two high speed logic banks. One bank is dedicated to the time based summation of the incoming data while the second bank delivers the prior summed files across the VME bus to the parallel processors. By this means, all of the information in every transient is captured and used and spectral files can be continuously generated, limited only by the size of the disk storage on the bus. Even when summing is used to reduce the rate and magnitude of the data to be stored, a summed transient production rate of 40 per second requires a rate of almost 2 megabytes per second to store the complete transients (equivalent to storing raw spectra with a scanning instrument). To further reduce the data storage rate and bulk to manageable levels, the ITR uses fast peak finding algorithms in parallel processors to reduce the summed transients to mass/intensity pairs. In this form, we have written summed spectra to disk across the VME bus as fast as 250 spectra per second.

Summing has the further advantage of extending the range of the measurable intensities by a factor equal to the number of sums. If the analog-to-digital converter is an 8-bit converter, its total range, per conversion, is 256. When 250 (100 ms) transients are summed to produce 40 summed transients per second, the total range is 64,000. To achieve this range enhancement, the summing registers must be long enough to contain the total sum. The 16,384 summing registers in the ITR are 24 bits long. The fact that direct summation is performed on raw data from the transients allows noise cancellation which decreases the magnitude of the noise of the summed files, greatly increasingly the dynamic range of the measurements.

Performance Characteristics of TOF/ITR/TAD

The optimum unit having been developed to date to enable TAD in TOFMS is the combination of a reflectron and the ITR as shown in Figure 4. The reflectron TOFMS itself is a modification of the unit provided by Professor Hermann Wollnik in our collaboration with the University of Giessen. In addition to solving the mass-independent focussing problem, two unique features of this configuration that are of value to the utility of TAD are 1) that the ion source is capable of storing ions between source extractions, and 2) the gridless ion mirror is capable of reasonable amounts of transverse ion focusing, enhancing the overall resolution and sensitivity of the system. This reflectron TOFMS has been interfaced to a Hewlett-Packard 5890 gas chromatograph. The eluent of the chromatograph flows directly into the ion source. Molecules that are ionized by electron impact ionization are extracted and accelerated with the brief application of a single field which produces a space focal plane of the extracted ion packet in the vicinity of the ion source. The subsequent ion packet is focused by an Einsel lens and directed towards the mirror. The reflection from the mirror reconstitutes the space focal plane at the surface of the detector. This

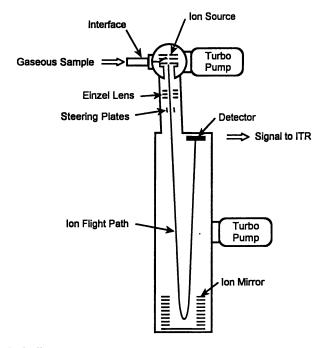


Figure 3 A diagram of the reflectron TOFMS used in these investigations.

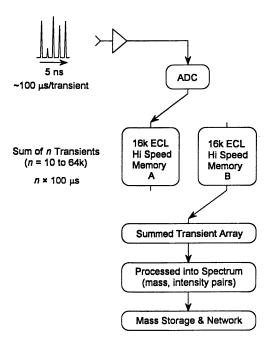


Figure 4 Block diagram of the integrating transient recorder indicating information flow and data rate reduction.

configuration allows for a very adequate (up to 2,000, 50 percent valley) resolution and corrects for the energetic variations existing in the source at the moment of extraction. This correction enables all of the m/z values throughout the mass range of each and every transient to be in temporal focus at the moment of impact with the detector. As mentioned above, this is a prerequisite for the successful application of TAD. The ion intensity information striking the detector is amplified and sent to the ITR. The two banks of the transient recorder enable successive summation of succeeding transients in one bank simultaneous with the transfer of a collected summed spectra from the other bank across the computer bus.

For GC and MS/MS applications, spectral generation rates in excess of 200 have readily been attained. However, more appropriate to the bandpasses of the information being sought and the time frames being desired, scan generation rates of approximately 40-50 are more common. For example, for a reflectron TOFMS utilizing a five kilohertz ion source extraction rate, successive summation of 100 transient waveforms would yield one summed mass spectrum in 1/50 of a second. As illustrated in Figure 5, this summation process has several benefits. The upper left hand spectrum of this figure is a mass spectrum generated without summation at the rate of 5,000 per second and clearly illustrates that the information from a single transient waveform is adequate to construct a mass spectrum. As more transients are summed, increases in the precision and signal-to-noise are evident as shown in Figure 5 where 200 transients are summed to produce a single mass spectrum. information in this mass spectrum will have a signal-to-noise improvement and hence a dynamic range increase of slightly over 14 times that for a single transient. The total range, obviously, will increase linearly with the summation having grown from 250 in a single transient (limited by the 8-bit analog-to-digital conversion) to 50,000 for the data from the 200 transient summation. This summation process can also increase the sensitivity as well as the dynamic range of the measurement. example, less abundant ions may occur at a rate of less than one per transient. Hence, in the summation of 200 transients, we have a probability of occurrence ranging from ions that may appear in all 200 transients down to ions that may appear in only one of the 200 transients summed. This constitutes an increase of over two orders of magnitude for the range of the measurement and extends the detectability down to a one in 200 occurrence probability. Additionally, the linear summation process will greatly reduce the effect of random noise increasing the overall quality (signal-tonoise) of the measurement system. In summary, because of the amount of information contained in a single transient and the random cancellation of noise, the summation process significantly increases the dynamic range, precision, signal-tonoise and sensitivity of subsequent analysis.

Another outstanding advantage of time-of-flight detection is the fact that the ions are extracted from the ion source in a very brief period of time. This provides a snapshot of the ion population within the source at that moment. Consequently, the mass spectrum generated as the ions strike the detector in their rapid time sequence is a true measurement of the population in the source at the instant of extraction. Hence, if only one molecular species were present, the fragmentation pattern resulting from this single extraction would be totally unskewed. There are no time-dependent variations affecting the magnitude of the low masses vis-a-vis the high masses that are related to changes in sample concentration in the ion source during the finite time of mass analysis. This ability to produce totally unskewed data cannot be done by

other types of mass spectrometers when analyzing dynamic samples, such as those produced by GC. The ion trap MS likewise has a snapshot extracting process, however, multiple collisions between analyte molecules and the buffer gas molecules utilized in this type of mass spectrometer can alter the fragmentation pattern, often as a function of concentration of the analyte species. This situation, in essence, leaves time-of-flight alone as the one mass spectrometer analyzer that will not produce skewed mass spectra. Fortunately the linear summation processes used by the ITR for TAD do not impair the ability of the analyzer to produce unskewed spectra. Linear summations of unskewed spectra result in unskewed summed spectra with the consequential increases in signal and signal-to-noise. The unskewed nature of the resulting spectra is of prime importance in the data processing and the deconvolution routines to be described below.

The ability of the operator to pre-select the number of transients to be summed in order to obtain a mass spectra adds another analytical parameter to the analysis itself. In practice, the mass spectral generation rate which is necessary to accommodate the band-pass of the chromatographic information and the extension of the summation processes which are essential to gain the advantages of signal-to-noise and sensitivity, are balanced against each other in an optimization process. This logically reduces to the situation where the number of transients summed are at the largest number which will still enable spectral generation rates sufficient to maintain the integrity of the chromatographic information. It is in accordance with this general precept that the ITR, which is capable of providing several hundred spectra per second, is actually utilized in the 40 to 50 spectra per second range for high resolution gas chromatography. Spectral generation rates up to 200 have been found to be necessary for some of the GC/MS/MS applications experienced to date (6). In either situation the ability to trade off scan file generation rate with sensitivity and signal-to-noise, provides an additional degree of freedom to the analyst.

Capacity for Increasing GC/MS Information Generation Rate

At this point, it is quite apparent that the speed with which the ITR can collect time-of-flight information is far in excess of that needed for capillary column chromatography. This excess capacity can be utilized in two contrasting approaches. In one approach more information can be gained from a chromatographic analysis performed in a normal "optimum" chromatography-time frame because of the high density and high quality of the data collected. Subsequent mathematical routines, such as peak finding and deconvolution, enable an increase in the effective resolution of the chromatography, providing more information in the same period of analysis time. The second approach would be to take advantage of the reserve capacity to actually perform the analysis in an attenuated period of time. This approach has catalyzed the genesis of a technique called "Time Compressed Chromatography" (TCC) wherein chromatographic analyses that typically take 50 minutes to an hour can be accomplished in 3 minutes or less. The TCC technique involves the following four steps:

 The compression of the time frame of the chromatographic analysis. This is accomplished by shortening the column length, increasing linear flow rate, and increasing temperature programming rate, etc.

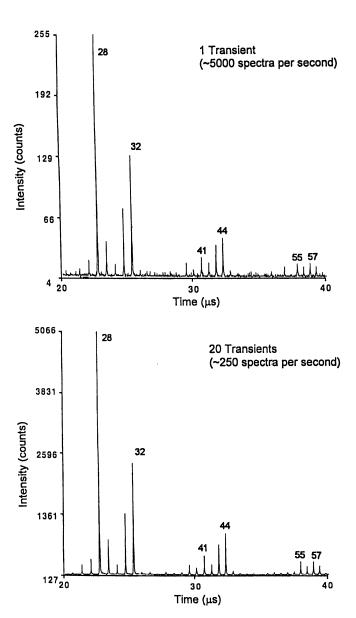


Figure 5 The mass spectra of a single transient compared with those of summations of 2, 20, and 200 transients.

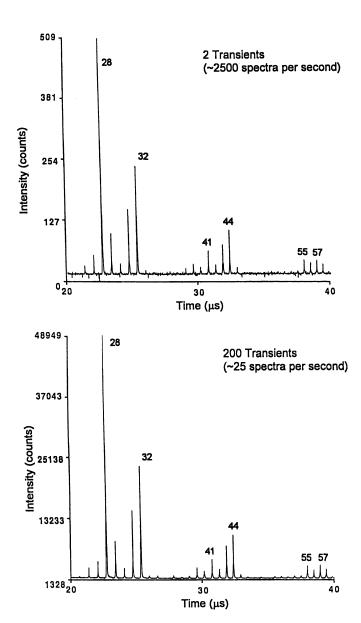


Figure 5. Continued.

- High speed, accurate GC/TOFMS/TAD detection utilizing the ITR. The scan file generation rates are set to accommodate the chromatographic information band-pass;
- 3) The mathematical extraction from the high density, high quality MS data files, of the chromatographic profiles of all of the components present. Chromatographic peak location routines identify the presence and positions of individual components and mathematical deconvolution routines will separate these components where overlapping elution occurs;
- 4) The application of qualitative and quantitative analysis routines to the reconstructed profiles to provide analytical information equal to or greater than that obtained by normal speed chromatography, recovering completely all of the information placed at risk by the initial compression technique.

Figure 6 illustrates the application TCC to a gasoline range hydrocarbon mixture in a 51 second elution time period. The range of hydrocarbons from cyclopentane to isopropylbenzene incorporates an elapsed time of approximately 48 seconds. To analyze this same compound utilizing state of the art capillary gas chromatography with hydrogen flame detection requires slightly over 50 minutes across the same span of mixture components. This represents an increase in speed (reduction of time) of over 60X with no loss of information. Figure 7 illustrates the results of the mathematical deconvolution of peak 6 of Figure 6. The peak finding algorithm of this routine identified this peak as a doublet. Iterative correlations identify the ions which are the most specific for each of these two compounds. Methods of cross correlation are used to determine the other ions arising from each component and to delegate apportionately any ions shared between the two. As shown in Figure 7, the pure spectra extracted by these mathematical deconvolution routines match exactly with the library spectra of the identified compounds; all this in spite of the fact that they elute within approximately a tenth of a second of each other. Indeed, these mathematical deconvolution routines, when applied to data files gathered from normal time-frame, high resolution chromatography, can be readily utilized to increase the effective resolution of the chromatography itself. Experience to date indicates that, even with manual injection of the sample into the chromatograph, component peak elution differences of 4 scans or more readily enable the effectiveness of the deconvolution and correlation processes. separation range implies that when data are generated at a rate of 40 spectra per second, component separation of a tenth of a second can be readily discriminated. This level of resolution is in excess of that is normally obtained by state-of-the-art gas chromatography utilizing any of the one dimensional universal detectors common to this methodology. In summary, to the already documented and established benefits of GC/TOFMS with TAD using the ITR, one must now add the benefits of greater chromatographic resolution and shorter analysis times.

Sensitivity Capabilities of TOFMS-TAD

The time-of-flight mass spectrometry of gaseous samples has a reputation for poor sensitivity, due largely to poor sample utilization factors. The process of creating a

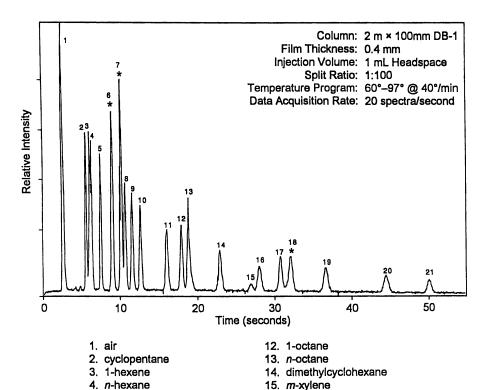


Figure 6 Analysis of a mixture of the hydrocarbon components of gasoline by capillary column chromatography and TOFMS detection utilizing the principles of time-compressed chromatography. Asterisks indicate co-eluting components.

p-xylene

21. solvent

17. 1-nonene

18.* o-xylene and n-nonane
19. 1,3,5-trimethylbenzene

isopropylbenzene

5. methylcyclopentane

10. methylcyclohexane

n-heptane
 diisobutylene

11. toluene

6.* benzene and cyclohexane

7.* isooctane and 1-heptene

temporally defined sample of ions which will be velocity-analyzed can be quite inefficient. Some sampling techniques operate by taking a small section out of a continuous ion beam. This process of beam slicing is accomplished by beam deflection (12). It has the advantage that, since all the ions are going in the same direction, there is no ion turn-around effect which is a major factor in limiting the resolution of TOF analysis. The disadvantage of beam slicing is that a very small fraction of the generated ions are sent through the analyzer to the detector. If a 20 ns slice is taken from a beam every 200 ms, the sample utilization is only one part in 104! Similar inefficiency is encountered when the sampling is achieved by pulsed sample ionization. In this approach, the electron beam or other ionizing energy source is applied to the source for only a short time. This technique, is very effective for solid or steady state samples that are consumed or used only when the ionizing radiation is applied, but is not efficient when the sample is gaseous and dynamic. If, in addition to these inefficient sampling methods, time-slice detection, in which the detected ion efficiency is less than one part in 1000, is used, the overall efficiency can be much worse than that of a scanning mass spectrometer. The ion collection efficiency of time-array detection can improve the signal-to-noise ratio of the resulting intensity measurement by the square root of the number of summed elements along the mass axis (Fellgett's advantage), such that the advantage of TAD can offset the disadvantage of sampling by beam-slicing or pulsed ionization.

Fortunately, the inefficiencies outlined above are not inherent in, and need not be an essential part of, time-of-flight mass spectrometry. Several approaches have been used to obtain much better utility of the sample. These techniques are based on continuous ion generation with pulsed ion extraction and some degree of ion storage between extractions. Figure 8 illustrates the advantages obtainable with ion storage. The transverse line represents the continuous ion generation rate for one of the m/z values in the analyte's mass spectrum over the 200 ms time interval between extractions. When beam slice or pulsed ionization bunching is used, the amplitude of this line is the value of the peak detector current at the arrival time for this m/z value. When continuous ion generation is used with pulsed extraction, some fraction of the ions formed between extractions may remain in the source region at the next extraction time. This approach to greater ion use is not compatible with time-lag focusing, but then, neither is the mass-dependance of time-lag focusing consistent with time-array detection. If no special attempt is made to store the ions, only those ions that have not yet left the source would be extracted. The mean velocity of a mass 200 molecule at room temperature is 0.17 mm/ms which suggests that most of the ions generated during the microsecond previous to extraction would still be in the source. The higher the ion mass, the greater the fraction of previously generated ions that will be present at the extraction time. Ions accumulated over 2 ms, if focused at the detector to a 20 ns arrival time will have a peak current 100 times that of the average ion generation current. This will result in an intensity measurement with signal-to-noise ratio equivalent to the averaging of the continuous ion current over 200 ms (assuming background white noise is limiting). In other words, with this degree of ion accumulation between extractions, the resulting detection limits by TOFMS/TAD approach that of a scanning mass spectrometer operated in single-ion monitoring mode (SIM), except that with TAD, this response is achieved for all ions in the mass spectrum simultaneously.

From the above arguments, it can be seen that with even further efficiency of

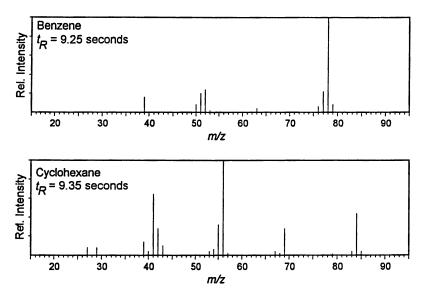


Figure 7 The deconvoluted mass spectra of two compounds co-eluting as peak 6 of Figure 6.

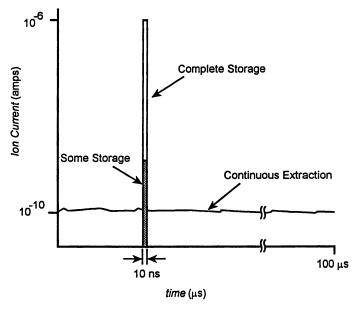


Figure 8 A graphic representation of the advantages of storage in the ion source prior to extraction.

ion accumulation between ion extractions, the detection limits for TOFMS/TAD have the potential to exceed those of quadrupole SIM without sacrificing mass spectral information. Several researchers have sought ways to increase the storage efficiency of ions between extractions. In an early publication, Studier employed the electrostatic attraction of a continuous electron ionization beam to provide, in essence, a third or trapping electrode for positive ions (16). Over two orders of magnitude increase in ion signals were observed. More recently, Wollnick introduced a source design in which a mid-source grid was used to introduce a potential well that would impede the loss of ions after their formation (17). Research in this area continues as the benefits to be gained are great. If complete ion storage between extractions could be achieved, the peak signal intensity at the arrival time of an isomass packet could be 10,000 times that of the average detectable ion generation current for that mass. Detection limits substantially greater than those currently achieved by SIM could be obtained while simultaneously enjoying full spectral information.

Along with the desire to improve ion storage efficiency comes the concern about space charge limitations on ion storage. Conventional wisdom, derived principally from ion behavior in ICR and ion trap MS, suggests a source storage capacity on the order of 106 ions per cc. For TOFMS, this should not be a problem. Based on the ion statistical arguments made earlier, there would be an ample number of ions in each extraction from which to obtain a quantitative spectrum. In other words, the ion storage limitations are ameliorated to a considerable extent by the speed of the extraction cycle. Of greater concern regarding ion storage capacity for chromatographic detection is the fraction of the stored ions that are due to the chromatographic mobile phase, vis-a-vis, the analyte and the relationship between analyte concentration and the kinetics of the storage mechanism. accumulation times and less frequent extractions have some statistical advantages, but unfortunately decrease the degree to which the dynamic range of the summed transients can exceed the dynamic range of the analog-to-digital converter. This loses some of the advantages gained by summing, and creates a greater vulnerability to the non-linearity of the storage mechanism itself.

Significance of TOF/TAD for Chromatographic Detection

The development of the ITR and its application to TAD, for the first time, produces an instrument system capable of gaining the full information provided by state-of-the-art capillary column chromatography. This was the initial objective of the research group at MSU and it has been more than achieved. Not only can capillary column gas chromatography be accommodated, but the present capability exceeds the requirements for speed, even for microbore gas chromatography and high pressure liquid chromatography (HPLC). The very sharp peaks of capillary electrophoresis (CE) likewise would be amenable to the techniques of TCC as would any technique requiring the collection of multi-dimensional data fields such as MS/MS. Indeed the full capability of time-array detection may reach one of its ultimate performances when utilized for the sweep axis for MS/MS applications. MS/MS data fields have been collected on the time frame of single component elution from packed column chromatography. The potential and probable utility of time-of-flight for both axes will enable the same two-dimensional information to be collected on the time frame of capillary column chromatography. This capacity would introduce a significant

potential to the range of applications of MS/MS since it is through gas and liquid columns that both in number and complexity the most efficient introduction of sample molecules into the ion source of mass spectrometers has been achieved. This development will combine the ideal inlet system with the ideal high speed analyzer, opening the avenue of MS/MS techniques for the direct analysis of complex mixtures.

In a general overview it can be anticipated that the reserve capacity of TOFMS/TAD can be utilized either to increase the effective resolution of chromatography or any other separations method to which mass spectrometry may be applied as a detecting system, or to reduce greatly the analysis time which is appropriate for MS/MS and the various applications of TCC. Utilizing either or both of these advantages, one can readily envision a broad spectrum of applications to which mass spectrometry may now be effectively employed as a detecting system. These include several techniques in which the sample introduction to the mass spectrometer is dynamic, such as the temporal based separations of chromatography, or situations where the sample itself is undergoing rapid chemical change. Fast gas chromatography is an emerging technology in which chromatographic peak widths are measured in terms of tens to one hundredths of milliseconds. It can readily be envisioned that the application of TCC will greatly enhance this technique for the analysis of complex or moderately complex mixtures. The immense strain on the reproducibility of the injection system for fast chromatography is greatly ameliorated by the use of the mass spectrometer as a detector. A single dimensional detector requires extreme precision in sample injection since only the elution time is of value in the qualitative assessments. The two dimensional information provided by the mass spectrometer allows for identification techniques to be applied effectively in situations where the actual elution times may vary beyond the point where it would be useful, if used as a single parameter. Only TOFMS-TAD applying the principles of TCC can accommodate this emerging analytical requirement. Indeed, one cannot readily envision a more appropriate detector for fast chromatography.

Other situations requiring a rapid analysis speed in addition to the chromatographic and the two- and three-dimensional techniques discussed above are cases where the sample being analyzed is either present in vanishingly small amounts or in dynamically short time periods. Smaller amounts of samples require the sensitivity that TAD is capable of producing. Dynamic sampling requires the speed which only TOF is capable of accommodating. For example, the instrument described above can analyze the exhaust emissions of a 6-cylinder gasoline engine idling at 600 rpm on a per cylinder basis with excellent sensitivity. Phase triggering of successive transients from the spark ignition can yield up to 160 complete informative mass spectra detailing the combustion process of a single explosion in a single cylinder.

In conclusion, it is readily apparent that TOFMS using the ITR to accomplish TAD creates enabling instrumentation for which complete new areas of analytical applications may be identified. The continued development and improvement of the ion storage processes between the source extractions and the applications of this new technology to other types of sample introduction and other types of sample ionization will continue to improve the performance and expand the applicability of TOFMS-TAD. One can envision that these developments may produce the "ideal" detector for chromatography or any other type of analysis which necessitates high speed and sensitivity. This detecting system would be capable of measuring and utilizing all of the information in each and every TOF transient waveform and storing all of the ions

generated in the time between ion source extractions. These two processes will maximize sample utility and allow optimization between the information bandpasses of the data generating process and the data collection and examination process. In addition to maximizing the amount of the analytical information gleaned from empirical experimentation, such a detector would have several orders of magnitude greater sensitivity than is currently available with the most sophisticated of the mass spectrometer detecting systems. Whether such an "ideal" detector can be eventually developed is problematic. What is clear, however, is that this is the beginning and not the ending of the developmental processes that will result from this new enabling technology.

Acknowledgments

The authors wish to acknowledge the DRR division of NIH, the State of Michigan, and Meridian Instruments, of Okemos, MI, for financial support; Dr. Hermann Wollnick of the University of Geissen, the Federal Republic of Germany, for providing major components and assistance in the construction of the reflectron mass spectrometer; and Ben Gardner of Michigan State University for technical assistance in preparation of the manuscript.

Literature Cited

- (1) Golke, R.S. Anal. Chem. 1959, 31, 538-554.
- (2) Henneberg, D. Anal Chem. 1961, 183, 12-23.
- (3) LKB 9000 GC/MS Technical Bulletin; LKB Productor: Stockholm, Sweden, 1965
- (4) Lawson, G.; Todd, J.F.J. Chem. Brit. 1971, 8, 373-380.
- (5) Holland, J.F.; Enke, C.G.; Allison, J.; Stults, J.T.; Pinkston, J.D.; Newcome, B.N.; Watson, J.T. Anal Chem. 1983, 55, 997A-1112A
- (6) Stults, J.T.; Enke, C.G.; Holland, J.F. Anal. Chem. 1983, 55, 1323
- (7) Cornish, T.J.; Cotter, R.J. Anal. Chem. 1993, 65, 1043-1047.
- (8) Puczycki, M.A.; McLane, R.D.; Vlasak, P.R.; Enke, C.G. Proc. 40th ASMS Conference, 1992, Washington, DC, 1332-1339
- (9) Holland, J.F.; Newcome, B.N.; Tecklenburg, R.E.; Davenport, M.; Allison, J.; Watson, J.T.; Enke, C.G. Rev. Sci. Instrum. 1991, 62(1) 69-76.
- (10) Stults, J.T.; Watson, J.T.; Enke, C.G.; Holland, J.F. Int'l. J. Mass Spectrom. and Ion Proc. 1968, 71, 169-181.
- (11) Pinkston, J.D.; Allison, J. Proc. 33rd ASMS Conference, 1985, San Diego, CA, 721-724.
- (12) Yefchak, G.E.; Enke, C.G.; Holland, J.F. Int'l. J. Mass Spectrom. and Ion Proc. 1987, 87, 313-330.
- (13) Mamyrin, B.A.; Karataev, V.I.; Shmikk, D.C; Zagulin, V.A. Sov. Phys. J.E.T.P. 1973, 37, 45-48.
- (14) Grix, R.; Kutscher, R.; Li, G.; Groma, U.; Wollnik, H. Rapid Comm. in Mass Spectrom. 1988, 2, 83-85.
- (15) McLane, R. D. Ph.D. Thesis, 1993, Chap. 7, Michigan State University
- (16) Studier, M.H. Rev. Sci. Inst., 1963, 34, No. 12, 1367-1370.
- (17) Grix, R.; Grüner, G.L.; Stroh, H.; Wollnik, H. Int. J. Mass Spec. and Ion Proc., 1989, 93, 323-330.

Chapter 10

Signal Processing for Time-of-Flight Applications

Ihor A. Lys

5545 Beeler Street, Pittsburgh, PA 15217

When compact disc players were first introduced, their cost, and the cost of the discs themselves, was astronomical. Economists will maintain that as volume grew, prices dropped. This is not the entire picture, however. The high cost was due to technological complexity, not just small volume. Today every CD player contains a significant amount of signal processing circuitry, yet because of the advances made in the early eighties, costs only a fraction of what comparable technology cost then. Music reproduction faced the same constraints in the eighties that signal processing for TOF faces today. This chapter examines the mathematical and practical aspects of analog and digital signal processing as applied to TOF application, but it should be noted that most of the material is quite generalized.

Time to Digital Conversion

Time to digital converters, or TDCs, are the most basic of signal acquisition elements. The basic block diagram is shown in Fig 1. A TDC consists of a counter and two discriminators. The counter is started by a pulse from the start discriminator, and stopped by a pulse from the stop discriminator. The time interval can then be read out and stored. The TDC is then reset and is ready for another event. This process is usually repeated thousands of times, and an output is presented to the user in histogram form.

TDCs have several properties which make them attractive for some forms of TOF work. They are inexpensive, and quite fast, with count rates of 6 GHz being common. They find many applications in high energy physics experiments, and pulse counting applications, where the number of pulses received is small (usually less than 5) and there is a long time between successive events. These applications were the original impetus for the development of TDCs.

TDC's properties may also preclude their use in many applications. A stop event terminates a TDCs cycle, and it is therefore required that there be a stop pulse, and that it occur before the next start pulse. TDCs need to have some maximum time

0097-6156/94/0549-0177\$06.00/0 © 1994 American Chemical Society to record in the case that no matching stop pulse is received. Until multi-stop TDCs were developed, there had to be a 1 to 1 correspondence between start and stop pulses. Multi-stop TDCs solve the problems associated with the 1 to many nature of many ionization events, but at a price in complexity and cost. A multi-stop TDC will record events separated by some minimum time, called the dead time, but will not record anything which happened in-between.

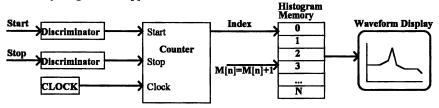


Figure 1. Block diagram of a TDC.

Signals of varying heights produce the same output, including the time value. This is not usually desired, because the height of the received signal may cause a slope-induced error from the leading edge. The recorded time always leads the time at which the peak of the signal occurred in a TDC, but the amount of this lead is dependent on the signal amplitude. TDCs do not quantify the size of the input signals, and the only information which is actually recovered is that there was some signal strength at the time recorded. Constant-fraction discriminators can be used to overcome the time error introduced by signal height variations, but the height of the signal is still not recorded.

TDC's do not have any ability to separate signals from noise. Signals with poor signal to noise ratio (SNR) will prematurely trigger the stop discriminator, and will therefore generate no usable data. There has been much discussion about the SNR required for good operation of a TDC. The SNR value needed can be expressed in terms of an arbitrary "falsing rate" which expresses the percentage of false stop pulses to true stop pulses through the use of noise distribution analysis. Obviously a lower falsing rate is better, but because of the nature of the analysis, some reasonable rate needs to be chosen. In any event, the signal must be larger than the noise level.

There has been interest in "windowed" TDCs, which impose some dead time after the start pulse is received, to remove early noise events. This can be quite useful in TOF applications where many of the stop bins in a multi-stop TDC can be wasted on useless low-mass ions, preventing the acquisition of high-mass ions. At this point however TDC's become more and more difficult to use, require much more careful setup, and often require experiments to be repeated in order to generate good data. After adding all of the improvements that TDCs have undergone, they become complex, expensive devices, and Analog to Digital converters should be a better choice.

Transient Recorders

Transient Recorders are the other option available today. Analog to digital conversion is the basis of much of this technology. In the mid 1980's several companies introduced the first commercially viable digital oscilloscopes. These devices quickly revolutionized the transient recorder field, and have replaced both

analog scopes and more traditional transient recorders. Their initially high cost and poor performance limits have been overcome. Today one can buy hand-held digital oscilloscopes for under \$1000 that have performance specifications comparable to those of expensive rack mount instruments of the early 1980's.

A Transient Recorder is composed of several components, as shown in Fig 2. The core is a Sample and Hold unit(S/H), Analog-to-Digital Converter (ADC), and a memory. When packaged like a traditional oscilloscope, a transient recorder is referred to as a Digital Storage Oscilloscope, or DSO.

When a trigger is received by the unit, sampling begins at a rate determined by the clock, called the Sample Rate, and the digital representation of the voltage present at the input is stored in successive memory locations. It is important to note that each start (trigger) pulse generates a complete representation of the entire signal. This is significantly more data than a TDC recovers. Each memory location corresponds to one minuscule segment in time. Its value represents the voltage of the input signal during that period. Each trigger can produce as much as 200000 data values.

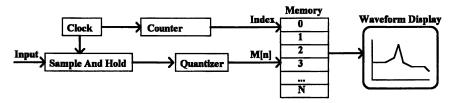


Figure 2. Block diagram of a transient recorder.

At first this may appear to be the complete solution to the TOF signal problem. Several issues remain however. TOF applications have constantly demanded more performance from DSOs. All of the general specifications of a DSO have been pushed by TOF needs. In many respects the fields of radar processing (the original impetus for the development of transient recorders) and TOF are similar in their demands. The signals have wide dynamic range, very wide bandwidth, poor signal to noise ratio, poor repeatability, long signal length, and low repetition rates. In addition, there is a desire to recover all of the signal produced at each point in time. These characteristics demand high sampling rates, long memories, high resolution A/D converters, and significant signal processing abilities. Furthermore, these characteristics must be met in *single shot* acquisitions.

In order to further understand the limiting factors affecting DSOs, an in depth discussion of signals and the operations performed on them is necessary.

Continuous Signals

All real world signals are continuous in nature. At each infinitesimal point in time the signal has some absolute amplitude. The signal can be analyzed, or processed to enhance certain aspects or to remove others. A mathematical representation of some continuous time signals would be:

$$x(t) = A \cdot Sin(\omega t), \quad y(t) = \frac{Sin(t)}{t}, \quad z(t) = A \cdot Sign[Sin(\omega t)], \quad v(t) = A$$
 (1)

In this list, x(t) is just a sine wave of amplitude A and of frequency ω ; y(t) is commonly referred to as the sinc function, essentially a rounded impulse at t=0; z(t) is a square wave of amplitude A and of frequency ω ; v(t) is a DC signal of amplitude A. Each of these signals has a value at every point in time, from $-\infty$ to $+\infty$, and x(t), y(t) and v(t) are also continuous. Continuous time signal manipulation operations have effects on these signals, often changing them in many subtle ways. For example a signal x(t) could be amplified, producing x'(t)=Ax(t). It could also be delayed, producing $x''(t)=Ax(t-t_0)$. Two signals can be added together, producing x'''(t)=Ax(t)+By(t). Many other operations are possible.

Fourier Transforms

Fourier analysis is a method of decomposing a signal into a series of sines and cosines, with differing amplitudes and frequencies. It can be shown that any signal that meets certain criteria, called the Dirchlet conditions, will have a Fourier representation. The Fourier transformation of a signal x(t) is $X(\omega)$, as given by the Fourier Integral:

$$X(\omega) = \int_{-\infty}^{+\infty} x(t)e^{-j\omega t}dt$$
 (2)

Note that this integral is an infinite integral, and that each evaluation of it produces one value of $X(\omega)$. The analytic notation $e^{-j\omega t}$ with $j=\sqrt{-1}$ is used to represent $\cos \omega t$, the different frequency sinewaves over which the integral is evaluated. In mathematics the variable i is commonly used for this value, but in electrical engineering, i is reserved to symbolize current, and so j is used instead. When a periodic signal is transformed, the limits of integration can be relaxed, and the signal need only be integrated over a single period. The importance of eq. (2) cannot be overemphasized. It transforms the time-domain to the frequency domain. A function such as $x(t) = A \cdot \cos(\omega_0 t)$ in the time domain corresponds to two impulses of amplitude $A \cdot \pi$ in the frequency domain at $\omega = \pm \omega_0$. $X(\omega)$ is zero at all other points. Note that there two impulses. Their relative amplitudes are proportional to the phase of the input sinusoid. This is graphically represented in Fig 3.

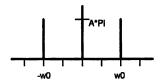


Figure 3. Fourier representation of $x(t) = A \cdot \cos(\omega_0 t)$.

Many functions will have more complex Fourier transforms. A square pulse in time will transform to an odd looking function shown in Fig 4. This transform relation is:

$$x(t) = \begin{cases} 1 & |t| < T_1 \\ 0 & T_1 < |t| \end{cases} \quad \Leftrightarrow \quad X(\omega) = \frac{2\sin(\omega T_1)}{\omega}$$
 (3)

There are several important aspects of this relationship. $X(\omega)$ is infinite in length even though x(t) is not. This is a result of the sharp discontinuity in x(t), which transforms to sinusoids extending to infinity in frequency, attempting to reproduce ever more faithfully the step. Infinite frequency is required because only infinite frequency sinusoids can reproduce the sharp (infinite) slope at the discontinuity.

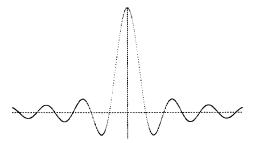


Figure 4. Fourier transform of a square pulse.

Inverse Fourier Transforms

Like many other transforms the Fourier Transform has an inverse. If the Fourier transform of a signal is known, then the signal itself can be determined through the transformation:

$$x(t) = \frac{1}{2\pi} \int_{-\infty}^{+\infty} X(\omega) e^{j\omega t} d\omega$$
 (4)

Note that this equation is very similar to the Fourier transform equation in (2). This is known as *duality*, and its meaning is quite important. A square pulse in time transforms to a sinc function in frequency, as shown in Fig 4. Likewise a square pulse in the frequency results in a sinc pulse in time!

Properties of the Fourier Transform

Fourier Transforms have many properties, which often help in determining the transform of a particular signal. They also show why the Fourier transform is so important and useful. Fourier Transform is abbreviated as FT here.

The FT is linear. That is, if two signals are added together, with some arbitrary scaling, then their combined FT will be the sum of their individual FT scaled by the same amounts as the original time functions.

$$ax_1(t) + bx_2(t) \stackrel{FT}{\longleftrightarrow} aX_1(\omega) + bX_1(\omega)$$
 (5)

The FT of a time-shifted function has the same magnitude as the original FT, but with different phases for the components.

$$x(t-t_0) \stackrel{FT}{\longleftrightarrow} e^{-j\omega t_0} X(\omega) \tag{6}$$

If a signal is scaled linearly in time the FT is scaled linearly in frequency, and its amplitude is multiplied by a constant.

$$x(at) \xleftarrow{FT} \frac{1}{|a|} X\left(\frac{\omega}{a}\right)$$
 (7)

Differentiation in time corresponds to multiplication by $j\omega$ in frequency.

$$\frac{dx(t)}{dt} \longleftrightarrow j\omega X(\omega) \tag{8}$$

Integration in time corresponds to division by $j\omega$ in frequency, and the addition of a not so arbitrary constant, the average or DC value of the signal.

$$\int_{-\infty}^{t} x(\tau)d\tau \xleftarrow{FT} \frac{1}{j\omega} X(\omega) + \pi X(0) \partial(\omega) \tag{9}$$

Parseval's relation transforms as would be expected. This relation states that the power in a signal, which as proved by Parseval, is the integral of the magnitude squared of a signal over all time. After FT, the equation states that the power in the signal can be obtained simply by integrating magnitude squared over all frequency.

$$\int_{-\infty}^{+\infty} |x(t)|^2 dt = \frac{1}{2\pi} \int_{-\infty}^{+\infty} |X(\omega)|^2 d\omega$$
 (10)

Finally, the most important property concerns convolution. The convolution of two signals is defined as:

$$y(t) = x(t) * h(t) \equiv \int_{-\infty}^{+\infty} x(\tau)h(t-\tau)d\tau$$
 (11)

In the FT domain, the FT of the convolution of two signals is just the product of the FT of each of the original signals.

$$y(t) = x(t) * h(t) \longleftrightarrow Y(\omega) = X(\omega)H(\omega)$$
 (12)

This is vitally important, since the filtering or processing of a signal in the time domain by a circuit corresponds to the convolution of the signal with the response of the circuit. Hence if the response of the system in the frequency domain is known, then the output of the system can be easily determined without the need to evaluate the integral in (11), which is often extremely difficult. Furthermore, we can determine many other characteristics of the circuit from its $H(\omega)$. A device called a Spectrum

Analyzer is used to determine $H(\omega)$ experimentally. Often this device is used in the design of a circuit, in tuning the circuit to the design specifications.

Filtering

Filters can be generally viewed as frequency selective amplifiers. They increase the amplitude of signals in a certain frequency range relative to other frequencies. Filters are necessary because most signals contain spurious components (noise) which are not of interest. The job of the filter is to remove those spurious components, while leaving as much of the original signal intact as possible. A filter can only remove noise when its frequency components are different from those of the signal of interest.

In a TOF spectrum, the signal information is contained in a relatively wide bandwidth. Frequencies of interest rarely exceed 100MHz, but often extend below 1MHz. From Parseval's equation it can easily be seen that high frequencies are more damaging. Consider a typical case. Noise in the real world can be considered "white", that is it has equal power per unit frequency. The input bandwidth of a Tektronix TDS 540 DSO is 500MHz. If only white noise were present, then for the typical TOF signal, 401 MHz of unnecessary noise power is captured. In other words 5 times as much noise would be captured than the input signal actually contained.

An ideal filter which removed all frequencies above 100MHz would improve the signal to noise ratio of the signal by a factor of 5, or 14dB! Luckily manufacturers of DSOs have recognized this problem, and usually provide filters that limit the input bandwidth. Note that the noise contributed by the DC to 1MHz band is minimal. As long as certain conditions are met, all of this noise can be removed later, by digital filtering (smoothing).

This can be seen graphically in Fig 5. Assume that the input signal is band-limited, as graphically represented in (a). The signal may contain any frequency within the box. Note that the box represents only the maximum frequency, and really does not signify anything about the actual amplitudes of the components of the input signal. Next wide band noise, extending out to infinity in frequency is added to the signal, and shown in (b). The new signal's frequency components or envelope is (c). If this signal were fed directly to the DSO, the cutoff frequency would be at ω_1 , and the FT of the captured signal would be (d). On the other hand, if the signal is first filtered, then the noise power present between ω_2 and ω_1 is removed, and the resulting signal has the FT in (e). The ideal filter used to remove this noise has the response in (f), and this response is convolved with the input signal in the time domain. In the frequency domain, the signal and response are simply multiplied, and the result is obvious. For TOF applications, this type of filter may not be ideal however.

A quick examination of the time-domain of the resulting signal will reveal that input peaks, originally sharp, now appear similar to Fig 4, the sinc function. The duality of FT explains why this pulse shape appears. This pulse is guaranteed to be the narrowest, but not necessarily to provide the best signal to signal separation. Bessel-Thompson filters have the "best" pulse shape, but have much less attenuation per unit frequency. Generally, the faster the cutoff, the worse the pulse response, although it is possible to obtain both poor pulse response, and slow cutoff at the same time. There has been much debate over the "best" filter response, and there exist some very

complicated, even non-linear filters (like Dolby). Essentially the aim is the same, to remove those components not of interest, or to minimize their addition.

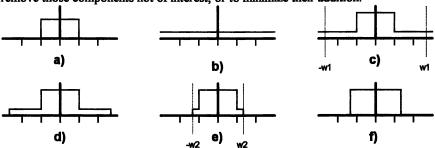


Figure 5. Graphical representation of reduction of noise bandwidth.

Signal Averaging

Signal averaging is a simple procedure which increases the Signal to Noise Ratio (SNR) of the recovered input signal. Signal averaging can theoretically be performed on continuous signals, but is usually done after A/D conversion, since this can actually be implemented. Nevertheless, the analysis is the same. If N random signals with an expected mean of zero, and average power P are summed together, the resulting signal will have an average power of NP and an expected mean of zero. The average amplitude of the resulting signal will rise by only the square root of N however. On the other hand, if the signal is not random, then summation will produce a signal with amplitude N times greater than the original signal, and power N^2P .

If two signals, one repetitive, and one not, are superimposed then the result is a signal with noise. If more than a few such signals are summed, then the power of the repetitive signal grows faster than the power of the non-repetitive signal. Most forms of noise can be considered uncorrelated with the signal of interest, and hence can be reduced by signal averaging. The SNR gain for signal averaging is:

$$SNR_{gained} = 20\log(\sqrt{N}) \tag{13}$$

The maximum SNR is limited by other factors, but the maximum gain can be quite substantial, often exceeding 20dB. This technique does not involve any filtering, and the noise and signal may occupy the same bandwidth. The procedure "extracts" the signal from the noise. A demonstration of this effect is quite astounding. The input SNR can even be negative! Peaks which are indistinguishable from the noise around them can become quite well separated. A signal at -3dB, of lower amplitude than the surrounding noise, can be recovered, and will appear 7 times larger than the surrounding noise if 100 shots are averaged together! The maximum gain is limited, primarily by the noise to signal correlation, and also by reality. If an instrument is capable of 10 scans per second, and the input SNR is -10dB, and we want an SNR of 10dB (signal 3 times as big as the noise) then the SNR gain needed is 20dB and the number of shots is 100. This takes 10 seconds. If however the signal is worse, and an SNR gain of 40dB is desired, then it takes 17 minutes, already a long time. At this point a different instrument would probably be desired. More averaging requires more

sample, and more sample may not be availiable. It may be necessary to reload the instrument, taking more time, etc.

Sampling

The first operation performed in a typical DSO is sampling of the input signal. Sampling has a mathematical representation. A sampling system essentially multiplies the time-domain signal by a series of impulses, each of amplitude 1, and spaced at some sample period T. This operation results in convolution, in the frequency domain. This vitally important result is graphically represented in Fig 6. The spacing between

successive copies of the input's FT is $\omega_s = \frac{2\pi}{T}$. The implications are quite obvious. If the input signal needs to be fully captured then the edges of the FTs of the input signal cannot overlap. The point at which the signals touch is when $\omega_s = 2\omega_m$; the signal is sampled twice as fast as the largest frequency in the input. This is the Nyquist criterion. This may seem to be a trivial operation, but nothing could be further from the truth. The Nyquist criterion sets a minimum limit on the sampling rate, but which frequency does ω_m refer to? The highest frequency of interest should be assigned to ω_m , but in this case all frequencies bigger than ω_m should first be removed. Usually it is too difficult to form such a sharp cutoff, and some wasted bandwidth is tolerated. The signal is oversampled (sampled faster than necessary), and the FTs of the input signal are separated by some gaps in the frequency domain, where no energy is present. Digital filtering can then be performed, and the sample rate reduced, such that no additional samples are present.

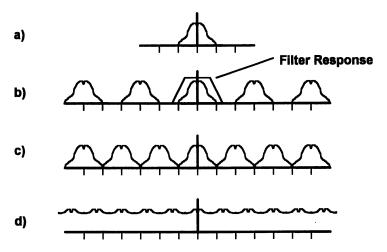


Figure 6. Original signal's frequency response (a), Oversampled signal (b), signal sampled at Nyquist rate (c), Undersampled signal (d).

Take the case of CD players, for example. As any audiophile will adamantly maintain, audio signals have a bandwidth up to about 40KHz. CDs have a defined

sample rate of 44.1KHz. If the higher frequency components of the signal are to be removed before sampling, as is absolutely necessary, and the frequency range of interest is 20Hz to 20KHz, then the filter must remove all frequencies above 22.05KHz, while not affecting frequencies of 20KHz. The amount of attenuation at 22.05KHz must be greater than the dynamic range of the A/D converter, which is 96dB (for 16 bits). If the maximum allowed deviation at 20KHz is 1dB, then the system will require an analog filter with 50 sections. CBS records initially purchased such a rediculous analog filter. It occupied an entire 1.5 meter high electronics rack, and was retuned every week.

The problem is not that a filter section is large, or difficult to manufacture, but rather that as more filter sections are added, the tuning requirements for all of the sections become more severe. Eventually a point is reached where random temperature fluctuations, and component variations will make it impossible to manufacture the filter.

Digital filtering significantly reduces the problem. Assume that the signal is sampled at eight times the original sample rate, and that the resulting samples are then digitally converted to a lower sampling rate. Now the input signal needs to be filtered to remove noise and spurious signals, but the bandwidth is now 176.4KHz. Now a much more reasonable analog filter, with only 5 sections is necessary. Such a filter can easily be manufactured on an integrated circuit, and purchased for about one dollar. The corresponding digital filter is not trivial, but can be implemented in less chip area than the 5 pole analog filter. As an added benefit, the D/A converter need not actually have 16 bit accuracy, since the digital filter will automatically "spread" the least significant bits among the multiple samples, and the analog filter will then "collect" them back into the waveform. Assuming everything is perfect, the converter only needs 13 bits. Hence the 14 bit converter used in many players is perfectly acceptable¹. Furthermore, the digital/analog filter combination is much more accurate and stable than the analog version, and usually requires no initial tuning. There is an obvious tradeoff here, with the digital and analog world being traded through oversampling.

The CD player example is one of low speed sampling at high accuracy. TOF signals usually have much higher sampling rates in the realm of 50MHz to 2GHz. If the same logic is applied to this case the result is similar. The TOF signal from a particular mass spectrometer has 35MHz of bandwidth. The sampling instrument in this case will be a Lecroy 9400A DSO. This instrument has 42dB of dynamic range, 175MHz of Bandwidth, and samples at 100MS/sec. In order to not undersample any part of the input signal and noise, the input filter must have a cutoff of less than 50MHz. This is especially troublesome because the DSO has 175MHz of bandwidth. An external filter is therefore required. This filter should have 1dB of error up to 35MHz, and 42 dB of attenuation above 50MHz. If a Chebyshev filter is used, it requires 7 poles. If pulse response in the time domain is to be optimized through the use of a Bessel filter then the filter would need about 15 to 20 poles. A digital filter would not be necessary nor useful.

¹The consumer electronics marketing people have consistently worked much too hard to get converters with too many bits.... Hence we have 18 bit converters (accuracy only 16 bits), and essentially useless claims of 102dB SNR (14 bit converter = 84dB + 8X filter = 18dB) and 108dB SNR (96dB from the converter and 12dB from the 4X filter).

If however, the DSO is a LeCroy 7242B then the sample rate is 1GS/sec, the bandwidth is 500MHz, and the dynamic range is 42dB. The filter must now cutoff from 35 to 500MHz, so a Chebyshev filter with 2 poles is needed. A Bessel filter with 3 poles would be more than adequate. Furthermore, these filters are unnecessary, since the 85Mhz Bandwidth limiter in the 7242B is more than sufficient. The digital resolution enhancement filters in the 7200 will do the digital filtering necessary, and the resulting waveform will be much cleaner than that of the 9400A.

Resolution enhancement

Note that the increase in sample rate is only part of the result, the digital filters will increase the effective SNR of the input signal from 7 to 9 bits, or from 42dB to 53dB. Essentially the filters do a modified form of signal averaging, this time using neighboring samples rather than successive acquisitions. The oversampling of the input not only significantly reduces the filter requirements, but it also increases the amount of signal recovered. This is because additional information about the low frequency portion of the waveform has been recovered. The larger the oversampling ratio, the greater the gain! There is also no reason why the two techniques cannot be used together. Hence an 8 bit digitizer with 7 bit actual performance can yield 9 bit SNR if the signal is properly sampled and processed! This same technique is used in CD players to obtain 18 bit resolution from 16 bit samples. The additional resolution is really not necessary, and the listener is challenged to distinguish between 16 and 18 In TOF applications however the gain is more visible and bit reconstruction. important. This is single shot performance. Multiple shots can easily push this value to 12 bits. This will be the new justification for higher sampling rates in TOF Single shot performance determines the root quality of the data recovered from a digitizer. A 4GS/sec digitizer will gain another bit of performance, and yield 59dB of SNR.

Sampling Errors

Sampling is one of the most difficult operations to perform accurately at high speeds. Along with the theoretical limitations of sampling, the true errors are usually frequency dependent. Sampling DSOs have a timebase, which controls when a particular sample is collected. At first it could be assumed that this timebase need only be a little more accurate than the sample interval, or 10ns for a 100MS/sec recorder. This is not the case. The sample and hold unit has some aperture, during which the signal is sampled. The width of this aperture is a function of the analog circuit used to perform the task. This Aperture Width is usually specified in terms of the maximum bandwidth which the DSO can capture. A DSO with a smaller Aperture will be capable of sampling a higher frequency signal. The signal may be aliased, if the sample rate is too low, but repetitive sampling can recover this signal. The Aperture Width should be at most 10% of the sample rate, to allow good sampling. The sample and hold system also has some aperture uncertainty, or jitter. This jitter is much more of a problem. The aperture width can be filtered away, as long as it is consistent, but the jitter, being random cannot be filtered away. Furthermore, the jitter results in a signal dependent error, whose magnitude is related to the slope of the input signal. Hence

faster inputs require better jitter performance. The aperture jitter must be maintained at

$$T_{\text{jitter}} < \frac{1}{\omega_{\text{max}}} \cdot \frac{1}{10^{(SNR/20)}} \tag{14}$$

In order to achieve 42dB of Signal to noise ratio, for the 175MHz input bandwidth of the LeCroy 9400A, the jitter must be below 7.22E-12 seconds or about 7 picoseconds! This is extremely hard to achieve, and is the primary reason why manufacturers have not introduced DSOs with 10 or 12 bit converters. The SNR necessary would increase by a factor of 4 or 16, and the aperture uncertainty specifications would not be met. The extra bits would be meaningless. The 9400A actually claims only 30 dB of SNR at this frequency, so the 10 picosecond aperture jitter of the sample and hold is 3 sigma away, quite conservative. At higher frequency inputs the problem becomes worse of course. In the case of the TEK TDS 540, the input bandwidth is 500MHz. The jitter would have to be below 2.5 picoseconds to achieve 7 bit performance. The performance is not 7 bit, and is probably not greater than 4 to 5 bits. Almost all manufacturers including TEK, LeCroy, and HP, specify a SNR at various input frequencies. By claiming only 30dB of SNR at the maximum input frequency, they reduce the jitter requirements to a point where thay can be met. This is how sampling jitter is represented to the user.

Luckily these errors do not depend on the sample rate. The jitter becomes a problem only if the application requires sampling of a signal with components at 500MHz. If the application only generates frequencies up to 100MHz the jitter is less important. It is the input bandwidth, not the sample rate which determines the S/H requirements.

Interleaved sampling

The problem of sampling at ever faster speeds has spawned an increasing number of schemes for increasing the effective sampling rate of a system. In its simplest form, two sampling units are ganged together, and the appropriate delay is inserted in the signal line connected to one of them. Both units sample at the same time, but a 1/2 sample time delayed version of the signal is presented to the first S/H. If the resulting data is later interleaved, then the resulting waveform has twice as many samples as the original, spaced at 1/2 of the original sampling period.

Unfortunately, these schemes usually make the jitter performance of the system worse, although the systematic portion of the jitter can be removed through later digital processing. DSOs usually perform this trick internally. The TEK TDS 540 contains 4 250MS/sec S/H and A/D units. The DSO allows the user to select certain modes of operation where these units are ganged, but the number of active inputs is reduced. Hence 4 inputs sampled at 250MS/sec can be turned into 1 input sampled at 1GS/sec.

Even on scopes which do not contain internal interleaving capabilities, these capabilities can be added. All that is needed is an appropriate signal distribution scheme. The LeCroy 7242 digitizer uses this trick, the external adapter is called the 7291. Interleaving the two channels of a LeCroy 9400A can be accomplished through

the use of some hard coaxial cable and two 50 Ohm resistors. The amplitude of the input signal is reduced by a factor of 2. All of this is contingent on a good match in input characteristics of the amplifiers, S/H's and A/D converters

Random Interleaved Sampling

If a signal is repetitive, then the interleaving samples do not need to be collected at the same time. The first set of samples can be collected during the sampling of the first transient, while each subsequent interleaved set of samples can be collected during subsequent transients. The trick is to synchronize the sampling with the signal. In practice it is usually impossible to synchronize the signal and the DSO, but it is possible to determine what the time offset between the signal and sample clock was, post mortem. Hence if an interleave value of 8 is desired, then the sample period is divided into eight sections, and the acquired samples are later rearranged into the appropriate "bins". The process is stochastic however, and so more than eight transients would be required. The expected value is 22, but of course more shots may be necessary. If interleaving by a larger amount is desired the number of shots necessary increases much faster.

It would appear that most of the shots are wasted, but this is not the case. Each successive shot can be utilized, since the time value can be stored, and the data later adjusted to reconstruct the waveform quite exactly. In fact it is not necessary to fill every bin. If the largest spacing between two acquired shots is acceptable, then the missing samples can be interpolated, given that enough total samples are actually acquired to produce an acceptable waveform. This reduces the number of random shots necessary, and reduces the number of wasted shots to zero. The waveforms must be digitally processed if equally spaced bins are desired. This is essentially a sample rate conversion, and many algorithms exist to implement this process.

Combining Methods

After the sample rate conversion of the previous section, resolution enhancement can be performed, and after that, traditional signal averaging. The resulting waveform is not limited to the sample rate or resolution of the DSO, but of course a better starting point yields a better finished product. Effective sample rate can be increased by a factor of 20 to 100, effective bits by 5 to 8, though the maximum frequency recovered determines how much of each will actually be attainable. Only the input amplifier bandwidth cannot be overcome so easily. This is the real limiting factor.

It is neither time consuming, nor complex to implement such a procedure, but it does require substantial hardware. No scope manufacturer currently processes interleaved data so thoroughly inside the DSO, primarily because no convenient method for storage of this large number of shots exists. This will change eventually change however, and the additional resolution and accuracy will be welcomed by the TOF community.

Maintaining Signal Integrity

The processing aspects of TOF signal acquisition are the back end of the process. Understanding the front end of the system is just as necessary. Many things can

happen to a perfectly good signal which will reduce its amplitude and add noise. Keeping the gremlins out of the signal path is a demanding but rewarding task. Signal destruction at the front end usually cannot be compensated for later.

Isolating the sensitive signal path from noise carried on metal parts, collected from the air and generated by the power supplies, pumps, and lasers is the first priority. Electrostatic noise can be reduced by shielding. Magnetic noise is more difficult, since it is able to penetrate the stainless steel used to house most TOF analyzers. The detector, feedthrough to atmosphere, and the digitizer should not form ground loops. The detector loop is usually the most sensitive, but the digitizer loop is often larger. Reducing the size of a loop has the beneficial effect of reducing its ability to gather magnetic and electrical noise. By reducing distance between the detector and the DSO, the loop can be made smaller.

Feedthroughs which carry high frequency signals, such as TOF signals need to be of the impedance matched variety, or ringing will result. When a high speed pulse approaches an impedance discontinuity, such as that found at the end of a cable, the energy in the pulse cannot simply traverse the discontinuity at the same amplitude, since this would be akin to generating energy, or instantaneously losing energy. Instead, the energy is divided into a forward component and a reflected component. The forward component is reduced in amplitude, and the reverse component is sent back to the source. Assuming that the source is properly terminated, the absorption of the pulse will not generate another reflection, but it will take some time for the correct voltage to appear at the cable end. When multiple discontinuities are present, the situation quickly degrades, since pulses bounce between the discontinuities many more times before their energy is dissipated. The resulting signal has less amplitude, and more width than the original. It is possible to digitally remove the "noise" generated by the reflections, but much of the amplitude has already been lost, and cannot be regained because it fades into wide short peaks. It is best to properly design the signal path, rather than to attempt to "fix" it later.

Achieving good signal path performance requires attention to detail. Bad as it is for the vacuum system, feedthroughs with connectors on both ends are needed, and they must be 50 Ohm impedance-matched feedthroughs. The SMA variety seem to work better than the BNC or N type, and are much smaller in either case. The signal path inside of the vacuum system should be kept as short as possible, preferably less than one inch. This reduces the size of the ground loop present, and makes it possible to use insulating mounting hardware to eliminate it completely, leaving the detector supported entirely by the feedthrough. The detector should be terminated. Series or parallel termination may be employed, but microscopic chip resistors should be used to minimize inductive effects. Designing the anode for a channel plate detector system is not a trivial task, and is best left to the detector companies. The conical shape of the anode is very precisely machined to maintain a 50 Ohm impedance to the surrounding machined shield. Changing either forms impedance discontinuities, and affects the signal. If the anode is made small enough, then some relaxation of the constraints may be possible, but experimentation is the only way to tell for sure.

It is usually possible to determine how well the system works by looking for random ion hits from a neighboring ion type vacuum gauge, and determine the system's pulse characteristics. The necessary hardware for testing is quite simple. Since most DSOs have BNC inputs, some terminators, and attenuators of the BNC variety would suffice. It is important to use good coaxial cable between the Vacuum

system and the DSO and to keep it as short as possible. This not only minimizes ground loops, but also keeps the pulse spreading which occurs in all cables (terminated or not) down to a minimum. It is very difficult to compensate for the pulse spreading later, because the amplitude changes linearly with frequency, not log frequency as in most filters. Hard coaxial cable should be used in the final version of an instrument, since it has much better impedance and frequency characteristics, and lower losses.

The 50 Ohm inputs to most DSOs are not exactly 50 Ohms and are not usually completely resistive. The TEK TDS 540 seems to have the largest deviation from 50 Ohms, or at least the most noticable. The addition of a 20dB attenuator at the input reduces reflections, and improves signal quality substantially. Other scopes may have similar problems. Usually use of an attenuator is possible, although it does reduce signal intensity. Otherwise, a matching network should be designed, and after that, the instrument must not be disturbed. Designing this matching network requires a Network Analyzer, and very careful construction techniques must be employed. Luckily this needs to be done only once.

Input protection is another important issue. An attenuator will usually provide good input protection for a DSO, but reduces the signal amplitude. Surge absorbers exist for may kinds of systems, but their effects on high frequency signals are undesirable. Perhaps some network matching is in order? If there is one non ideal component in a system, then why not add a few more and compensate the whole mess later, at the same time. A neon lamp (just like the one on your power strip, but without the resistor) will make a fine surge protector if the scope input can take 100 volt surges.

Coupling a signal from a high DC voltage is a vexing problem. Straight capacitive coupling has been employed with some success, but at the expense of regular repairs to the input amplifiers on the DSO. It seems that the voltage normally present on the plate has a tendency to discharge, dumping the capacitor's stored charge into the DSO input. Lasers seem to trigger the effect, and hence the problem. Perhaps some form of optical shielding is in order, although the shiny stainless steel parts of a TOF analyzer would make this impractical. There is no good way to couple such a system. Every approach has its drawbacks.

Triggering

Trigger signals are just as important for averaging as is the input signal. The stability of the trigger is vital to the accurate acquisition of an averaged or interleaved spectrum. The SYNC outputs of most lasers are insufficiently precise, and have much too high a jitter for this application. A fast photo diode viewing split portion of the beam of the laser is the only way to ensure trigger signal consistency. The trigger point is also important. It should be 3/4 of the way up the output pulse. There should be no electrical coupling between the laser and the photo diode. It is best to route the beam away from the laser, and to keep the laser away from the instrument, DSO, detector and photo diode, since the magnetic pulse from the laser will introduce ringing and transients, and will affect the trigger pulse if this is not done.

Digitizer Tradeoffs

Choosing the appropriate digitizer is not an easy task. In some sense the target is constantly moving, as new DSOs become available, and old ones decline in price. Not surprisingly, there has been a lot of "black magic" in digitizer selection. Generally speaking higher sample rates have been the biggest attraction, but input bandwidth has also been valued highly. No amount of signal processing can recover lost input bandwidth. There is also no substitute for deep memories. This was a bit of a problem in the early days of DSOs, when memories were limited. Now however it is difficult to find a scope with less than 32K of memory, and additional memory is usually available. Desktop digitizers with 1Meg of sample memory are available (the LeCroy 7242B-L1, and others) and the next raft of digitizers to be introduced will probably have even more memory. How then does one decide which digitizer to purchase, and how much memory to have?

The first step is to determine the time resolution and flight time of the instrument. This is best done mathematically, although it is possible to simply connect the instrument up, and use Random Interleaved Sampling on a particularly small compound to determine the pulse width. The necessary analog bandwidth is related to the pulse rise time as follows:

$$BW_{Min} = 0.35 \frac{1}{2\pi T_R} \tag{15}$$

The minimum sample rate should be $Sample\ Rate_{Min} = 2BW_{Min}$ and the DSO should have at least 40dB of SNR at the BW_{Min} chosen in the previous step. The memory required is $MEM = Sample\ Rate_{DSO} * FlightTime_{Max}$. The sample rate is the first parameter which should be considered for improvement, assuming that the others can be met at the higher sample rate. This reduces the requirements placed on the input filter, and allows resolution enhancement to be performed. Higher sample rate never hurts, because the time base can always be increased, or samples can be discarded.

On the other hand excess bandwidth will necessitate the addition of an antialiasing filter to the system, and usually will increase the sampled noise. Note that these are single shot specifications. Interleaved sampling is not acceptable for meeting these criteria, because the system will lose too much of the input signal. Interleaving may be used once these specifications are met, but care must be taken in the processing of the data, to keep pulse spreading down to a minimum.

Conclusions

This section has focused on the complete digitzation system, from the detector onward. Signal processing allows the mass spectroscopist the luxury of time. A signal can be modified after it is produced, to enhance, purify and improve it. No amount of signal processing however can compensate for lost information, and hence it is always preferable to create more data rather than less. The data handling aspect of these procedures is currently the biggest problem. Techniques exist for extracting

the last little bit of information from a signal, but they require too much memory and processing in real life.

The material here has been of an introductory nature. The reader is encouraged to consult texts on signal processing, which will better explain the development of such techniques, as well as provide proofs of all of these equations in excruciating detail. Furthermore, some liberty has been taken with these equations, limiting them to first order effects. More accurate results can be obtained, and explanations of many algorithms can be found in signal processing texts. Most such texts have the added side effect of curing most forms of insomnia.

In conclusion I leave you with the three requirements for good data acquisition.

- 1. More signal.
- More signal.
- More signal.

Suggested Reading

A reader interested in signal processing should look into the following two texts for additional information regarding analog, digital and discrete time signals. Both of these texts contain extensive bibliographies, organized by subject. Many of these books are much too advanced for MS applications, but selected chapters may be of intrest.

Oppenheim, Alan Victor, and Willsky, Alan S. Signals and Systems. Englewood Cliffs, N. J.: Prentice-Hall, 1983.

Oppenheim, Alan Victor, and Schafer, Ronald W. Digital Signal Processing. Englewood Cliffs, N. J.: Prentice-Hall, 1975.

A reader interested in amplifiers, noise, basic analog circuit sections, and basic filters will find the following text quite enlightning. It is also not that bad to read, and contains lots of diagrams, pictures and graphs to keep things lucid. It even covers A/D and D/A converters.

Kennedy, E. J. Operational Amplifier Circuits, Theory and Applications. New York, N.Y. Holt Rinehart and Winston, 1988.

Analog filters and digital filters often share many characteristics. A good text on analog filters is:

Van Valkenburg, M. E. Analog Filter Design. New York, N.Y. Holt Rinehart and Winston, 1982.

RECEIVED October 12, 1993

Chapter 11

Protein Processing in Herpes Viruses

Amina S. Woods, Wade Gibson, and Robert J. Cotter

Middle Atlantic Mass Spectrometry Facility, The Johns Hopkins University School of Medicine, Baltimore, MD 21205

The gene encoding cytomegalovirus assembly protein (AP) has been cloned, sequenced and found to be organized within a nested set of four in-frame, 3'-coterminal genes. These genes code for a precursor of the enzyme (assemblin) 64 kDa, a pre-45 kDa protein 46 kDa, a preassembly protein 34 kDa, and a 27 kDa protein. A new approach to protein sequencing that combines enzymatic and chemical digestion with high sensitivity molecular weight measurements by mass spectrometry was developed. In particular it involved mass-mapping of unfractionated enzymatic digests using plasma desorption mass spectrometery (PDMS), purification of peptides, transfer of peptides to the mass spectrometer using blotting techniques, and mass analysis following in situ digestion with carboxypeptidases to reveal amino acid sequence, post translational modifications and/or cleavage sites. This approach is a 100 fold more sensitive than those which rely upon fragmentation in tandem mass spectrometers, and enables the analysis of proteins available in very small quantities (10 to 50 picomoles). PDMS was used to determine the exact cleavage site of the pre-assembly protein. C-terminal peptide fragments were generated by Endoproteinase-Lys C and Endoproteinase-Glu C. A nitrocellulose coated sample foil was used for on foil digestion of the carboxy terminal fragment of the AP with carboxypeptidase. identification of alanine 277 as the carboxy terminal amino acid of the mature AP enabled the recognition of a consensus proteinase cleavage sequence of $V/L-X-A^{\dagger}-S/V$ at the carboxylic end of all herpes viruses AP homologs. This finding also predicts that the mature enzyme is generated by cleavage at YVKA⁺S. In addition PDMS was used to determine phosphorylation sites on the AP. Our results suggest a single site at S_{144} . The sequence RS₁₄GALKRRR is a concensus sequence for cellular protein kinase C. AP from other herpes viruses also have a consensus sequence that could be phosphorylated by protein kinase C. This area is conserved in all Herpes viruses, strongly suggesting that phosphorylation of the AP might play a role in its function.

> 0097-6156/94/0549-0194\$06.00/0 © 1994 American Chemical Society

Importance of CMV. Cytomegalovirus (CMV) is one of the seven herpesgroup viruses known to be indigenous in the human population. Its recurrence from latency appears to be potentiated by a weakened immune system and with the rising number of immunocompromised patients, CMV has become an increasingly significant pathogen. There is a great need to develop new antivirals to CMV and to the other herpes group viruses because of resistance to the currently available drugs.

Role of the AP and Organization of the Gene that Encodes the AP. The AP, a herpesvirus group-common species, is regarded as a potential target. The AP appears to be involved in capsid assembly and maturation (1) as well as DNA Packaging (2), and its correct processing appears to be essential for the production of infectious virions (3). The AP is derived from a precursor by cleavage of its carboxyl terminal end (4), and is not found in the mature virion. The gene encoding the AP has been cloned, sequenced and found to be organized within a nested set of four in-frame, 3'coterminal genes. These genes code for a precursor of the enzyme assemblin, the proteinase responsible for the maturational cleavage of the AP precursor, a pre-45 kDa protein, a pre assembly protein and a 27 kDa protein (5). The cloned assemblin and assembly protein genes have been used in transfection assays. The enzyme gene encodes a 590 amino acid, the N-terminal half of which is the mature enzyme (6,7). The pre AP gene encodes a 310 amino acid protein. These residues are the same as the last 310-amino acid residues of the enzyme precursor. The enzyme precursor has to cleave itself at two sites before the enzyme matures and can process the AP precursor. The first site is the same as the maturational site for the AP. The second cleavage site is the enzyme maturational site (7). The same genetic organization is found in the proteinase/assembly protein coding region of other herpesviruses (7).

Focus of the Work. We determined the cleavage site $(VNA\downarrow S)$ at the carboxyl end of the assembly protein precursor (PAP) by using plasma desorption mass spectrometry (PDMS). Both the proteinase and its consensus cleavage site $(V/L-X-A\downarrow S)$, where X=D, E, E, E or E0 in the PAP are conserved in the other herpesviruses (7).

The AP is also distinguished from the other capsid proteins as being the only one that is phosphorylated (8). Considering the possibility that this modification may also be of functional importance, it was of interest to identify the site(s) involved and determine the nature of the modification. We have used PDMS to investigate these questions, and we show that the CMV AP is phosphorylated at a single serine residue near its midpoint. The amino acid sequence of the AP has been deduced from its nucleotide sequence (Fig. 1)

Mass Spectrometric Strategy. The recent advances in mass spectrometry have resulted in a new way of looking and approaching protein structural problems. This new approach can be used by itself or as a complement to Edman degradation and DNA sequencing.

Until recently there were two ways to approach protein structural problems. If enough of the protein was available, it was sequenced by Edman degradation and in cases where getting enough of the protein was practically not possible, isolating and sequencing of the gene encoding the protein of interest was the other alternative.

MSHPMSAVATPAASTVAPSQAPLALAHDGVYLPKDAFFSLIGASRPLAEAAGARAAYPAVPPPPAYPVMNYEDPSSRHFD	20 30 40 50 60 70 80	* ** ** ** ** ** ** ** ** ** ** ** ** *	EDMSFPGEADHGKARKRLKAHHGRUNNNSGSDAKGDRYDDIREALQELKREMLAVRQIAPRALLAPAQLATFVASPTTTT	SHQAEASEPQASTAAAASPSTASSHGSKSAERGVVNASCRVAPPLEAVNPPKDMVDLNRRLFVAALNKWEZ
ASTVAPSQAPI	 20	VPPLPPPVMF 100	КАККЕГКАННG 	raaaspstas 260
MSHPMSAVATPA	10	YSAWLRRPAYDA 	EDMSFPGEADHG 170	SHQAEASEPQAST

Figure 1. Amino acid sequence of the pre-assembly protein.

Time of flight mass spectrometry (TOF) is a technique which is highly sensitive and requires a picomolar amount of sample to study maturation and post translational modifications of proteins. The following is a general strategy that could be applied to a variety of proteins.

- 1. The molecular weight (MW) of the protein should be obtained using Matrix assisted laser Desorption (MALD) to verify if the MW obtained by gel electrophoresis (SDS-PAGE) is close to the MW deduced from the DNA sequence, or if any post translational modifications are present. If the protein is glycosylated or if glycosylation is a possibility, a spectrum of the protein could be acquired then the protein is deglycosilated and another spectrum acquired.
- 2. Reduction. To find out if the protein is made of one or more chains, the protein is reduced with dithiothreotol, then a spectrum is acquired.
- 3. Digestion. For large peptides CNBr digests and for small ones enzymatic digest using trypsin or any one of a number of endoproteinases to generate peptides. A mass spectrometric peptide map of the digest could be studied, then the peptides could be separated by HPLC allowing the isolation of each peptide. Mass spectra of these peptides makes it easier and more likely to detect and study post translational modifications as well as maturational sites.

We used a combination of enzymatic and chemical reactions, RP HPLC and mass spectrometry to forge new strategies that allowed the location of the carboxyterminus of the AP as well as the confirmation of the sequence and determination of the postranslational modifications of the AP.

Mapping

Cleavage site. The mature AP is processed by C-terminal cleavage from a slightly larger precursor (40kDa) the pre-assembly protein (PAP) (Fig. 1) (4). The site of cleavage of the PAP is unknown and until now conventional methodology has failed to isolate and sequence the carboxyterminus of the assembly protein. Identification of the cleavage site is of importance. The knowledge of the amino acid at the cleavage site could indirectly help to determine the type of protease acting at that cleavage site.

CMV strain Colburn was grown in human foreskin fibroblasts (3). Infected cells were separated into nuclear and cytoplasmic fractions and B-capsids were recovered from the nuclear fraction of infected cells as previously described (3). Bcapsids were disrupted in 8M guanidine and 10 % \beta-mercaptoethanol with heating at 45° for 5 min, and proteins were separated by RP HPLC. A C₄ column was used, and the flow rate was 1 ml/min. The column was equilibrated with 0.1% trifluoroacetic acid (TFA) in water (buffer A) for 5 min. A gradient using 0.1% TFA in 80% acetonitrile (buffer B) was increased linearly from 0 to 60 % B in 30 minutes. Fractions were collected, an aliquot of each fraction was dried, resuspended in loading buffer and submitted to SDS-PAGE. The AP eluted at 32.5 min and 48% acetonitrile (Fig. 2a). The fraction containing the assembly protein was lyophilized and the AP was suspended in 100 mM Tris pH 8.5, and digested with Endoproteinase-Lys C (Endo-Lys C) for 24 hr at 37°C. A similar assembly protein preparation was resuspended in 25 mM ammonium bicarbonate pH 7.8 and digested with Endoproteinase-Glu C (Endo-Glu C) for 24 hr at room temperature. All digests were separated by RP HPLC using a flow rate of 0.5 ml/min (Figs 2b and 2c). A C₁₈

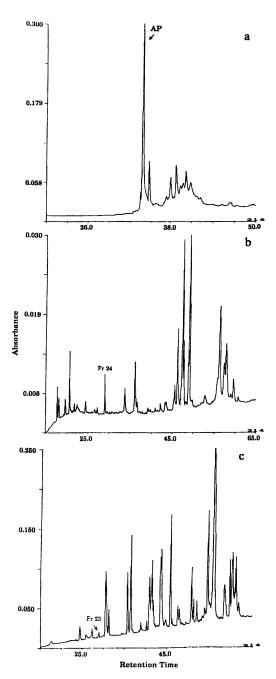


Figure 2. HPLC chromatograms of: (a) B-capsids showing the AP; (b) Peptide map of the Endo-Lys C digest of the AP; and (c) Peptide map of the Endo-Glu C digest of the AP.

column was used to separate the peptides. It was equilibrated in buffer A and a gradient of buffer B was increased linearly from 0 to 70 % B in 75 min, to 100 % B in 5 min, and maintained at 100% for 10 min. The column was equilibrated again for 30 min with buffer A before use (9). Fractions were collected. PD mass spectra of the Endo-Lys C and Endo-Glu C peptides from the AP were utilized to determine the cleavage site of the PAP. The results of that study are summarized in Tables 1 and 2. Although cleavages at lys and glu are expected from these two enzymes, additional cleavages at arg and asp were also observed resulting in 32 possible cleavage sites in the case of Endo-Lys C and 34 in the case of Endo-Glu C. Cleavages were often incomplete, resulting in peptides that contain two or more fragments. In the case of Endo-Glu C cleavage at ala occured if the ala was followed by glu or asp (10) (Fig. 3b). Fr 24 from the Endo-Lys C digest reveals the Cterminus of the AP as ala₂₇₇ (Table 1), and Fr 23 from the endo-Glu C digest reveals the same cleavage site (Table 2). Fr 24 gave a molecular ion (MH+) of 903.3 amu, the calculated MH⁺ for SAERGVVNA is 902.5 amu (Fig 3a). Fr 23 gave a MH⁺ of 616.2 amu, the calculated MH⁺ for RGVVNA is 615.4 amu (Fig. 3b). Both the Endo-Lys C and the Endo-Glu C digests accounted for residues 1 to 277.

Possible phosphorylation site. The AP is also distinguished from the other capsid proteins as being the only one that is phosphorylated (8) and some fragments of both digests were 80 amu larger than the predicted molecular weight (MW), suggesting the presence of a phosphorylated ser, thr or tyr.

The mass spectrum of Fr 28 from the Endo-Lys C digest (Table 1) gave peaks corresponding to the protonated MH⁺ for SGALKR (m/z 632.3), SRSGALK (m/z 717.4) and SGALKRRRER (m/z 1221.0). An additional peak was observed at m/z 799.0 amu that could correspond to the phosphorylated peptide SRSGALK-HPO₃ containing ser residues: S₁₄₂ and S₁₄₄. Fr 41 gave a MH⁺ of (m/z 3291.3) that may correspond to GYAPSAYDHYVNNGSWSRSRSGALKRRR-HPO₃, which contains the same ser residues. The mass spectrum of Fr 37 from the Endo-Glu C digest (Table 2) gave peaks that could correspond to protonated MH⁺ (m/z 3485.2) of peptide HYVNNGSWSRSRSGALKRRERDASSDEE-HPO₃.

Confirmation of the Cleavage Site by On-Foil Carboxypeptidase P Digests.

Fr 24 from the Endo-Lys C digest and Fr 23 from the Endo-Glu C digest were each submitted to direct digestion on the sample foil. The sample foil was covered with 10 ul of carboxypeptidase P (0.4 ug/10 ul) in 25 mM sodium citrate buffer and incubated for 5 minutes. The excess fluid was spun off, and the disc dried. The disc was washed with 30 ul of 0.1 % TFA in water, dried and a spectrum acquired (9). The spectrum of HPLC Fr 24 containing peptide SAERGVVNA shows a significant reduction in peak height at 903.3 amu and the appearance of a new peak at m/z 462.2 amu that was not seen at that site before the digestion. 462.2 amu could be generated by SAERGVVNA - GVVNA (calculated 463.3 amu). The spectrum of HPLC Fr 23, RGVVNA, shows a new peak at m/z 547.6 which could be generated by RGVVNA - A (calculated 545.7), confirming that the last residue on the AP is an ala (Fig. 4). A MH⁺ of 744.5 amu is also seen in Figure 3b it corresponds to the following peptide ERGVVNA glu₂₇₁ in this peptide is preceded by ala₂₇₀. This is one of those rare cases where Endo-Glu C cleaves at an ala (10). We also note that the difference in mass

TABLE 1: Peptide Fragments Observed in the Plasma Desorption Mass Spectra of HPLC Fractions of the Endoproteinase-Lys C Digest of CMV Assembly Protein

Assem	ora Lighter			
HPLC	Peptide	Amino Acid		ular Ion
Frac.	Fragments	Residues	Calculated	Observed
14	18-19-20	ARKR	530.3	530.2
15	22-23	AHHGRDNNNSGSDAK	1579.7	1580.3
15	26-27	EALOELKR	986.6	989.4
15	26	EALOELK	830.5	830.4
15	27-28	REMLAVR	874.5	874.6
15	28-29	EMLAVROIAPR	1283.7	1283.4
16	20-21	RLK	416.3	416.6
16	23	DNNNSGSDAK	1021.4	1018.0
18	17-18-19	DASSDEEEDMSFPGEADHGKARK	2508.0	2503.9
19	28	EMLAVR	717.4	718.5
24	31-32	Saergv <u>vna</u>	902.5	903.3
28	11-12	SRSGALK	718.4	717.4
28 *	11-12-HPO ₃	SRSGALK (HPO ₃)	798.4	<u>799.0</u>
28	12-13	SGALKR	631.4	632.3
28	12-13-14-15-16		1228.0	1221.0
31	26-27-28-29	EALQELKREMLAVRQIAPR	2253.4	2253.7
31	19-20-21-22	KRLKAHHGRDNNNSGSDAKGDRYDDI	4767.5	4764.0
	23-24-25-26	REALQELKREMLAVR		
	27-28		2000 1	0000
41	10-11	GYAPSAYDHYVNNGSWSRSR	2288.1	2290.6
41*	10-11-12-13-	GYAPSAYDHYVNNGSWSRSRS	3291.7	<u>3291.3</u>
42	14-15-HPO ₃	GALKRRR (HPO ₃)	1000 0	1001 3
42 42	24-25-26 ² 25-26-27	GDRYDDIREALQELK	1820.9	1821.3
42 43*		YDDIREALQELKR GYAPSAYDHYVNNGSWSRSRS	1648.9 2823.3	1649.4 2825.7
	10-11-12-HPO ₃	GALK (HPO ₃)		
43	15-16-17	RERDASSDEEEDMSFPGEADHGK	2594.1	2592.2
45*	6-7-8-9-	RRDPMMEEAERAAWERGYAPSAY	4993.4	<u>4995.8</u>
	10-11-12-	DHYVNNGSWSRSRSGALKR (HPO ₃)		
46	13-HPO ₃	EW NUMBER OF THE PROPERTY OF	E777 0	E710 7
46	28-29-30	EMLAVRQIAPRALLAPAQLATPVASP TTTTSHQAEASEPQASTAAAASPSTA SSHGSK	5722.9	5719.7
49	2	DAFFSLIGASRPLAEAAGAR	2020.1	2021.3
52	27-28-29	REMLAVRQIAPR	1441.0	1443.6
53	2-3-4-5-6-7-8-	DAFFSLIGASRPLAEAAGARAAY	12746.3	12741.1
	9-10-11-12	PAVPPPPAYPVMNEDPSSRHFDY		
		SAWLRRPAYDAVPPLPPPPVMPMPY RRRDPMMEEAERAAWERGYAPSAY DHYVNNGSWSRSRSGALKRR		
54	27-28-29	REMLAVROIAPR	1441.0	1441.0
54	19-20-21-22-	KRLKAHHGRDNNNSGSDAKGDRYDDI	3907.1	3909.6
	23-24-25-26	REALQELK		
57	1-2-3	<u>MSH</u> PMSAVATPAASTVAPSQAPLAL	7859.0	7863.8
		AHDGVYLPKDAFFSLIGASRPLAEAA ARAAYPAVPPPPAYPVMNYEDPSSR	G	
57	5-6	RPAYDAVPPLPPPPVMPMPYRR	2517.6	2515.5
57	7-8	RDPMMEEAER	1263.6	1265.2
57	1-2-3-4-5-6	MSHPMSAVATPAASTVAPSQAPLALAH		11539.7
		DGVYLPKDAFFSLIGASRPLAEAAGA AYPAVPPPPAYPVMNYEDPSSRHFDY AWLRRPAYDAVPPLPPPPVMPMPYRR	S	

a Molecular ions are MH unless otherwise indicated.

TABLE 2: Peptide Fragments Observed in the Plasma Desorption Mass Spectra of HPLC Fractions of the Endoproteinase-Glu C Digest of CMV Assembly Protein

Page	Assem	bly Protein			
Frace Fragments Residues Calculated Concepts	HPIC	Peptide	Amino Acid	Moleci	ular Ton
20					
23 34 RGUVNA 615.4 616.3					
23 34 RGVVNA					
24 25-26-27 AKGELERE 986.6 985.8 24 25-26-27 AKGENYDD 939.5 939.5 939.5 939.5 939.5 939.5 939.5 939.5 939.5 939.5 939.5 939.5 939.5 936.6 985.8 26 26-27 RYDD 568.2 568.8 8 28 31-32-33 MLAVRGIAPRALLAPAQLATPVASP 5881.0 5880.8 30 29 ALQE 460.2 460.5 31 32-33-34 ASEPQASTAAAASPSTASSH 2984.5 2985.9 34 24-25-26-27 NINSGSDAKGDRYDD 1627.7 1625.7 36 14 15-16-17- HYVNINGSWSKSGALKRRRE 3485.7 3485.2 37* 14-15-16-17- HYVNINGSWSRSGALKRRE 3485.7 3485.7 3485.2 40 7 YSAWLRPATO 4710.4 4710.4 4710.4 40 8 AVPLIPPPVMPMPYRRD 2186.2 2187.5 41 22-2-32.4 ADHGKARKRLKAHGRDNINSG					
24 25-26-27 AKGDRYDD 939.5 939.9 26 32 ASE 306.1 306.1 306.9 28 31-32-33 MLAVRQIAPRALLAPAQLATPVASP 568.2 568.8 TATSISHGSKSAERGVVNA 30 29 ALQE 460.2 460.5 31 32-33-34 ASEPQASTAAAASPSTASSH 2984.5 2985.9 32 11-12 AERAAME 832.4 833.0 36 14 HYVNNGSWGRSGALKRRRE 2516.3 2517.6 37* 14-15-16-17- HYVNNGSWGRSGALKRRE 3485.7 3485.2 18-HPO3 RDASSDEE (HPO3) 1397.7 1397.6 40 7 YSAMIRPRADI 1397.7 1397.6 40 8 AVPPLPPPPMPMPYRRD 2186.2 2187.5 41 22-23-24 ADHGKARKRIKAHHGRDNNNSGSD 2261.4 2642.3 42 23-24-25 HGKARKRIKAHGRDNNN 2826.5 2822.8 43 6 PSSRHFD 973.5 972.7 44 24 NNNSGSD 707.3 705.6 <t< td=""><td></td><td>34</td><td></td><td></td><td></td></t<>		34			
26 32					
26 26-27 RXDD 568.2 568.8 28 31-32-33 MLAVRQIAPRALLAPAQLATPVASP TTTTSHQAEASEPQASTAAAASPS 5881.0 5880.8 30 29 ALQE 460.2 460.5 31 32-33-34 ASEPQASTAAAASPSTASSH 2984.5 2985.9 GSKSAERGVVNA 32 11-12 AERAAWE 832.4 833.0 34 24-25-26-27 NNNSGSDAKGDRYDD 1627.7 1625.7 37* 14-15-16-17- HYVNNGSWSRSGALKRRRE 2516.3 2517.6 37* 10-11-12-13- EAERAAWERGYAPSAYDHYVN 4710.4 4710.9 40 7 YSAMLRPRAYD 1397.7 1397.6 40 8 AVPPLPPPPPWMPYTRRD 2186.2 2187.5 41 22-23-24 ADHGARRRLKAHGRDNNNSGSD 2641.4 2642.3 42 23-24-25 HGKARKRLKAHGRDNNN 2826.5 2822.8 43 4-5-6 AAGRARATYAPAVPPPPAYPWNYE 3314.6 3314.4 44 24 NNNSGSD 707.3 705.6 44 29-20-21-22 EDMSFFGEAD 1097.5				939.5	939.9
Table Tabl					
TTTTSHOARASEPQASTARAASPS TASSHGKSAERGVVNA 30 29 ALQE					
32-33-34 ASEPQASTAAAASPSTASSH 2984.5 2985.9	28	31-32-33	TTTTSHQAEASEPQASTAAAASPS	5881.0	5880.8
SSKSAERGVVNA S32.4 S33.0	30	29	ALQE	460.2	460.5
34	31	32-33-34		2984.5	2985.9
36 14 HYVNINGSWSRSGALKRRRE 2516.3 2517.6 37* 14-15-16-17- HYVNINGSWSRSGALKRRRE 3485.7 3485.2 18-HPO, 14-15 RDASSDEE (HPO ₃) 4710.4 4710.9 40 7 YSAWLRRPAYD 1397.7 1397.6 41 22-23-24 ADHGKARKRLKAHHGRDNNNSGSD 2641.4 2642.3 42 23-24-25 HGKARKRLKAHHGRDNNN 2826.5 2822.8 43 4-5-6 AAGARAAYPAVPPPPAYPVMNYE 3314.6 3314.4 43 6 PSSRHFD 845.4 846.1 44 24 NNNSGSD 707.3 705.6 44 27-28-29 DIREALQE 973.5 972.7 44 19-20-21-22 EDMSFPGEAD 1097.5 1095.0 46 19-20-21-22 EDMSFPGEAD 1779.0 1784.0 28-29 DMSFPGEADHGKARKRLKAHHGRD 2716.4 2717.7 46 20-21-22-23 DMSFPGEADHGKARKRLKAHHGRD 2716.4 2717.7 47 1 MSHPMSAVATPAASTVAPSQAPLALAHD 2729.2 48 4-5-6-7 AAGARAAYPAVPPPPAYPVMN 6358.1 6359.0 54* 11-12-13-14- 15-16-17-18- 29-20-21-22- AAGARAYPAVPPPAYPVMN	32		AERAAWE	832.4	833.0
37* 14-15-16-17-	34	24-25-26-27	NNNSGSDAKGDRYDD		
18-HPQ			HYVNNGSWSRSGALKRRRE		
14-15	37*	14-15-16-17- 18-HPO		3485.7	<u>3485.2</u>
40 7 YSAWIRRPAYD 1397.7 1397.6 40 8 AVPPLPPPPVMPMPYRRD 2186.2 2187.5 41 22-23-24 ADHGKARKILKAHHGRDNNNSGSD 2641.4 2642.3 42 23-24-25 HGKARKILKAHHGRDNNN 2826.5 2822.8 SGSDAKGD 43 4-5-6 AAGARAAYPAVPPPPAYPVMNYE 3314.6 3314.4 49 DPSSRHFD 845.4 846.1 44 24 NNNSGSD 707.3 705.6 44 27-28-29 DIREALQE 973.5 972.7 44 19-20-21-22 EDMSFPGEAD 1097.5 1095.0 44 25-26-27- AKGPYDDIREALQE 1779.0 1784.0 28-29 14-15-16-17 HYVNNGSWSRSGALKRRER 3276.7 3280.3 46 20-21-22-23 DMSFPGEADHGKARKIKAHHGRD 2716.4 2717.7 47 1 MSHPMSAVATPAASTVAP SQAPLALAHD 2729.3 2729.2 48 4-5-6-7 AAGARAAYPAVPPPPAYPVMN 4693.3 4692.2 YEDPSSRHFDYSAWLRRPAYD 4693.3 4692.2	37			4710.4	4710.9
40 8 AVPPLPPPPVMPMPYRRRD 2186.2 2187.5 41 22-23-24 ADHGKARKRIKAHHGRDNNN 2641.4 2642.3 42 23-24-25 HGKARKRIKAHHGRDNNN 2826.5 2822.8 43 4-5-6 AAGARAAYPAVPPPPAYPVMNYE 3314.6 3314.4 43 6 PSSRHFD 845.4 846.1 44 24 NNNSGSD 707.3 705.6 44 27-28-29 DIREALQE 973.5 972.7 44 19-20-21-22 EDMSFPGEAD 1097.5 1095.0 44 25-26-27- AKGDRYDDIREALQE 1779.0 1784.0 28-29 HYVNNGSWSRSGALKRRER 3276.7 3280.3 46 20-21-22-23 DMSFPGEADHGKARKRLKAHHGRD 2716.4 2717.7 47 1 MSHPMSAVATPAASTVAPSQAPLALAHD 2729.3 2729.2 48 4-5-6-7 AAGARAAYPAVPPPPAYPUMN 4693.3 4692.2 49 14-15-16 HYVNNGSWSRSGALKRRERDASSD 3147.6 3150.7 54* 11-12-13-14- AERAAWERGYAPSAYDHYVNN 6358.1 6359.0	40			1397.7	1397.6
### 22-23-24 ADHGKARKRLKAHHGRDNNNSGSD 2641.4 2642.3 ### 23-24-25 HGKARKRLKAHHGRDNNN 2826.5 2822.8 ### SGSDAKGD					
A2 23-24-25 HGKARKILKAHHGRDININ SGSDAKGD		_			2642.3
DPSSRHFD 43 6	42			2826.5	2822.8
43 6 PSSRHFD 845.4 846.1 44 24 NNNSGSD 707.3 705.6 44 27-28-29 DIREALQE 973.5 972.7 44 19-20-21-22 EDMSFPGEAD 1097.5 1095.0 44 25-26-27- AKGDRYDDIREALQE 1779.0 1784.0 28-29 46 14-15-16-17 HYVNNGSWSRSGALKRRER 3276.7 3280.3 DASSDE DMSFPGEADHGKARKRLKAHHGRD 2716.4 2717.7 47 1 MSHPMSAVATPAASTVAPSQAPLALAHD 2729.3 2729.2 48 4-5-6-7 AAGARAAYPAVPPPPAYPVMN 4693.3 4692.2 YEDPSSRHFDYSAWLRRPAYD 4693.3 4692.2 YEDPSSRHFDYSAWLRRPAYD 3147.6 3150.7 54* 11-12-13-14- AERAAWERGYAPSAYDHYVNN 6358.1 6359.0 15-16-17-18- GSWSRSRGALKRRERDAS 29-20-21-22- SDEEEDMSPGEAD (HPO ₃) HPO ₃ 55 11-12-13-14- AERAAWERGYAPSAYDHYVNN 6278.1 6274.6 15-16-17-18- GSWSRSRSGALKRRERDASSD 19-20-21-22 EEEDMSPGEAD 56 2-3 GVYLPDAFFSLIGASRPLAE 2251.2 2251.1 57 6-7-8-9 PSSRHFDYSAWLRRPAYDAVPPLP 58 7-8-9-10 YSAWLRRPAYDAVPPLPPPVMPM 4182.1 4177.9	43	4-5-6		3314.6	3314.4
44 27-28-29 DIREALQE 973.5 972.7 44 19-20-21-22 EDMSFPGEAD 1097.5 1095.0 44 25-26-27- AKGDRYDDIREALQE 1779.0 1784.0 28-29 46 14-15-16-17 HYVNNGSWSRSGALKRRER 3276.7 3280.3 46 20-21-22-23 DMSFPGEADHGKARKRLKAHHGRD 2716.4 2717.7 47 1 MSHPMSAVATPAASTVAPSQAPLALAHD 2729.3 2729.2 48 4-5-6-7 AAGARAAYPAVPPPPAYPWN 4693.3 4692.2 YEDPSSRHFDYSAWLRRPAYD 4693.3 4692.2 YEDPSSRHFDYSAWLRRPAYD 3147.6 3150.7 54* 11-12-13-14- AERAAWERGYAPSAYDHYVNN 6358.1 6359.0 55 11-12-13-14- GSWSRSRSGALKRRERDAS 3 6274.6 15-16-17-18- GSWSRSRSGALKRRERDASSD 6278.1 6274.6 19-20-21-22- SDEEEDMSPGEAD 6278.1 6274.6 56 2-3 GVYLPDAFFSLIGASRPLAE 2251.2 2251.1 57 6-7-8-9 PSSRHFDYSAWLRRPAYDAVPPLP 4879.5 4877.1					

a Molecular ions are MH unless otherwise indicated.

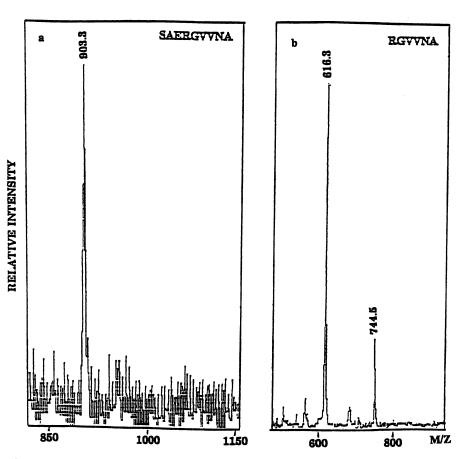


Figure 3. Mass spectra of the carboxy terminus of the AP: (a) Mass spectrum of HPLC Fr 24 obtained from the Endo-Lys C digest of the AP; and (b) Mass spectrum of HPLC Fr 23 obtained from the Endo-Glu C digest of the AP.

between m/z 616.3 and 744.5 corresponds to a glu. Figure 4 shows a peak at m/z 673.6 which corresponds to ERGVVN. The peak at 744.5 (ERGVVNA) that was seen in Figure 3b has disapeared. The difference between 744.5 and 673.6 amu is 70.9 amu which again corresponds to an ala.

Determination of the Phosphorylation Site Using 32P-Labeled Assembly Protein.

The observations of possible phosphorylation sites motivated additional experiments to determine whether such residues were phosphorylated, and whether additional phosphorylation sites were present. We added [32P]-orthophosphate (200 µci/ml of complete medium) to the CMV infected cultures two days before recovering the B-capsids. The labeled AP was isolated and digested with Endo-Lys C and endo-Glu C following the same protocol used in the above experiments.

Endoproteinase-Lys C digest. The resulting peptide fragments were separated by HPLC, and fractions were collected and counted for radioactivity. In the Endo-lys C digest Fr 28, 32 and 43 had 1947, 5292 and 197 CPM, respectively, while the rest of the Fr showed no radioactivity. PDMS spectra of these 3 Fr were obtained (Fig. 5 a,b,c, and Table 3). The peak observed at m/z 554.7 in the mass spectrum of Fr 28 (Fig. 5a) corresponds to the mass of the phosphorylated pentapeptide, SGALK-HPO₁, while the peaks at m/z 719.1 and 798.2 correspond to the unphosphorylated and phosphorylated heptapeptides, SRSGALK and SRSGALK-HPO₁, respectively. These same peaks are observed in the mass spectrum of Fr 32 (Fig. 5b), as well as peaks at m/z 475.1 and 954.7 corresponding to the unphosphorylated pentapeptide, SGALK, and an additional phosphorylated peptide, SRSGALKR-HPO, respectively. The mass spectrum of Fr 43 (Fig. 5c) reveals a single major peptide peak at m/z 3293.9, whose mass corresponds to that of a larger phosphorylated peptide that contains the region of the peptides observed in fractions 28 and 32. These results suggest that S_{144} is the site of phosphorylation, although S_{142} cannot be ruled out as an alternative phosphorylation site. Because PDMS is a very sensitive technique that detects as little as one picomole of a peptide most of the peptides detected were seen with a different intensity in as much as three to five fractions preceding and following the fraction where the peptide was most prominent. The multitude of peptides containing the phosphorylated site of the AP is due to the cleavage of the following: R₁₄₀SRSGALKRRERDASSDEEED₁₆₂ contains six arg and one lys, four glu and three asp, resulting in seven possible sites to be cleaved by each of the endoproteinase used.

Endoproteinase-Glu C digest followed by digestion of labeled fractions with Trypsin. The HPLC chromatogram for the Endo-Glu C digest of the AP produced three peaks with radioactivity, corresponding to Fr 31/32 (972 and 302 CPM), Fr 33/34 (931 and 236 CPM) and Fr 35/36/37 (611, 274 and 189 CPM). The next step was to find out if any of these fractions contained fragments that had residues S_{142} or S_{144} in their sequence. By looking at the AP sequence one can see that the shortest peptide that could be generated by the Endo-Glu C digest and that contained the possible phosphorylation site is $H_{132}YVNNGSWSRSGALKRRRE_{152}$ (this peptide contains 6 arg and one lys that could be cleaved by trypsin). However the phosphorylated peptides seen in Table 2 are both larger and contain several other ser

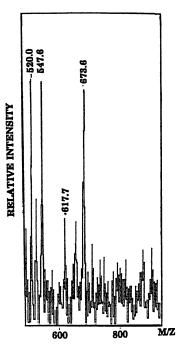


Figure 4. Mass spectrum of the on-foil digest of Fr 23.

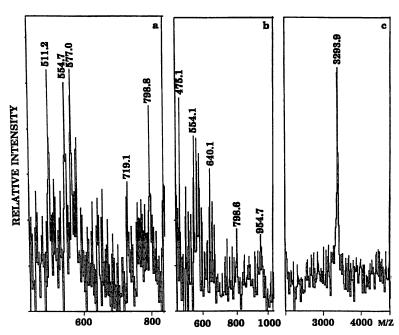


Figure 5. Mass spectra of the radioactive HPLC fractions of the Endo-Lys C digest of ³²P-labeled CMV AP: (a) Fr 28; (b) Fr 32; and (c) Fr 43.

In Time-of-Flight Mass Spectrometry; Cotter, R.; ACS Symposium Series; American Chemical Society: Washington, DC, 1993.

and thr. To find out if we could generate the SGALK-HPO₃ and the SRSGALK-HPO₃ peptides found in the Endo-Lys C digest fractions, a trypsin digest of the radio active fractions was done.

The fractions forming each peak were pooled dried, redissolved in 100 mM Tris pH 8.5 and digested with trypsin for 24 hours at 37°C. Phosphorylated peptides dissolved in Tris gave better spectra than the same peptides dissolved in 0.1% acqueous TFA. The mass spectrum for the tryptic digest of Fr 31/32 is shown in figure 6. In the low mass portion of the spectrum (Fig. 6a), the peaks include some of those observed in the mass spectra of the Endo-Lys C fractions. These include the MH⁺ and MNa⁺ ions for the phosphorylated pentapeptide, SGALK-HPO₃, at m/z 555.4 and 577.8, respectively, and the MH⁺ and (M+2Na-H)⁺ ions for phosphorylated peptides SGALKR-HPO, (at m/z 711.4 and 756) and SRSGALKR-HPO, (at m/z 799.4 and 844.0), respectively. In addition, the MH⁺ and MNa⁺ ions for a larger phosphorylated peptide, SGALKRRR-HPO₃, at m/z 1024.6 and 1047.1, respectively, are also observed, as well as an additional peptide, MSFPGE, at m/z 665.6, which is not phosphorylated. The high mass portion of the spectrum of Fr 31/32 (Figure 6b) reveals 3 larger peptides at m/z 2597.0, 4594.5 and 4950.4. The MH⁺ at m/z 2287.3 amu is seen in the trypsin blank digest. The measured masses correspond to protonated MH $^+$ of phosphorylated peptides containing the S_{142} and S_{144} residues. These 3 peptides all contain glu as the C-terminal residue, reflecting incomplete tryptic digestion of Endo-Glu C peptides. Two of these peptides were also observed in Fr 33/34 and 35/36/37. From the above results as well as some unpublished data we found that phosphorylated peptides dissolved in 100 mM Tris gave better spectra then the same peptides dissolved in 0.1% TFA in water.

Identification of Phosphoserine with Ethanethiol

B-capsids were harvested and treated with ethanethiol (11). Ethanethiol in the presence of NaOH specifically converts phosphoserine (MW=167 amu) to S-ethylcystein (MW=132 amu) by a β-elimination of the phosphate group on the phosphoserine followed by a Micheal addition of the ethanethiol, resulting in a loss of 35 amu. The AP was separated using RP HPLC, yielding two unresolved peaks, at 32.2 and 32.8 min, that probably represents a mixture of underivatized and derivatized AP (Fig. 7). These fractions were pooled, dried, resuspend in 100 mM Tris and digested with Endoproteinase-Lys C for 24 hours at 37°C and the resulting fragments separated by RP HPLC, and analyzed by PDMS. Phosphoserine is more hydrophilic than N-ethylcysteine. The AP with a phosphoserine is more hydrophilic than the derivatized AP that contains an N-ethylcysteine.

The mass spectra of fractions 28 and 29 are shown in Fig. 8 a and b, respectively. In addition to the phosphorylated peptides containing S_{144} , peaks observed at m/z 520.9, 988.8 and 1517.0 correspond to peptides carrying an S-ethylcysteine

Discussion

Determination of the Carboxyterminus of the Assembly Protein. The amino acid sequence of the PAP has been deduced from its nucleotide sequence (12). The amino terminus was determined by chemical digests and probing with antisera (13); and was

TABLE 3: Peptide Fragments Observed in the Plasma Desorption Mass Spectra of Radioactive HPLC Fractions of the Endoproteinase-Lys C Digest of P-labeled CMV Assembly Protein from Fig. 4

HPLC	Peptide	Peptide	Molecular ions	
Fraction		Fragment	Calculated	Observed
28	SGALK (HPO_)	424-428	555.2	554.7
	SGALK (HPO ₃) SRSGALK (HPO ₃)	422-428	798.4	798.8
32	SGALK	424-428	475.2	475.1
	SGALK (HPO ₂)	424-428	555.2	554.1
	SRSGALK (HPO ₃)	422-428	798.4	798.6
	SRSGALKR (HPÖ ₂)	422-429	954.1	954.7
43	GYAPSAYDHYVNNGSWSR SGALKRRRER (HPO ₃)	404-433	3291.7	3293.9

a. Molecular ions are MH unless otherwise indicated.

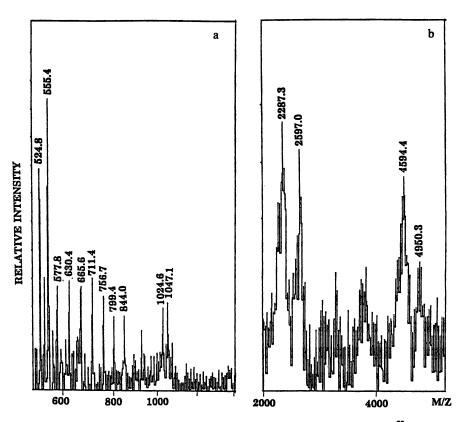


Figure 6. Mass spectra of HPLC Fr 31/32 of the Endo-Glu C digest of ³²P-labeled CMV AP following digestion with trypsin: (a) low mass region; and (b) high mass region.

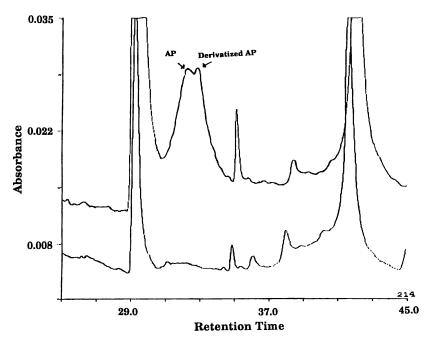


Figure 7. HPLC chromatogram of the separation of the AP after treatment of B-capsids with ethanethiol.

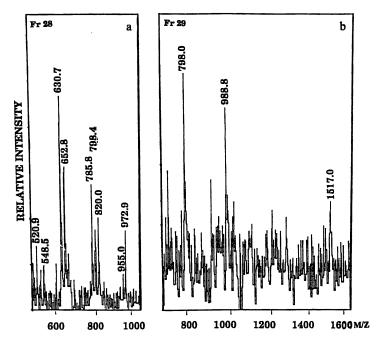


Figure 8. Mass spectra of HPLC fractions (a) 28 and (b) 29 of the Endo-Lys C digest of ethanethiol-treated CMV AP.

In Time-of-Flight Mass Spectrometry; Cotter, R.; ACS Symposium Series; American Chemical Society: Washington, DC, 1993.

also seen in fragments generated by the Endoproteinases digests (Table 1 and 2). The carboxy terminus however had escaped localization. We do know from previous work (4) that the one cysteine in the deduced sequence (residue 279) of the PAP is not part of the mature AP. In our current approach, the AP was isolated, purified, and enzymatically digested. The resulting peptides were isolated by RP HPLC and their MW determined by PDMS and compared with the MW calculated from the DNA sequence in order to verify the primary sequence of the AP and locate the carboxy terminal fragment.

Cleavage of the PAP by assemblin generates the mature AP. Endo-Lys C and Endo-Glu C were utilized. Cleavage at C-terminal end of lys268 could be expected to give the peptide SAERGVVNAS (m/z 989.5), SAERGVVNA (m/z 902.5), or SAERGVVN (m/z 831.5) etc., while cleavage at glu271 would give the peptide RGVVNAS (m/z 702.4), RGVVNA (m/z 615.4), or RGVVN (m/z 544.4) etc., depending on where the viral protease assemblin cleaved the PAP. Table 1 shows the peptides that were obtained from the enzymatic digests and compares these MH⁺ to the expected MH⁺ calculated from the deduced amino acid sequence. The Endo-Lys C digest fragments accounted for every residue from residue 1 to 277. Fr 24 gave a MH⁺ of m/z 903.3, while the calculated MH⁺ for SAERGVVNA is m/z 902.5 (Fig. 3a). The Endo-Glu C digest accounted for every predicted fragment that would result from the AP digest. Fr 23 gave a MH⁺ of m/z 616.2, while the calculated MH⁺ for RGVVNA is m/z 615.4 (Fig. 3b). These results suggest that ala277 is the last residue in the amino acid sequence.

On-foil digests with carboxypeptidase P verified that ala₂₇₇ is the terminal amino acid residue of the mature AP.

The proteinase (assemblin) has been characterized by Welch (7) using the cloned enzyme and substrate (AP) genes in transient transfection assays. The enzyme precursor (64kDa, 590 amino acid residues) is encoded by the whole open reading frame, that gives rise to a 64kDa protein, while the mature enzyme is generated by self-cleavage of the precursor at ala_{249} . The activated enzyme then proceeds to cleave the PAP (34kDa, 310 amino acid residues) that is encoded by the 3'-terminal half of the open reading frame at ala_{277} , generating the mature AP. Because the enzyme cleaves itself, determination of the cleavage site of the AP as ala_{277} allowed the recognition of a consensus proteinase cleavage sequence of $\underline{V}/L-X-A^{\perp}-\underline{S}/V$ at the carboxylic end of all herpes viruses assembly protein homologs. This finding also predicts that the mature enzyme is generated by cleavage at $\underline{YVKA^{\perp}S}$ that is also highly conserved in Herpes viruses.

Concensus Sequence. Protein kinase C-like enzymes phosphorylate basic sites, while casein kinase I and II type enzymes phosphorylate acidic sites (Table 4). The above work showed that the assembly protein is phosphorylated, identified the serine residue that is phosphorylated, but did not give a ratio of the phosphorylated to non phosphorylated AP.

Phosphorylation of proteins often plays an important role in the activation and regulation of cellular function. Phosphorylation/dephosphorylation usually works as an on/off switch. Phosphorylated proteins as well as the enzymes that phosphorylate them have been extensively studied. Protein kinases often phosphorylate more than one site on the same protein, and act on more than one substrate. In the past thirty years the observations of several researchers (14) implied that these enzymes

recognize the primary structure surrounding the S/T residue that is phosphorylated. They concluded that sites phosphorylated by a given kinase have a common set of amino acid residues, the "consensus sequence", whose presence is needed for recognition by the phosphorylating enzyme. Kennelly and Krebs emphasized that secondary and tertiary structures do play a role in substrate recognition, and that most phosphorylation sites are in that part of the sequence located at or near the surface of the folded protein, or within β -turns (14). The DNA sequence encoding the AP of the various herpes viruses is part of a large open reading frame. The sequence information shows possible phosphorylation site for the AP of various herpes group viruses at aproximately the same site where the CMV Colburn AP is phosphorylated. In all cases there is only one basic phosphorylation site. These findings strongly suggest that phosphorylation and dephosphorylation of the AP might play a role in its function or processing.

Kishimoto et al (15) and Woodget et al (16) have shown that phosphorylation of proteins at serine or threonine by protein kinase C is favored whenever the target T/S has a basic residue such as arg or lys at the amino terminus of T/S, and one or more residues after the carboxy terminus, i.e. the sequence R/K-S/T-X-R/K, where X is 0 to 2 uncharged residues (Table 10), (24). They also showed that additional basic residues at both the amino and carboxy sides of the target amino acid enhanced the V_{max} and K_m of the phosphorylation. In the sequence RSGALKRRR, S_{144} has an arg at its amino terminus, and 3 uncharged residues followed by 4 basic residues at its carboxy terminus, thereby suggesting that S_{144} is a likely site for phosphorylation by the protein kinase C enzyme of the host cells or a viral protein kinase C-like enzyme. S_{142} is preceded and followed by arg residues, which makes it a possible target for phosphorylation by protein kinase A or C, although phosphorylation efficiency would be expected to be lower. In addition, the mass spectral data suggests S_{144} rather than S_{142} as the most likely site. Another possible phosphorylation site was found distal to the RSGALKRRR site. the sequence $S_{157}DEEED_{162}$ is a classic consensus site for casein kinase II-type protein kinase. These two adjacent consensus sites are located in the most hydrophilic portion of the AP. Such site could include a beta turn. The AP could be phosphorylated at the $S_{157}DEEED_{162}$, but no peptide with this sequence only had the additional 80 amu.

Smith and Smith (17) identified protein kinase-related genes in three herpes viruses. The amino acid sequences of herpes simplex virus (HSV) gene UL13, varicella-zoster virus (VZV) gene 47, and Epstein Barr virus (EBV) gene BGLF4 resemble serine/threonine kinases. If we verify the analysis of the protein-coding content of the sequence of human CMV compiled by Chee (18), Table 2 of the article shows that UL97 of HCMV has the following homologs: HSV UL13, VZV47 and EBV BGLF4. It is now known that the VZV serine kinase phosphorylate the AP (19). These kinases could present additional opportunity for inhibiting or blocking viral growth and replication. UL97 phosphorylates the antiviral drug Ganciclovir, a nucleoside analogue which incorporates into the virus DNA sequence acting as a chain terminator, thus stopping viral DNA synthesis. Ganciclovir is one of the very few effective drugs used for treating HCMV infections, however extensive resistance to Ganciclovir has developped, making it even more pressing to find other therapeutic compounds.

In conclusion, the above work has shown that the new approaches that have been used to tackle the problem of the AP post-translational modifications can be used to successfully solve structural problems. These approaches could

Enzyme	Most common Concensus sequence (R/K _{1.3} , X _{2.4})-S°/T°-(X _{2.4} , R/K ^{1.3})		
Protein Kinase C			
cAMP dependent PK	R-R-X-S*/T*		
cGMP dependent PK	R/K ₂₋₃ -X-S [*] /T [*]		
Casein Kinase I	$S(P)-X_{1,2}S^*/T^*$		
Casein Kinase II	$S'/T'-(D/E/S(P)_{1,2}, X_{2,4})$		
Alphaherpesvirus PK	R.,-X,-S'-Z		
CMV Colburn PK ?	R/K-S ^o -x ₃₄ -R/K ₁₄ ? (Putative concensus site)		

S(P) = phosphorylated residue. X = amino acid residues Z = not Glu or Pro

be used by themselves or in conjunction with classic protein techniques to give information sought after with a minimal amount of sample, greater precision and accuracy and an easy way to detect and determine post-translational modifications.

Literature Cited

- 1. Lee, J.Y.; Irmiere, A.; Gibson, W. Virology, 1988, 167,87-96.
- 2. Preston, V.G.; Coates, J.V.; Rixon, F.J. J. Virol., 1983, 45, 1056-1064.
- 3. Gibson, W. Virology, 1980, 111, 516-537.
- 4. Gibson, W.; Marcy, A.I.; Comolli, J.C.; Lee, J. J. Virol. 1991, 64, 1241-1249.
- 5. Welch, A.R.; McNally, L.M.; Gibson, W. J. Virol., 1991, 65, 4091-4100.
- 6. Liu,F.; Roizman, B. J. Virol., 1991, 65, 5149-5156.
- Welch, A.R.; Woods, A.S.; McNally, L.M.; Cotter, R.J.; Gibson, W. Proc. Natn'l. Acad. of Sci., 1991, 88, 10792-10796.
- 8. Gibson, W.; Roizman, B.J. J. Virol., 1972, 10, 1044-1052.
- Woods, A.S.; Cotter, R.J.; Yashiyoka, M.; Bullesbach, E.; Schwabe, C. Int. J. Mass Spectrom. Ion Proc., 1991, 111, 77-88.
- 10. Dognin, M.J.; Whittmann-Liebold B. FEBS. 1977, 84, 342-346.
- 11. Holmes, C.F.B. FEBS Lett., 1987, 215, 21-24.
- 12. Robson, L.; Gibson, W. J. Virol., 1989, 63, 669-676.
- 13. Schenk, P.; Woods, A.S.; Gibson, W. J. Virol., 1991, 65, 1525-1529.
- 14. Kennely, P.J.; Krebs, E.G. J. Biol. Chem., 1991, 266, 15555-15558.
- Kishimoto, A.; Nishiyama, K.; Yuko, U.; Hideaki, N.; Takeyama, Y.;
 Nishizuga, Y. J. Biol. Chem., 1985, 260, 12492-12499.
- 16. Woodget, R.J.; Gould, L.K.; Hunter T. Eur. J. Biochem., 1986, 191, 177-184.
- 17. Smith, R.F.; Smith, T.F. J. Virol., 1989, 63, 450-455.
- Chee, M.S.; Bankier, A.T.; Beck, S.; Bohni, R.; Brown, C.M.; Cerny,R.; Horsnell, T.; Hutchison III, C.A.; Kouzarides, T.; Martignetti, J.A.; Preddie, E.; Satchwell, S.C.; Tomlinson, P.; Weston, K.M.; Barrell, B.G., 1990, 154, 125-169.
- 19. Ng, T.I.; Grose, C., Virol. (In Press).

RECEIVED September 20, 1993

Chapter 12

Laser Desorption Mass Spectrometry in Protein Analysis

Off and On Membranes

Martha M. Vestling

Department of Chemistry and Biochemistry, University of Maryland Baltimore County, Baltimore, MD 21228

Because matrix-assisted laser desorption mass spectrometry (LDMS) provides considerably more accurate molecular weights than the important well-established and widely used protein technique, gel electrophoresis, several LDMS instruments have recently become commercially available. The short analysis time, ease of operation, and price of these instruments is changing the way proteins are characterized. This report describes several ways LDMS can be used to analyze proteins and peptides. First the utility of the technique will be illustrated with data from cyanogen bromide and tryptic digests. Second, acquisition of laser desorption spectra of proteins and peptides absorbed on membranes will be described. And lastly, some guidelines for preparing proteins and peptides for LDMS will be presented.

Analysis of Cyanogen Bromide Digests and Mass Balance Strategy

Cyanogen bromide reacts with protein methionine residues in the presence of acid and leads to cleavage of the protein chain at the C-terminal of each methionine. Since proteins usually contain only a few methionine residues, cyanogen bromide digestion produces only a few peptides. By determining the molecular weights of the peptides, a protein with a predicted sequence can be searched or mapped for unexpected Two different amino acid sequences in the literature for the protein Staphylococcus aureus V8 protease made it a candidate for mapping (1, 2). S. aureus V8 protease itself is widely used to generate peptides for sequencing, since it catalyzes the hydrolysis of amide bonds whose carbonyls are contributed by glutamic acid residues. The molecular weight of S. aureus V8 protease was determined by LDMS to be 29768 ± 300 (3), which was considerably larger than the value of 29024 calculated from the structure derived from the cDNA sequence (1). It should be noted here that a routine gel electrophoresis experiment would give a value of 30000 ± 3000, and consequently would not have picked up the difference observed with LDMS. To locate the source of the mass difference, the cyanogen bromide digest of S. aureus V8 protease was subjected to analysis by LDMS and fast atom bombardment mass spectrometry (FABMS). The molecular weights measured are

> 0097-6156/94/0549-0211\$06.00/0 © 1994 American Chemical Society

listed in Table I and showed that the bulk of the molecular weight discrepancy was located in the C-terminal cyanogen bromide fragment. Treatment of the C-terminal cyanogen bromide fragment with α-chymotrypsin produced a peptide with 61 amino acids consisting almost entirely of proline, aspartic acid, and asparagine residues. Using mass spectrometry in conjunction with microchemical (Edman) sequencing, a sequence was derived that fits the requirements of the molecular weight data (4). The logic of this mass balance strategy requires that all pieces be accounted for at each step and that their sums correspond to the molecular weight determined originally.

Analysis of the Tryptic Digest of a Glycoprotein

Avidin, found in chicken eggs, is extensively glycosylated at a single asparagine site. LDMS was used to confirm the site and to determine the extent of glycosylation. After its disulfide bonds were reduced with dithiothreitol and the thiol groups alkylated with iodoacetamide, avidin was subjected to tryptic digestion. The products were divided in half. Half of the mixture was treated with water and half with an aqueous solution of N-glycosidase F, which catalyzes the cleavage of carbohydrate from asparagine side chains, leaving behind an aspartic acid residues. After partial fractionation by high performance liquid chromatography (HPLC), the various fractions from both the N-glycosidase F treated peptides and the non-treated peptides were analyzed by LDMS. Ions for most of the tryptic peptides predicted from the amino acid sequence (5) were found. Figure 1 shows the spectra obtained from fractions 6 of both treatments. The presence of a major peak may be noted in the Nglycosidase F treated fraction (panel a) that is absent in the non-treated fraction (panel b). This peptide has a molecular weight of 1836 daltons which corresponds to the tryptic peptide [10-26] whose asparagine at position 17 has been changed to an aspartic acid residue. Only micrograms of avidin were needed for the digestion, chromatography, and LDMS analysis.

Laser desorption of the whole protein provided a broad signal, reflecting carbohydrate heterogeneity, with an average molecular weight of 16033 daltons. For this measurement, avidin was dissolved in 0.1 % trifluoroacetic acid (TFA) and then mixed with sinapinic acid (3, 5-dimethoxy-4-hydroxycinnamic acid) (6). The molecular weight of avidin was determined by sedimentation equilibrium in 1970, as 69300 (5), which indicates that 16033 is a measurement of the molecular weight of the subunit. TFA and sinapinic acid are undoubtedly denaturing agents. Subtracting the molecular weight of 14456 derived from the protein sequence provided the average weight of the carbohydrate, 1577 daltons. This indicates that avidin is about 10% carbohydrate by weight.

The time required to obtain the LDMS spectrum of a tryptic digest fraction or of a protein is very short, on the order of two to five minutes using commercially available instrumentation. At least two or three days are needed to reduce and alkylate a protein, digest with trypsin, treat with N-glycosidase F, and fractionate by HPLC. This suggests that one laser desorption mass spectrometer can serve a number of biochemical researchers.

Desorption of Proteins and Peptides from Membranes

For LDMS to achieve its potential, it must be able to handle proteins and peptides as

Table I

Molecular weight of the products of cyanogen bromide cleavage of S. aureus V8 protease (a).

peptide	calc. MH+	observed m/z	technique
[1-117]	12520	12511	LDMS
[1-143]	15220	15243	LDMS
[118-143]	270 1	2701	FABMS
[144-158]	1693	1693	FABMS
[159-end]	12020	13154	LDMS

^{*}adopted from reference 3.

bcalculated from cDNA derived sequence, reference 1.

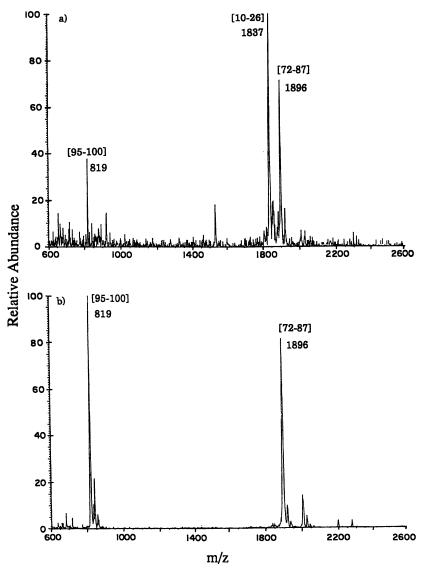


Figure 1. a) LDMS spectrum of HPLC fraction 6 from the N-glycosidase F treated trypsin digest of reduced and alkylated avidin. b) LDMS spectrum of HPLC fraction 6 from non-treated trypsin digest of reduced and alkylated avidin. The peak at m/z 1836 is only present in the deglycosylated sample. Approximately 100 μg of digest were treated with N-glycosidase F while another 100 μg were not treated. Each HPLC fraction was freeze dried and redissolved 60 μL of 0.1% TFA. An aliquot (0.5 μL) of this solution was mixed with an equal volume of 50 mM α-cyano-4-hydroxycinnamic acid solution (acetonitrile (70% by volume) and 0.1% TFA/water (30%)). All the spectra in the figures of this report were acquired with a Kratos Kompact MALDI III Mass Spectrometer (Kratos Analytical, Manchester, UK) which has a 337 nm nitrogen laser.

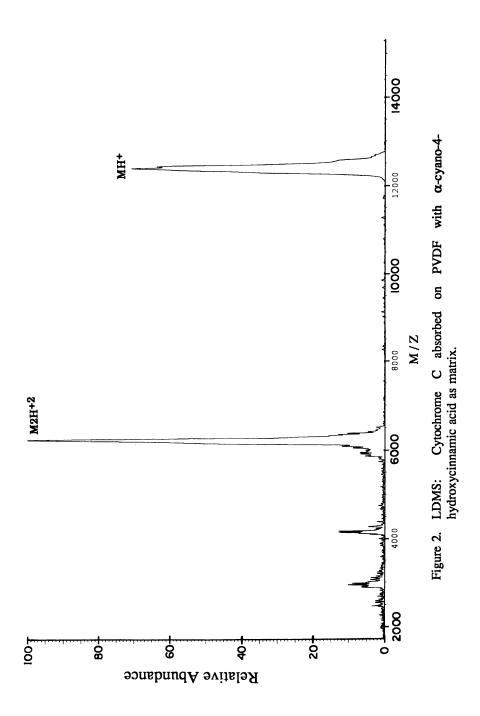
they are purified. Gel electrophoresis, HPLC, and capillary electrophoresis are the major techniques used for purification, and one way to transfer from one place to another the small amounts of material provided by these techniques is to absorb them directly onto membranes. Samples collected on polyvinylidene difluoride (PVDF) membranes are routinely subjected to microchemical (Edman) sequencing (7). Laser desorption spectra can be obtained of proteins and peptides absorbed on the PVDF. Figure 2 shows the spectrum of cytochrome C which had been absorbed on PVDF. The matrix was α-cyano-4-hydroxycinnamic acid (8). In this experiment, a piece of PVDF membrane was taped to a sample slide for a Kratos Kompact mass spectrometer, which has a 337 nm nitrogen laser. The instrument was calibrated with peptides standards absorbed on the membrane. It is important to note that these membranes can be removed from the mass spectrometer with most of the protein intact.

A spectrum for bovine insulin is shown in Figure 3a. The matrix (6-aza-2-thiothymine) was applied to the membrane, and the membrane was placed in the mass spectrometer. When the insulin sample was removed from the instrument, treated with dithiothreitol, and reinserted, the spectrum shown in Figure 3b was obtained. The appearance of both the A-chain (m/z 2342) and B-chain (m/z 3401) demonstrates that reduction of disulfide bonds carried out on the membrane can be monitored by LDMS (9).

Laser desorption of products produced by protease digestion directly on PVDF can also be carried out (9). After cyctochrome C was digested on PVDF with trypsin in 5 µL of 10 mM Tris.HCl at pH 8.5, the partial spectrum shown in Figure 4 was obtained using 6-aza-2-thiothymine as the matrix. Horse heart cytochrome C has 104 amino acids and was first sequenced in 1961 (10). The major peaks at 1168, 1296, 2249, and 3137 are assigned to peptides [28-38], [28-39], [9-22], and [1-37] while the minor peaks at 1435, 1469, 1509, 1563, 1604, 1713, 2557, and 3379 are assigned to peptides [26-38], [40-53], [92-104], [26-39], [88-100] or [87-99], [40-55], [6-22], and [1-25]. Two poorly shaped peaks near m/z 4924 and 5842 were recorded and appear to rise from large pieces of cytochrome C. The digestion was allowed to proceed during the time it took the 5 µL of buffer (only a few minutes) to evaporate in the laboratory atmosphere. The spectrum in Figure 4 was acquired without prior HPLC fractionation suggesting that LDMS could be used to monitor the progress of protein digestions. Chemical reactions and protease digestions have been carried out on nitrocellulose for PDMS (11, 12) and chemical and protease digestions on PVDF are known (13), but measuring molecular weights of the products on membranes is a recent advance (9). This capability of analyzing membrane-absorbed proteins and peptides by LDMS provides a way to refine the rough molecular weights achieved by gel electrophoresis and size-exclusion chromatography.

Preparation of Proteins and Peptides for LDMS

The typical biochemical protein buffer contains a number of inorganic compounds such as sodium chloride, sodium phosphate, potassium acetate, and magnesium chloride as well as other additives. Thus the compounds deposited on the sample holder or absorbed onto a membrane will not be just proteins and peptides. The presence of these salts affects the quality of the mass spectra obtainable. The laser desorption spectrum of gramicidin S shown in Figure 5a was obtained in the presence



In Time-of-Flight Mass Spectrometry; Cotter, R.; ACS Symposium Series; American Chemical Society: Washington, DC, 1993.

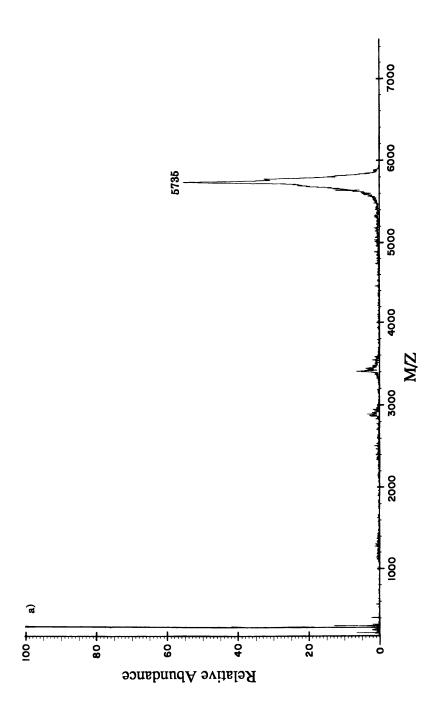
of sodium ions. Note the strong M+Na⁺ ion signal at m/z 1164. The gramicidin S signal is divided between the M+H⁺ ion at m/z 1142 and the M+Na⁺ ion, requiring more gramicidin S to see the same signal intensity as one would need from a pure gramicidin S sample. The presence of inorganic salts reduces the overall sensitivity of the measurement. The effect of the inorganic salts can be minimized by rinsing the dried mixture of matrix and peptide with ice cold water (14). The spectrum shown in Figure 5b was obtained by applying 10 µL of ice cold water to the sample spot used to obtain the spectrum shown in Figure 5a. The water was pulled off the sample mixture immediately with an automatic pipet and the sample slide was reinserted into the LDMS. As long as the matrix and analyte have only limited water solubility, rinsing can improve peak shape and sensitivity. Small peptides of the sort that elute early in reverse phase HPLC can be washed off the sample holder, though perhaps not so easily off a membrane. At an instrument resolution of 0.1 %, sodium adduct peaks can be easily recognized for peptides such as gramicidin S. With proteins, adducts blend in with the broad isotope distribution. For proteins larger than 10,000 daltons, at 0.1 % resolution, protein isotopic distributions (15) merge with adduct isotopic distributions to produce broad peaks with m/z values at the apex shifted higher than those expected for pure proteins. So while LDMS spectra are easy to obtain, the presence of other ions in the sample must be considered in the interpretation of the values measured.

The choices of matrix and matrix/analyte ratio are also critical to the success of the LDMS experiment. For example, an equimolar mixture of the peptides gramicidin S (MW = 1141), melittin (MW = 2847), and aprotinin (MW = 6512) in a α -cyano-4-hydroxycinnamic acid matrix produced ions for all three peptides. The same mixture in an equivalent amount of sinapinic acid showed ions for only gramicidin S and melittin. These spectra are shown in Figure 6. The laser powers used are not the same. With a 337 nm laser, sinapinic acid and 2,5-dihydroxybenzoic acid usually require higher laser power than α -cyano-4-hydroxycinnamic acid does. The molar ratio of matrix to analyte in both spectra in Figure 6 was 5000/1. The ratio of matrix to analyte also effects the quality of LDMS measurements. Low matrix/analyte ratios require higher laser power. And molecular ion peaks for heavy molecules are usually broader at higher laser power (16).

An equimolar mixture of lysozyme, cytochrome C, ubiquitin, and aprotinin was mixed with α-cyano-4-hydroxycinnamic acid for the spectrum shown in Figure 7a. The molar/matrix ratio per analyte was 2500/1. Note the variation in signal intensity. Cytochrome C which contains a strong visible chromophore (the solid is red-brown in appearance) dominates the spectrum suggesting that photochemical effects are important. The same mixture in sinapinic acid and at a matrix/analyte ratio of 5000/1 showed variation in signal intensity and the suppression of aprotinin (Figure 7b). Thus it may be advisable when dealing with unknown mixtures to try several matrices and matrix/analyte ratios.

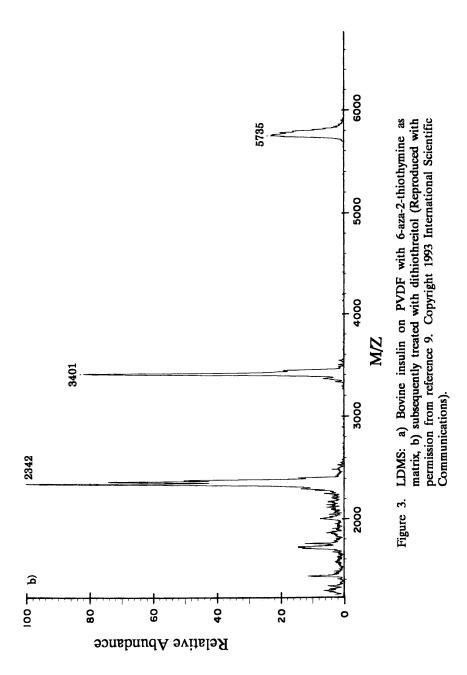
Conclusion

The examples cited here make a case for installing a LDMS in every biochemistry and biotechnology laboratory. A low cost, rugged, multi-user instrument can quickly provide accurate molecular weights for proteins and peptides isolated by the whole array of biochemical separation tools. Direct coupling of gel electrophoresis or other

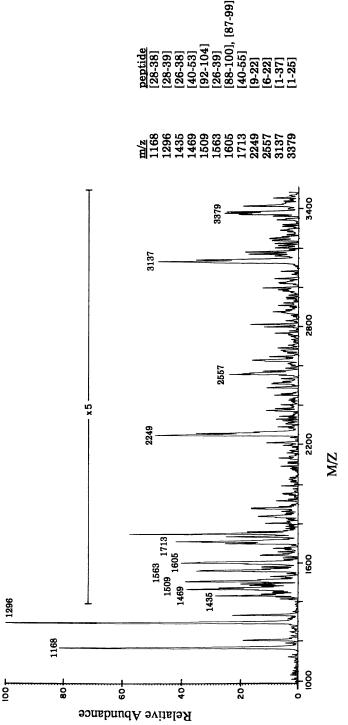


In Time-of-Flight Mass Spectrometry; Cotter, R.; ACS Symposium Series; American Chemical Society: Washington, DC, 1993.

12.



In Time-of-Flight Mass Spectrometry; Cotter, R.; ACS Symposium Series; American Chemical Society: Washington, DC, 1993.



numbered peaks are matched in the table and the text to expected tryptic peptides (Reproduced with permission from reference 9. Cytochrome C digensted on PVDF with trypsin. Copyright 1993 International Scientific Communications) LDMS: Figure 4.

In Time-of-Flight Mass Spectrometry; Cotter, R.; ACS Symposium Series; American Chemical Society: Washington, DC, 1993.

12. VESTLING

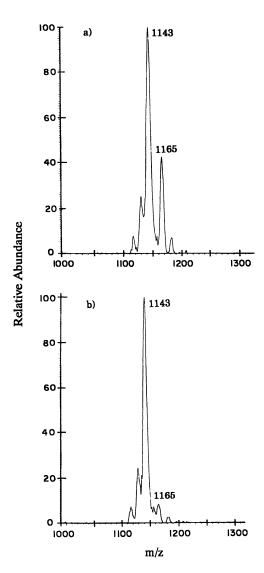


Figure 5. a) LDMS spectrum of gramicidin S in the presence of sodium ions (matrix = α-cyano-4-hydroxycinnamic acid). b) subsequently rinsed with ice cold water.

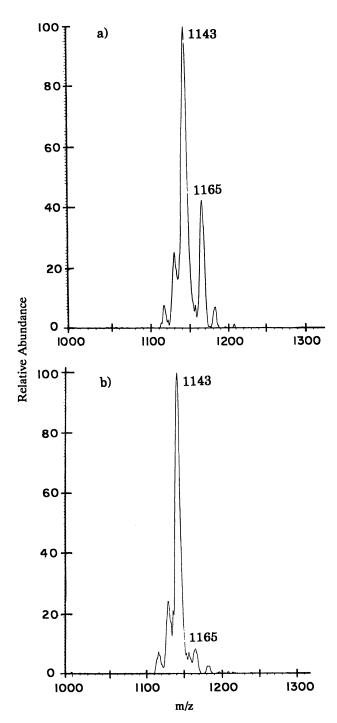


Figure 6. LDMS spectra of an equimolar peptide mixture in two different matrices. The same ratio of matrix to peptides was used for both spectra. a) α-cyano-4-hydroxycinnamic acid. b) sinapinic acid.

In Time-of-Flight Mass Spectrometry; Cotter, R.; ACS Symposium Series; American Chemical Society: Washington, DC, 1993.

12. VESTLING

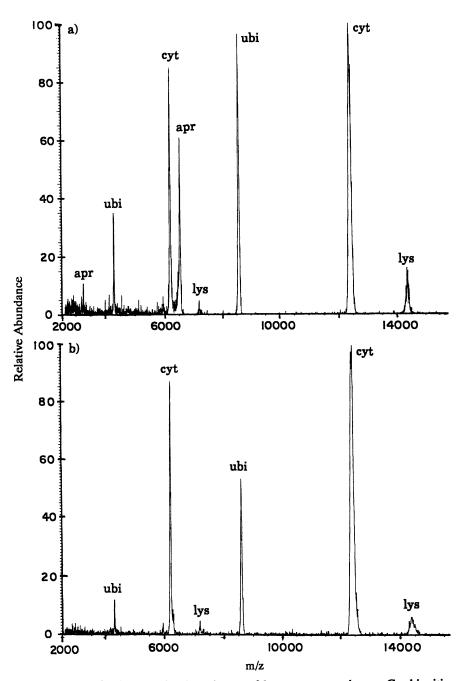


Figure 7. LDMS: a) an equimolar mixture of lysozyme, cytochrome C, ubiquitin, and aprotinin in α -cyano-4-hydroxycinnamic acid, b) in sinapinic acid.

protein separation techniques to LDMS is not necessary and may not be even desirable, since membranes can be used to transfer the samples efficiently and the time-scales for the experimental techniques are usually very different (hours versus minutes).

Acknowledgments

The author thanks Catherine Fenselau for much helpful discussion. Support for this work was provided by Sterling Winthrop Inc. and the National Science Foundation.

References

- 1. Carmona, C.; Gray, G. L., Nucleic Acids Res. 1987, 15, 6757.
- 2. Drapeau, G. R., Can. J. Biochem. 1978, 56, 534-544.
- 3. Hua, S.; Vestling, M.; Murphy, C.; Fenselau, C.; Spengler, B.; Pan, Y.; Wang, R.; Cotter, R. J; Theibert, J.; Collins, J. H., Techniques in Protein Chemistry 1991, II, 95-106.
- 4. Hua, S.; Vestling, M. M.; Murphy, C. M.; Bryant, D. K.; Height, J. J.; Fenselau, C.; Theibert, J.; Collins, J. H., Int. J. Peptide Protein Res. 1992, 40, 546-550.
- 5. DeLange, R. J.; Huang, T., J. Biol. Chem. 1971, 246, 698-709.
- 6. Beavis, R. C.; Chait, B. T., Rap. Comm. Mass Spectrom. 1989, 3, 432-435.
- 7. Matsudaira, P., J. Biol. Chem. 1987, 262, 10035-10038.
- Beavis, R. C.; Chaudhary, T.; Chait, B. T., Org. Mass Spectrom. 1992, 27, 156-158.
- Vestling, M. M.; Fenselau, C., 41st Annual Conference on Mass Spectrometry and Allied Topics, American Society for Mass Spectrometry, San Francisco, May 1993.
- Margoliash, E.; Smith, E. L.; Kreil, G.; Tuppy, H. Nature 1961, 192, 1125-1127.
- 11. Cotter, R. J., Anal. Chem. 1988, 60, 781A-793A.
- 12. Woods, A. S. this volume.
- Patterson, S. D.; Hess, D.; Yungwirth, T.; Aebersold, R., Anal. Biochem. 1992, 202, 193-203.
- 14. Beavis, R. C.; Chait, B. T., Anal. Chem. 1990, 62, 1836-1840.
- Yergy, J.; Heller, D.; Hansen, G.; Cotter, R. J.; Fenselau, C., Anal. Chem. 1983, 55, 353-357.
- 16. Pan, Y.; Cotter, R. J., Org. Mass Spectrom. 1992, 27, 3-8.

RECEIVED July 15, 1993

Author Index

Allison, J., 157
Beavis, Ronald C., 49
Chernushevich, I. V., 108
Conzemius, Robert J., 124
Cornish, Timothy J., 95
Cotter, Robert J., 16,95,194
Dodonov, A. F., 108
Duncan, M. A., 61
Enke, C. G., 157
Gibson, Wade, 194
Holland, J. F., 157

Laiko, V. V., 108 Lys, Ihor A., 177 Price, Dennis, 1 Robbins, D. L., 61 Russell, D. H., 73 Strobel, F. H., 73 Vestling, Martha M., 211 Watson, J. T., 157 Willey, K. F., 61 Woods, Amina S., 194 Yeh, C. S., 61

Affiliation Index

Iowa State University, 124
The Johns Hopkins University School of Medicine, 16,95,194
Memorial University of Newfoundland, 49
Michigan State University, 157
Russian Academy of Sciences, 108 Texas A&M University, 73 University of Georgia, 61 University of Maryland Baltimore County, 211 University of Salford, 1

Subject Index

Α

Accelerating voltages, values, 17
Assembly protein, 195
Atmospheric pressure ionization—
reflecting time-of-flight mass
spectrometer
advantages, 108
application of electrospray, 118–122
instrumentation, 109–113
mass resolution, 113–118
parameters, 111,112t
storage modulator, 109–110
Atmospheric pressure ionization techniques,
examples, 108
Atomically coexcited desorption, 154–155
Avidin, laser desorption—MS, 212,214f

В

Bendix Corporation, instrument, 5–6 Biological mass spectrometry, 73–74 Boxcar methods, ion recording, 39–40

C

Carboxypeptidase P digests, confirmation of cytomegalovirus assembly protein cleavage sites, 199,203,204f
Chromatographic detection by mass spectrometry approaches, 157–162
capacity for increasing GC–MS information generation rate, 167,170,171f,173f

Author Index

Allison, J., 157
Beavis, Ronald C., 49
Chernushevich, I. V., 108
Conzemius, Robert J., 124
Cornish, Timothy J., 95
Cotter, Robert J., 16,95,194
Dodonov, A. F., 108
Duncan, M. A., 61
Enke, C. G., 157
Gibson, Wade, 194
Holland, J. F., 157

Laiko, V. V., 108 Lys, Ihor A., 177 Price, Dennis, 1 Robbins, D. L., 61 Russell, D. H., 73 Strobel, F. H., 73 Vestling, Martha M., 211 Watson, J. T., 157 Willey, K. F., 61 Woods, Amina S., 194 Yeh, C. S., 61

Affiliation Index

Iowa State University, 124
The Johns Hopkins University School of Medicine, 16,95,194
Memorial University of Newfoundland, 49
Michigan State University, 157
Russian Academy of Sciences, 108 Texas A&M University, 73 University of Georgia, 61 University of Maryland Baltimore County, 211 University of Salford, 1

Subject Index

Α

Accelerating voltages, values, 17
Assembly protein, 195
Atmospheric pressure ionization—
reflecting time-of-flight mass
spectrometer
advantages, 108
application of electrospray, 118–122
instrumentation, 109–113
mass resolution, 113–118
parameters, 111,112t
storage modulator, 109–110
Atmospheric pressure ionization techniques,
examples, 108
Atomically coexcited desorption, 154–155
Avidin, laser desorption—MS, 212,214f

В

Bendix Corporation, instrument, 5–6 Biological mass spectrometry, 73–74 Boxcar methods, ion recording, 39–40

C

Carboxypeptidase P digests, confirmation of cytomegalovirus assembly protein cleavage sites, 199,203,204f
Chromatographic detection by mass spectrometry approaches, 157–162
capacity for increasing GC–MS information generation rate, 167,170,171f,173f

Chromatographic detection by mass spectrometry-Continued data rate analysis for maximum sample utilization, 162–165f time-of-flight MS-integrating transient recorder-time array detection, performance characteristics, 164-169 time-of-flight MS-time array detection sensitivity capabilities, 170-174 significance for chromatographic detection, 174-176 Cluster(s), photodissociation studies of H⁺-transfer reactions, 84–85,87f,t Cluster ion photodissociation and spectroscopy in reflectron time-of-flight mass spectrometer application, 62,64 cluster ion distribution, 62,63f design advantages and disadvantages, 64 experimental description, 62 instrument configuration, 62,63f instrument operation, 62,64 metal-molecular complexes, 66-71 pure metal clusters, 64-66 Coaxial dual-stage reflectron, 37,38f Collisionally induced dissociation fragmentation technique, 95 use in time-of-flight MS, 95-96 Commercial analog transient digitizers, description, 163-164 Compact disc players, technological advances vs. cost, 177 Continuous ionization, description, 44 Continuous signals, mathematical representation, 179-180 Correlated reflex spectrum, 37,38f Cyanogen bromide digests, laser desorption-MS, 211-213tα-Cyano-4-hydroxycinnamic acid, dual reflectron tandem time-of-flight MS, 104,105f Cytomegalovirus, importance, 195 Cytomegalovirus assembly protein amino acid sequence, 195,196f carboxy terminus determination, 205,208 cleavage site confirmation by carboxypeptidase P digests, 199,203,204f cleavage site mapping, 197-202

consensus sequence, 208-210t

experimental objective, 195

Cytomegalovirus assembly protein— Continued

MS strategy, 195,197
phosphorylation site determination,
203–206t,f
phosphorylation site mapping, 199
phosphoserine identification with
ethanethiol, 205,207f

D

Data acquisition, tandem magnetic sectorreflectron time-of-flight MS, 79-83 Desorption, peptides and proteins from membranes, 212,215-220 Digitizer, selection for time-of-flight signal processing, 192 Drift lengths, values, 17 Dual reflectron tandem time-of-flight mass spectrometer collision cell, 101 design, 96,97f,99 experimental objective, 96 gating, 101 instrumentation, 96-99 mass dispersion, 101,103 operation, 104-106f reflectron operating modes, 99-102f timing sequence diagram, 96,98f Dual-stage reflectron, description, 31–34f Dynamic field focusing, description, 162

E

Electrospray ionization on reflecting time of flight mass spectrometer advantages, 118,120,122 ion source design, 118,119t,121f ion structure determination, 120,121f mass determination, 120,122f resolution, 119–120,121f sensitivity, 119,121f Electrostatic energy analyzers, 31,33f Endoproteinase–Glu C digest, phosphorylation site determination of labeled assembly protein, 203,205,206f Endoproteinase–Lys C digest, phosphorylation site determination of labeled assembly protein, 203,204f,206t

INDEX 229

Energy focusing, improvements, 5
Energy focusing devices
coaxial dual-stage reflectron, 37,38f
dual-stage reflectron of mamyrin,
31-32,34f
electrostatic energy analyzers, 31,33f
single-stage reflectron, 32,35-37
tandem MS, 37,39
European Time-of Flight Mass Spectrometry
symposium, functions, 6-8

F

Fast atom bombardment, 29,30f
Filtering, 183–184
First-order one-stage reflectron, behavior, 58f,60
First-order two-stage reflectron, behavior, 57f,59–60
Flight times, values, 17
Flight tube, fragmentation, 26
Fourier transforms
Fourier integral, 180
properties, 181–183
representation, 180f
transform of square pulse, 180,181f

G

Gas chromatography—mass spectrometry data rate requirements, 157,159 limitations, 159 rates of information along two axes of information, 157,158f Glycoprotein tryptic digest, laser

desorption-MS, 212,214f

Η

H*-transfer reactions within clusters, photodissociation studies, 84-85,87f,t Herpes viruses, protein processing analysis, 195-210

I

Initial kinetic energy distribution, mass resolution effect, 19–21f

Instruments, tandem time-of-flight MS, 75 - 76Integrated transient recording, ion recording, 42,43f Interleaved sampling, description, 188-189 Interpretation, reflectron time-of-flight MS, Inverse Fourier transforms, transform equation, 181 Ion(s), behavior in reflectron analyzer, 51-60 Ion arrival time detectors, description, 163 Ion deflection, mass resolution effect, 116 Ion(s) desorbed from surfaces, improvement of mass resolution, 23-24 Ion recording integrated transient recording, 42,43f oscillographic and boxcar methods, 39-40 time-to-digital conversion, 40-42 Ion source velocity distributions, 52–53 Ion unimolecular decomposition, 54-55 Iron-benzene complexes, photodissociation and spectroscopy in reflectron time-of-

K

Kinetic energy of ions, definition, 16 Knudsen cell, description, 8

flight MS, 67,68f

L

Large ionic molecules, 75

Laser(s), use in biological MS, 74

Laser desorption—laser multiphoton ionization—high-resolution time-of-flight mass spectrometer, development, 10

Laser desorption—mass spectrometry advantages, 211

cyanogen bromide digests, 211–213t desorption of proteins and peptides from membranes, 212,215–216,218–220 glycoprotein tryptic digest, 212,214f proteins and peptides, preparation, 215,217,221–223f

Linear analyzers ion source velocity distribution effects, 52

ion unimolecular decomposition, 54

M

tion and spectroscopy in reflectron time-of-flight MS, 67,69-71 Mamyrin, dual-stage reflectron, 31-32,34fMass calibration, determination, 17,18f Mass difference spectrometry concept, 132,134f,135 instrumentation for basic measurement, 135,136*f* mass difference spectra negative ions, 139,142-146 positive ions, 147,149-154 nonrandom negative ions, 137,139t–141f nonrandom positive ions, 145,147t,148f random observation and predictions, 135,137t,138f Mass dispersion, determination for dual reflectron tandem time-of-flight MS, 101,103 Mass measurement accuracy, determination, 17,18f Mass reflectron, schematic representation, 7,12fMass resolution determination, 17,18f,21 ion deflection effect, 116 ion(s) desorbed from surfaces, 23-24 mass dependence of bottom resolution, 116-118 metastable fragmentation effect, 25-30 role of time, space, and kinetic energy distributions, 17,19-21 time lag focusing, 22-23 time spread compensation in two-stage

Magnesium-CO, complexes, photodissocia-

chromatographic detection, 157–176
problems for analytical
characterization, 124
Mass spectrometry—mass spectrometry, twodimensional mass axis scanning, 160

electrostatic mirror, 113-117f

Mass resolution limitations for linear

uncertainties in initial time and position

maximum characterizing power for

kinetic energy problem, 24-25

of ion formation, 24

instruments

Mass spectrometry

Matrix-assisted laser desorption—ionization, description, 25,42,43f

Matrix-assisted laser desorption—ionization—tandem mass spectrometry, comparison to MS, 88–92

Metal—molecular complexes, cluster ion photodissociation and spectroscopy in reflectron time-of-flight MS, 66–71

Metastable fragmentation—mass resolution relationship fragmentation in flight tube, 26 fragmentation in source—accelerating region, 25–26 postacceleration effects, 27–28

N

Neutral ion correlation experiment, 79-80

time-delay techniques, 29,30f

0

On-line pile-up rejection method, 80–83f Orthogonal extraction, description, 44 Oscillographic methods, ion recording, 39–40

P

Peptides, preparation for laser desorption-MS, 215,217,221–223f Peptides from membranes, desorption, 212,215-220 Performance characteristics, time-of-flight MS-integrating transient recorder-time array detection, 164,166-169 Photodissociation tandem magnetic sector-reflectron timeof-flight MS, 82–84,86–87 use in time-of-flight MS, 95-96 See also Cluster ion photodissociation and spectroscopy in reflectron time-offlight mass spectrometer Plasma desorption, conditions, 29 Plasma desorption-mass spectrometry assembly protein analysis, 195–210 description, 40-42

development, 8

INDEX 231

Postacceleration, mass fragmentation effects, 27–28

Protein(s), preparation for laser desorption–MS, 215,217,221–223f

Protein analysis, use of laser desorption–MS, 211–222

Protein(s) from membranes, desorption, 212,215–220

Protein processing in herpes viruses, techniques, 195–210

Pulsed ion extraction, description, 44,45f

Pulsed laser ionization, development, 9

Pure metal clusters, cluster ion photodissociation and spectroscopy in reflectron time-of-flight MS, 64–66

R

Radically new time-of-flight mass spectrometric instrumentation advantages and disadvantages, 154-155 concept, 125 mass difference spectrometry, 132,134-154 reasons for development, 124-125 single-event laser desorption-time-of-flight MS, 125-133 Random interleaved sampling, 189 Reflectron(s) classifications, 79 coaxial dual stage, 37,38f description, 49,51 dual stage, 31-32,34f mass measurement, 51 single stage, 32,35-37 tandem magnetic sector-reflectron timeof-flight MS, 79 temporal correction, 51 Reflectron analyzers examples, 55-58f first-order one-stage reflectron, 58f,60 first-order two-stage reflectron, 57f,59-60 ion source velocity distribution effects, 52-53 ion unimolecular decomposition, 54-55 second-order two-stage reflectron, 56f,59 Reflectron time-of-flight mass spectrometer, cluster ion photodissociation and spectroscopy, 61-71

Reflectron time-of-flight mass spectrometry detector techniques, 162–164 diagram, 162,165f integrating transient recorder, 163–165f Resonance ionization mass spectrometry, 10 Rhodamine 6–G, dual reflectron tandem time-of-flight MS, 104,106f

S

Sampling description, 185f digital filtering, 185-186 errors, 187 examples, 186-187 resolution enhancement, 187 Second-order two-stage reflectron, behavior, 56f,59 Secondary ion mass spectrometry, 9-10 Sensitivity capabilities, time-of-flight MStime array detection, 170,172-174 Signal averaging, 184–185 Signal integrity, maintenance for time-offlight signal processing, 189-191 Signal processing for time-of-flight applications combining methods, 189 continuous signals, 179-180 digitizer selection, 192 filters, 183,184*f* Fourier transforms, 180-183 interleaved sampling, 188-189 inverse Fourier transforms, 181 maintaining signal integrity, 189-191 random interleaved sampling, 189 resolution enhancement, 187 sampling, 185f-187 sampling errors, 187-188 signal averaging, 184-185 time-to-digital conversion, 177,178f transient recorders, 178,179f triggering, 191 Single-event laser desorption-time-of-flight mass spectrometry application, 126,129f approach and development, 125-127f ion association, 130,132,133f

ion source, 126,128f

multiplicity of ions, 126,130t,131f

Single-event laser desorption-time-of-flight mass spectrometry—Continued single-event information, 126,130–133
Single-stage reflectron mass calibration in instruments, 32,35 metastable fragmentation, 36–37
Source-accelerating region, fragmentation, 25–26
Source distance, values, 17
Spatial distribution, mass resolution effect, 19,20f
Spiratron, description, 51
Surface-induced dissociation description, 37 use in time-of-flight MS, 95–96

T

160,162

Tandem magnetic sector-reflectron time-offlight mass spectrometer background signal, 81,83f data acquisition, 79-83 diagram, 76,77f future, 92 H+-transfer reactions within clusters, 84–85,87*f*,*t* parameters, 76,79 photodissociation, 82-84,86-87 reflectrons, 79 schematic representation, 76,78f Tandem mass spectrometric studies of biomolecules, objectives, 74 Tandem mass spectrometry advantages, 73-74 applications, 95 description, 37,39 development, 11 fragmentation techniques, 95 process, 95 Tandem time-of-flight mass spectrometry future, 92 instruments, 75–76 magnetic sector-reflectron, 76-87,92 matrix-assisted laser desorption-ionization, 88-92 Temporal distribution, mass resolution effect, 19,20f Time array detection, requirements for use,

Time-compressed chromatography description, 167 gasoline range hydrocarbon mixture analysis, 170,171f,173f steps, 167,170 Time lag focusing, improvement of mass resolution, 22-23 Time of flight, definition, 1,3 Time-of-flight mass analyzer, 49-51 Time-of-flight mass spectrometers advantages and disadvantages, 61-62 atmospheric pressure ionization reflecting, See Atmospheric pressure ionizationreflecting time-of-flight mass spectrometer components, 16,18f drift region, 17 dual reflectron tandem, See Dual reflectron tandem time-of-flight mass spectrometer parameters, 16-17 source region, 16 Time-of-flight mass spectrometry advantages, 11-12t, 108 applications, 44,46 Bendix Corp. instrument, 5-6 continuous ionization, 44 Dynamic Mass Spectrometry symposiums, 10-11 energy focusing, 5 energy focusing devices, 30-39 European Time-of-Flight Mass Spectrometry symposiums, 6-9 future developments, 13 future improvements, 46 history, 1,2tinitial kinetic energy distribution vs. mass resolution, 19-21 instrument(s), 1,2tinstrument development, 3,4f interpretation of reflectron spectra, 49-60 ion recording, 39-43 laser desorption-laser multiphoton ionization-high-resolution MS, 10 mass calibration and resolution, 17,18f mass resolution improvement approaches, mass resolution limitations for linear instruments, 24-25 metastable fragmentation vs. mass

resolution, 25-30

INDEX 233

Time-of-flight mass spectrometry— Continued orthogonal extraction, 44 plasma desorption-MS, 8 principle, 1,3 problems, 12,13 pulsed ion extraction, 44,45f pulsed laser ionization, 9 reasons for interest, 108 resonance ionization MS, 10-11 secondary ion MS, 9-10 signal processing, 177–192 space distribution of ions, 5 space distribution vs. mass resolution, 19,20f speed, 159-160 strategy for protein analysis, 197 tandem MS, 11 temporal distribution vs. mass resolution, 19,20f time array detection, 160,161f Wiley-McLaren instrument, 3-5 Time-of-flight mass spectrometry-integrating transient recorder-time array detection, performance characteristics, 164,166–169 Time-of-flight mass spectrometry-time array detection sensitivity capabilities, 170,172-174 significance for chromatographic detection, 174-176

Time of flight of ions, definition, 8,17 Time-of-ion formation, determination, 21 Time-resolved ion kinetic energy spectroscopy, description, 162 Time-resolved ion momentum spectroscopy, description, 160,162 Time slice detector, description, 162–163 Time-to-digital conversion, ion recording, 40-42 Time-to-digital converters description, 40 properties, 177-178 Time-to-pulse height converter, 40 Transient recorders, 178-179 Triggering, description, 191 Tryptic digest of glycoprotein, laser desorption-MS, 212,214f

V

Velocities of ions, definition, 16

W

Wiley-McLaren instrument, description, 3-5